

Design, Synthesis and Pharmacological Evaluation of Novel Adenosine A₂ Modulators for Treatment of Epilepsy and Pain

THESIS

Submitted in partial fulfilment
of requirements for the degree of
DOCTOR OF PHILOSOPHY

by

SRIKANTH RACHARLA

ID No 2011PHXF023H

Under the supervision of
Prof. P. YOGEE SWARI



Pilani | Dubai | Goa | Hyderabad

BIRLA INSTITUTE OF TECHNOLOGY & SCIENCE, PILANI

2016

CERTIFICATE

This is to certify that the thesis entitled “**Design, Synthesis and Pharmacological Evaluation of Novel Adenosine A₂ Modulators for Treatment of Epilepsy and Pain**”, submitted by **SRIKANTH RACHARLA** ID No.**2011PHXF023H** for award of Ph.D. of the Institute embodies the original work done by him under my supervision.

Signature of the Supervisor:

Name in capital letters : **Dr. P.YOGEESWARI**

Designation : **Professor**

Date:

ACKNOWLEDGEMENTS

*First and foremost, I would like to thank **Lord Vinayaka** who has given me this opportunity and for his blessings.*

*It's a great pleasure and immense satisfaction in expressing my deep gratitude towards my research supervisor, **Prof.P.Yogeeswari**, Professor and Associate Dean (Sponsored Research and Consultancy Division), Department of Pharmacy, BITS Pilani Hyderabad Campus for her continuous guidance, suggestions and support. She has always been an inspiration to me for my research work. I am thankful to her for her enthusiasm, patience and love for research. The work environment she has given to me, the experiences gained from her and her creative working culture have been great and will be remembered throughout my life.*

*I deeply acknowledge the valuable suggestions and guidance given to me during the period of my research by **Prof.D.Sriram**, Professor, Department of Pharmacy, BITS-Pilani Hyderabad Campus.*

*I thankfully acknowledge the support and encouragement given by **Prof.A.Sajeli Begum**, DAC member, during this period.*

*I am grateful to **Prof.Bijendra N. Jain**, Ex Vice-Chancellor, BITS-Pilani Campus and **Prof.V.S.Rao**, Acting Vice Chancellor, BITS Pilani, and Director, BITS Pilani Hyderabad Campus for allowing me to carry out my doctoral research work in the institute.*

*I am thankful to **Prof.M.M.S.Anand**, Registrar and **Prof.S.K.Verma**, Dean, Academic Research (Ph.D. Programme), BITS Pilani for their support in doing my research work.*

*I would like to thank **Prof.M.B.Srinivas**, Dean, Administration and **Prof.Vidya Rajesh**, Associate Dean, Academic Research (Ph.D Programme), BITS Pilani Hyderabad Campus for their continuous support and encouragement during my research work.*

*I would like to express my gratitude to **Dr.Shrikant Charde**, Assistant Professor & Head, Department of Pharmacy, BITS Pilani Hyderabad Campus for providing me with the required laboratory facilities and helping me at various stages of my research work.*

*I sincerely acknowledge the help rendered by **Dr.Punna Rao Ravi,Dr.Vamsi Krishna, Dr.Balram Ghosh, Dr. Swati Biswas, Dr.Arti Dhar and Dr.Onkar Kulkarni**, faculty at the BITS Pilani, Hyderabad campus.*

*I am grateful to my friends **Dr. Monika, Dr. Mallika, Aditya, Jean, Patrisha, Rahul, Praveen, Madhu, Rukkaiyya, Mahibalan, Shailender, Brindha, Koushik, Manoj, Reshma.A, Shalini, Ganesh.S, Saketh, Gangadhar, Poorna, Ganesh.P, Santhosh, Brahmam, Renuka, Priyanka.S, Radhika, Vijay, Suman, Bobesh, Anup, Sridevi, Preeti, Hasitha, Omkar, Bomba, Reshma.L, Priyanka.P, Suresh, late Thimmappa and late Srividya** for the time they had spent for me and helped me complete my work.*

*I am very much thankful to the post graduate student **Sushruth Jay** for his help in setting up the experiments.*

*I am greatly indebted to **Dr. Pushkar Kulkarni**, Scientist (Zee Phase Laboratory), **Mr. Raghavender and Ms. Swapna**, Dr. Reddy's Institute of Life Sciences, University of Hyderabad Campus, Gachibowli, Hyderabad in helping me perform the zebrafish experiments.*

*I express my thanks to our laboratory technicians and attenders **Mrs. Saritha, Mr. Rajesh, Mr. Venkat, Mr. Ramana Babu, Mr. Uppalaya, Mr. Ramu, Mr. Seenu and Mrs. Rekha** for all their support.*

*I deeply acknowledge the **Department of Science & Technology (DST)**, Ministry of Science & Technology, Government of India, New Delhi; for providing financial assistance in the form of **Inspire Fellowship (IF: 110052)** for five years.*

*I take this opportunity to sincerely acknowledge the support of the **Indian Council of Medical Research (ICMR)**, Government of India, New Delhi, by providing international travel grant and **European Congress** for providing travel bursary for attending 11th European Congress on Epileptology, Stockholm, Sweden, 29th June-3rd July, 2014.*

*I would like to begin by dedicating this piece of work to my parents **Mr. R. Dhanunjaya and Mrs. R. Kousalya**, whose dreams of my getting the highest degree in education are to materialize. I owe my doctorate degree to my parents who kept my morale high with their continuous care, support and encouragement. Thanks are due if I don't dedicate this thesis to*

*my whole **Racharla** family whose constant and continuous support, love and affection made me reach this level.*

*Last but most important, I would like to thank and deeply appreciate my beloved wife **Mrs. Swapna** for her invaluable patience and support, and the youngest member of my family, **Vedha Sri** for showering me with the joys of fatherhood.*

To everyone who took part in this journey, many, many thanks.

April, 2016

Srikanth Racharla

ABSTRACT

Epilepsy is a neurological disorder, characterized by the recurrent appearance of spontaneous seizures due to neuronal hyperactivity in the brain. Most of the existing antiepileptic drugs possess toxicities and many adverse side effects including cognitive impairment, anorexia, depression, somnolence, and birth defects. This led us to undertake a research to develop more tolerable and less toxic antiepileptic drugs (AEDs) based on protein targets to yield broader spectrum of antiepileptic activity. Pain is an ill-defined, complex unpleasant phenomenon, usually evoked by an internal or external noxious stimulus (nociception). An analgesic is the drug that relieves pain by acting on the peripheral or central pain mechanisms, without significantly altering consciousness. Several extensive research reports reveal that, adenosine A_{2R} 's has crucial role in CNS disorders like epilepsy, acute pain and inflammation. Hence, in the present thesis we mainly focus on CNS disorders like epilepsy ($A_{2A}R$ antagonists), acute pain and inflammation ($A_{2B}R$ antagonists).

$A_{2A}R$ antagonists play a key role in regulating a variety of neurodegenerative diseases like epilepsy, depression, schizophrenia, parkinson's and alzheimer's diseases. Under chronic epilepsy, density of A_{2A} receptors increases robustly and hence it has been proposed to be a potential and attractive target for the development of novel antiepileptic compounds. This research work describes the successful design and identification of 1,3,5 triazine 2,4,6 triamine derivatives as novel adenosine A_{2A} receptor antagonists for treatment of epilepsy. Efforts were taken to discover novel drug candidates targeting A_{2A} as antagonists to suppress various types of seizures with minimal or no adverse effects compared to existing AEDs, by utilizing structure-based pharmacophore modelling. Energy based pharmacophore modeling, cAMP inhibitory IC_{50} by HPLC assay and subsequent *in vivo* screening in an adult zebrafish model including cardio, hepato and neuro tox studies resulted in an initial hit compound Ligand 9 with an IC_{50} of 2.06 μM which was slightly higher than SCH-58261, a standard selective A_{2A} adenosine receptor antagonist. This was further optimized by a combination of pharmacophore modeling and synthetic chemistry (SAR optimization). Expansion of Ligand 9 by chemical synthesis led to the development of two potent A_{2A} receptor antagonists i.e compound 19 and 7 with cAMP inhibitory IC_{50} values of 0.966 μM and 0.292 μM respectively, which are more potent than SCH-58261 (IC_{50} 1.399 μM). Results of *in vivo* anti-epileptic models indicate that 1,3,5 triazine 2,4,6 triamine derivatives, modified at the R-position with cyclohexyl ring show promising anticonvulsant activity. Thus the identified

lead 19 constitutes a prototypical molecule for further optimization and development as antiepileptic compound. We believe that the present class of drugs could be useful as potential leads for further optimization through lead optimisation using the knowledge of medicinal chemistry, in-vivo studies, and pharmacokinetic approaches.

In the second study, pharmacophore model was generated considering a dataset of 265 compounds. A five-point pharmacophore model AADRR was developed. A valid 3D QSAR model was generated based on the developed pharmacophore model which displayed a rational predictive capacity with $R^2 = 0.9661$, $Q^2 = 0.5839$ and Pearson-R = 0.7861. The model was further externally validated which resulted in statistically significant parameters – $R = 0.926$, $r_{cv}^2 = 0.858$ and $r_{pred}^2 = 0.594$. This validated model was further utilized to identify diverse scaffolds against A_{2B} from BITS in-house database based on the fitness and predicted activity of hits. The present study was carried out to evaluate the anti-nociceptive and anti-inflammatory activities of A_{2B} R antagonists (30 mg/kg) using acetic acid induced writhing, formalin induced paw licking, hot plate and tail immersion methods. In acetic acid induced writhing test, all test compounds (RS-4, 6, 9 and 12) produced significant ($p < 0.05-0.001$) reduction in the number of writhing in mice. In formalin induced paw licking test, test compound RS-9 and indomethacin produced significant ($p < 0.001$) reduction in paw licking time. In eddy's hot plate model, the reaction time in test compound (RS-4, 6, 9 and 12) treated groups increased significantly ($p < 0.05-0.001$) in comparison to the control group, except RS-6 at 120 min. In tail immersion test, the reaction time in test compound (RS-9 and RS-12) treated groups increased significantly ($p < 0.05-0.01$) in comparison to the control group.

These test compounds were further evaluated for their anti-inflammatory activity by carrageenan-induced mice paw edema. Further, we measured the levels of tumour necrosis factor (TNF- α), interleukin-1 β (IL-1 β), interleukin-6 (IL-6) and nuclear factor (NF κ B) in the edema paw tissue using real-time quantitative RT-PCR analysis. Among the three tested compounds, **RS-9** was found to diminish the levels of inflammatory mediators like TNF- α , IL-6 and NF κ B but not IL-1 β level suggesting its underlying mechanism of anti-inflammatory action. These results suggested that RS-9 was found to possess promising anti-nociceptive and anti-inflammatory properties. We can conclude that **RS-9** emerged as a novel A_{2B} R antagonist and it may be further developed into a therapeutic agent for treatment or prevention of acute pain and inflammatory diseases.

Table of contents

	Page No
CERTIFICATE	i
ACKNOWLEDGEMENTS	ii-iv
ABSTRACT	v-vi
List of figures	xii-xiv
List of tables	xv
List of Abbreviations and symbols	xvi-xix
CHAPTER 1 - Introduction to Adenosine Receptors as Targets for Therapeutic Intervention	1-18
1.1 Adenosine receptors	1
1.2. Adenosine formation and metabolism	2
1.3. Adenosine receptors and their classification	4
1.3.1. A ₁ adenosine receptors	6
1.3.2. A ₃ adenosine receptor	7
1.3.3. A ₂ adenosine receptor	7
1.3.3.1. Adenosine A _{2A} receptor	8
1.3.3.2. Adenosine A _{2B} receptor	9
1.4. Therapeutic potential for various adenosine receptors	11
1.4.1. Immunomodulatory activity	12
1.4.2. Anti-inflammatory activity	12
1.4.3. Cardiovascular disorders	12
1.4.4. Bacterial sepsis	12
1.4.5. Asthma and glaucoma	13
1.4.6. Bronchial asthma	13
1.4.7. Inflammatory bowel diseases (IBDs)	13
1.4.8. Parkinson's disease	13
1.4.9. Pain	14
1.4.10. Epilepsy	14
1.4.10.1. Modulatory role of adenosine and its receptors in epilepsy	16
1.5. Pain	17
1.6. Zebrafish, a model organism to screen AED'S	18
1.6.1. Use of larval Zebrafish in the toxicity studies	18
CHAPTER 2 - Review of literature	19-37
2.1. Adenosine A _{2A} receptors	19
2.1.1. The Adenosine A _{2A} receptor-mediated signaling pathways	19
2.1.2. Newer potential therapeutic roles of adenosine A _{2A} R agonists and antagonists	21
2.1.3. Possible role of Adenosine A ₁ receptors in epilepsy	22
2.1.4. Possible role of Adenosine A _{2A} receptors in epilepsy	23
2.1.5. Why A _{2A} R receptors are preferable than A ₁ R	24
2.1.6. A _{2A} adenosine receptor antagonists	26

2.2. Adenosine A _{2B} receptors	28
2.2.1. Adenosine A _{2B} receptor antagonists	31
2.2.1.1. Xanthine analogues as antagonists	31
2.2.1.2. 9-Deazaxanthines	33
2.2.1.3 Non-xanthine analogues as antagonists	34
2.2.1.4. Triazolotriazine analogues	36
2.2.2. Pharmacological aspects of selective A _{2B} R antagonists	37
CHAPTER 3 - Objectives and plan of work	38-41
3.1. Objectives	38
3.2. Plan of work	38
CHAPTER 4 - Materials and methods	42-71
4.1. Energy based pharmacophore drug design	42
4.1.1. Computational details	42
4.1.2. Protein target	42
4.1.3. Protein and ligand preparation	42
4.1.4. Glide (XP) docking	43
4.1.5. E-pharmacophore generation	44
4.1.6. Enrichment calculations	44
4.1.7. Preparation of commercial database	45
4.1.8. High-Throughput Virtual Database Screening and Docking Studies	46
4.2. Ligand based drug design	47
4.2.1. Molecular modeling	47
4.2.2. Pharmacophore modeling	48
4.2.3. 3D QSAR model generation	48
4.2.4. PLS analysis and cross validation	49
4.2.5. External validation of the developed 3D QSAR model	50
4.3. Biology	51
4.3.1. Cell culture	51
4.3.2. Selectivity index analysis	52
4.3.2.1. Cytotoxicity studies	52
4.3.2.2. Growth inhibition assay	52
4.3.3. Determination of gene expression analysis of A _{2A} and A _{2B} adenosine receptors (ARs) in two prostate cancer cell lines	52
4.3.3.1. Total RNA isolation and cDNA conversion	52
4.3.3.2. Detection of A _{2A} and A _{2B} (ARs) gene expression	53
4.4. Quantitative estimation of Cyclic AMP in MCF-7 breast cancer cell lines by HPLC assay	54
4.4.1. Materials	54
4.4.2. Sample preparation	54
4.4.3. Mobile phase optimization	55
4.4.4. Preparation of mobile phase	55
4.4.5. Preparation of standard solutions	55
4.4.6. Construction of calibration curve	56

4.4.7. Cyclic AMP-HPLC assay, method development	56
4.5. Pharmacological activity	56
4.5.1. Zebrafish behavioural studies	56
4.5.1.1. Zebrafish-animal husbandry	56
4.5.1.2. Drugs	57
4.5.1.3. Oral drug administration for behavioural assessment in adult zebrafish	58
4.5.1.4. Experimental setup for behavioural monitoring	58
4.5.1.5. Dose response evaluation of Ligand-9	59
4.5.1.6. Drug treatment protocol	59
4.5.1.7. Zebrafish toxicity studies	59
4.5.1.7.1. Drug exposure to zebrafish embryos for toxicity evaluation	60
4.5.1.7.2. Cardiotoxicity assay	60
4.5.1.7.3. Hepatotoxicity assay	61
4.5.1.7.4. Neurotoxicity assay	61
4.5.1.8. Statistical analysis	62
4.5.2. In-vivo anti-epileptic evaluation	62
4.5.2.1. Chemicals	62
4.5.2.2. Experimental animals and treatment	62
4.5.2.3. Toxicity assessment (Neurotoxicity screening)	63
4.5.2.3.1. Rotarod test	63
4.5.2.3.2. Behavioural test using actophotometer	64
4.5.2.4. Anticonvulsant screening methods	64
4.5.2.4.1. Maximal Electroshock induced Seizures (MES): (Mouse model)	65
4.5.2.4.2. Pentylenetetrazole induced seizures (PTZ): (Mouse model)	65
4.5.2.4.3. Strychnine induced seizures (STY): (Rat model)	66
4.5.2.4.4. Picrotoxin induced seizures (PTX): (Rat model)	66
4.5.3. Anti-nociceptive and anti-inflammatory evaluation	66
4.5.3.1. Eddy's hot-plate test in mice	66
4.5.3.2. Tail immersion test in mice	67
4.5.3.3. Acetic acid induced writhing model in mice	67
4.5.3.4. Formalin induced paw licking model in mice	68
4.5.3.5. Carrageenan-induced mice paw edema	68
4.6. Gene expression analyses of inflammatory mediators using RT-PCR studies	69
4.6.1. Total RNA isolation and cDNA conversion	69
4.6.2. Detection of expression levels of inflammatory mediators	70
4.7. HPLC method development for purity analysis of synthesised compounds	70

Chapter 5- Results and discussion:Design, synthesis and pharmacological evaluation of novel A_{2A} antagonists 72-134

5.1. Design, synthesis and pharmacological evaluation of novel A _{2A} antagonists in the treatment of epilepsy	72
5.2. Energy based pharmacophore drug design	73
5.2.1. Protein preparation and active site validation	75
5.2.2. Pharmacophore generation	76
5.2.3. Validation of constructed pharmacophore models	77
5.2.4. Docking analysis of compounds in human A _{2A} receptor	78
5.3. Biology	84
5.3.1. Effect of ethanol on Cyclic AMP	84
5.3.2. Validation of Cyclic AMP Peak	85
5.3.3. Linearity	86
5.4. Zebrafish behavioural and toxicity studies	88
5.4.1. Visual assessment of seizure-like behaviour in response to PTZ and Ligand-9	88
5.4.2. Toxicity evaluation of potent compound (Ligand 9)	94
5.4.2.1. Cardiotoxicity assay	94
5.4.2.2. Hepatotoxicity assay	95
5.4.2.3. Neurotoxicity assay	96
5.5. Estimation of cAMP levels by HPLC-assay (for synthesised compounds)	97
5.6. Experimental section	100
5.6.1. Chemistry	100
5.6.2. General	100
5.6.3.1. General procedure for the synthesis of compounds (2a-d)	102
5.6.3.2. General procedure for the synthesis of compounds (3a-d)	103
5.6.3.3. General procedure for the synthesis of designed analogues (4-27)	105
5.6.4. Structure-Activity Relationship	117
5.6.5. Purity analysis	125
5.7. Pharmacological activity	130
5.8. Summary and conclusion	133
Chapter 6- Results and discussion: Identification of novel A_{2B}R antagonists by using Pharmacophore-Based 3D-QSAR and its anti-nociceptive and anti-inflammatory effects	135-197
6.1. Identification of novel A _{2B} R antagonists by using pharmacophore-based 3D QSAR and its anti-nociceptive and anti-inflammatory effects	135
6.2. Ligand based drug design	135
6.2.1. Determination of pharmacophore and validation	135
6.2.2. 3D QSAR model development and PLS analysis	173
6.2.3. External validation of 3D QSAR model	174
6.2.4. Contour map analyses	175
6.2.5. ADME analysis	180
6.3. Gene expression analysis of A _{2A} and A _{2B} in PC3 and DU145 cell lines	182
6.4. In-vitro cAMP assay	182

6.5. Selectivity index analysis	184
6.6. Pharmacological evaluation	185
6.6.1. Neurotoxicity screening	185
6.6.2. In-vivo anti-nociceptive evaluation	186
6.6.2.1. Acetic acid induced writhing model in mice	186
6.6.2.2. Formalin induced paw licking model in mice	187
6.6.2.3. Eddy's hot-plate test	189
6.6.2.4. Tail immersion test	190
6.7. Effects of test compounds RS-4, RS-9 and RS-12 on carrageenan-induced mice paw edema	191
6.8. Effects of test compounds RS-4, 9 and 12 on TNF- α , IL-1 β , IL-6 and NF κ B levels	193
6.9. Summary and conclusion	196
CHAPTER 7 - Recapitulation and future perspectives	198-202
References	203-224
APPENDIX	225-228
List of publications	225
Papers presented at national/international conferences	226
Biography of Srikanth Racharla	227
Biography of Prof. P. Yogeewari	228

List of figures

Figure No	Description	Page No
Figure 1.1	Chemical structure of adenosine	1
Figure 1.2	Overview of the intra- and extracellular adenosine metabolism	3
Figure 1.3	Adenosine receptor model	4
Figure 1.4	Signal transduction pathways associated with the activation of four human adenosine receptors	8
Figure 1.5	Schematic representation of intracellular pathways coupled to adenosine A _{2B} receptors in various cells	10
Figure 1.6	Alignment of primary amino acid sequences of human A _{2A} and A _{2B} adenosine receptor subtypes in one-letter-code	11
Figure 1.7	Neuromodulatory role of adenosine in epilepsy	17
Figure 2.1	Simplified overview of A _{2A} R induced signal transduction	20
Figure 2.2	Novel disease targets for selective adenosine receptor ligands	21
Figure 2.3	Possible mechanisms operated by adenosine A _{2A} receptors to control spreading of seizure activity and resulting neurodegeneration	24
Figure 2.4	Structures and binding affinities of known hA _{2A} adenosine receptor antagonists	27
Figure 2.5	Model of excessive adenosine signalling in erythrocyte sickling via A _{2B} R	28
Figure 2.6	The chemical structures of some selective antagonists (CVT-6883, CVT-6694 and LAS-101057) for adenosine A _{2B} receptor	31
Figure 2.7	Chemical structures of some nonselective antagonists (theophylline and caffeine) and selective antagonists (MRS-1754, CVT-5440, PSB-1115, MRE-2029F20 and PSB-603) for adenosine A _{2B} receptor	33
Figure 2.8	Chemical structures of selected deazaxanthines as antagonists for adenosine A _{2B} receptor	34
Figure 2.9	Chemical structures of some nonxanthine antagonists for adenosine A _{2B} Receptor	36
Figure 5.1	Workflow for identification of initial hits of Adenosine A _{2A} antagonists by e-pharmacophore modeling and in silico docking.	74
Figure 5.2	The 2.6 Å crystal structure of human A _{2A} receptor (3EML) bound to ZMA241385	75
Figure 5.3	E-Pharmacophore hypothesis	76
Figure 5.4	2D chemical structures of top nine compounds and selective A _{2A} receptor antagonist (SCH-58261)	79
Figure 5.5	Interaction picture of most active compound (Ligand 9)	80
Figure 5.6	Ligand interaction pictures of lead molecules from Ligand 1 to 9 along with crystal structure (3EML).	81
Figure 5.7	RT-PCR of adenosine in MCF-7 cells	84
Figure 5.8	HPLC Chromatogram of standard cAMP at a concentration of 12.5ppm	85

Figure 5.9	Over lay of HPLC Chromatogram of standard cAMP and Ligand 9 along with blank	86
Figure 5.10	Calibration curve of standard cAMP	86
Figure 5.11	Dose-response curve of top active compound (Ligand 9) Vs SCH-58261	87
Figure 5.12	Rotational movements of orally administered Ligand 9 on seizure-like activity induced by intraperitoneal injection of PTZ	89
Figure 5.13	Overall seizure scores for fish treated with various compounds	90
Figure 5.14	Seizure score at every minute time point, representative to neuro-protection to PTZ challenge	91
Figure 5.15	Seizure score at every minute time point, suggesting no neuro-protection to PTZ challenge	91
Figure 5.16	Visual assessment of seizure-like activity in adult zebrafish at different concentrations of Ligand 9	92
Figure 5.17	Overall seizure score for fish treated with Ligand 9	93
Figure 5.18	Heart rates of atria and ventricles of Ligand 9 treatment groups	94
Figure 5.19	Score of atrio-ventricular ratio of Ligand 9 treatment groups	95
Figure 5.20	Representative images of hepatotoxicity assay	95
Figure 5.21	The graph represents qualitative data of % liver size, % liver degeneration & % yolk sac retention of Ligand 9 at different concentrations	96
Figure 5.22	Qualitative data of percentage induction of apoptosis of Ligand-9	96
Figure 5.23	Representative images of embryos treated with compounds and assayed for Apoptosis	97
Figure 5.24	Dose-response curve of most active lead 19 and SCH-58261	98
Figure 5.25	Synthetic protocol used to achieve target compounds	101
Figure 5.26	MASS spectra of compound 19	120
Figure 5.27	Spectral representation ¹ H NMR spectra of most active compound 19	121
Figure 5.28	Spectral representation ¹³ C NMR spectra of most active compound 19	122
Figure 5.29	MASS spectra of compound 6	123
Figure 5.30	Spectral representation ¹ H NMR spectra of most active compound 6	124
Figure 5.31	HPLC chromatogram of most active compound 6	126
Figure 5.32	HPLC chromatogram of most active compound 19	126
Figure 5.33	Ligand interaction pictures of lead molecules from Ligand 4 to 15	127
Figure 5.34	Ligand interaction pictures of lead molecules from Ligand 16 to 27	128
Figure 5.35	Structures of 24 synthetic lead molecules	129
Figure 5.36	Over all workflow of anti-epileptic evaluation of A _{2A} antagonists	133
Figure 6.1	Pharmacophore hypothesis AADRR	137
Figure 6.2	Scatter plot plotted between observed versus predicted activity	174
Figure 6.3	3D QSAR contour map representation for hydrogen bond acceptor property for most active compound C1 and least active compound C257	176
Figure 6.4	3D QSAR contour map representation for hydrogen bond donor property for most active compound C1 and least active compound C257	176
Figure 6.5	3D QSAR contour map representation for hydrophobic property for most active compound C1 and least active compound C257	177

Figure 6.6	Determination of gene expression analysis of A _{2A} and A _{2B} adenosine receptors (ARs) in two prostate cancer cell lines	182
Figure 6.7	Dose-response curves of top active compounds (RS-4, 6, 9, 12 and 15)	183
Figure 6.8.1	Effects of test compounds (RS-4, RS-9 and RS-12) and Indomethacin on carrageenan-induced mice paw edema	192
Figure 6.8.2	Effects of test compound RS-9 (3, 10 and 30 mg/kg) and Indomethacin on carrageenan-induced mice paw edema	193
Figure 6.9	Normalised gene expression levels of pro inflammatory cytokines in carrageenan-induced edema paws with test compounds RS-4, RS-9 and RS-12 and indomethacin (n=3).	195
Figure 6.10	Over all workflow of anti-nociceptive and anti-inflammatory effect of A _{2B} antagonists	197

List of tables

Table No	Description	Page No
Table 1.1	Classification of adenosine/P1 receptors	6
Table 1.2	Distribution and expression of adenosine receptors	7
Table 4.1	Oligonucleotide sequences used for RT-PCR in mice brain samples	70
Table 5.1.	Validation of pharmacophore hypothesis	77
Table 5.2	<i>In silico</i> parameters of Asinex compounds including crystal ligand (3EML).	82
Table 5.3	ADME prediction for designed 9 compounds from Asinex database	83
Table 5.4	Biological data of selected Asinex molecules	88
Table 5.5	Biological data of synthesized molecules	99
Table 5.6	Physical data of 1,3,5 triazine 2,4,6 triamine derivatives	106
Table 5.7	Anticonvulsant activity and minimal motor impairment of 1,3,5 triazine 2,4,6 triamine derivatives	132
Table 6.1	Top five pharmacophore hypothesis generated and given with their scoring parameters	136
Table 6.2	Training set compounds of dataset used in QSAR model development along with observed, predicted activity and fitness over pharmacophore model	138-158
Table 6.3	Test set compounds of dataset used in QSAR model development along with observed, predicted activity and fitness over pharmacophore model	158-172
Table 6.4	Results of external statistical validation for developed 3D QSAR model for hypothesis AADRR	175
Table 6.5	Selected hits based on their predicted activity and fitness to model AADRR	179
Table 6.6	Predicted ADME properties for selected 15 compounds	181
Table 6.7	Biological data of the selected compounds from in house database	184
Table 6.8	Neurotoxic Activity of test Compounds	185
Table 6.9	Effect of test compounds (RS-4, 6, 9 and RS-12) on Acetic acid induced writhing model in mice	187
Table 6.10	Effect of test compounds (RS-4, 6, 9 and RS-12) on Formalin induced paw licking model in mice	188
Table 6.11	Effect of test compounds (RS-4, 6, 9 and RS-12) on Eddy's hot-plate test in mice	189
Table 6.12	Effect of test compounds (RS-4, 6, 9 and RS-12) on Tail immersion test in mice	190

Abbreviations

^{13}C NMR	Carbon Nuclear Magnetic Resonance
^1H NMR	Proton Nuclear Magnetic Resonance
3D-QSAR	Three Dimensional Quantitative Structure Activity Relationships
A	Acceptor atom
A ₁ R	A ₁ receptor
A _{2A} R	A _{2A} receptor
A _{2B} R	A _{2B} receptor
A ₃ R	A ₃ receptor
ADMET	Absorption, Distribution, Metabolism, Elimination and Toxicity
AEDs	Anti-epileptic drugs
AMP	Adenosine Monophosphate
ANOVA	Analysis of Variance
ARs	Adenosine Receptors
ATP	Adenosine Triphosphate
BBB	Blood Brain Barrier
BEDROC	Boltzmann-enhanced discrimination of receiver operating characteristic
cAMP	Adenosine 3', 5'-cyclic monophosphate
CC ₅₀	Cell cytotoxicity 50%
CC ₅₀	Cell cytotoxicity 50%
CDCl ₃	Chloroform deuterated
cDNA	Complementary DNA
CHN	Carbon Hydrogen Nitrogen
CNS	Central Nervous System
D	Donor atom
d	Doublet
DCM	Doublet of Doublet
dd	Dichloromethane
DIPEA	N,N-Di-IsoPropyl Ethyl Amine
DMF	Dimethyl Sulphoxide
DMSO	N,N-Dimethyl formamide
DMSO d ₆	Dimethyl Sulphoxide deuterated
dpf	Day post fertilization
DRC	Dose response curve
EC ₅₀	Effective concentration 50
EF	Enrichment factor
E-pharmacophore	Energetically optimized structure-based pharmacophores
ESI-MS	Electro spray ionization-mass spectroscopy
FBS	Fetal bovine serum
GABA	γ -aminobutyric acid

GAPDH	Glyceraldehyde-3-Phosphate Dehydrogenase
GH	Goodness of hit
GIC ₅₀	Growth Inhibitory concentration 50%
GLIDE	Grid based Ligand Docking and Energetics
GPCRs	G protein-coupled receptors
G-protein	Guanine nucleotide binding protein
GScore	Glide Score
H	Hydrophobic moiety
HEK	Human embryonic kidney cells
hERG	Human Ether-a-go-go-Related Gene
HPLC	High-performance liquid chromatography
HTVS	High throughput virtual screening mode of docking
IC ₅₀	Inhibitory concentration 50%
IL-1 β	Interleukin-1 β
IL-6	Interleukin-6
<i>J</i>	Coupling constant
K _i	Inhibitor constant
LCMS	Liquid Chromatography-Mass Spectrometer
LOO	Leave-one-out
m	Multiplet
M.P	Melting Point
MCF-7	Michigan Cancer Foundation-7
MEM	Minimum Essential Medium
MES	Maximal electroshock seizure test
mg	Milligram
ml	Milliliter
mmol	Millimole
mRNA	Messenger RNA
MTT	((3-(4,5-dimethylthiazol-2-yl)-2,5- diphenyltetrazolium bromide)
NaCl	Sodium chloride
NCCS	National Centre For Cell Science
NF κ B	Nuclear factor kappa B
NIH	National Institutes of Health
NT	Neurotoxicity
Oligo-dT	Short sequence of deoxy-thymine nucleotides
OPLS	Optimized Potentials for Liquid Simulations
PBS	Phosphate-buffered saline
PCR	Polymerase Chain Reaction
PDB	Protein Data Bank
PEG	Polyethylene glycol
PHASE	Pharmacophoric Search Engine
pIC ₅₀	-log IC ₅₀
PLS	Partial least square

ppm	Parts per million
PPW	Protein Preparation Wizard
PRESS	Predictive Residual Error Sum of Squares
QPlogBB	QuickProp predicted Blood Brain partition coefficient
QPlogHERG	QuickProp predicted the human Ether-a-go-go-Related gene
QPlogPo/w	QuickProp Predicted octanol/water partition coefficient
QPPCaco	QuickProp predicted Caco-2 cell permeability
QSAR	Quantitative Structure-Activity Relationship
R	Aromatic ring
r^2	Squared correlation coefficient
r^2_{cv}	Cross validated correlation coefficient
r^2_{pred}	Predictive correlation coefficient
RCSB	Research Collaboratory for Structural Bioinformatics Protein Data Bank
RIE	Robust initial enhancement
RMSD	Root-mean-square deviation
ROC	Receiver operating characteristic
rpm	Rotation per minute
RPMI	Roswell Park Memorial Institute medium
rt	Room temperature
RT	Retention time
RT Enhancer	Reverse transcriptase enhancer
RT-PCR	Real Time Polymerase Chain Reaction
s	Singlet
SAR	Structure-Activity Relationship
scPIC	Subcutaneous picrotoxin
scPTZ	Subcutaneous pentylenetetrazole
scSTY	Subcutaneous strychnine
SEM	Standard error of mean
SI	Selectivity index (CC_{50}/EC_{50})
SNAr	Nucleophilic aromatic substitution
SP	Standard Precision
t	Triplet
TLC	Thin layer chromatography
Tm	Melting temperature
TMS	Tetramethyl silane
TNF- α	Tumor Necrosis Factor A
TRI reagent	TRIZOL reagent
XP	Extra precision
zERG	Zebrafish ether-a-go-go-related gene

List of symbols used

%	Percent
°C	Celsius
cm	Centimeter
g	Gram
h	Hour
m	Meter
mg	Milligram
MHz	Megahertz
mL	Milliliter
mm	Millimeter
m/z	Mass-to-charge ratio
nm	Nanometre
nM	Nanomolar
W	Watt
α	Alpha
β	Beta
δ	Chemical shift, δ scale (in NMR)
λ_{\max}	Wavelength of maximum absorption
μL	Microliter
\AA	Angstrom
μM	Micromole
μm	Micrometer

Introduction to Adenosine Receptors as Targets for Therapeutic Intervention

1.1. Adenosine receptors

Adenosine (**Figure 1.1**) is an endogenous nucleoside composed of adenine attached to a ribose. It is an essential compound of life distributed in several mammalian tissues (Cacciari *et al.*, 2005).

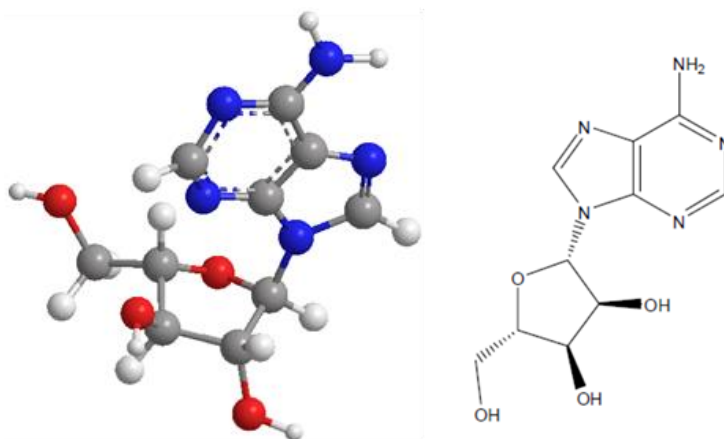


Figure 1.1: Chemical structure of adenosine.

Adenosine may either leave the intracellular space by exocytosis, or generate by the enzymatic breakdown of extracellular ATP (universal energy molecule in animal and plant kingdoms). ATP is released from injured neurons and glial cells by passing the damaged plasma membrane (Tautenhahn *et al.*, 2012). In addition to its role in cellular energy metabolism, adenosine acts in mammalian tissues as a signal molecule to produce a broad spectrum of physiological effects through cell signalling. Most of these responses are mediated by activation of cell surface adenosine receptors which are members of the guanine nucleotide protein (G protein) coupled receptor family.

The adenosine directly affects a variety of synaptic processes, signaling pathways, and plays an important role in regulation of several neurotransmitters in the central nervous system (CNS). Unlike a classical neurotransmitter, adenosine is neither stored in synaptic vesicles nor does it act exclusively on synapses. Its release and uptake are mediated by bidirectional nucleoside transporters whereby the direction of transport solely depends on concentration gradient between cytoplasm and extracellular space. Adenosine is therefore considered a neuromodulator affecting neural activity through multiple mechanisms presynaptically by controlling neurotransmitter release, postsynaptically by hyper or depolarizing neurons, and nonsynaptically mainly via regulatory effects on glial cells (Boison *et al.*, 2012). It exerts its actions through interaction with receptors, and its actions can be blocked by specific antagonists. Its actions are terminated by an efficient reuptake system and a metabolizing system (Cacciari *et al.*, 2005).

Adenosine plays a vital role in various physiological functions. It is involved in synthesis of nucleic acids, when linked to three phosphate groups; and it forms ATP, the integral component of the cellular energy system. It produces various pharmacological effects, both in periphery and in the central nervous system, through an action on specific receptors localized on cell membranes (Matsumoto *et al.*, 2012). The intracellular production of adenosine is increased up to 30 millimolar and more, during hypoxia or ischemia (Linden *et al.*, 1994) and (Hagberg *et al.*, 1987). Adenosine is a metabolite of adenosine triphosphate (ATP), having a very short half-life of 1.5sec due to its rapid metabolism. It accumulates in the area where ATP is utilised but not reformed as observed during ischemia and possibly during sepsis (Jacobson *et al.*, 2006).

1.2. Adenosine formation and metabolism

Adenosine is formed at both intracellular and extracellular sites by two distinct pathways that involve two different substrates, namely, AMP and S-adenosyl homocysteine, and transported across cell membranes by nucleoside transporters (Zhou *et al.*, 2009; Livingston *et al.*, 2004). After intracellular reuptake, adenosine undergoes rapid phosphorylation to AMP by adenosine kinase, or deamination to inosine by adenosine deaminase (**Figure 1.2**). These pathways ensure maintenance of intracellular adenosine concentrations through a strict enzymatic control. So, it is clear that there are essentially three systems that can account for inactivation and/or removal of adenosine in tissue; adenosine deaminase, kinase, and the uptake system (**Figure 1.2**). Strategies to increase local concentrations of adenosine have

included inhibition of enzymes responsible for the metabolic transformation of adenosine. Specifically, inhibitors of adenosine deaminase (ADA) and adenosine kinase (AK) have received considerable attention in an attempt to increase concentrations of endogenous adenosine. Inhibition of adenosine kinase displays neuroprotective potential in areas as pain and inflammation (Matulenko *et al.*, 2007). Under hypoxic conditions, adenosine reaches high concentrations inside the cell through a cascade of enzymatic actions and leads to release of adenosine into extracellular space through nucleoside transporters (Antonioli *et al.*, 2008). The other major pathway that contributes to high extracellular adenosine concentrations during metabolic stress is release and degradation of precursor adenine nucleotides (ATP, ADP and AMP) by a cascade of ectonucleotidases, which include CD39 (nucleoside triphosphate diphosphohydrolase) and CD73 (50-ectonucleotidase). Adenosine accumulation is limited by its catabolism to inosine by adenosine deaminase.

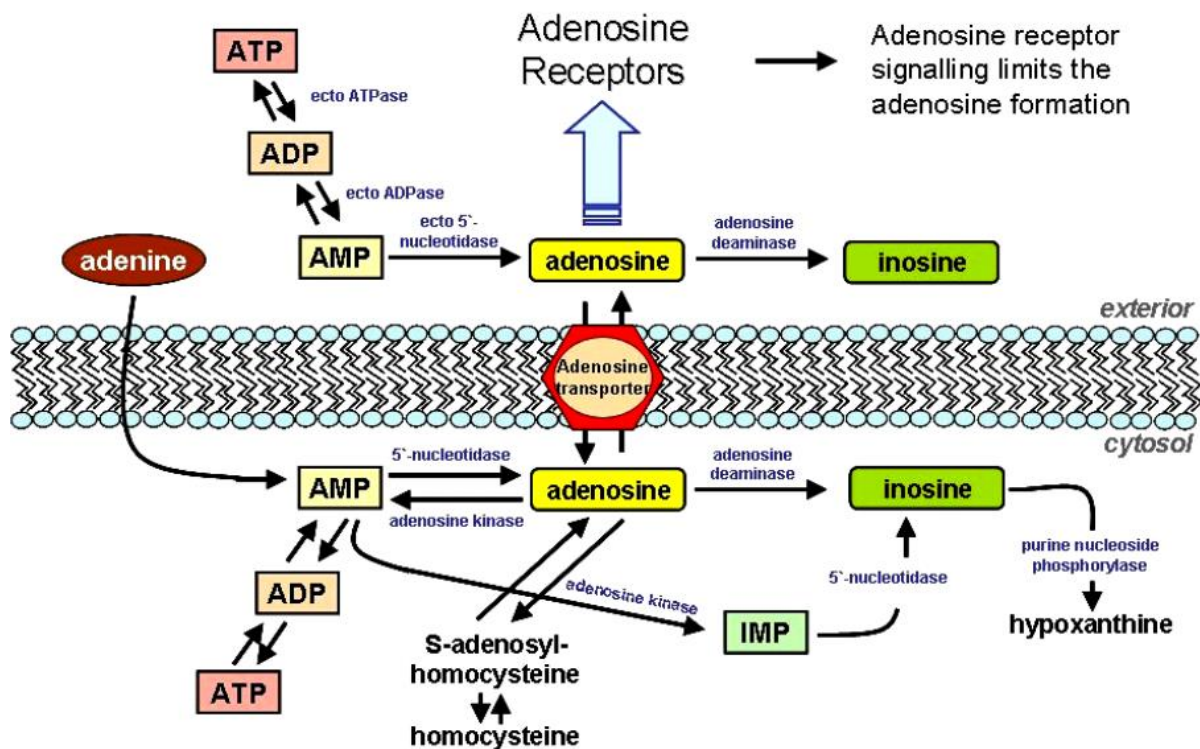


Figure 1.2: Overview of the intra and extracellular adenosine metabolism. Abbreviations: AT(D,M)P, adenosine tri-(di, mono-) phosphate; IMP, inosine monophosphate. (Modified from G. Schulte, Dissertation, 2002).

1.3. Adenosine receptors and their classification

Burnstock *et al.* in 1978, He classified purinoceptors into two subtypes: P1 and P2 receptors, based on their pharmacological properties and molecular cloning (Ralevic and Burnstock, 1991). P1 purinoceptors recognize adenosine as principal natural ligand and P2 receptors have broad natural ligand specificity, recognizing ATP, ADP, UTP, UDP and some dinucleotides. The P1 and P2 receptor families are both further subdivided according to convergent molecular, biochemical, and pharmacological evidences (Matsumoto *et al.*, 2012). Based on the extensive roles of adenosine-receptor subtypes in both physiologic and pathophysiologic events, these receptors are becoming important drug targets in treatment of a variety of diseases because of their key roles in controlling physiological processes.

The adenosine receptors (ARs) are members of the superfamily of GPCRs belonging to the subfamily of rhodopsin-like receptors and thus, show the typical heptahelical structure. The adenosine receptor subtypes in a tissue or isolated cells are characterized by their G protein coupling preference. Similar to other GPCRs, adenosine receptors consist of seven transmembrane helices which accommodate binding site for ligands. **Figure 1.3** represents adenosine receptor model. Each helix is constituted of approximately 21-28 amino acid residues. The transmembrane helices are connected by three extracellular and three cytoplasmic loops of unequal size of amino acid residues. The N-terminal of protein is on extracellular side and C-terminal on cytoplasmic side of the membrane. (Hutchinson and Scammells, 2004).

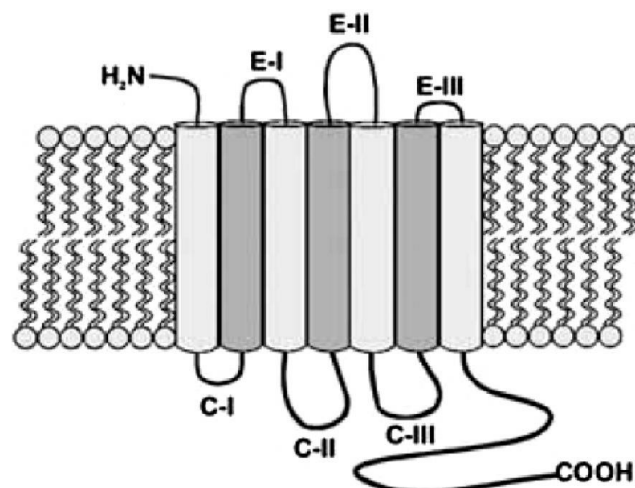


Figure 1.3: Adenosine receptor model (Figure adapted from Hitchinson *et al.*, 2004).

Depending on the Nomenclature of the International Union of Basic and Clinical Pharmacology (NC-IUPHAR) subcommittee, a group of receptors named by their preferred endogenous agonists adenosine was classified into A₁, A_{2A}, A_{2B}, and A₃ (Fredholm *et al.*, 2001). The A₁, A_{2A}, A_{2B} and A₃ subtypes, the subscripts (1, 2A, 2B and 3) represent classification neutral labels. The A₁ and A₃ receptor subtypes, which couple to a G protein (G_i) inhibiting intracellular adenylyl cyclase (AC) lead to a decrease of cAMP; and the A_{2A} and A_{2B} adenosine receptors, which couple to a G protein (G_s) that stimulate AC activity lead to elevate intracellular cAMP concentration (Fredholm *et al.*, 1997) (**Figure 1.4**).

Each of the subtypes has been characterized by molecular cloning, agonist activity profile, antagonist activity profile, G protein-coupling and effector systems. The classification of adenosine receptors was clearly depicted in **Table 1.1**. Experimental evidence has been reported for existence of two different histidine residues at the active site of adenosine receptor, one of which is involved in binding with agonists while the other binds with antagonists of adenosine (Shukla and Mishra, 1995).

The four adenosine receptors have been cloned from several mammalian species, including human. There is extensive sequence similarity between species for A₁, A_{2A} and A_{2B} receptors, whereas A₃ receptors are more variable (Londos *et al.*, 1980). Each adenosine receptor has different but overlapping functions. Each of them is unique in pharmacological profile, tissue distribution and binding partners. Coupling to other second messenger systems, e.g. activation of K⁺ channels (A₁), or phospholipase C (all subtypes) has been described (Fredholm *et al.*, 2001). Generally, A_{2B} receptor requires higher concentration of adenosine than other subtypes to be significantly activated. In particular, all of the adenosine receptor subtypes can also be characterized according to the potency of natural agonist adenosine. In most native systems, the rank order of potency for adenosine is as follows: A₁ ≥ A_{2A} >> A₃ ≈ A_{2B} (Müller *et al.*, 1996), i.e. the A₁ and A_{2A} subtypes are high-affinity receptors activated by adenosine in nanomolar concentrations (A₁ receptors occurs at 0.3–3 nM and A_{2A} receptors at 1–20 nM, concentration of adenosine), while the A_{2B} and A₃ receptors are low-affinity subtypes that require high (more than 1 μM) concentrations for activation. However, in artificial systems with high receptor expression at least A₃ receptor can also be activated by low adenosine concentrations (Muller *et al.*, 2000).

Table 1.1: Classification of adenosine/P1 receptors.

	A1	A2A	A2B	A3
Molecular mass	36.5 kDa	44.7 kDa	36.3 kDa	36.2 kDa
Amino acids	326	412	332	318
G protein coupling	G _i /0	G _s	G _s , G _q	G _i , G _q
Effects	↓ cAMP ↑ IP3 ↑ K ⁺ ↓ Ca ²⁺	↑ cAMP	↑ cAMP ↑ IP3	↓ cAMP ↑ IP3
Selective agonists	CPA, CCPA, CHA, R-PIA	CGS-21680, HE-NECA, APEC, CV1808, DPMA, WRC0470	—	IB-MECA, 2CI-IB- MECA
Selective antagonists	DPCPX, XAC, KW-3902, ENX, KFM19, N 0861, FK 453, WRC 0571	KF 17837, ZM 241385, CSC, SCH 58261	—	I-ABOPX, L 268605, L 249313, MRS-1067, MRS-1097, MRS-1220

AC, adenylate cyclase; PLC, phospholipase C; K⁺, potassium channels; Ca²⁺, calcium channels. ↑ and ↓ denote stimulation or inhibition, respectively. Sequence information is given as SwissProt accession number for human adenosine receptors.

1.3.1. A₁ adenosine receptors

A₁R is the most abundant adenosine receptor and is densely expressed throughout CNS with high abundance in the neocortex, cerebellum, hippocampus and the dorsal horn of spinal cord, and are also found in adipose tissue, heart muscle, and inflammatory cells, such as, neutrophils (**Table 1.2**). A₁ receptors mediate the inhibition of adenylate cyclase. A₁ receptor activation can also inhibit G-protein-coupled activation of voltage dependent Ca²⁺ channels and is reported to induce phospholipase C activation (Yuzlenko and Kononowicz, 2006).

Table 1.2: Distribution and expression of adenosine receptors

Expression level	A ₁ receptors	A _{2A} receptors	A _{2B} receptors	A ₃ receptors
High expression	Brain (cortex, hippocampus, cerebellum), spinal cord, eye, adrenal gland, atria (Poulsen and Quinn, 1998)	Blood platelets, olfactory bulb Spleen, thymus, leukocytes (Fredholm <i>et al.</i> , 2001)	Cecum, colon, bladder (Cacciari <i>et al.</i> , 2005)	Testis (rat), mast cells (rat) (Poulsen and Quinn, 1998)
Intermediate expression	Other brain regions, skeletal muscles, liver, kidney, adipose tissue (Poulsen and Quinn, 1998)	Heart, lung, blood vessels, peripheral nerves (Fredholm <i>et al.</i> , 2001)	Lung, blood vessels, eye, mast cells (Cacciari <i>et al.</i> , 2005)	Cerebellum, hippocampus (Poulsen and Quinn, 1998)
Low expression	Lungs (but probably higher in bronchi), pancreas (Poulsen and Quinn, 1998)	Other brain regions (Fredholm <i>et al.</i> , 2001)	Adipose tissue, adrenal gland, brain, kidney (Cacciari <i>et al.</i> , 2005)	Thyroid, most of brain adrenal gland, spleen, liver, kidney, heart (Poulsen and Quinn, 1998)

1.3.2. A₃ adenosine receptor

The A₃ receptor is distributed widely, being found in the kidney, testis, lung, mast cells, eosinophils, neutrophils, heart and the brain cortex (**Table 1.2**) (Livingston *et al.*, 2004). As with the A₁ receptor, stimulation of the A₃ adenosine receptor leads to inhibition of adenylate cyclase. It has also been shown to stimulate directly phospholipases C and D. A₃ receptor activation also results in the influx of calcium and its release from intracellular stores (Jacobson, 1998). However, A₃ receptor is not present on human lung mast cells. The presence of A₃ receptors in human eosinophils and macrophages suggests other mechanisms for the involvement of A₃ receptors in inflammatory conditions including asthma (Livingston *et al.*, 2004).

1.3.3. A₂ adenosine receptor

In contrast to A₁ receptor, A₂ receptor stimulation leads to activation of adenylate cyclase resulting in the elevation of intracellular cAMP. A₂ receptors are more widely distributed than A₁ receptors, being found in pre and postsynaptic nerve terminals, mast cells, airway smooth muscle and circulating leukocytes (**Table 1.2**). They bind adenosine with less affinity than A₁ receptors. A₂ receptors are subdivided into the A_{2A} and A_{2B} receptors, based on high and low affinity for adenosine, respectively (Livingston *et al.*, 2004).

1.3.3.1. Adenosine A_{2A} receptor

The human A_{2A} adenosine receptor (A_{2A}AR) has been mapped on chromosome 22 and it is composed of 409 amino acids. Its size is larger than other human adenosine receptors (hA₁AR 326 residues, hA_{2B}AR 328 residues, and hA₃AR 318 residues) because of their carboxyl-terminal tail, which is much longer than those of the other AR subtypes.

The A_{2A} adenosine receptor has been found in both periphery and central nervous system (CNS) and it is abundant in basal ganglia, T lymphocytes, vasculature and platelets.

In the peripheral system, A_{2A}AR is mainly coupled with G_s proteins, while in the striatum with G_{olf} proteins. Both the G proteins increase adenylyl cyclase activity and, hence the intracellular concentration of cyclic adenosine monophosphate (cAMP) (Fredholm *et al.*, 2000). The cAMP generation leads to activation of protein kinase A, which can activate various receptors, ion channels, phosphodiesterases and cAMP responsive element binding protein (CREB) that is critical for many neuronal functions (**Figure 1.4**).

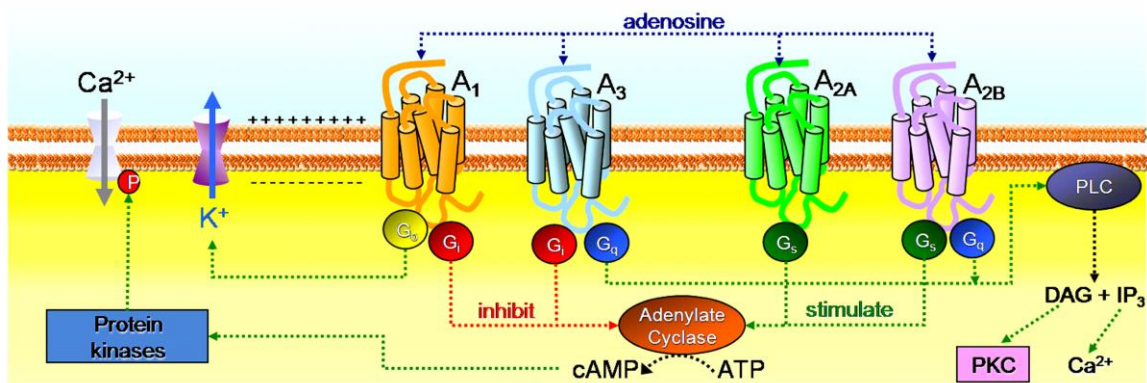


Figure 1.4: Signal transduction pathways associated with activation of four human adenosine receptors. Abbreviations: ATP, adenosine triphosphate; cAMP, cyclic adenosine monophosphate; PKC, protein kinase C; PLC, phospholipase C; DAG, diacylglycerol; IP₃, inositol (1,4,5)- trisphosphate; P, phosphate moiety; G_i, G_s, G_q, G_o, different families of G proteins.

1.3.3.2. Adenosine A_{2B} receptor

A_{2B} receptors are highly expressed in gastrointestinal tract, lung, bladder, and on mast cells (**Table 1.2**). The A_{2B} receptor, although structurally closely related to the A_{2A} receptor and is able to activate adenylate cyclase, is functionally very different. It has been postulated that this subtype may utilize signal transduction systems other than adenylate cyclase because of these functional differences (Livingston *et al.*, 2004). Among all adenosine receptors, A_{2B} adenosine receptor is a low affinity receptor, thought to remain silent under physiological conditions and activated in consequence of increased extracellular adenosine levels (Ryzhov *et al.*, 2008). Among the four subtypes, A_{2B} receptor is functionally active on both human airway smooth muscle cells and lung fibroblast cells, indicating the role of A_{2B} receptors in inflammation and asthma (Fredholm *et al.*, 2001).

A_{2B} receptors are coupled to adenylyl cyclase (AC) in all cells shown in **Figure 1.5**. Activation of this pathway results in accumulation of cAMP and stimulation of protein kinase A (PKA). (A) A_{2B} receptors are coupled to phosphatidylinositol- specific phospholipase C (PI-PLC) via a G protein of the Gq family [G(q)] in mast cells (Auchampach *et al.*, 1996). Activation of this pathway results in increase in diacylglycerol (DAG) and inositol trisphosphate (IP₃). Diacylglycerol stimulates protein kinase C (PKC). Inositol trisphosphate activates mobilization of calcium from intracellular stores. (B) A_{2B} receptors potentiate calcium influx directly by coupling with G_s protein in HEL cells (Feoktistov *et al.*, 1994). (C) In contrast, A_{2B} receptors potentiate calcium influx via cAMP and activation of protein kinase A in pyramidal neurons from the CA3 region of guinea pig hippocampus (Mogul *et al.*, 1993).

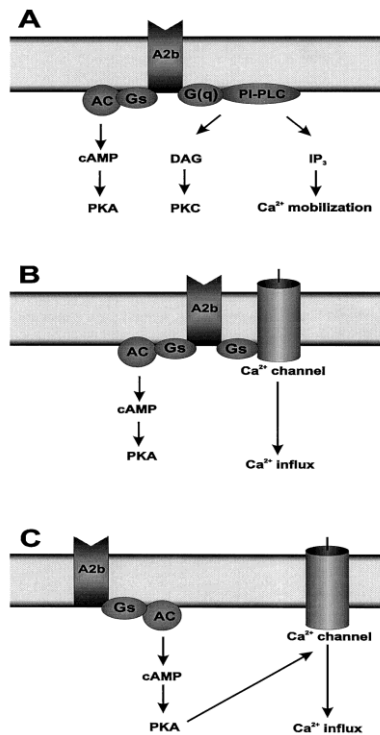


Figure 1.5: Schematic representation of intracellular pathways coupled to adenosine A_{2B} receptors in various cells. (Feoktistov, I and Biaggioni, I 1997).

The adenosine A_{2B} receptor has been generally defined as “low-affinity adenosine receptor,” due to its considerably lower affinity for endogenous ligand, adenosine. Recently, significant advancement has been made in the understanding of molecular pharmacology and physiological relevance of the adenosine receptors in general. However, the knowledge of A_{2B} adenosine receptors fall behind that of other receptor subtypes mainly because of lack of specific agonists for the A_{2B} receptor subtype. As a result, the quantitative tissue distribution of the A_{2B} adenosine receptor is so far unknown. Activation of AC in membranes and accumulation of cAMP in cells are used to characterize the A_{2B} adenosine receptor.

A_{2B} receptor encodes a protein of 328 to 332 amino acid residues depending on the species. As in case of other adenosine receptor subtypes, there are differences in the amino acid sequences of A_{2B} receptor among species. For example, there is approximately 86% amino acid sequence homology between the rat and human A_{2B} receptors (Pierce *et al.*, 1992) and 45% amino acid sequence homology with human A₁ and A_{2A} receptors. For closely related species, e.g. rat and mouse, the A_{2B} receptors share 96% amino acid sequence homology.

The proposed 3D-protein structure of A_{2B} receptors is the typical one of GPCRs, i.e. seven transmembrane domains connected by three extracellular and three intracellular loops, flanked by an extracellular N-terminus and an intracellular C-terminus (Rivkees *et al.*, 1992).

Since the A_{2B} adenosine receptor shares a high similarity with the A_{2A} adenosine receptor in the primary sequences (**Figure 1.6**), extensive knowledge of A_{2A} adenosine receptors will provide a useful guide for the research on A_{2B} adenosine receptor.

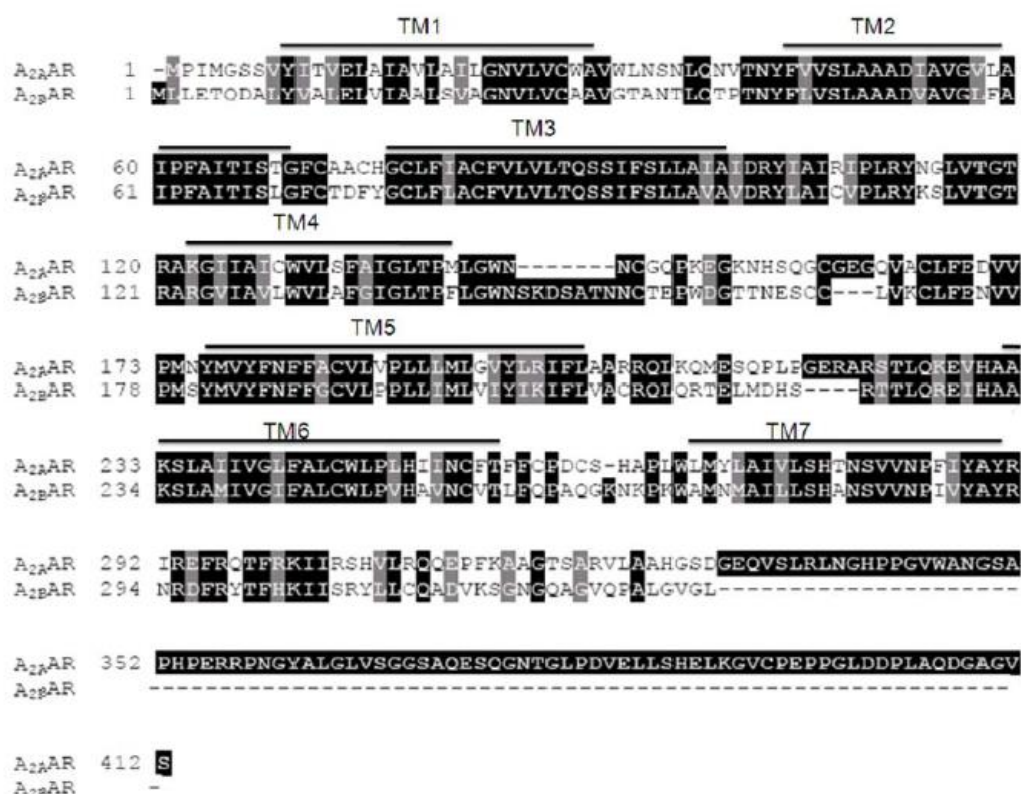


Figure 1.6: Alignment of primary amino acid sequences of human A_{2A} and A_{2B} adenosine receptor subtypes in one-letter-code. Domains presumably spanning the membrane are indicated by bars and labelled accordingly. Black-background indicates identity among amino acid residues, while closely similar amino acid residues are highlighted grey. Dashed lines represent gaps which were introduced to optimize the degree of alignment.

1.4. Therapeutic potential for various adenosine receptors

Adenosine receptors are major targets of caffeine, the most commonly consumed drug in the world. There is growing evidence that they could also be promising therapeutic targets in a wide range of conditions, including cerebral and cardiac ischaemic diseases, sleep disorders, immune and inflammatory disorders and cancer. After more than three decades of medicinal chemistry research, a considerable number of selective agonists and antagonists of adenosine receptors has been discovered, and some have been clinically evaluated, although none has yet received regulatory approval.

1.4.1. Immunomodulatory activity

Protective effects of adenosine receptor stimulation (mainly A_{2A} and A₃) have been observed in models of ischemia reperfusion as well as autoimmune diseases, such as, rheumatoid arthritis, multiple sclerosis, colitis, and hepatitis (Hasko *et al.*, 2007). Ezeamuzie and Khanin 2007 found that the inhibition of TNF- α release by adenosine is mediated by A_{2A} receptors whereas enhancement of PGE₂ release appears to be mediated by A_{2B} receptors.

1.4.2. Anti-inflammatory activity

Adenosine is an important modulator of inflammation and it can show pro-inflammatory as well as anti-inflammatory activities, depending on the conditions, cell type and adenosine concentrations, probably by the activation of various subtypes of adenosine receptors (Akkari *et al.*, 2006; Livingston *et al.*, 2004). A_{2A} agonist CGS 21680 inhibits neutrophil accumulation and protects heart from reperfusion injury (Jordan *et al.*, 1997). The A_{2B} receptor antagonist, CVT-6883 had been used in laboratory studies and also showed inhibition of pulmonary inflammation and injury in adenosine deaminase deficient mice and a mouse model of bleomycin-induced pulmonary fibrosis (Baraldi *et al.*, 2008). It has been proposed that adenosine contributes to the pathogenesis of inflammatory airways disease by acting on the mast cell A_{2B} receptor to enhance release of pro-inflammatory mediators (Livingston *et al.*, 2004).

1.4.3. Cardiovascular disorders

The A₁ receptor is potential therapeutic target for a number of disorders including atrioventricular (AV) node block and supraventricular tachyarrhythmia (adenosine agonist), AV block of cardiac arrest (adenosine antagonist), bradyarrhythmias in transplanted hearts (adenosine antagonists) and diuresis (adenosine antagonists) (Dhalla *et al.*, 2003). In patients with documented paroxysmal supraventricular tachycardias involving the AV node, 99% are successfully terminated with standard doses of adenosine (Strickberger *et al.*, 1997). Ellenbogen *et al.* in 2005 found that tecadenoson is a potent selective A₁ adenosine receptor agonist with a dose-dependent negative dromotropic effect on AV node.

1.4.4. Bacterial sepsis

AR agonists increase mouse survival in endotoxemia and sepsis via A_{2A} AR-mediated mechanisms and reduce the number of live bacteria in blood. In a bacterial sepsis model

(*Escherichia coli*) treatment with an A_{2A} -receptor agonist ATL-146e in combination with antibiotic therapy increased survival from 40% to 100 %.(Sullivan *et al.*, 2004).

1.4.5. Asthma and glaucoma

The potent adenosine A_3 receptor antagonists have been developed for therapeutic treatment of inflammatory diseases, such as, asthma and glaucoma (Jung *et al.*, 2004).

1.4.6. Bronchial asthma

Theophylline, a non-selective adenosine receptor antagonist and bamiphylline, a selective A_1 adenosine receptor antagonist (which does not bind to human A_{2B} and A_3 receptors), improve lung function and symptoms in humans with asthma (Catena *et al.*, 1988; Crescioli *et al.*, 1991).

1.4.7. Inflammatory bowel diseases (IBDs)

The involvement of the adenosine system in anti-inflammatory action has been recognized since early 1990s. In recent years, focus is on the search for drugs that act via a direct stimulation of adenosine receptor subtypes, in particular A_{2A} and A_3 or through an increase in local adenosine concentration and could offer novel therapeutic options for treatment of IBDs.

In a study by Odashima *et al.*, 2005, the potential anti-inflammatory effect of ATL-146e, a selective A_{2A} receptor agonist was investigated on acute and chronic model of colitis evoked by formalin-immune complex in rabbits, as well as in a model of spontaneous ileitis in SAMP1/YitFc mice (Odashima *et al.*, 2005). Adenosine A_3 receptors are also emerging as possible targets for treatment of bowel inflammation (Rybczyk *et al.*, 2007). It has been shown that adenosine A_{2B} receptor is known to induce angiogenesis, to reduce vascular permeabilisation and to increase anti-inflammatory cytokine levels. Thus, adenosine A_{2B} receptor selective agonists are proposed for treatment of septic shock, cystic fibrosis, and cardiac, kidney and pulmonary diseases associated with hyperplasia (Volpini *et al.*, 2003).

1.4.8. Parkinson's disease

Istradefylline (KW-6002) is an adenosine A_{2A} receptor antagonist that is now in phase III clinical trials for PD (Hauser *et al.*, 2005). Specific A_{2A} receptor antagonists consistently reverse motor deficits or enhance dopaminergic treatments in animal models of PD. For

example, in rats with unilateral 6-hydroxydopamine (6-OHDA) lesions of the dopaminergic pathway, A_{2A} receptor antagonists including KF17837, KW-6002 and MSX-3 potentiated the contralateral turning behaviour induced by Levodopa or a dopamine agonist (Koga *et al.*, 2000). Further, the case for developing adenosine A_{2A} receptor antagonists as anti-parkinsonian therapy has been built on a solid foundation of preclinical evidence (Xu *et al.*, 2005).

1.4.9. Pain

Adenosine receptor agonists might just become important in pain management. Intrathecal adenosine is a potential treatment for neuropathic pain (adenosine 0.5 or 2.0mg) which through this route antagonises capsaicin-induced hyperalgesia and allodynia (Eisenach *et al.*, 2003).

1.4.10. Epilepsy

Epilepsy is a neurological disorder, characterized by the recurrent appearance of spontaneous seizures due to neuronal hyperactivity in the brain. A seizure is a symptomatic, behavioural manifestation of abnormal, disordered, spontaneous but synchronized, high frequency firing of neuron populations in the central nervous system (McNamara, 1999). Each year, about 150,000 Americans are diagnosed with the central nervous system disorder that causes seizures. Over a lifetime, one in 26 people will be diagnosed with it. Around 50 million people worldwide have epilepsy. Up to 50,000 Americans die each year from seizures and related causes. Approximately 1.8 million people were affected by therapy-resistant epilepsy.

Epileptic seizures are generally classified into focal (partial) and generalized. The clinical manifestation of focal seizures varies depending upon the origin of epileptic discharges (the epileptic focus) and includes motor, sensory, autonomic and psychic symptoms. Seizures are defined as simple partial if there is no loss of consciousness, but complex partial if there is loss of consciousness. When the seizure discharge becomes sufficiently widespread (or generalized) and includes a strong participation of motor system circuitry, the result is a convulsive response that typically includes both tonic (sustained contractions) and clonic (oscillating contractions and relaxations) components. Absence seizures are primary generalized seizures that do not include strong motor system recruitment. Such seizures appear to be nearly immediately generalized. Even focal seizures, however, can become generalized (secondary generalized seizures).

According to the causal aetiology, epilepsy is also classified into idiopathic and symptomatic or acquired. Almost 50% of epilepsy cases that occur in the absence of other brain abnormalities are called idiopathic epilepsy, including absence seizures and they are age-dependent and benign. They are thought to have a genetic predisposition, in which several candidate genes have recently been identified, mainly at ion channel loci (Hirose *et al.*, 2000).

It has long been proposed that increased seizure susceptibility may be caused by an abnormality in the transmitter systems of the brain, such as, impaired inhibitory transmission (through GABA), excessive excitatory transmission (through glutamate) or an imbalance between neuronal excitatory and inhibitory systems (Meldrum *et al.*, 1999; Coulter, 2001). This transformation of healthy CNS tissue with a functional balance between excitation and inhibition to brain tissue having a hyper excitable neuronal population of neurons is called epileptogenesis (McNamara, 1999), i.e. the process that leads to epilepsy and spontaneous seizures is thought to be triggered by an initial acute brain injury, e.g. status epilepticus, followed by progressive neuronal cell loss, mossy fibre sprouting and formation of an astrogliotic scar (Pitkanen *et al.*, 2002).

Until the early 1990s there were six major compounds used for treatment of epilepsy: carbamazepine, ethosuximide, phenobarbital, phenytoin, primidone and valproic acid. Thus, the initial group of anti-epileptic drugs was barbiturates, which bolster the inhibitory GABAergic system. They are effective in controlling seizures, but they cause sedation. In general, for partial epilepsies carbamazepine is recommended initially; whereas for generalized epilepsies, first line choice is usually valproate (French *et al.*, 2004a, b). Since 1991, new drugs have been developed and marketed to reduce the number of patients with drug-resistant epilepsy: namely lamotrigine, gabapentin, topiramate, tiagabine, levetiracetam, oxcarbazepine and vigabatrin (Berkovic, 2005). All are effective for partial epilepsies and some of them are also for generalized epilepsies. However, none of them has been shown to be more efficient than the older drugs, at least in the new onset of patients. Most of the older drugs as well as most of the newly developed drugs exert numerous adverse effects and toxicities, such as, anaemia, cognitive impairment, anorexia, depression, somnolence, birth defects, rash, and visual field effects, etc. (Beghi, 2004 and Begley *et al.*, 1994). The newer drugs have the advantages of lower risk of side effects, less drug interactions and less enzyme induction (Berkovic, 2005).

1.4.10.1. Modulatory role of adenosine and its receptors in epilepsy:

It is presently unclear why some brain injuries evolve into epilepsy while others do not. Therefore, identification of diagnostic markers to predict epileptogenesis is of utmost importance. Identification of astrogliosis as a hallmark in brain of epileptics, and identification of astrocytes as important modulators of neuronal activity imply that dysfunction of astrocytes might play a key role in the pathogenesis of epilepsy (Tian *et al.*, 2005). These inhibitory actions of adenosine can be used therapeutically to suppress seizures and are considered important for maintaining postictal depression and restoring metabolic equilibrium following seizures (Huber *et al.*, 2001; Etherington *et al.*, 2004; Dunwiddie *et al.*, 1999).

However, despite more than 20 years of research on the role of adenosine in experimentally induced seizures and identification of adenosine as endogenous anticonvulsant of brain (Dragunow *et al.*, 1985), the pathogenic role of the adenosine system in epileptogenesis remains understudied. Alterations in the adenosinergic system (adenosine and its receptors) have been referred by many previous studies indicating that deficiencies or modifications in the function of this purinergic system may contribute to epileptogenesis. Due to this emerging implication of adenosine in managing seizures, a new field of adenosine-based therapies has been introduced including adenosine itself, adenosine receptor agonists and antagonists, and adenosine kinase inhibitors. The method with the least side effects (heart rate, blood pressure, temperature or even sedation) is being questioned including intracerebral implantation of adenosine releasing cells or devices.

As mentioned above, adenosine acts as an important neuromodulator with mostly inhibitory effects on neuronal activity in CNS. In healthy brain, development and spread of seizures are thought to be prevented by a tonic anticonvulsant effect mediated by endogenous adenosine, which is kept in the range of 25–250 nM (Dunwiddie and Masino, 2001) (**Figure1.7**).

However, during situations of metabolic stress, such as epileptic seizures or during periods of oxygen stress, extracellular adenosine concentrations rise rapidly to micromolar levels, that are able to activate all types of adenosine receptors (Berman *et al.*, 2000). Microdialysis probes implanted in the hippocampi of patients with intractable complex partial epilepsy revealed 6- to 31-fold increases of extracellular adenosine during seizure activity (During and

Spencer, 1992). This seizure-induced rise in adenosine was considered to be sufficient to terminate ongoing seizure activity.

Several studies have also reported changes in density of adenosine receptors in various epileptic models of rodents as well as in human epileptic tissues. These changes are not uniform but seem to be different depending on the duration of treatment as well as the epileptogenic drug used.

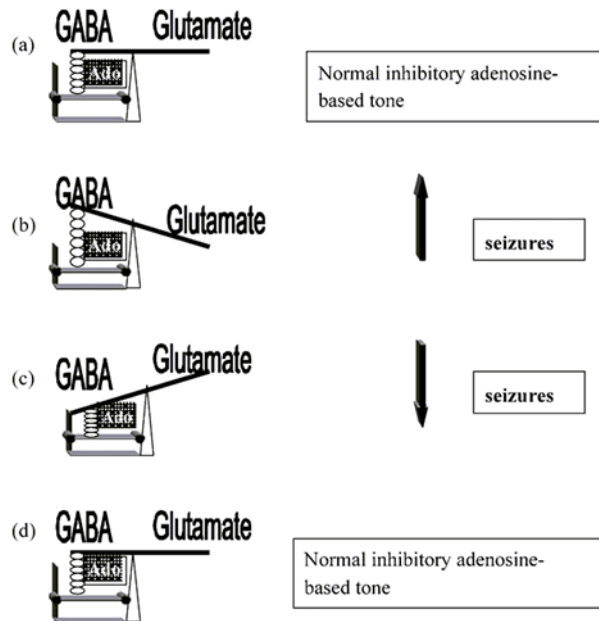


Figure1.7: Neuromodulatory role of adenosine in epilepsy under normal conditions: (a) adenosine (tension spring in this model) is fine-tuning the actions of GABA (inhibition) and glutamate (excitation) in order to achieve normal nerve cellmembrane firing. Abnormalities such as excessive excitatory transmission (b) may lead to membrane depolarization and hence seizure activity. Sustained adenosine release (increased tension on the string) as shown in (c) may lead to increase of inhibitory neurotransmitter release, thus contributing to seizure suppression and finally return to normal balanced condition (d).(Pagonopoulou *et al.*, 2006).

1.5. Pain

Pain is an ill-defined, complex unpleasant phenomenon, usually evoked by an internal or external noxious stimulus (nociception). An analgesic is the drug which relieves pain by acting on peripheral or on central pain mechanisms, without significantly altering consciousness. However, the origin of inflammatory pain is partly from the tension of

damaged tissues due to swelling, but pain sensing nerve terminals are directly excited by inflammatory mediators.

1.6. Zebrafish, a model organism to screen AED'S

Zebrafish (*Danio rerio*) is fresh water vertebrate, used as a valuable, versatile model organism to study the basis of epilepsy and for evaluation of new AED (Kari *et al.*, 2007) and it is an attractive preliminary *in-vivo* model for screening compounds with potential, hERG blockade & QT prolongation. Now-a-days, it serves as an important tool in pharmaceutical research, due to its small size, inexpensive, rapid organogenesis, high fecundity, transparent embryos and high degree of conservation with human genome (approximately 75%) (Chakraborty *et al.*, 2009). Here we have used adult zebrafish as an effective model for investigating several CNS disorders including epilepsy rather than larval zebrafish. Limitations of larval zebrafish include incompletely developed brain, and the BBB (starts functioning after 10 dpf, whereas adult zebrafish has fully developed brain regions and blood brain barrier (BBB) and it is very difficult to detect seizures in larval form because of its small size. BBB of adult zebrafish is similar to that of higher vertebrates, so that this model serves as an attractive organism for discovery of novel AED (Berghmans *et al.*, 2007).

1.6.1. Use of larval Zebrafish in the toxicity studies

Larval zebrafish assays have been utilized in pharmaceutical industry in several different aspects of drug discovery namely target validation, toxicology and safety (Fleming *et al.*, 2013). Use of larval zebrafish in toxicities like Hepatotoxicity, Cardiac function, was reported earlier by several pharmaceutical companies during 2006-February 2012. Similar to other mammals, zebrafish larvae have the ability to perform both phase I and phase II metabolism reactions (Alderton *et al.*, 2010). Traditionally larval zebrafish have been used to demonstrate human disease, and serve as an excellent model for evaluating toxicity studies because of their small size and suitability to conduct experiments in multi well plates.

Review of Literature

2.1. Adenosine A_{2A} receptors

2.1.1. The Adenosine A_{2A} receptor-mediated signaling pathways

As already mentioned, A_{2A} receptor is coupled to stimulatory G proteins. Thus, the activation of receptors leads to stimulation of adenylate cyclase activity, resulting in increased cyclic AMP (cAMP) accumulation in cells. But there are also other types of known G proteins which interact tissue-specific with the A_{2A} receptor, for example, the G_{olf} (70% homologous to G_s) in striatum. It was already shown that the elements of third intracellular loop, and not the carboxyl terminal tail, are responsible for G_s interaction (Tucker *et al.*, 2000). Moreover, A_{2A} receptor interacts most preferably with G proteins containing β4 subunits (McIntire *et al.*, 2001). There is evidence that A_{2A}R can occur as receptor homodimer as well as heterodimers with other receptors, such as, dopamine D2 receptor (Fredholm *et al.*, 2007).

The effects of A_{2A} receptor activation on enzymes and ion channels can be predicted due to the present knowledge of G protein signaling, including mobilisation of calcium among others. There is also evidence that A_{2A} receptors increase mitogen-activated protein kinases (MAPK) activity; more precisely they initiate phosphorylation of the ERK1/2 (Schulte and Fredholm, 2000). In CHO cells, ERK phosphorylation occurs via G_s - cAMP - protein kinase A (PKA) - Src kinase - MAPK/ERK kinase 1 (MEK1) - pathway (Klinger *et al.*, 2002). Small G proteins of the Ras family and protooncogene serine/threonine-protein kinases Raf-1 and B-Raf are involved in this pathway as well (Neves *et al.*, 2002). This signaling is cell type-specific and might vary in other cells. However, A_{2A} receptor activation can also inhibit phosphorylation of ERK1/2, for example, in nerve growth factor-induced manner (Arslan *et al.*, 2000). Moreover, recent studies have shown that there are many proteins interacting with cytoplasmic tail of the activated A_{2A}R resulting in G-protein-independent signaling pathways (Fredholm *et al.*, 2007).

A_{2A} receptors coupled to G_s proteins are believed to desensitize very quickly. Various mechanisms were shown to be involved, including phosphorylation of threonine at position 298 via receptor kinases as well as phosphorylation by PKA. The involvement GRK2 is still controversial as it usually phosphorylates in alkaline micro milieu which is not the case of acidic area around Thr298 (Palmer *et al.*, 1997). **Figure 2.1** illustrates a simplified overview of the $A_{2A}R$ -mediated signal transduction regarding to G protein-dependent signaling.

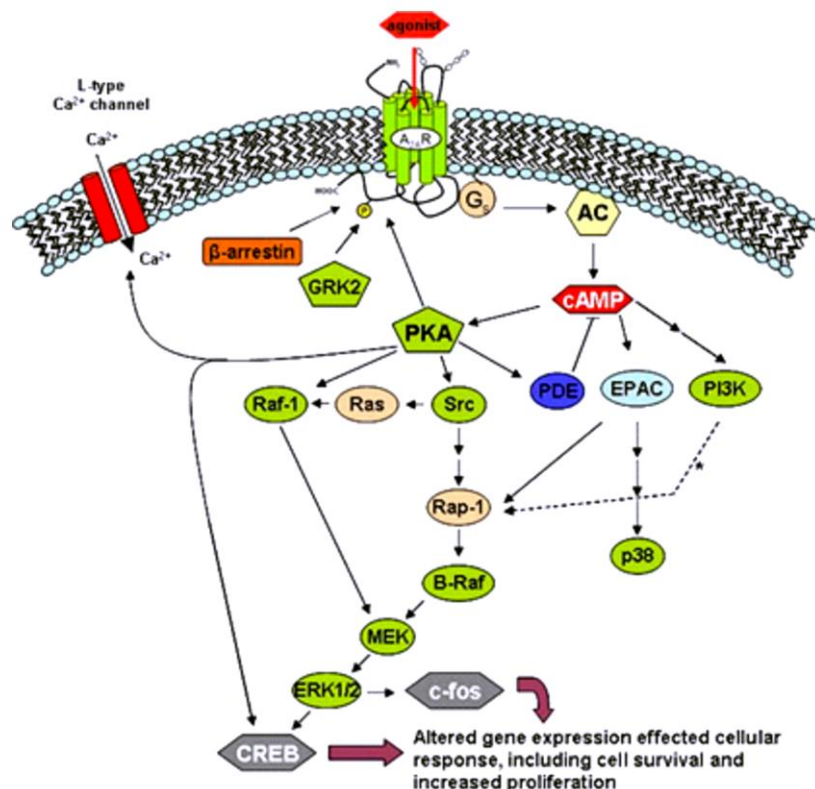


Figure 2.1: Simplified overview of $A_{2A}R$ induced signal transduction. Activation of G_s coupled receptor results in activation of several transcription factors via ERK1/2 activation, including CREB and *c-fos* (modified from Neves *et al.*, 2002; Fredholm *et al.*, 2007). Abbreviations : $A_{2A}R$, adenosine A_{2A} receptor; AC, adenylyl cyclase; B-Raf, B-Raf proto-oncogene serine/threonine-protein kinase; cAMP, cyclic adenosine monophosphate; CREB, cAMP response element binding protein; EPAC, exchange factor protein activated by cAMP; ERK1/2, extracellular signal-regulated kinase; G_s , stimulatory G protein; GRK2, G protein-coupled receptor kinase; MEK, MAPK/ERK kinase; p38, p38 mitogen-activated protein kinase; PDE, phosphodiesterase; PI3K, phosphatidylinositol 3-kinase; PKA, cAMPdependent kinase; Raf-1, RAF proto-oncogene serine/threonine-protein kinase; Rap-1 proto-oncogene small G protein of the Ras family; Ras, proto-oncogene small G protein; Src, tyrosine-protein kinase Src.

2.1.2. Newer potential therapeutic roles of adenosine A_{2A}R agonists and antagonists

The development of selective and potent synthetic agonists and antagonists of adenosine receptors has been the subject of medical chemistry research for more than thirty years (Jacobson and Gao, 2006).

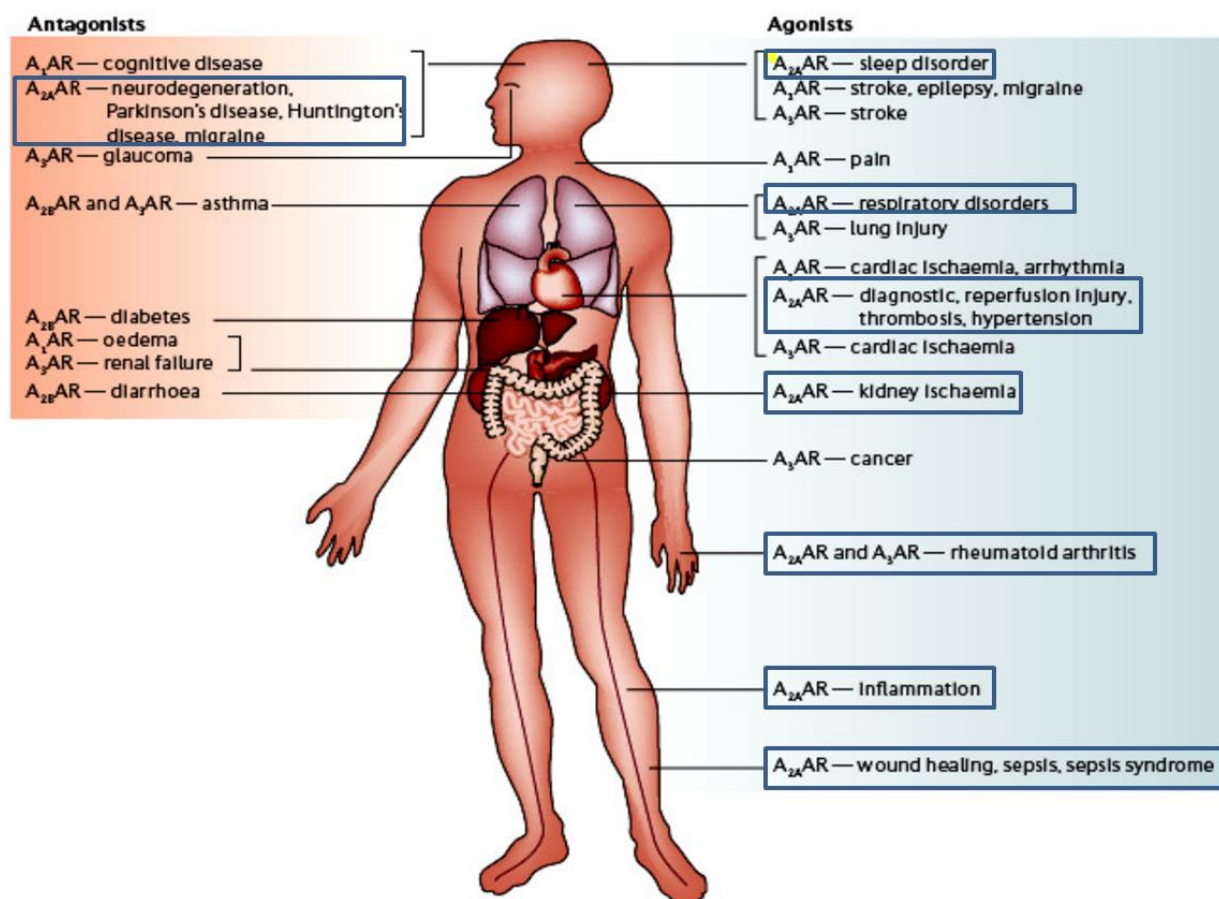


Figure 2.2: Novel disease targets for selective adenosine receptor ligands. Among many different approaches of adenosine receptors, treatment of arrhythmias, ischemia of heart and brain, pain, neurodegenerative diseases, sleep disorders, inflammation, diabetes, renal failure, cancer and glaucoma, and in cardiovascular imaging are the most promising areas. Therapies involving A_{2A} receptor agonism or antagonism are deposited in the boxes (modified from Jacobson and Gao, 2006)

A summary of novel targets for selective adenosine receptor ligands is given in **Figure 2.2**. On the one hand, selective agonists are well advanced in clinical trials for treatment of atrial fibrillation, pain, neuropathy, pulmonary and other inflammatory conditions, as well as cancer, and on the other hand, antagonism is useful in the treatment of Parkinson's disease and congestive heart failure for which selective antagonist is already in clinical trials (Jacobson and Gao, 2006). As previously described A_{2A} receptor activation is involved in

vasodilation in aorta and coronary arteries, thereby, hypotensive effect is gained from peripheral A_{2A}Rs which inhibit platelets aggregation. Three potential A_{2A}R selective agonists, referred to as Regadenoson, ATL-146e, and Binodenoson, have currently entered the third phase of clinical trials (Jacobson and Gao, 2006). Furthermore, the blockade of A_{2A}R has a clear antidepressant effect (Ledent *et al.*, 1997).

In addition, A_{2A}R activation was found to promote myelination in Schwann cells, suggesting opportunity of selective agonist use in treatment of demyelinating diseases, such as, multiple sclerosis (Stevens *et al.*, 2002). A high-affinity A_{2A}R agonist, called CGS21680, provokes a wide spectrum of anti-inflammatory activities in an allergic asthma animal model. This suggests potential use of agonists as alternatives to glucocorticosteroids in treatment of asthma (Fozard *et al.*, 2002). The previously mentioned A_{2A}R agonist ATL-146e could also be applied in treatment of sepsis (Sullivan *et al.*, 2004) as well as inflammatory bowel disease (Odashima *et al.*, 2005).

Neurons that express A_{2A}AR also express dopamine D2 receptors, and one of the roles of dopamine is to suppress the A_{2A}AR signaling. This interaction has interesting implication on the treatment of pathologies related to an abnormal function of dopamine neurons, such as schizophrenia and Parkinson's disease. In CNS, A_{2A}AR antagonists play a role in neuroprotection and are implicated in several pathologies such as Parkinson's disease, Huntington's disease, and Alzheimer's disease.

2.1.3. Possible role of Adenosine A₁ receptors in epilepsy

Adenosine has long been considered an endogenous anti-epileptic compound. Since the activation of A₁R seems the most evident effect of adenosine and it selectively decreases excitatory rather than inhibitory transmission, inhibits calcium influx through voltage sensitive calcium channels and also inhibits NMDA responses, adenosine acting through A₁R has long been considered an endogenous neuroprotective system. The ability of A₁R to hyperpolarise principal neurons further suggests that adenosine acting through A₁R should be a major anti-epileptic system (Dunwiddie *et al.*, 1999).

There are robust evidences showing that A₁R are still able to efficiently control chronic epileptic-like conditions. Thus, it seems evident that in a naïve system, A₁R effectively constitute a hurdle curtailing seizure activity. This is confirmed by the ability of A₁R to control the spreading of seizure activity and the greater susceptibility of A₁R knockout mice

to epilepsy (Fedele *et al.*, 2006). Caffeine is a non-selective antagonist of A₁R and A_{2A}R (and likely of other adenosine receptors) and its established mechanism of action at non-toxic doses is the antagonism of these receptors. The long term consumption of moderate doses of caffeine (0.3 g/L) was found to prevent neuronal damage in different models of epilepsy (Rigoulot *et al.*, 2003). A₁R still emerge as the most efficacious purinergic modulation system to control seizure activity. However, it is becoming increasingly clear that anti-epileptic role of A₁R is probably operated through non-synaptic mechanisms.

2.1.4. Possible role of Adenosine A_{2A} receptors in epilepsy

The major interest of the adenosine neuromodulation system has been the inhibitory A₁R system, an increasingly number of studies are now focusing on facilitatory A_{2A}R. However, recent elegant studies make it evident that the blockade of A_{2A}R, either using genetic deletion of A_{2A}R or selective A_{2A}R antagonists or non-selective antagonists such as chronic caffeine administration (El Yacoubi *et al.*, 2008) can afford robust protection against the seizure evolving severity. Furthermore, chronic caffeine administration or A_{2A}R blockade effectively prevent neuronal damage following convulsions (Rigoulot *et al.*, 2003).

The blockade of adenosine A_{2A} receptors (A_{2A}R), in animal models of epilepsy, can attenuate seizure activity and prevent seizure-induced neurodegeneration. A_{2A}R are also located in astrocytes and microglia cells, where they control uptake and clearance of glutamate (Nishizaki *et al.*, 2002). Thus, given that A_{2A}R are densely located in glutamatergic synapses where they control the release of glutamate (Rodrigues *et al.*, 2005) and the activation of NMDA receptors (Azdad *et al.*, 2009). Thus, A_{2A}R seem to control the evolution and consequences of seizures, both seizures-beget-seizure and seizure-induced neurodegeneration.

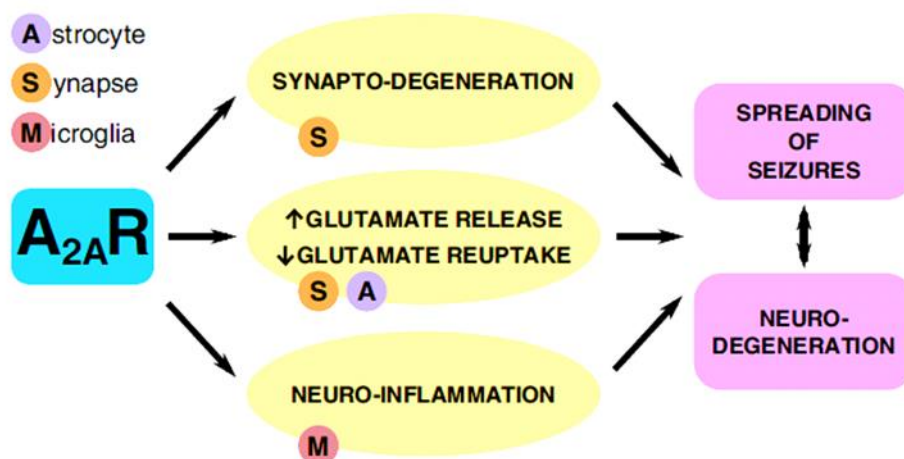


Figure 2.3: Possible mechanisms operated by adenosine A_{2A} receptors to control spreading of seizure activity and resulting neurodegeneration. (Tome *et al.*, 2010).

Adenosine A_{2A} receptors are mostly located in synapses, namely in excitatory synapses of limbic cortex. A_{2A} receptors play a key role in controlling one of the early features found to depress the functioning of limbic circuits in different neurodegenerative diseases. A_{2A} receptors have also been found to control release of glutamate, the activity of glutamate transporters and activation of NMDA receptors (**Figure 2.3**). These may be potential mechanisms explaining the ability of A_{2A} receptors to control synaptic degeneration or may constitute a parallel mechanism by which A_{2A} receptors control excessive glutamatergic transmission involved both in spreading seizures as well as on associated neurodegeneration.

The accumulating evidence is that A_{2A}R are up-regulated in animal models of epilepsy, blockade of A_{2A}R prevents seizure activity, and the resulting neurodegeneration prompts a novel key concept. Adenosine can no longer be considered an anti-epileptic agent, since it can also contribute to worsen this condition through A_{2A}R-mediated actions.

2.1.5. Why A_{2A}R receptors are preferable to A₁R?

Adenosine A₁R agonists have been traditionally reported as anti-epileptic drugs. However, the therapeutic application of A₁R agonists has several limitations that hamper its usefulness as novel neuroprotective drugs. The first major drawback of A₁R agonists is cardiovascular side effects (Shryock *et al.*, 1997); the second limitation of A₁R agonists is their poor brain permeability (Schaddelee *et al.*, 2004); the third limitation is related to the short window of opportunity of A₁R agonists, which is limited to a few hours, (Sweeney *et al.*, 1997), and

finally, the last major limitation of A₁R agonists as neuroprotective drugs is that the effect of A₁R activation desensitizes in chronic stressful brain conditions. In conclusion, the use of A₁R agonists as neuroprotective drug is limited to acute noxious brain conditions, i.e., to control the onset or enhance the threshold of neuronal damage.

A_{2A}R are widespread throughout the brain; and upon chronic epilepsy there is a robust increase (over 200%) of the density of A_{2A}R (Rebola *et al.*, 2005). A_{2A}R are also located in astrocytes and microglia cells where they control the uptake of glutamate (Nishizaki *et al.*, 2002), given that A_{2A}R are densely located in glutamatergic synapses where they control the release of glutamate and the activation of NMDA receptors. Previous studies have demonstrated that, A_{2A}R are up-regulated in various animal models of epilepsy and their blockade can attenuate seizure activity which leads to the prevention of seizure-induced neurodegeneration, and provides a novel concept for the discovery of potential anti-epileptic drug candidates.

From the earlier reports it was found that A_{2A} receptor antagonism reduced I_{GABA} run down (Sebastiao *et al.*, 2010; Roseti *et al.*, 2008). A_{2A}R activation decreased NKA activity selectively in astrocytes to inhibit glutamate uptake (Matos *et al.*, 2013). Further, A_{2A} and A₃ antagonists were found to alter the GABA_A desensitization (Roseti *et al.*, 2009), suggesting a possible association between ARs and GABA_Aergic system. The role of adenosine A_{2A} receptors (A_{2A}AR) seems globally less explored than that of A₁R for epileptic therapy. Till date, research reports very few A_{2A} antagonists (ZM241385) having antiepileptic activity (Li *et al.*, 2012). In a majority of cells and models tested, A_{2A} receptor antagonism reduced I_{GABA} rundown, suggesting that A_{2A} receptor activation by endogenous adenosine exacerbates GABA_A receptor desensitisation. This could be expected since receptor desensitisation often occurs through phosphorylation (frequently mediated by cAMP and PKA, the well-known transduction pathways of A_{2A} receptors) (Sebastiao *et al.*, 2010).

The interest on targeting adenosine A_{2A} receptors in the treatment of epilepsy first arose based on the control of glutamate release which might be the reason for its neuroprotective effects in cerebral cortex, hippocampus and striatum. Hence, research has been focused on A_{2A} antagonists as an important target in the treatment of epilepsy, because their neuroprotective doses are considerably lower than those producing peripheral cardiovascular side effects (Monopoli *et al.*, 1998) as well as their acceptable pharmacokinetic profile. Consequently, selective and potent antagonists at the adenosine A_{2A} receptor subtype are

needed for therapeutic intervention and could be useful for treatment of several diseases like epilepsy.

2.1.6. A_{2A} adenosine receptor antagonists

Relevant potential therapeutic indications of A_{2A}AR antagonists are neurodegenerative diseases, such as Parkinson's and Alzheimer's, restless legs syndrome, depression and addiction (Muller *et al.*, 2011). Several selective A_{2A}AR antagonists have been evaluated in clinical trials for treatment of Parkinson's disease. In **Figure 2.4** some representative A_{2A}AR antagonists, with their binding affinities, are reported.

The first A_{2A}-selective antagonists were developed modifying xanthine nucleus at the 8-position with alkenes (notably styryl groups) and the 8-styrylxanthine istradefylline (1, KW6002) was one of the first A_{2A}AR antagonists reported.

Substitution of xanthine core with various heterocyclic ring systems has led to some compounds with very high affinity and selectivity toward the A_{2A} subtype. The triazoloquinazoline CGS15943 (2) was one of the early examples of a heterocyclic structure showing A_{2A}AR antagonist activity but with only slight selectivity. Subsequent refinement of triazoloquinazoline core by the addition of a third ring or alteration of pattern of N inclusion in the heterocyclic system greatly improved the A_{2A}AR selectivity.

Examples of highly potent A_{2A}AR antagonists of later generation are the triazolotriazine ZM241385 (3), the triazolopyrimidine vipadenant (4), and the pyrazolotriazolopyrimidine SCH442416 (5). Another pyrazolotriazolopyrimidine compound with a very good affinity and selectivity profile at the hA_{2A}AR is preladenant (6) that is undergoing clinical trials for treatment of Parkinson's disease.

Examples of further non-xanthine A_{2A}AR antagonists, which are being clinically evaluated, are adenine derivative ST-1535 (7) and benzothiazole derivative SYN-115 (8).

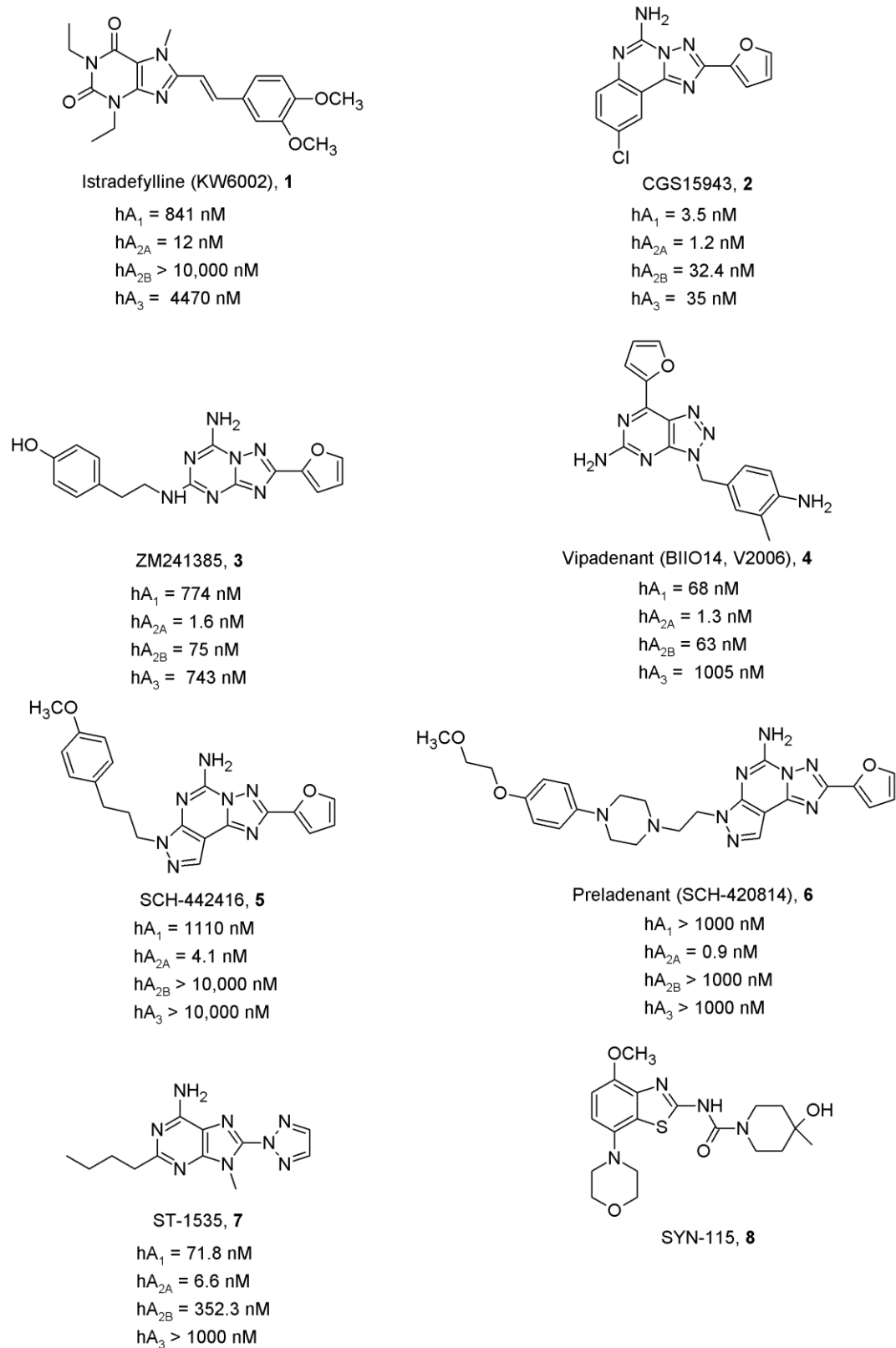


Figure 2.4: Structures and binding affinities of known hA_{2A} adenosine receptor antagonists.

2.2. Adenosine A_{2B} receptors

A_{2B} receptor plays a central role in tissue adaptation to hypoxia and has a protective role in hypoxia-induced tissue inflammation (Koeppen *et al.*, 2011). Van der Hoeven *et al.* (2011) indicated that A_{2B} receptor suppresses oxidase activity and inhibits superoxide production in murine neutrophils regulating the proinflammatory action of neutrophils.

In hypoxic conditions, increased adenosine-mediated activation leads to production of 2, 3-DPG which decreases binding of hemoglobin (HbS) to O₂, resulting in increased amount of deoxy-HbS, sickling and hemolysis. Erythrocyte hemolysis further promotes tissue damage and more ATP is released in the damage response from these tissues. ATP is converted to adenosine by action of CD39/CD73 enzymes and function as a positive feedback of adenosine stimulated erythrocyte sickling. Treatment with polyethylene glycol-modified adenosine deaminase (PEG-ADA) or application of A_{2B} antagonist could reduce production of erythrocyte 2, 3-DPG and sickling (**Figure 2.5**) (Zhang *et al.*, 2011).

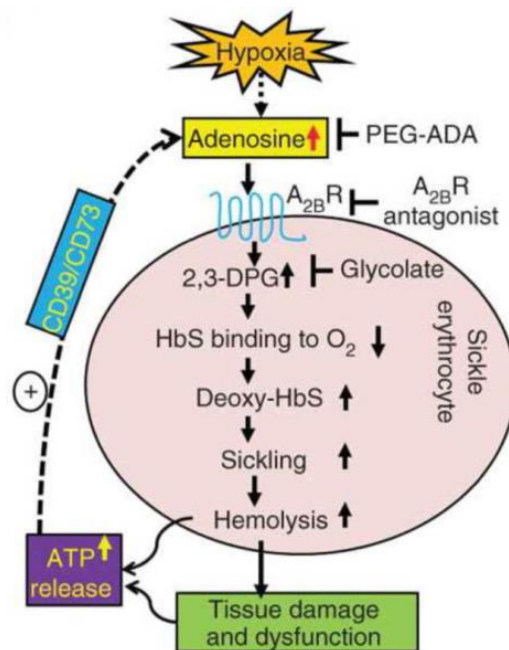


Figure 2.5: Model of excessive adenosine signalling in erythrocyte sickling via A_{2B}R. (Modified from Zhang *et al.*, 2011).

Due to widespread occurrence of the adenosine A_{2B} receptor in diverse tissues, it is a target for a large number of therapeutic applications. In particular, an A_{2B} selective antagonist was found to prevent development of pulmonary inflammation and airway fibrosis in lungs. All

this evidences point to an important role of adenosine A_{2B} receptors in the pathophysiology of lung diseases and suggests that this receptor might become a key player in the therapy of lung diseases (Sun *et al.*, 2006). Thus, treatment of asthma with selective A_{2B} adenosine receptor antagonist is proposed to be a therapeutic approach due to their bronchodilatory and anti-inflammatory effects. Besides, the therapeutic benefit of A_{2B} antagonists includes treatment of type-II diabetes, Alzheimer's disease and many other diseases (Rosi *et al.*, 2003).

A_{2B}R is located on immune cells, and expressed predominantly in the colonic epithelia cells (Kolachala *et al.*, 2008). Up-regulation of A_{2B}R can be seen in models of intestinal inflammatory diseases; hence it might be an important target to modulate inflammatory responses in the colon (Kolachala *et al.*, 2005). Activation of A_{2B} receptors increases release of histamine and interleukin (IL)-8 from mast cells (Feoktistov *et al.*, 1997). Adenosine A_{2B} receptors may exert effects on central inflammatory processes by regulating glial function (Fiebich *et al.*, 1996; Peakman *et al.*, 1994). Until 2006, the role of this receptor (A_{2B}R) has been unexplored due to lack of selective A_{2B}R agonists as well as an A_{2B} knockout mouse. Recently, Abo-Salem *et al.*, 2004 demonstrated that novel selective adenosine A_{2B}R antagonists produced a similar anti-nociception to caffeine in the hot-plate test in mice. Furthermore, A_{2B}R antagonists were potent in attenuating pulmonary inflammation (Sun *et al.*, 2006) as well as in reducing inflammatory pain and inflammatory hyperalgesia (Bilkei-Gorzo *et al.*, 2008). Similarly, Yang *et al.*, 2006 indicated that A_{2B}R knockout mice showed a phenotype with increased inflammatory responses. Selective A_{2B} receptor antagonists may play an important role in pathologies such as Anti-nociceptive (Abo-Salem *et al.*, 2004), Inflammation diseases like Asthma and Rheumatoid Arthritis (RA) (Fozard *et al.*, 2002) and chronic obstructive pulmonary disease (COPD) (Sun *et al.*, 2006), Alzheimer's disease (Papassotiropoulos *et al.*, 2001), Diabetes (Harada *et al.*, 2001), Prostate and Breast cancers (Wei *et al.*, 2013; Cekic *et al.*, 2012). Few years back, Sawynok *et al.*, 2000 reported that enprofylline an A_{2B} antagonist reduced the edema formation suggesting an anti-inflammatory role of blockade of A_{2B} receptors. Recently, Sun *et al.*, 2006 and Mustafa *et al.*, 2007 reported a novel, selective A_{2B} antagonist, CVT-6883, shown to attenuate pulmonary inflammation. Similarly, Belikoff *et al.*, 2011 reported MRS-1754, a novel selective A_{2B} antagonist shown to reduction of plasma TNF- α and IL-6 levels in an experimental model of polymicrobial sepsis in mice. In particular, A_{2B} receptor activation leads to increase in the TNF- α level from bronchial epithelial cells (Zhong *et al.*, 2006) and its blockade reduced IL-6 production by dendritic cells (Wei *et al.*, 2013). However, pharmacological blockade of

A_{2B}R or their absence was found to be associated with increased levels of inflammatory cytokines and chemokines, with enhanced NFκB in the plasma, spleen and heart (Csoka *et al.*, 2010).

Based on the earlier reports, it was clear that among the four AdoR subtypes, A_{2B}R antagonists has been the recent target for a medicinal chemistry researcher to identify its therapeutic applications in various disorders. Thus, A_{2B}R antagonists seem to be an attractive therapeutic target (Kalla *et al.*, 2009) for drug discovery and also prompted our recent attention towards therapeutic intervention in acute pain and inflammation.

Adenosine constricts airways of asthmatic patients through the release of histamine and leukotrienes from sensitized mast cells. The receptor involved seems to be the A_{2B}AR in humans, or the A₃AR in rats. Recently, A_{2B}ARs have been reported to mediate several proinflammatory effects of adenosine in inflammatory cells of the lung. In addition to mast cells, functional A_{2B}ARs have been found in bronchial smooth muscle cells and lung fibroblasts. In these cells adenosine increases release of various inflammatory cytokines through stimulation of the A_{2B} subtype, supporting the evidence that A_{2B}AR plays a key role in the inflammatory response associated with asthma (Spicuzza *et al.*, 2006).

The first evidence for involvement of A_{2B}AR in asthma derived from studies concerning selectivity of enprofylline, a methylxanthine structurally related to theophylline. Low expression of A_{2B}ARs was also found in lung parenchyma of patients affected by chronic obstructive pulmonary disease (COPD) (Varani *et al.*, 2006). In bronchoalveolar lavage macrophages from COPD patients A_{2B}ARs were down regulated compared to smokers with normal lung function. In addition, A_{2B}AR mRNA and protein expression were selectively decreased by oxidative/nitrosative stress, but not by inflammatory mediators in a human leukaemic monocytelike cell line (U937 cells), supporting the potential for modulating A_{2B}AR function in alveolar macrophages as a novel treatment for COPD (Varani *et al.*, 2010).

It has also been reported that adenosine deaminase-deficient mice treated with the selective A_{2B}AR antagonist (CVT-6883) showed reduced elevations in proinflammatory cytokines and chemokines, as well as mediators of fibrosis and airway destruction (Sun *et al.*, 2006).

The N-1 propyl derivative of CV Therapeutics (CVT-6694) has a very high A_{2B} affinity (7 nM) and very weak affinity for the A₁, A_{2A}, and A₃ AdoRs. When dosed orally in rats compound CVT-6694 exhibited very low systemic exposure.

The pyrazine-based A_{2B} AR antagonists discovered by the Almirall group, include LAS- (101057) a potent, selective, and orally efficacious A_{2B} R antagonists that was identified as a clinical development candidate (Eastwood *et al.*, 2010) (**Figure 2.6**).

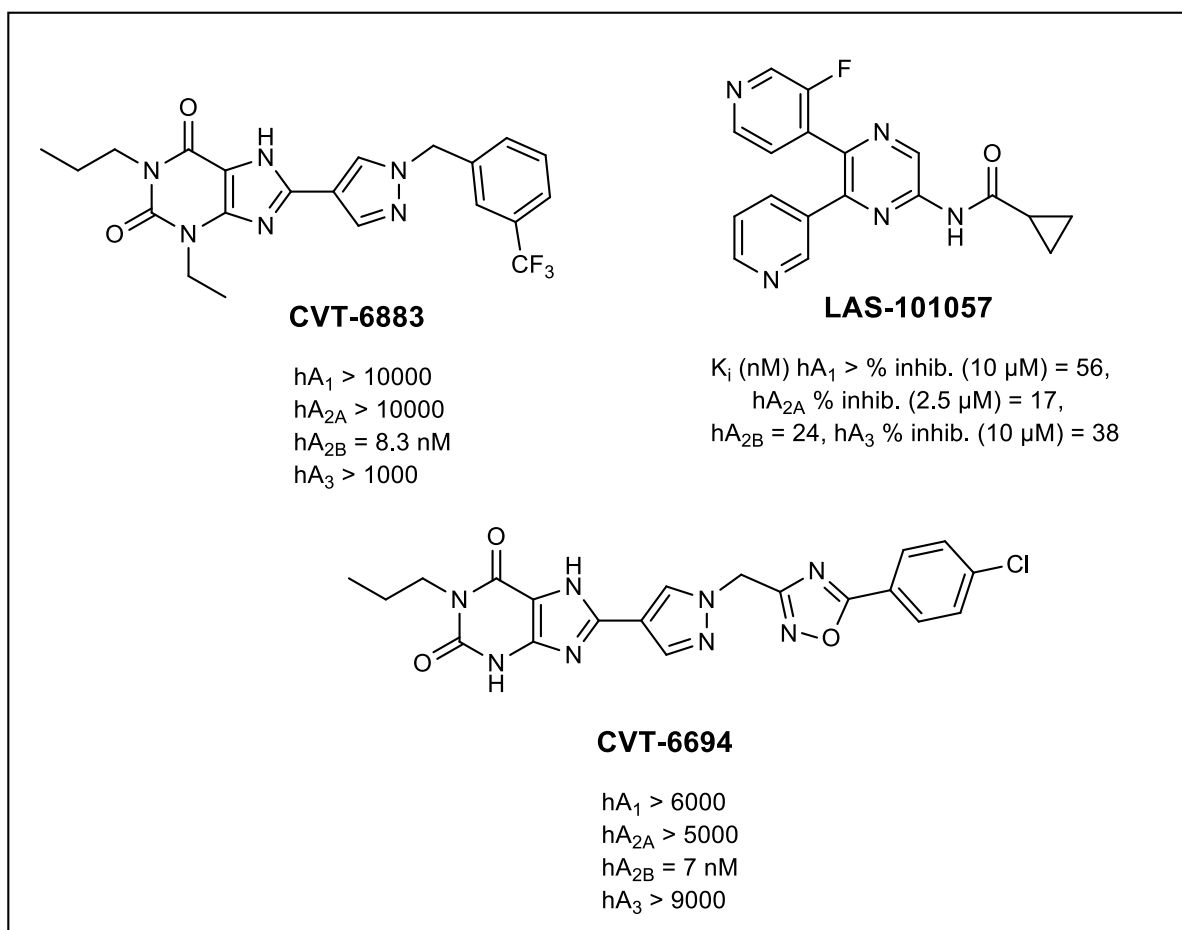


Figure 2.6: The chemical structures of some selective antagonists (CVT-6883, CVT-6694 and LAS-101057) for adenosine A_{2B} receptor

2.2.1. Adenosine A_{2B} Receptor Antagonists

A_{2B} antagonists can be divided into two classes of compounds; xanthine and non-xanthine derivatives. Between these types of compounds, the best results were initially achieved with xanthine and pyrrolopyrimidine scaffolds.

2.2.1.1. Xanthine analogues as antagonists

Extensive research on the adenosine receptor subtypes (A_1 , A_{2A} and A_3) showed that xanthines contain a promising core structure, modification of which led to the identification of selective antagonists for these receptor subtypes. Therefore, initial efforts to develop selective antagonists for adenosine A_{2B} receptor are focused on this class of compounds. The first adenosine receptor antagonists identified were the naturally occurring xanthines caffeine

and theophylline, which are used therapeutically for treatment of asthma. These compounds are of weak affinity and thus, are non-selective at the adenosine receptor subtypes and theophylline has a narrow therapeutic window. Thus identification of selective antagonists for adenosine A_{2B} receptor is desirable. Therefore, similar to agonists, structure-activity relationships (SAR) of the xanthines have been extensively studied in an attempt to improve their potency and selectivity at adenosine receptors (Baraldi *et al.*, 2004).

Alkylxanthines are classical antagonists for adenosine receptors and have considerable potency at the adenosine A_{2B} receptor subtype. Following further structural exploration of the xanthine moiety by several groups, led to the discovery of 8-phenylxanthines as selective A_{2B} adenosine receptor antagonists. Among these 8-phenylxanthine derivatives, pcyanonilide MRS-1754 displayed high affinity for human adenosine A_{2B} receptor ($K_i=1.97$ nM) and 210-, 260-, and 290-fold selectivity versus A_1 , A_{2A} and A_3 adenosine receptor subtypes (Kim *et al.*, 2000). However, this compound is not metabolically stable. Consequently, Zablocki *et al.*, 2005, used MRS-1754 as a lead compound to synthesize a series of metabolically more stable analogs. Within this series, CVT-5440 was identified by high selectivity and an affinity of 50 nM for human adenosine A_{2B} receptor.

Furthermore, a negatively charged compound PSB-1115 was found to display one of the most selective compounds of this family, exhibiting a K_i value of 53.4 nM at human A_{2B} adenosine receptor and selectivity versus rat A_1 adenosine receptors (41-fold), and versus the other human adenosine receptor subtypes ($A_{2A} > 400$ -fold and $A_3 > 180$ -fold). This compound is highly water soluble due to its sulfonate functional group (Hayallah *et al.*, 2002). Several heterocycles, such as, pyrazole, isoxazole, pyridine and pyridazine linked by different spacers (substituted acetamido, oxyacetamido and urea moieties) at the 8-position of xanthine nucleus were investigated, e.g. Baraldi *et al.*, 2004 has discovered a series of 8-heterocyclic substituted xanthines as antagonists for adenosine A_{2B} receptor subtype. The 5-pyrazolyl class resulted in a lead compound MRE-2029F20 (K_i h A_{2B} = 5.5 nM; K_i h A_1 = 200 nM; K_i h A_{2A} , $A_3 > 1000$), that has high affinity and selectivity for the adenosine A_{2B} receptor. In addition, PSB-603, of Muller *et al.* with high potency and specificity across species, including rodents and humans, was demonstrated to possess excellent A_{2B} affinity and promising selectivity which displayed a K_i value of 0.553 nM for binding to human A_{2B} adenosine receptors. A selective and high affinity radioligand, [3 H] PSB-603 was prepared that could be a useful tool in further characterization of adenosine A_{2B} receptor subtype (Borrmann *et al.*, 2009) (**Figure 2.7**).

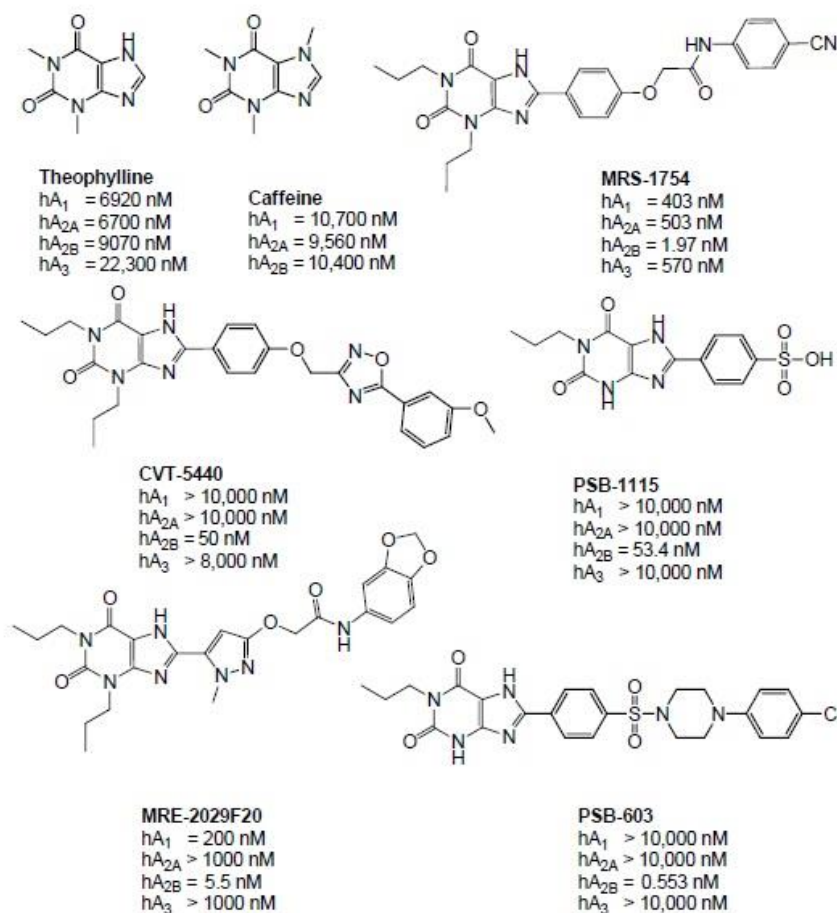


Figure 2.7: Chemical structures of some nonselective antagonists (theophylline and caffeine) and selective antagonists (MRS-1754, CVT-5440, PSB-1115, MRE-2029F20 and PSB-603) for adenosine A_{2B} receptor

2.2.1.2. 9-Deazaxanthines

In the xanthine family, 9-deazaxanthines (pyrrolo[2,3-*d*]pyrimidinones) were initially investigated by Grahner *et al.* 1994 and Hayallah *et al.* 2002 as antagonists for the A₁ and A₂ adenosine receptors. The authors observed that the structure-activity relationships of 9-deazaxanthines are similar to those of xanthine derivatives and also noticed an increased selectivity over A₁ adenosine receptor. They also concluded that the xanthines and 9-deazaxanthines bind in the same mode to the adenosine receptors, and thus, they have similar structure-activity relationships. Further, the 9-deazaxanthine derivative (**11**), with a meta-fluoro substitution on the pyrazole ring has the same affinity as the direct xanthine analog (Kalla *et al.*, 2009). However, the meta-CF₃-substituted derivative displayed a lower affinity

for A_{2B} adenosine receptor but with good selectivity. Vidal *et al.*, 2007 have identified a series of 8-phenyl-9-deazaxanthines that have a sulfonamide linker at the para-position of the phenyl group, and many compounds exhibited good A_{2B} adenosine receptor affinity (Esteve *et al.*, 2006) For instance, compound (**12**) of the above series showed 6 nM affinity for A_{2B} adenosine receptor and displayed good selectivity versus A₁ and A₃ receptor subtypes. Recently, Carotti *et al.* have presented and evaluated several 9-deazaxanthines that have a piperidine substituent (Stefanachi *et al.*, 2008). Among the compounds tested, compounds (**13**) (5.5 nM) and (**14**) (11 nM), respectively, displayed both high affinity and selectivity for A_{2B} adenosine receptor. Overall the 9-deazaxanthines afforded similar SAR to the parent xanthines with respect to A_{2B} adenosine receptor affinity (**Figure 2.8**).

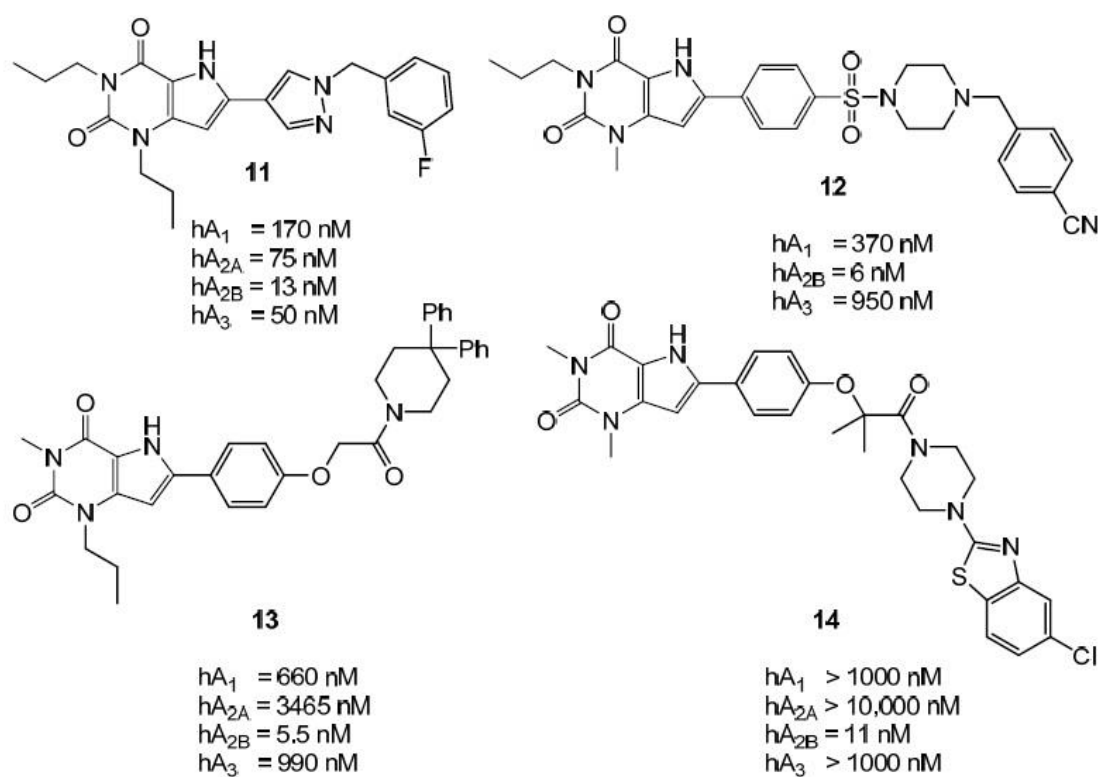


Figure 2.8: Chemical structures of selected deazaxanthines as antagonists for adenosine A_{2B} receptor

2.2.1.3 Non-xanthine analogues as antagonists

In order to identify highly potent and selective A_{2B} ligands, a large number of non-xanthine structures have been screened to search for adenosine receptor antagonists. Therefore, numerous classes of heterocycles were identified as antagonists at the adenosine A_{2B} receptor and other receptor subtypes as well. SAR of those non-xanthine heterocycles has been extensively studied and a number of highly potent and selective antagonists have been obtained.

Two series of compounds, 2-aminopyridines and 2-aminopyrimidines, were published as A_{2B} adenosine receptor antagonists. From these series of compounds, Vidal *et al.* recently published, a novel series of N-heteroaryl-4'-(2-furyl)-4,5'-bipyrimidin-2'-amines, as A_{2B} adenosine receptor antagonists. In particular, the 2'-amino-(3-pyridyl) derivative LAS38096 has an A_{2B} affinity of 17 nM and has very good selectivity. In addition, LAS38096, which represents the lead for this series, was capable of inhibiting A_{2B} adenosine receptor mediated NECA-dependent increases in intracellular cAMP, with IC₅₀ values of 321 nM and 349 nM in cells expressing human and mouse adenosine receptors, respectively (Vidal *et al.*, 2007).

Modifying pyrrolopyrimidines resulted in an even more potent antagonist with a decent selectivity: Scientists at OSI Pharmaceuticals have shown that 2-phenyl-7- deazaadenines (pyrrolopyrimidines) display good A_{2B} adenosine receptor affinity, such as OSIP-339391 which had an affinity of 0.5 nM towards human adenosine A_{2B} receptor and had a selectivity greater than 70-fold with respect to the human A₁, A_{2A}, and A₃ receptors subtypes (K_i hA_{2B} = 0.5 nM; K_i hA₁ = 37 nM; K_i hA_{2A} = 328 nM; and K_i hA₃ = 450 nM) (Stewart *et al.*, 2004) (**Figure 2.9**)

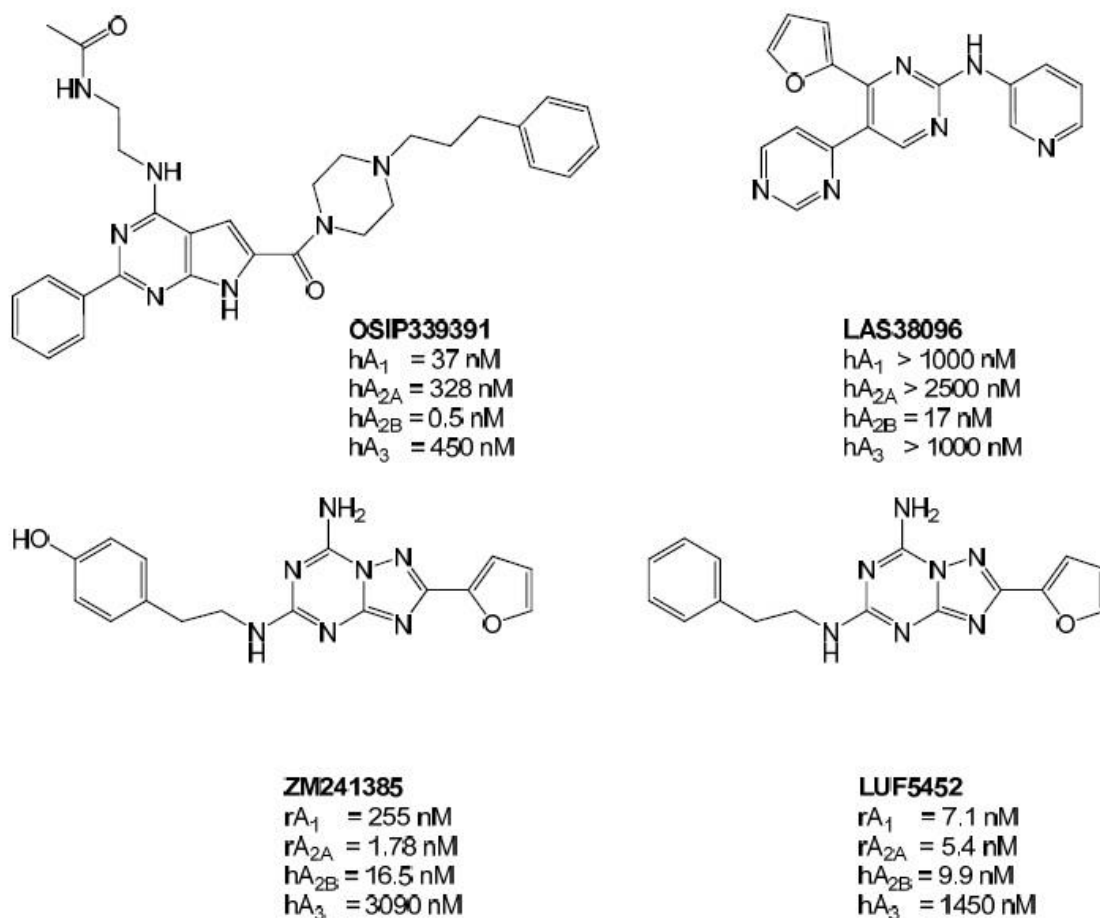


Figure 2.9: Chemical structures of some nonxanthine antagonists for adenosine A_{2B} Receptor

2.2.1.4. Triazolotriazine analogues

One of the most attractive bicyclic cores is represented by triazolotriazine nucleus, which led to the discovery of ZM241385. ZM241385, an excellent radioligand for A_{2A} receptors, is slightly (10-fold) selective for the adenosine A_{2A} versus the A_{2B} receptor subtype (De Zwart *et al.*, 1999). It had a K_i value of 16.5 nM at A_{2B} receptors in radioligand binding studies on Chinese hamster ovary cells expressing human A_{2B} receptors. Elimination of the 4-hydroxyl group on the phenyl ring of ZM241385, yielding LUF5452, resulted in a slightly improved affinity for A_{2B} and A_3 adenosine receptors and increased affinity for adenosine A_1 receptor. The affinity of this compound for adenosine A_{2A} receptor, on the other hand, was reduced indicating that the hydroxyl group contributes to increasing adenosine A_{2A} receptor selectivity (**Figure 2.9**).

2.2.2. Pharmacological aspects of selective A_{2B}R antagonists

Since the goal of obtaining a high affinity and selective A_{2B} antagonist has been achieved by several research groups, the agents obtained have been used to establish the anti-inflammatory properties in both *in vitro* cellular studies and in asthma models. CVT chemists have synthesized several A_{2B}-selective antagonists including CVT-6694 and CVT-6883. Following stimulation with a nonselective agonist NECA, compound CVT-6694 attenuated the increased production of both interleukin (IL)-6 and monocyte chemoattractant protein-1 (MCP-1) in bronchoalveolar lavage smooth muscle cells (Zhong *et al.*, 2004). These experiments suggest a novel mechanism whereby adenosine acts as a proinflammatory mediator in the bronchiole airways.

Compound CVT-6883, a potent selective, orally available, and potentially first in class A_{2B} AdoR antagonist, has entered the clinical trials by CV Therapeutics. In a mouse asthma model (ragweed challenge), compound CVT-6883 (dose: 1 mg/kg IP, 14-day treatment) was as effective as montelukast in reducing AMP-induced airway reactivity (Mustafa *et al.*, 2007). Compound CVT-6883 reduced significantly bleomycin (3.0 U/kg)-induced pulmonary fibrosis and inflammation in mice (Sun *et al.*, 2006).

The selective A_{2B} AdoR antagonist, MRE-2029-F20 synthesized by Baraldi's group, shows the inhibition of cAMP levels in neutrophils, lymphocytes, and HMC1 cells that naturally express the A_{2B} AdoR that may play a role in inflammatory diseases (Gessi *et al.*, 2005). The selective A_{2B} AdoR antagonist LAS38096 synthesized by Almirall has been shown to inhibit the NECA-induced production of IL-6 in a dose-dependent manner in both human and mouse fibroblasts (Vidal *et al.*, 2007). This further confirms the anti-inflammatory properties of A_{2B} AdoR antagonists.

Objectives and plan of work

3.1 Objectives

After thorough review of the literature, design of small molecule inhibitors of human adenosine A₂R receptors (A_{2A} and A_{2B}) was considered important and hence the thesis work focused on the following objectives:

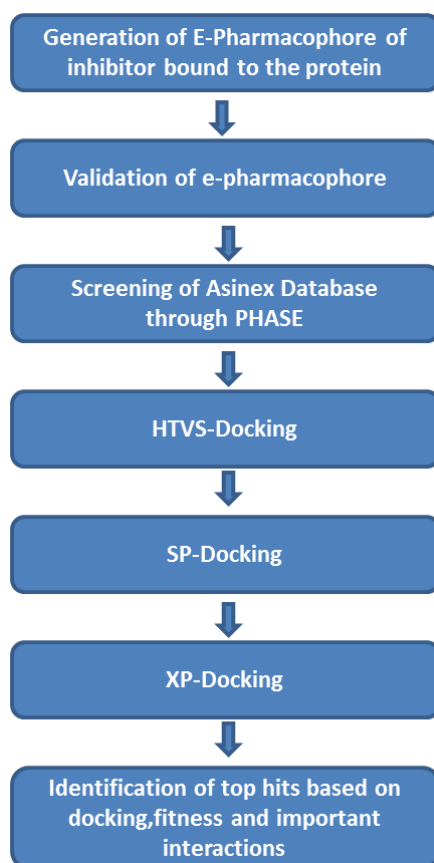
- To design novel potential adenosine modulators for the treatment of CNS disorders like epilepsy, acute pain and inflammation by utilizing the knowledge from the fields of computational chemistry and drug design, bioinformatics, medicinal chemistry, biotechnology and pharmacology.
- We utilized adenosine A₂R receptors (A_{2A} and A_{2B}) as primary targets. Lead molecules were identified using *in silico* methods. Identified compounds were further characterized using cAMP-HPLC assay, lead optimisation (SAR) by using knowledge from medicinal chemistry and extensive pre-clinical studies using animal models.

3.2 Plan of work

Part-1

The compounds were identified *in silico* using Schrodinger suite of softwares. A_{2A} inhibitory, neuroprotective and anti-epileptic profile of identified compounds were established using various *in vitro* assays and *in vivo* models as outlined below:

- a. Identification and validation of suitable feature template (pharmacophore) from crystal structure utilizing structure based drug design



b. *In vitro* cAMP-HPLC assay screening in MCF-7 cell lines

c. *In vitro* cell based studies on cell lines like alcohol induced MCF-7 and cytotoxicity studies in HEK-293 cells

d. *In vivo* behavioural studies in PTZ-induced seizures in adult Zebrafish

e. Toxicity studies of potent lead compound for Neuro, Cardio and Hepato tox in larval zebrafish

f. Synthesis of various analogues of lead molecule selected from Zebrafish behavioural studies

g. *In vivo* pharmacological studies

i. Determination of neurotoxicity

a. Rotarod Test

b. Behavioral Test Using Actophotometer

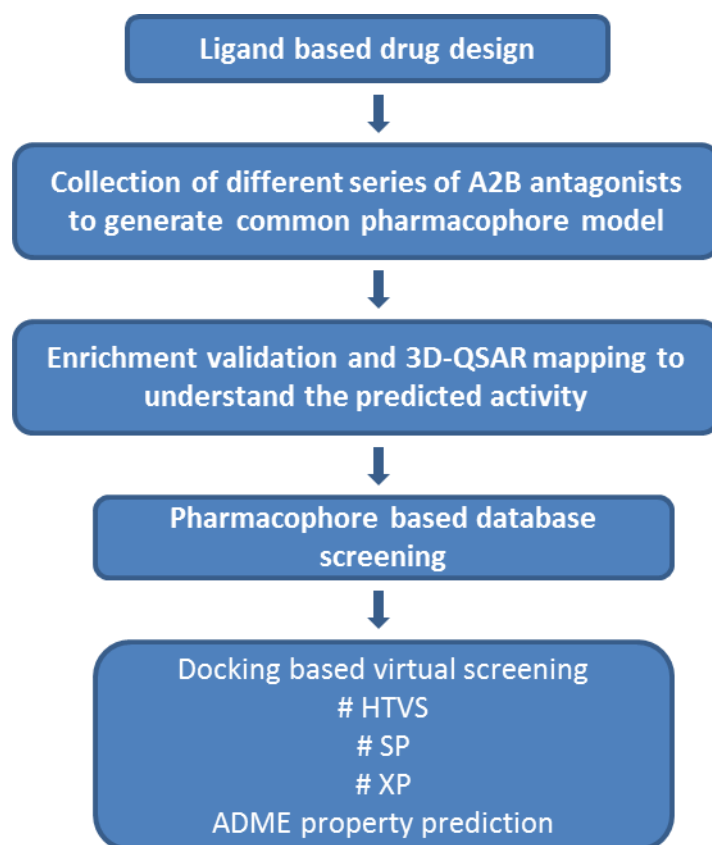
ii. Efficacy in Anticonvulsant Screening Methods

- a. Maximal Electroshock Induced Seizures (MES): (Mouse model)
- b. Pentylentetrazole induced Seizures (PTZ): (Mouse model)
- c. Strychnine induced Seizures (STY): (Rat model)
- d. Picrotoxin induced Seizures (PTX): (Rat model)

Part-2

The plan of work was classified into following stages

3.2.1. Design and development of new A_{2B} inhibitors using computational methods (3D-QSAR)



3.2.2. *In vitro* cAMP-HPLC assay screening in PC-3 cell lines

3.2.3. *In vitro* cell based studies on cell lines like PC-3 and cytotoxicity studies in HEK-293 cells

3.2.4. *In vivo* pharmacological studies

i. Determination of neurotoxicity

- a. Rotarod Test
- b. Behavioral Test Using Actophotometer
 - ii. Efficacy in Anti-Nociceptive Screening Methods
 - a. Eddy's hot-plate test in mice
 - b. Tail immersion test in mice
 - c. Acetic acid induced writhing model in mice
 - d. Formalin induced paw licking model in mice
 - iii. Evaluation of Anti-Inflammatory activity on carrageenan-induced paw edema in mice
 - iv. Measurement of *in vivo* gene expression levels of various key regulators NF κ B, IL-1 β , IL-6 and TNF- α using RT-qPCR

Materials and methods

4.1. Energy based pharmacophore drug design:

4.1.1 Computational details: An Intel Core i7 2600, 3.40GHz capacity processor with memory of 12GB RAM running with the CentOS 6.1 X 86_64 bit operating system was used to carry out the computations. The e-pharmacophore models were generated using Glide and PHASE applications implemented in the Maestro 9.3 software package (Schrodinger, LLC, New York, 2012). Finally, ADME prediction of molecules was checked with QikProp 3.5. 2D sketcher tab on Maestro graphical user interface was used to draw all structures. Structures were energetically minimized and stereo isomers generation were done at neutral pH 7 using ionizer subprogram of LigPrep 2.6 (Maestro 9.3).

4.1.2. Protein target: The crystal structure of Human A_{2A} receptor in complex with one of the antagonists (PDB code: 3EML) was retrieved from protein data bank (PDB) and was utilized for structure-based drug design. Hydrogen atoms, bond orders and formal charges were added using protein preparation wizard of Maestro software package.

4.1.3. Protein and ligand preparation: Protein Preparation Wizard (PPW) was used to assign bond orders, add missing hydrogens to heavy atoms and predict coordinates of missing loops. Five protonation states were generated for the native ligand (pH 7.0 ± 4.0) (Schrödinger, 2012) and the state with the lowest state penalty of 0.18 kcal/mol and charge of

+1 was selected. Hydrogen-bonding network was optimized by reorienting hydroxyl and thiol groups, amide groups of asparagine and glutamine, and imidazole ring in histidine. Protonation states of histidine, aspartic acid and glutamic acid, and tautomeric states of histidine were predicted at neutral pH. Finally, the structure was refined by minimization (Impref utility of Impact module) using OPLS 2005 force field with a maximum RMSD of 0.30 Å for heavy atoms. The reference ligand structure was downloaded from PDB and minimized using impact energy minimization using Impref module. The three dimensional structure of compounds was retrieved from Asinex database and employed for virtual screening. The database compounds were energy-minimized, and used as a single file using LigPrep module (Schrodinger, LLC: New York, 2012).

4.1.4. Glide (XP) docking: Receptor binding site was defined by grid generation using Glide (Glide, 2012). Each field on the grid is identical in size (10 Å), and represents the shape and properties of the active site. Glide uses two cubic boxes to define where the energetic calculations should be done. The outer cube contains all atoms of the binding ligand and all the acceptable positions of the ligand center lies in the inner cube. Centers of both the outer cube of 20 Å size and the inner cube of 10 Å size were chosen as centroid of the native ligand, ZMA of the PDB complex (3EML). Van der Waals radii of non-polar atoms were scaled to 0.8 with 0.25 partial charge cut-offs to provide flexibility to the rigid receptor and to relax binding site, which is a buried cavity between PH and kinase transmembrane helical domains of the protein, by decreasing penalties for close contacts in the binding site. The generated grid file from the prepared protein was used for Glide XP docking calculations. The minimized conjugate gradient output of the reference ligand was used. “Write XP descriptor information” option and “Compute RMSD” option were enabled and settings were kept default for the rest of the parameters. The XP Glide scoring function was used to order the best ranked compounds and specific interactions like π -cation and π - π stacking were

analyzed using XP visualizer in Glide module. The input RMSD of the ligand was also ascertained.

4.1.5. E-pharmacophore generation: E-pharmacophores script was used for pharmacophore modelling based on antagonist binding site of Human A_{2A} receptor. Reference ligand was docked to grid generated Human A_{2A} structure using Glide XP mode. E-pharm script used the information stored in Glide XP descriptor file, which carries information about reference ligand binding modes to receptor and energetic terms, to sum the energetic contributions that construct GlideScore of ligand on each atom center. The summed values allowed detection of five possible pharmacophore sites; A2, D9, R13, R14 and R15 (hydrogen bond acceptor (A), hydrogen bond donor (D), hydrophobic group (H), negatively charged group (N), positively charged group (P), and aromatic ring (R)) on atoms with the energy scores -1.17, -0.69, -0.89, -0.75 and -0.71 respectively. These sites were ranked based on their energies and two pharmacophore hypotheses were developed with selected sites of A2, D9, R13 and R14 (ADRR hypothesis) and of A2, D9 and R13 (ADR hypothesis). Generated ASINEX database was filtered separately to 5,25,807 compounds using ADRRR, ADRR and ADR hypotheses for reducing the number of structures to be used in docking runs.

4.1.6. Enrichment calculations: For validating reliability of the best three-pharmacophore hypotheses, enrichment calculation was performed. A decoy set molecules (contains no activity) were acquired from Schrödinger online database, from which 1000 decoy molecules were grouped with 20 known active molecules of human A_{2A} inhibitors (Total of 1020 molecules), compiled as a database. Further, decoy set database was utilized to check the hypothesis ability to discriminate the active human A_{2A} inhibitor compounds 20 from other molecules. Enrichment factor (EF) and goodness of fit (GH) was calculated using the following equations.

$$EF = \frac{(Ha \times D)}{(Ht \times A)}$$

$$GH = \left(\frac{Ha}{4HtA}\right) \times (3A + Ht) \times \left(1 - \frac{Ht - Ha}{(D - A)}\right)$$

Where, 'Ht' represented total number of hit compounds from the database; 'Ha' was the total number of active molecules in hit list; 'A' was the total number of actives in the decoy set and 'D' was total number of molecules in the decoy set.

Enrichment calculator script provided by Schrodinger application package, was utilized for internal validation properties such as EF1%, 10%, BEDROC, RIE. EF(X) % inferred the ability of the e-pharmacophore to select active molecules in the first X% of the match finds. Boltzman enhanced discrimination receiver operating characteristic (BEDROC) and robust initial enhancement (RIE) were good metrics which had the advantage to discriminate between early and late recognition problem of true positives. In this study, exponential weighting scheme of $\alpha=20$ was used for BEDROC, corresponding to 80% of the score from top 8% of the list. Validated pharmacophore hypothesis with above parameters was considered for use in virtual screening.

4.1.7. Preparation of commercial database: Asinex database containing 5,25,807 unique structures and synthesized compounds BITS in-house database of 2500 compounds were used in this study. Database molecules were prepared using LigPrep and Epik to expand protonation and tautomeric states at pH 7.0. Conformational sampling was performed for all molecules using ConfGen search algorithm. We employed ConfGen with OPLS_2005 force field and a duplicate pose elimination criterion of 1.0 Å RMSD to remove redundant conformers. A distance-dependent dielectric solvation treatment was used to screen electrostatic interactions. A maximum relative energy difference of 10.0 kcal/mol was chosen

to exclude high energy structures. Using Phase, the database was indexed with automatic creation of pharmacophore sites for each conformer to allow rapid database alignments and screening.

4.1.8. High-Throughput Virtual Database Screening and Docking studies: For the e-pharmacophore approach, explicit matching was required for the most energetically favourable site (scoring better than 1.0 kcalmol⁻¹) that found matching pharmacophores in the ligands. For filtering database molecules, a minimum of 2–4 sites were required to match for hypotheses with 3–5 sites. The above criterion was followed in the present work to screen the Asinex database. In the order of their fitness score, database hits were ranked to measure how well the aligned ligand conformer matched the hypothesis based on RMSD, site matching, vector alignments and volume terms. Virtual docking experiments were performed using Glide module with three docking modes which were High throughput virtual screening (HTVS), standard precision (SP) and extra precision (XP). For scoring the binding affinity of poses, Glide employs its own scoring function, GlideScore (GScore). Two different docking runs were performed for each hypothesis separately. Docking 5,25,807 ASINEX compounds obtained by filtering with ADRRR, ADRR and ADR hypotheses to grid generated Human A_{2A} structure with HTVS mode, and scoring with HTVS scoring function were followed by re-docking the top scored 5125 molecules. Top 20% molecules were subjected to SP docking to obtain SP scoring; and top 10% were docked using XP docking mode and scoring with XP scoring function. The numbers 5, 00,000 and 5125 were determined as optimum values considering the CPU time required for docking calculations. For both docking modes, ten poses per compound state (at maximum) were generated and only best scoring state was kept in the final hit list. For each ligand pose, a tightly constrained minimization and an unconstrained minimization were performed with Macro Model module. Ligands with more than 5 kcal/mol energy difference between the docked and free conformations received

penalties and quarter of this energy difference was added to GlideScore. GlideScore values were used for further evaluation of hits.

4.2. Ligand based drug design

4.2.1. Molecular modeling

In the present study, a dataset containing 265 reported A_{2B} antagonists were considered for development of three dimensional pharmacophore which was further utilized in the identification of novel A_{2B} inhibitors. The dataset consisted molecules with various scaffolds which include derivatives of Xanthines (Stefanachi *et al.*, 2008; Fernandez *et al.*, 2009; Kim *et al.*, 2000; Hayallah *et al.*, 2002; Elzein *et al.*, 2008; Borrmann *et al.*, 2009; Baraldi *et al.*, 2012; Kalla *et al.*, 2008), N-Heteroaryl 4'-Furyl-4,5'-bipyrimidin-2'-amines (Vidal *et al.*, 2007), 2-Amino-4,6-substituted Nicotinitriles (Mantri *et al.*, 2008), 4-Substituted-7-N-alkyl-N-acetyl 2-aminobenzothiazole amides (Cheung *et al.*, 2010), N-(5,6-diarylpyridin-2-yl)amide derivatives (Eastwood *et al.*, 2010), 2-Amino-6-furan-2-yl-4-substituted Nicotinitriles (Mantri *et al.*, 2008), 7-Aryltriazolo[4,5-d]pyrimidines (Gillespie *et al.*, 2008), Quinolinone (McGuinness *et al.*, 2010), pyrrolopyrimidin-6-yl benzenesulfonamides (Esteve *et al.*, 2006). All these molecules were sketched using Maestro graphical user interface. Activity of the compounds which was reported as IC₅₀ was converted into pIC₅₀ which was further used in categorizing compounds into active and inactive molecules. The geometry of compounds was cleaned, hydrogens were added, energy minimized and checked for any stereoisomers at pH 7 using (Schrodinger, 2012; LigPrep v2.5). The compounds were subjected for generation of their conformers employing the ConfGen v2.3 of Schrodinger 2012, where generated conformers were energy-minimized and redundant conformers were eliminated (Schrodinger, 2012; ConfGen v2.3). Energy minimizations were carried out using

MacroModel using OPLS_2005 force field (Schrodinger, 2012; MacroModel v9.10). These prepared compounds were used in developing pharmacophore model and 3D QSAR model.

4.2.2. Pharmacophore modeling

Pharmacophore development for dataset compounds was carried out using PHASE v3.4 Schrodinger. Total dataset was divided into three categories: active, inactive and moderately active based on their activity profiles. The prepared compounds were subjected to generation of pharmacophore features which were further used in the generation of common pharmacophore based on these compounds. A threshold was set during development of common pharmacophore, stating the ideal number of active compounds that the pharmacophore would match so as to retain the important features of active compounds. Common pharmacophores were identified using a tree-based partitioning method in which groups similar pharmacophores were based on their intersite distances. This mapping of pharmacophore according to its intersite distances was done into a box of finite size. All pharmacophores that are found to be mapped in the same box are observed to be enough in the identification of common pharmacophore. In the present study, the tree partition technique was used with a minimum distance of 2 Å. 5 was set as the maximum tree depth with an initial and final box size of 32 Å and 1 Å respectively. Scoring procedure was applied for each box to identify the best pharmacophore that greatly aligns with the chosen number of active molecules. The hypotheses were rescored to attain accurate data by applying a weightage of 0.5 to the activities of ligand.

4.2.3. 3D QSAR model generation

Pharmacophore based 3D QSAR model was generated which includes important structural features from active compounds so as to identify potential A_{2B} inhibitors. Total dataset was categorized into test set and training set of molecules which were used during the QSAR

model development. A 3D QSAR model was developed using the activity data of compounds in the dataset for selected pharmacophore hypothesis. The developed model divides available three dimensional spaces into a grid of uniformly sized cubes to produce negative and positive contours that will be useful in the analysis of various structural properties of compounds. Various parameters were considered in order to analyze the significance of the developed model. A partial least square (PLS) regression analysis was carried out for the developed model to analyze the predictability of the model.

4.2.4. PLS analysis and cross validation

Accuracy of the model can be increased by increasing the number of PLS factors employed until a point where over-fitting starts to occur for the developed model. Stability of the predicted model was determined by employing cross validation methods such as leave-one-out technique (LOO). Methodology can be explained as exclusion of one molecule from the dataset and development of model over the remaining molecules in an iterative manner. This iteration was repeated till all the compounds had been kept out once. Analysis of the exclusion of molecule was carried out based on properties of the built model. The cross validated correlation coefficient (r_{cv}^2) and predictive correlation coefficient (r_{pred}^2) are the other two properties which determine predictive ability of the developed QSAR model.

The cross validated correlation coefficient was calculated using the formula given in equation (1), where Y_{obs} , Y_{pred} and Y_{mean} are the observed, predicted and mean of the pIC_{50} values respectively.

$$r_{cv}^2 = 1 - \frac{\Sigma(Y_{pred} - Y_{obs})^2}{\Sigma(Y_{obs} - Y_{mean})^2} \quad (1)$$

The statistical significance of developed model was calculated with the help of predictive correlation coefficient (r_{pred}^2) according to the formula given in equation (2). r_{pred}^2 indicates

the predictive power of the model which is calculated over the test set molecules according to the equation (3).

$$r_{\text{pred}}^2 = \frac{\text{SD-PRESS}}{\text{SD}} \quad (2)$$

PRESS (Predictive Residual Error Sum of Squares) is the sum of squared deviation between the predicted and the observed activity values for each molecule in the test set (Pan *et al.*, 2010; Sharma *et al.*, 2010). SD is the sum of squared deviations between experimental values of test set and mean activities of training set molecules. PRESS can be considered one of the crucial factors which estimate prediction error of the model. The lesser the value of PRESS than that of SD, the better is the predictive ability of the model and it ultimately conferring the statistical significance of the model.

$$\text{PRESS} = \Sigma(Y_{\text{obs}} - Y_{\text{pred}})^2 \quad (3)$$

4.2.5. External validation of developed 3D QSAR model

True predictive ability of the model was evaluated as it is necessary to analyze the developed model (Doweyko *et al.*, 2004; Schuurmann *et al.*, 2008). This was done using external validation which involved calculation of squared correlation coefficient r^2 (or R) according to the equation (4):

$$R = \frac{\Sigma(y_i - \bar{y}_o) * (\tilde{y}_i - \bar{y}_p)}{\sqrt{\Sigma(y_i - \bar{y}_o)^2 * \Sigma(\tilde{y}_i - \bar{y}_p)^2}} \quad (4)$$

Where y_i and \tilde{y}_i are observed and predicted activity of total dataset molecules; \bar{y}_o and \bar{y}_p are average of the observed and predicted values of test set molecules. The model can be considered highly predictive only if it is close to 1. Regression of y against \tilde{y} through the origin,

i.e. $y^{ro} = k\tilde{y}_i$ should be contained by k nearer to 1. The slope can be calculated using Equation (5):

$$k = \frac{\sum y_i \tilde{y}_i}{\sum \tilde{y}_i^2} \quad (5)$$

Another essential parameter that was used for external validation is r_m^2 (Mitra *et al.*, 2010), which was calculated according to Equation (6), where r^2 is referred to as non-cross-validated correlation calculated from the PLS regression method. r_o^2 was calculated according to the Equation (7) and value of y_i^{ro} was calculated from Equation (8):

$$r_m^2 = r^2(1 - \sqrt{|(r^2 - r_o^2)|}) \quad (6)$$

$$r_o^2 = 1 - \frac{\sum (\tilde{y}_i - y_i^{ro})^2}{\sum (\tilde{y}_i - \tilde{y}_p)^2} \quad (7)$$

$$y_i^{ro} = K\tilde{y}_i \quad (8)$$

4.3. Biology:

4.3.1. Cell culture: Human breast cancer cell lines HEK 293 and MCF-7 were procured from NCCS, Pune, India. Cell lines were cultured in MEM growth medium supplemented with 10 $\mu\text{g/ml}$ Human insulin (as supplement for MCF-7 cell lines procured from (Sigma, St. Louis, MO, USA) 10% fetal bovine serum (Sigma, St. Louis, MO, USA) and 1% Penicillin-Streptomycin solution (Sigma, St. Louis, MO, USA) at 37 °C in a humidified 5% CO_2 /95% air incubator and were sub cultured in 1:5 ratio twice a week. Absolute ethanol was diluted in sterile distilled water as per requirement. All inhibitors were diluted in DMSO (10%).

Human prostatic carcinoma cells, DU145, and PC-3 (NCCS, Pune, India), were cultured at 37 °C in a humidified incubator with 5 % CO₂ in RPMI-1640 medium supplemented with 10 % FBS, 100 U/ml penicillin, 100 µg/ml streptomycin, and 3 mM/l glutamine. Cells used in the present study were within 20 passages after purchasing from NCCS.

4.3.2. Selectivity index analysis

4.3.2.1. Cytotoxicity studies: MTT ((3-(4,5-dimethylthiazol-2-yl)-2,5-diphenyltetrazolium bromide) reduction assay was used to measure cytotoxicity (Van Meerloo *et al.*,2011). 10,000 cells/well HEK 293 cells were seeded in a 96-well plate in MEM medium containing 1% FBS, treated with different concentrations of compound from 100 µM–10 nM for 48 h. 10 mg/mL of MTT solution (dissolved in 1X PBS) was added to the wells and incubated for 3 h. Violet crystals formed were dissolved in 100% DMSO and absorbance measured at 595 nm in spectrophotometer (Spectra Max, Molecular Devices, LLC). The experiment was done in triplicates, and % cytotoxicity was calculated to draw CC₅₀.

4.3.2.2. Growth inhibition assay of A_{2A} antagonists: Inhibition of growth of the 0.1% EtOH treated MCF-7 cells by the compounds was measured in a dose response curve in triplicate. Approximately 5000 cells per well were utilized for this investigation, and growth inhibition was measured by MTT addition, similar to the cell cytotoxicity studies. GIC₅₀ values were calculated using GraphPad prism 5.01.

4.3.3. Determination of gene expression analysis of A_{2A} and A_{2B} adenosine receptors (ARs) in two prostate cancer cell lines

4.3.3.1. Total RNA isolation and cDNA conversion

Cells from 35 mm petridish were treated with TRI reagent (Chomczynski *et al.*, 1993), according to protocol of the manufacturer (Sigma-Aldrich Co. LLC. USA). Concentrations

and purity of RNA were quantified with Perkin Elmer VICTOR X3 (Perkin Elmer, Shelton, CT, USA) according to optical density. Purity of RNA was determined with $A_{260/280}$ ratio (1.8–2.0 was considered pure). cDNA synthesis of respective samples was acquired according to the Verso cDNA synthesis kit (Thermo Fisher Scientific Inc. USA) protocol. Equal amount of RNA (about 1 μ g) from the samples was suspended in 5 μ l of RNase-free water. RNA sample was further added to reaction mixture containing final volumes of 1X cDNA synthesis buffer, 500 μ M of dNTP Mix, 500 ng of Anchored Oligo-dT primers, 1 μ L of RT enhancer (to remove contaminating DNA), Verso enzyme mix (includes Reverse transcriptase) and the final volume was adjusted with water (PCR grade). Reverse transcription cycling program was set at the temperature 42 °C in 1 cycle of 30 min and at 95 °C for 2 min for reaction termination using MJ Mini Thermal Cycler (Bio-Rad Laboratories, Inc. USA.).

4.3.3.2. Detection of A_{2A} and A_{2B} (ARs) gene expression

Transcript levels of Human A_{2A} and A_{2B} primers were assessed using BIO-RAD CFX Connect Real Time System (BIO-RAD Laboratories, Inc). 1 μ g of total RNA was used as a template to make the first strand cDNA by Anchored oligo dT priming using a commercial cDNA synthesis kit (Verso cDNA synthesis kit, Thermo Fischer scientific, Inc). Real time PCR was performed according to the manufacturer's instructions using a BIO-RAD CFX Connect with SYBR green (Kapa Biosystems) as the fluorescent dye enabling real-time detection of PCR products. Synthetic gene specific primer sets used in PCR for human A_{2A} primer forward 5'AACCTGCAGAACGTCACCAA'3 and reverse 5' GTCACCAAGCCATTGTACCG'3 (Etique *et al.*, 2009) and for human A_{2B} forward primer 5' GTGCCACCAACAACACTGCACAGAAC3' and reverse 5'

CTGACCATTCCCACTCTTGACATC 3' were used to assess gene expression levels of A_{2A} and A_{2B} in cancer cell lines (Wei *et al.*, 2013).

4.4. Quantitative estimation of Cyclic AMP in MCF-7 breast cancer cell lines by HPLC assay

4.4.1. Materials: Adenosine 3', 5'-cyclic monophosphate (cAMP), methanol (HPLC grade) were purchased from Sigma Aldrich, Mumbai, India. Formic acid was purchased from SD Fine-Chem Limited, Mumbai, India; Milli-Q water purification system (Millipore®, MA, USA) was used for obtaining high quality HPLC grade water.

4.4.2. Sample preparation: From earlier reports it was demonstrated that A_{2A} receptor is activated upon treating with the 0.1% of ethanol (Etique *et al.*, 2009 and Dohrman *et al.*, 1997). Different concentrations of ethanol were added to the 1, 00,000 cells (incubated in MEM complete medium in 6-well plate) for 24hrs. A_{2A} gene expression studies reveal that at 0.1% of ethanol has over expressed A_{2A} receptor at transcript level, compared to all other concentrations. This is also evident from the cAMP measurement in cells using HPLC at different concentrations of ethanol. Prior to sample analysis, 300 µL of each solution was extracted using 500 µL of 100% methanol for protein precipitation. Further, each of the cell mixtures was sonicated for a period of 1 min in a sonicator (SONICS, vibra cell, Sonics & Materials, Inc.) with subsequent centrifugation at 10,000 rpm, for a period of 10 min at 4 °C using a centrifuge (Sorvall WX Floor Ultra Centrifuges - Thermo Scientific. Inc). For each sample, supernatant was finally collected and directly injected into the HPLC system. For estimating the compound efficacy, compounds were incubated with 0.1% ethanol at different concentrations 25 µM, 12.5 µM, 6.25 µM, 3.12 µM and 1.5 µM for 24hrs and later cAMP was extracted using methanol precipitation. The chromatographic precision for each compound was evaluated by repeated analysis (n=3) of same sample at all five

concentrations. Dose response curves for each compound were plotted using Graphpad prism 5.01 and IC_{50} were calculated.

4.4.3. Mobile phase optimization

The chromatographic conditions were selected on the basis of backpressure, tailing factor, peak resolutions, peak shapes and reproducibility of retention time. For selecting a mobile phase initial trial was taken using potassium dihydrogen phosphate buffer of different pH and in varying proportions with acetonitrile, and methanol was investigated. But the peaks were not of a good shape. Utilization of 0.4% HCOOH buffer in place of phosphate buffer improved the peak shapes and hence, 70:30, %v/v of formic acid buffer-methanol was selected as mobile phase for further trials.

4.4.4. Preparation of mobile phase

For preparing a mobile phase, HPLC grade methanol and 0.4 % HCOOH buffer were filtered through a 0.22 μ m Membrane filter and subjected to degassing in an ultrasonic bath for a period of 15 min.

4.4.5. Preparation of standard solutions

A primary stock solution (1 mg/ml) was prepared by dissolving 10 mg of cAMP in 10 ml of Milli-Q water. Stock solution was suitably diluted with Milli-Q water to obtain working range of standard solutions. Calibration curve sample (100 PPM) was prepared by spiking 900 μ l of Milli-Q water with 100 μ L of primary stock solution. Remaining calibration curve samples were prepared by spiking 500 μ l of Milli-Q water with 500 μ l previously diluted working standard solution in order to obtain final concentrations of 3.125, 6.25, 12.5, 25 and 50 PPM. All samples were stored at 2-8° and equilibrated to room temperature prior to use.

4.4.6. Construction of calibration curve

The values of peak areas were plotted against their respective concentrations in order to construct the calibration curve for cAMP. Linear regression analysis was performed using Microsoft Excel® version 2010 (Microsoft Corporation, Washington, USA).

4.4.7. Cyclic AMP-HPLC assay, method development: A method for detection of cAMP was developed using a HPLC system (Elnatan *et al.*, 1994) consisting of two solvent delivery LC-20AD pumps, a SIL-20A HT auto injector, a CTO-10AS VP column oven and a SPD-M20A photo diode array (PDA) UV detector (Shimadzu, Tokyo, Japan). Data collection and integration were accomplished using LC Solutions 1.25 SP2 version software. A combination of 0.4% formic acid in water and methanol (70:30, %v/v) was selected as mobile phase. Samples were analysed by using Vydac 218TP C18 column (250 × 4.6 mm i.d., 5 µm) maintained at 40 °C. The mobile phase was injected to the system using binary pumping mode at a flow rate of 0.7 mL/min. For all samples, injection volume and run time were fixed at 10 µL and 7 min, respectively. Peaks were monitored at a wave length of 254 nm. HPLC system was stabilized for 1 h at 0.7 mL/min flow rate, through baseline monitoring prior to actual analysis. The prepared 0.4% formic acid in water and methanol was filtered through a 0.22 µm Millipore filter and ultra sonicated to degas before use.

4.5. Pharmacological activity:

4.5.1. Zebrafish behavioural studies:

4.5.1.1. Zebrafish-animal husbandry: Zebrafish (*Danio rerio*) is fresh water vertebrate, used as a valuable, versatile model organism to study the basis of epilepsy and for evaluation of new AED (Kari *et al.*, 2007 and Berghmans *et al.*, 2007), and it is an attractive preliminary *in-vivo* model for screening compounds with potential, zERG blockade & QT prolongation (Chaudhari *et al.*, 2013). It serves as an important tool in pharmaceutical research, due to its

small size, inexpensive, rapid organogenesis, high fecundity, transparent embryos and high degree of conservation with human genome (approximately 75%)(Chakraborty *et al.*, 2009). Here we have used adult zebrafish as an effective model for investigating epilepsy rather than larval zebrafish, as larval zebrafish have incompletely developed brain, and the BBB (starts functioning after 10 dpf) (Goldsmith *et al.*, 2005)), whereas the adult zebrafish has fully developed brain regions and BBB (Eliceiri *et al.*, 2011 and Berghmans *et al.*, 2007).

Adult wild-type male zebrafish, around (5-7 months old), were used for this study (obtained from Vikrant Aquaculture, Mumbai, India). Fish were acclimated for 2 weeks before the experiment in a polysulfone housing tanks fitted with continuously aerated purified water (Millipore ELIX system grade) maintained at PH 7.0-8.0 with 150 mg/L sea salt at 27±2 °C under a 14-10 h light/dark cycle photoperiod as most favourable conditions for their growth and development (Banote *et al.*, 2013). Zebrafish were fed 2-3 times daily with flake food and live hatched brine shrimps *ad libitum*. Use and maintenance of zebrafish were as per the Guidelines for Use of Zebrafish in the NIH Intramural Research Program (<http://oacu.od.nih.gov/ARAC/documents/Zebrafish.pdf>) and the Zebrafish Book (Westerfield, M., 2000). Embryos are obtained by breeding a ratio of 2 females: 3males; embryos obtained were collected, sorted and allowed to grow in E3 medium (5mM NaCl, 0.17 mM KCl, 0.33 mM CaCl₂ and 0.33 mM MgSO₄.) at 28 °C.

4.5.1.2. Drugs: PTZ used in this study was purchased from Sigma-Aldrich (St. Louis, MO, USA). Terfenadine, Amiodarone, Atrazine and tricaine were purchased from Sigma Aldrich, Mumbai, India. DMSO was purchased from HiMedia Laboratories, Mumbai, India. Test compounds were purchased from ASINEX database. A stock solution of PTZ was prepared in de-ionized water at a concentration of 7.33mg/ml for Seizure Induction and stored at -20 °C for future use. Prior to use test compounds were dissolved in 0.5% methyl cellulose at 50

mg/ml and stored at 4 °C in an air-tight container. Working solutions were prepared from each stock solution by adding sterile distilled water to provide a final concentration.

4.5.1.3. Oral drug administration for behavioural assessment in adult zebrafish:

Conventional studies on adult zebrafish are conducted by addition of chemicals to the aquarium water which requires large amounts of drugs. We have used a reported method of oral drug administration which helps administer precise quantities of drugs orally to adult zebrafish [Zang *et al.*, 2011].

4.5.1.4. Experimental setup for behavioural monitoring (Banote *et al.*, 2013):

In order to allow acclimatization, 2 h before starting the experiment, zebrafish were kept in polysulfone tank. Acclimatized fish were pretreated with 50 mg/kg test compounds administered orally (p.o.). Ten minutes later, intraperitoneal (i.p.) injection of 220 mg/kg PTZ (Sigma-Aldrich, USA) was done (dose volume: p.o. Test compound—4 µL; i.p. PTZ—15 µL). Control fish were treated with p.o. methyl cellulose and i.p. saline. Behavioral testing was performed using an observation tank (30cm length×15cm width×10cm height) maximally filled with aquarium water. Videos were recorded using a digital camera for 8 min, beginning 2 min after PTZ injection. All behavioral tests took place between 10 AM to 4 PM to reduce behavioral variations. Qualitative seizure scoring was conducted by trained observers in a blinded fashion. All fish were observed for 8 min to evaluate seizure-like behavior, and a score was assigned according to the following scale—stage 1: intermittent immobility and hyperventilation; stage 2: rotational swimming; stage 3, side-to-side movements; stage 4: visible muscular spasms and contractions; stage 5: quick convulsions of the entire body; stage 6: spasms and high frequency convulsions lasting several minutes including sinking of fish to tank bottom and; stage 7: complete immobility and death. 66 male fish were distributed in 11 treatment groups with 6 fish per group. The different groups (with treatment) were the

following: Control (p.o. methyl cellulose+i.p. saline), PTZ (p.o. methyl cellulose+i.p. PTZ 220 mg/kg), Ligand-1-50+PTZ (p.o. Ligand-1-50 mg/kg+i.p. PTZ 220 mg/kg), Ligand-2-50+PTZ (p.o. Ligand-2-50 mg/kg+i.p. PTZ 220 mg/kg), Ligand-3-50+PTZ (p.o. Ligand-3-50 mg/kg+i.p. PTZ 220 mg/kg), Ligand-4-50+PTZ (p.o. Ligand-4-50 mg/kg+i.p. PTZ 220 mg/kg), Ligand-5-50+PTZ (p.o. Ligand-5-50 mg/kg+i.p. PTZ 220 mg/kg), Ligand-6-50+PTZ (p.o. Ligand-6-50 mg/kg+i.p. PTZ 220 mg/kg), Ligand-7-50+PTZ (p.o. Ligand-7-50 mg/kg+i.p. PTZ 220 mg/kg), Ligand-8-50+PTZ (p.o. Ligand-8-50 mg/kg+i.p. PTZ 220 mg/kg), Ligand-9-50+PTZ (p.o. Ligand-9-50 mg/kg+i.p. PTZ 220 mg/kg).

4.5.1.5. Dose response evaluation of Ligand-9: In this study, test compound (Ligand-9) was evaluated against Pentylene-tetrazole (PTZ) induced seizure in adult zebrafish. PTZ at a dose of 220mg/kg was used for seizure Induction. Six fish were assigned to each of the five groups: 1. Vehicle Control (p.o. methyl cellulose+i.p. saline). 2. PTZ (p.o. Methyl cellulose+i.p. PTZ 220 mg/kg). 3. Ligand 9 + PTZ (p.o Lig-9-25 mg/kg + i.p. PTZ 220 mg/kg). 4. Ligand 9 + PTZ (p.o Lig-9-50 mg/kg + i.p. PTZ 220mg/kg). 5. Ligand 9 + PTZ (p.o Lig-9-75 mg/kg + i.p. PTZ 220 mg/kg)

4.5.1.6. Drug treatment protocol: Seizure induction was done using PTZ at a dose of 110 µg/fish intra-peritoneally. Vehicle control group was administered Methylcellulose orally. Treatment of different doses (Ligand 9) was carried out orally (25 mg/kg, 50 mg/kg & 75 mg/kg) and videos were recorded. Fish were evaluated for Seizure score at every minute and overall seizure score was calculated.

4.5.1.7. Zebrafish toxicity studies:

Larval zebrafish assays have been utilized in the pharmaceutical industry for toxicological evaluation especially hepatotoxicity, cardiac function and neurotoxicity safety (Fleming *et al.*, 2013, Hill *et al.*, 2012 and Mittelstadt *et al.*, 2008). Similar to other mammals, zebrafish

larvae have the ability to perform both phase I and phase II metabolism reactions (Alderton *et al.*, 2010). Traditionally larval zebrafish have been used to demonstrate human disease, and serves as an excellent model for evaluating toxicity studies because of their small size and suitability to conduct experiments in multi well plates (Kari *et al.*, 2007). Toxicological evaluation was carried out in a blinded fashion. Terfenadine for cardiotoxicity, Amiodarone for Hepatotoxicity assay, & Atrazine for Neurotoxicity assay, were taken as positive controls where toxic effects are reported and known. Various Concentrations of Ligand 9 (1 to 30 μ M) were screened in zebrafish larvae using standardized toxicity assays.

4.5.1.7.1. Drug exposure to zebrafish embryos for toxicity evaluation: 1 day post fertilization (dpf) embryos were collected into Petri dishes, checked for its developmental stage and condition. Embryos were dechorionated using 0.5mg/ml pronase E treatment followed by washes with E3 medium and allowed to grow in incubator in E3 medium at 28°C temperature until 5 dpf. Working concentrations of the compound was prepared by serially diluting the compound in final concentration of 100% DMSO. Embryos (n=6) were distributed in 24 well plate along with 250 μ l of 0.1% DMSO. Each well was then added with 250 μ l of working concentration of the drug. Embryos were allowed to incubate at 28°C for 4 hrs. After 4 hrs of incubation, embryos were treated with tricaine and immediately used for reading the heart rate.

4.5.1.7.2. Cardiotoxicity assay: Zebrafish ether-a-go-go-related gene (zERG) which is orthologous to the human ether-a-go-go-related gene (hERG) with these finding suggest it to be an effective model for cardiotoxicity screening. In this regard Ligand 9 was evaluated on the heart rate and atrio-ventricular block and thereby assess arrhythmogenic potential. The respective drug concentrations of Ligand 9 were exposed and the heart rates were measured, time taken for 30 atrial and ventricular beats was measured for each embryo from which

number of heart beats per minute was calculated and the atrioventricular ratio was calculated by the formula: $1800/X = \text{beats /minute}$ (where X = time in seconds). Terfenadine (20 μ M) was used as a positive control.

4.5.1.7.3. Hepatotoxicity assay: The transparency of zebrafish larvae and similarity in toxicity profiles with human allow them for testing compounds causing hepatotoxicity. After the evaluation for cardiotoxicity, this larva was oriented onto lateral view to focus liver, and the images were captured. These images were analyzed using ImageJ software for their liver size, liver degeneration and yolk sac retention. The areas of liver and yolk sac were traced to get liver size, and yolk sac retention and grey value of liver were measured to get liver degeneration.

Formulae for calculating these parameter were:

- Liver size = liver area (drug)/liver area (control) *100
- Percentage liver degeneration= [1-liver optical density (drug)/liver optical density (control)]*100
- Yolk sac retention=yolksac area (drug)/ yolksac area (control)*100

4.5.1.7.4. Neurotoxicity assay: Zebrafish is a good model to assess compound effects on developmental neurotoxicity. Acridine orange staining for apoptosis in brain is a good indicator of more specific neurotoxicity and the assay is simple and fast which provide a relatively high throughput whole-animal assay to identify compounds that are potentially neurotoxic. After collecting the data for cardiotoxicity (heart beats of each chamber) and hepatotoxicity (liver images), the larvae were stained with acridine orange using 2 μ g/ml solution of dye in E3 medium for 30min. The larvae were rinsed thoroughly twice in fresh E3 medium to wash the acridine orange solution. Stained larvae were anesthetized with tricaine and photographed under UV illumination using Zeiss AxioCamMR camera attached to a

Zeiss fluorescence microscope (GFP filter set : excitation 473, emission 520) under 5X magnification. Images were taken and analyzed for number of apoptotic cells in the brain region using ITCN plugin for imageJ.

4.5.1.8. Statistical analysis: Statistical analysis was performed using GraphPad Prism 5.01 software. The data were expressed as the mean and standard error of the mean (\pm SEM), and subjected to One-way ANOVA followed by Tukey's Multiple Comparison Test, and all treatment groups were compared with the PTZ treated group. Seizure score for dose response evaluation of Ligand-9 was done using two-way ANOVA followed by Bonferroni's post tests. Statistical significance was set at the $p < 0.05$ level. Toxicity evaluation of Ligand 9 was done by using Two way & One way ANOVA followed by Bonferroni's & Dunnet's post-test.

4.5.2. In-vivo anti-epileptic evaluation

4.5.2.1. Chemicals: Sodium valproate, Phenytoin, Pentylnetetrazole, (PTZ) and strychnine, (STY) (Sigma-Aldrich, India), Picrotoxin (PIC) (Himedia, Mumbai, India), Acetic acid, Formalin, Indomethacin, Carrageenan, MTT (3(4, 5dimethylthiazol2yl)-2, 5-diphenyltetrazolium bromide) were purchased from Sigma Chemical Co. (St. Louis, MO, USA). All other reagents used were analytical grade.

4.5.2.2. Experimental animals and treatment: Male Swiss albino mice (sainath agencies, Hyderabad) of average body weight of 25 ± 3 g and Wistar rats (200-250g) for scSTY & scPIC induced convulsions that were used in this investigation. The animals were housed in plastic cages with sawdust as beddings, and kept in an animal house where the temperature was $26^{\circ}\text{C} \pm 1^{\circ}\text{C}$, relative humidity of 45-55%, and 12:12 h light/dark cycles were maintained. All animals were acclimatized for at least 5-7 days before experiment and supplied with a standard animal feed and water *ad libitum*. They were fasted overnight before the experiment. All experiments were carried out between 10:00 a.m. to 04:00 p.m. Animal tests used in this

study were conducted in accordance with institutional animal ethics committee for the Care and Use of Laboratory Animals. All animals were treated with diethyl ether before sacrificing them.

The test compounds for the screening of anti-nociceptive and anti-inflammatory effects were coded as RS-4, RS-6, RS-9 and RS-12 were dissolved in 5% polyethylene glycol-400 for the various experimental procedures, and indomethacin was dissolved in carboxymethylcellulose before use.

4.5.2.3. Toxicity assessment (Neurotoxicity screening): In order to assess possible toxic effects of synthetic compounds (1,3,5-triazine-2,4,6-triamine derivatives) at the maximum dose (300 mg/kg), we observed the animals for 15 days after treating them with 24 different compounds (A_{2A} antagonists) and animal groups survived without any noticeable signs of toxicity or complications and did not display any abnormality in their gait and posture within this period. Those compounds were selected for further anticonvulsant activity assessment studies. Additionally, we assessed the possible effects of A_{2A} antagonists on the motor coordination and/or fatigue resistance on mice by using Rotarod test. A_{2A} antagonists treated animal groups which performed similar to control group animals in Rotarod test showing no alteration in motor performance, and only those (17 out of 24 A_{2A} antagonists) were considered for further studies.

4.5.2.3.1. Rotarod test

Minimal motor impairment was measured in mice (n=3) by the rotarod test (Rao *et al.*, 2005). Mice were trained to stay on an accelerating rotarod that rotates at 25 revolutions per minute. The rod diameter was 3.2 cm. Trained animals were given an ip/sc injection of the test compounds in doses of 300 and 100 mg/kg and were subjected to rotating rod before and after dosing (60 min and 120 min) respectively. Neurotoxicity was indicated by the inability

of the animal to maintain equilibrium on the rod for at least 2 min in each of the three trials. The animals were subjected to rotating rod before dosing and 1 and 2 h after dosing respectively.

4.5.2.3.2. Behavioural test using actophotometer: Test compounds (300 and 100 mg/kg) were screened for their behavioural effects using a photoactometer (Dolphin, India) at 30 min and 60 min after ip injection to mice. Behaviour of the animals inside the photocell was recorded as a digital score (Boissier *et al.*, 1965). Increased scores suggested good behavioural activity. The control animals were administered 10% PEG + citrate buffer (pH 4.5). Phenytoin was used as reference for comparison at a dose of 30mg/kg (p.o., in a 0.5% methylcellulose/water mixture). The observations are tabulated. The photoactometer was placed in a soundproof box, and mice were placed inside. The duration of the experimental observation was up to 10 min (2+8). After an initial period of 2 min during which the animals became accustomed to the new environment, the counter was reset and the remaining 8 min reading was noted. After each trial, the base was cleaned with 20% v/v ethyl alcohol.

4.5.2.4. Anticonvulsant screening methods: The initial anticonvulsant evaluation of the 1,3,5-triazine-2,4,6-triamine derivatives was established using slight modifications in standard protocols taken from NIH guidelines and from reported procedures (Yogeewari *et al.*, 2007; Krall *et al.*, 1978 and Swinyard *et al.*, 1952). Initially, all compounds were administered i.p. at doses of 30, 100 and 300 mg/kg to each group (4 animals mice/rat for doses 30 and 100 mg/kg and 1 animal for 300 mg/kg; if protected, tested in the remaining 3 animals (NIH standard protocol). Activity was established using one electrical and three chemical tests i.e. maximal electroshock seizure test (MES), subcutaneous pentylenetetrazole (scPTZ) seizure threshold (Mice models), subcutaneous strychnine (scSTY), subcutaneous picrotoxin (scPIC) seizure threshold test (rat models) and neurotoxicity tests. All observations

are tabulated at respective time points in each model for all synthesized compounds (1,3,5 triazine 2,4,6 triamine derivatives) and compared to the clinically proven antiepileptics, such as, sodium valporate and phenytoin.

4.5.2.4.1. Maximal Electroshock induced Seizures (MES): (Mouse model): One day prior to the administration of test compounds, animals were tested for sensitivity to electric shock and the animals which were unable to show hind limb extension were rejected. Animals were assigned into three groups viz., control, standard and test groups. The control group received 10% PEG + citrate buffer (pH 4.5) i.p, standard group animals were given phenytoin 25mg/kg i.p and test groups were injected with 1,3,5-triazine-2,4,6-triamine derivatives at dose levels of 300, 100 and 30mg/kg i.p. A maximal electroshock seizure threshold test was also performed for assessment of threshold for convulsions. Convulsions were induced with rectangular current pulses delivered by an Electroconvulsometer (Dolphin, India) with a constant current in milli amperes using corneal electrodes. Electrodes were soaked with saline containing 1% lidocaine was applied to the ears in order to ensure sufficient electrical conduction and to avoid pain. MES was applied at 60Hz alternating current of 30-36 mA intensity for 0.2 sec. Maximal seizure was defined by the tonic extension of the hind limbs to an angle close to 180° to the plane of body axis.

4.5.2.4.2. Pentylenetetrazole induced seizures (PTZ): (Mouse model): A dose of 60 mg/kg was given intraperitoneally to produce consistent generalized clonic seizures, and was used throughout the study. Maximal seizure was defined by the tonic extension of hind limbs to an angle close to 180° to the plane of body axis. Animals were assigned into three groups viz., control, standard and test groups. The control group received 10% PEG + citrate buffer (pH 4.5) i.p, standard group animals were given diazepam 5mg/kg i.p and test groups were injected with 1,3,5-triazine-2,4,6-triamine derivatives at dose levels of 300, 100 and 30mg/kg

i.p. 30 min after the administration of these substances to the respective groups, all the animals of assigned groups were administered with PTZ (60mg/kg; i.p). The time period before initiation of the first generalized convulsion and the duration of convulsion were accepted as a measure of anticonvulsive effect.

4.5.2.4.3. Strychnine induced seizures (STY): (Rat model):

Convulsions were induced with 1.8 mg/kg Strychnine hydrochloride (STY HCl) given in sub-cutaneous route. Maximal seizure was defined by tonic extension of the hind limbs to an angle close to 180° to the plane of the body axis. Compounds were given at 300, 100 and 30 mg/kg doses 30 minutes prior to STY injection. The time period before initiation of the first generalized convulsion and the duration of convulsion were accepted as a measure of anticonvulsive effect.

4.5.2.4.4. Picrotoxin induced seizures (PTX): (Rat model): In this model convulsions were induced with 2 mg/kg Picrotoxin (PIC) given in sub-cutaneous route.

4.5.3. Anti-nociceptive and anti-inflammatory evaluation

4.5.3.1. Eddy's hot-plate test in mice

This test was performed according to the method described previously by (Eddy and Leimbach, 1953), with some modifications. Groups of mice ($n = 3$) were treated with test compounds, RS-4, RS-6, RS-9 and RS-12 (10, 30 and 100 mg/kg, i.p), 10 mg/kg of indomethacin i.p. (positive control), and normal saline (normal control, 0.9%). After 30 min of treatment, animals were placed individually on hot plate warmed to 55 ± 0.5 °C and latency time (time for which mouse remains on the hot plate) was recorded in seconds by observing either jumping from hot surface or the first licking of the hind paws. Readings should be taken at an interval of 0, 30, 60, 90, 120 and 180 min after administration of test

compounds. A cut-off time of 20 sec was imposed for all animals, in order to prevent any damage to the animal's paws.

4.5.3.2. Tail immersion test in mice

This test was performed according to the method described previously by Sanchez-Mateo *et al.*, 2006, with some modifications. Groups of mice ($n = 3$) were treated with test compounds, RS-4, RS-6, RS-9 and RS-12 (10, 30 and 100 mg/kg, i.p), 10 mg/kg of indomethacin i.p. (positive control), and normal saline (normal control, 0.9%). Thereafter, terminal 2 cm portion of the mice tail was immersed into the water bath containing hot water maintained at 55 ± 0.5 °C. Pain response was taken as the time interval between immersion and withdrawal of the tail by the mice and these were taken at 30, 60, 90, 120 and 180 minutes after treatment. A cut-off time of 10 sec was maintained. After each reading the tail was dried carefully.

4.5.3.3. Acetic acid induced writhing model in mice

This test was carried out as described by (Koster *et al.*, 1959), with few modifications. Groups of mice ($n = 3$) were treated with test compounds, RS-4, RS-6, RS-9 and RS-12 (10, 30 and 100 mg/kg, p.o.), indomethacin (10 mg/kg, p.o.) (positive control), and normal saline (normal control, 0.9%). In this model, animals were pretreated with test and standard drugs and were given orally. After 30 minutes writhing was induced by intraperitoneal injection of 1% acetic acid in volume of 10 ml/kg body weight to each mouse. After 5 min of acetic acid administration, the number of writhes (abdominal constrictions) that occur within subsequent 30 min per animal was counted. Percentage of inhibition in writhing syndrome was calculated and compared with standard drug, which was taken as an index of analgesia.

Percentage of inhibition was evaluated using following formula:

$$\% \text{ inhibition} = \{(W_c - W_t) \times 100\} / W_c$$

Where, W_c = number of writhing of the control group

W_t = number of writhing of the treated group

4.5.3.4. Formalin induced paw licking model in mice:

The test was performed as described by (Hunskar and Hole *et al.*, 1987). In this model, groups of mice ($n = 3$) were treated with test compounds, RS-4, RS-6, RS-9 and RS-12 (10, 30 and 100 mg/kg, i.p), indomethacin (10 mg/kg p.o) (positive control), and distilled water (normal control, 0.9%) 30 min before formalin injection. Antinociceptive activity of test compounds was assessed by observing licking time in the treated groups. 30 minutes after treatment, 20 μ l of 5% formalin in 0.9% NaCl was injected subcutaneously into the subplantar surface of the mouse's right hind paw and the time spent for licking the paw injected with formalin was recorded from 0 to 5 min (phase 1, neurogenic) and from 20 to 30 min (phase 2, inflammatory) after the formalin injection. Percentage of inhibition was evaluated using following formula:

$$\% \text{ inhibition} = 100 - (\text{Mean licking time of test drug} / \text{Mean licking time of control} \times 100)$$

4.5.3.5. Carrageenan-induced mice paw edema

The anti-inflammatory activities of test compounds RS-4, RS-9 and RS-12 were achieved by carrageenan-induced paw edema test in the hind paws of mice according to the method described by (Vinegar *et al.*, 1969). Groups of mice (6 per each group) were fasted for 24 h before conducting the experiment with free access to water. Test compounds RS-4, RS-9 and RS-12 were dissolved in 5% poly ethylene glycol-400 (PEG-400), and administered at the

doses of 30 mg/kg, i.p. The other groups were injected with standard drug (indomethacin, 20 mg/kg, i.p.) or vehicle (PEG-400). After 30 min, 50 μ L of 1% v/v carrageenan suspension in normal saline was injected into plantar side of right hind paws of the mice. Paw volume was measured by using plethysmometer (UgoBasile, Italy), immediately prior to the carrageenan injection and after 1, 2, 3, 4 and 5 h. The degree of swelling or paw edema volume was evaluated by delta volume ($x - y$), where x and y represents volume of the right hind paw after and before the carrageenan treatment, respectively. After measurement of paw edema, mice were sacrificed by an overdose of diethyl ether. Thereafter, the inflamed right hind paws of carrageenan-induced groups and normal group (non-carrageenan-induced) were excised at the fifth hour. The right hind paw tissue was rinsed and placed immediately in its four volumes (1g/4ml) of ice cold normal saline and homogenized at 4 °C. Then the homogenate was centrifuged at 12,000 rpm for 5 min. The supernatants were stored at -80 °C for the Gene expression analyses of inflammatory mediators like TNF- α , IL-1 β , IL-6 and NF κ B using Real Time PCR studies.

4.6. Gene expression analyses of inflammatory mediators using RT-PCR studies

4.6.1. Total RNA isolation and cDNA conversion

Total RNA was extracted in triplicate from the carrageenan-induced, naive and test compound treated hind paw tissues of mouse. The paw tissue was minced and treated with TRI reagent (Chomczynski *et al.*, 1993), according to the manufacturer's instructions (Sigma-Aldrich Co. LLC. USA). Concentrations and purity of RNA were quantified with Perkin Elmer VICTOR X3 (Perkin Elmer, Shelton, CT, USA) according to optical density. Purity of RNA was determined with A260/280 ratio (1.8–2.0 was considered pure). The protocol was described previously in the experiment section **4.3.3.1**

4.6.2. Detection of expression levels of inflammatory mediators

Real time PCR was performed according to the manufacturer's instructions using a BIO-RAD CFX Connect with SYBR green (Kapa Biosystems) as the fluorescent dye enabling real-time detection of PCR products. Synthetic gene specific primer sets used in PCR were shown in **Table 4.1**.

Table 4.1: Oligonucleotide sequences used for RT-PCR in mice brain samples

Primer	Oligonucleotide sequence	Tm (°C)	Reference
Mouse-TNF- α -FP	GACCCTCACACTCAGATCATCTTC	60.6	[Riekenberg <i>et al.</i> , 2009)
Mouse-TNF- α -RP	CCTCCACTTGGTGGTTTGCT		
Mouse-IL-1 β -FP	CTGGTGTGTGACGTTCCCATTA	64	[Liu <i>et al.</i> , 2006]
Mouse-IL-1 β -RP	CCGACAGCACGAGGCTTT		
Mouse-NF κ B-FP	GGCGGCACGTTTTACTCTTT	61.2	[Walmsley <i>et al.</i> , 2005]
Mouse-NF κ B-RP	CCGTCTCCAGGAGGTTAATGC		
Mouse-IL-6-FP	GCCCACCAAGAACGATAGTCA	62.2	[Liu <i>et al.</i> , 2004]
Mouse-IL-6-RP	GAAGGCAACTGGATGGAAGTCT		
Mouse-GAPDH-FP	GACATGCCGCCTGGAGAAAC	58	[Tsujiita <i>et al.</i> , 2006]
Mouse-GAPDH-RP	AGCCCAGGATGCCCTTTAGT		

4.7. HPLC method development for purity analysis of synthesised compounds

All final compounds were checked for purity with a common method for detection and developed using a Shimadzu HPLC system (Shimadzu Corporation, Kyoto, Japan). Chromatographic separation was achieved on an end capped Promosil C8 analytical column

(250 × 4.6 mm i.d., 5 μm) with pore size 100 Å, maintained at 40°C. A combination of acetonitrile and 10mM ammonium acetate (60:40, %v/v) was selected as mobile phase. The mobile phase was injected to the system using binary pumping mode at a flow rate of 1 mL/min. For all samples, injection volume and run time were fixed as 20 μL and 30 min, respectively and detection wavelength was at 254nm.

Results and discussion:
**Design, synthesis and
pharmacological evaluation
of novel A_{2A} antagonists**

5.1. Design, synthesis and pharmacological evaluation of novel A_{2A} antagonists in treatment of epilepsy

Epilepsy is a neurological disorder, characterized by the recurrent appearance of spontaneous seizures due to neuronal hyperactivity in the brain. In recent times, several new drugs, such as, felbamate, topiramate, gabapentin, lamotrigine, and levetiracetam have been used for treatment of epilepsy, although they are less efficacious than established AEDs. Current treatment strategies are found to be effective in only one third of epileptic patients. So there is a need to develop more tolerable and less toxic new antiepileptic drugs (AEDs) based on protein targets to yield broader spectrum of antiepileptic activity. The A_{2A} AR antagonists as antiepileptic drugs were less explored globally than A_1 AR agonists. Our research work describes the design and identification of 1, 3, 5-triazine-2, 4, 6-triamine derivatives as novel A_{2A} AR antagonists for treatment of epilepsy. Energy based pharmacophore modelling, cAMP inhibitory IC_{50} by HPLC assay and subsequent *in vivo* screening in an adult zebrafish model including cardio, hepato and neuro toxicity studies resulted in an initial hit compound Ligand-9. Docking-based SAR optimization of Ligand-9 and results of *in vivo* anti-epileptic models allowed us to identify two potent A_{2A} AR antagonists as novel antiepileptic drugs.

5.2. Energy based pharmacophore drug design

Potential antagonists that were expected to bind the extra cellular domain combined with a subtle repacking of transmembrane helices relative to the adrenergic and rhodopsin receptor structure were defined by a pocket distinct from other structurally determined GPCRs and was identified by using pharmacophore modelling and docking methods. Pharmacophore models were built either based on information of binding site of the receptor or based on the previously identified antagonists for human A_{2A}. ASINEX drug-like database was filtered based on 3D similarity to pharmacophore hypotheses. Two-step docking was applied using Glide to predict binding modes and affinities of compounds in the filtered database. After thorough visual inspection, the compounds were further filtered based on interaction with Asn253 and Glu169, fitness to pharmacophore hypothesis. These hits were analyzed in detail to propose a set of antagonists for human A_{2A} receptor. Workflow of the study is shown in

Figure 5.1.

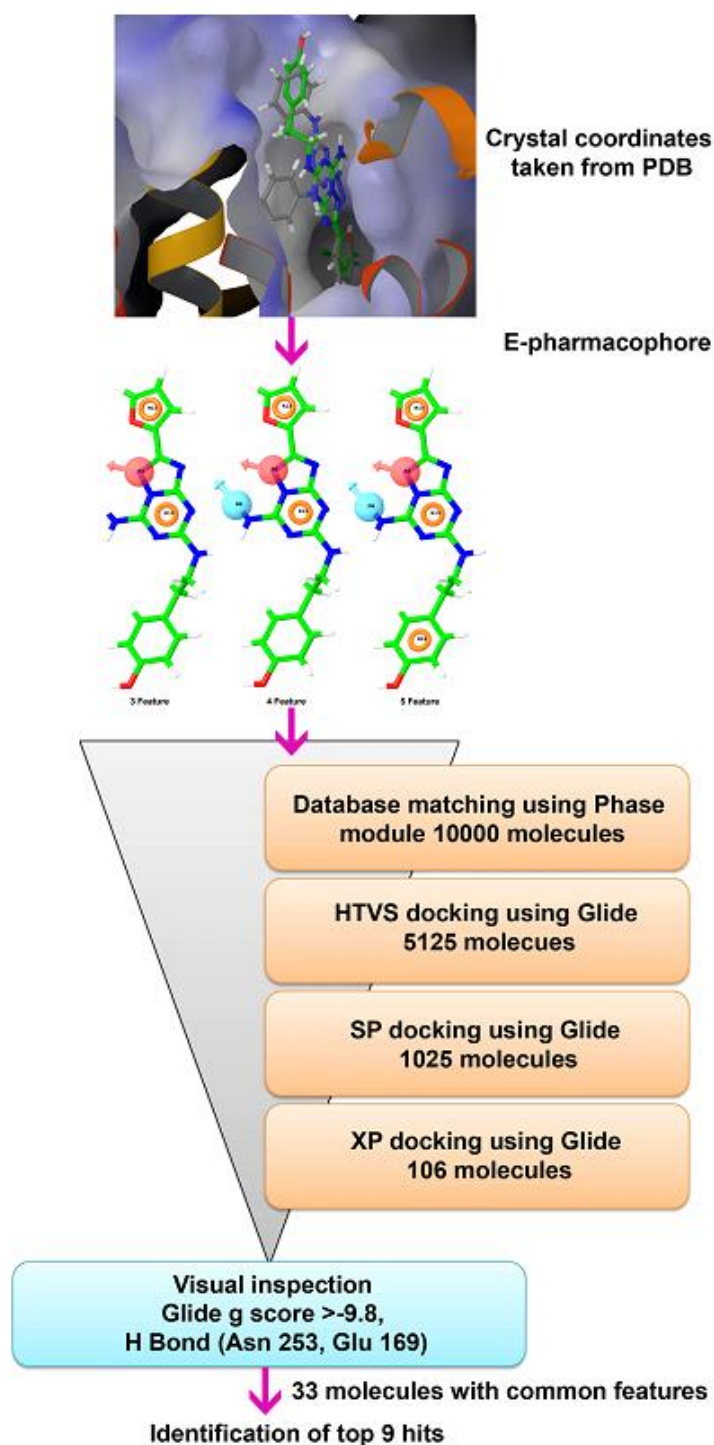


Figure 5.1: Workflow for identification of initial hits of Adenosine A_{2A} antagonists by e-pharmacophore modeling and in silico docking. The protocol started by using crystalstructure of Human A_{2A} receptor in complex with one of the antagonists (PDB code: 3EML) as a template.

5.2.1. Protein preparation and active site validation

The 2.6 Å crystal structure of human A_{2A} receptor bound to ZMA241385 was retrieved from protein data bank and used for structure-based pharmacophore modelling (**Figure 5.2**).

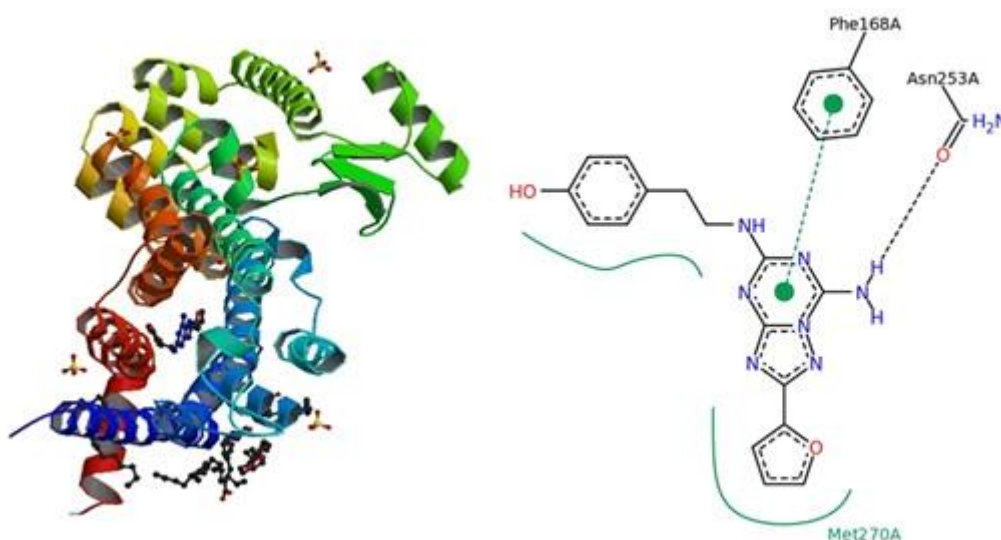


Figure 5.2: 2.6 Å crystal structure of human A_{2A} receptor (3EML) bound to ZMA241385.

The extra cellular domain combined with a subtle repacking of transmembrane helices consisted of one chain and the inhibitor was bound within helices II, III and V domains. The reference inhibitor showed two key interactions with Asn253 and Glu169. For validation of active site cavity, inhibitor bound to the protein was removed and prepared using Ligprep, and redocked with active site residues of the human A_{2A} receptor protein. The redocked ligand exhibited a glide score of $-9.01 \text{ kcal mol}^{-1}$ and was found in the vicinity of important amino acids like Asn253, Phe168, Glu169, Leu249, His250, His278, Asn181, Ile274 and Leu267 (**Figure 5.2**). Redocking results showed that the ligand exhibited similar interactions to that of original crystal structure with a RMSD of 0.798 Å.

5.2.2. Pharmacophore generation

Structure-based pharmacophore sites were identified using redocking of crystal ligand to allosteric binding site of human A_{2A} receptor. The descriptive information from energetic terms and binding modes of different conformers of antagonist were used to determine five pharmacophore sites (site score ≥ 2.0) by e-Pharmacophores script of Phase module. Hypotheses composed of three sites were selected to allow sampling of a wider range of compounds, and as the number of sites increases, pharmacophore model becomes more restrictive. Sites with higher energy contribution were included if they were less than 10 Å away from each other. The only ring feature detected among the seven sites was R15 which was included to assure the π - π stacking interaction between the ligand and Phe168 of human A_{2A} receptor. Consequently, one hypothesis was created using A2, D9, R13, R14 and R15 (ADRRR hypothesis), another one was created using A2, D9, R13 and R14 (ADRR hypothesis) and one more with A2, D9 and R13 (ADR hypothesis) (**Figure 5.3**).

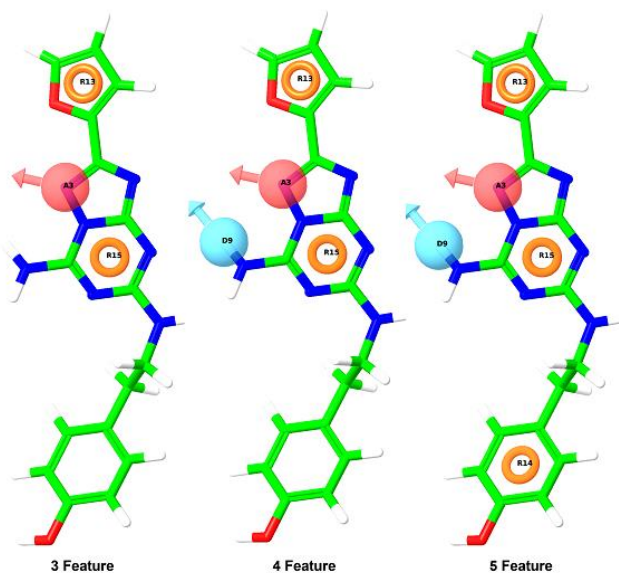


Figure 5.3: E-pharmacophore hypothesis.

Note that ADRR and ADRRR might select ligands that have similar hydrophobic character with double ring substructure of crystallised antagonist, while ADR hypothesis would select ligands with a different chemical scaffold from crystallised antagonist. Pharmacophore filtering with ADRRR, ADRR and ADR hypotheses were performed separately for the generated ASINEX database and 5,00,000 compounds with the highest fitness scores were saved for each hypothesis.

5.2.3. Validation of constructed pharmacophore models

The enrichment results for all the three pharmacophoric hypotheses were compared based on enrichment factor (EF), BEDROC ($\alpha = 20.0$) and % of active based on recovery rate of actives against ranked decoy database as shown in **Table 5.1**.

Table 5.1: Validation of pharmacophore hypothesis.

Pharmacophore	EF	GH	%Ya	%A	F(-ve)	F(+ve)
A2D9R13R14R15	11.6	0.281	25	40.9	13	27
A2R13R14R15	5.29	0.173	11.39	40.9	13	70
A2D9R13R14	9.5	0.246	20.45	40.9	13	35
D9R13R14R15	2.51	0.179	5.41	100	0	384
A2D9R13	8.44	0.008	18.18	36.36	14	36

EF	Enrichment Factor
GH	Goodness of hits
%Ya	% Yield of actives
%A	% Ratio of actives
F(-ve)	False negatives
F(+ve)	False positives

This not only helped us to eliminate the pharmacophore sites which lacked significant interactions but also to prioritize sites for further virtual screening. Hence, from this methodology we obtained both good enrichment as well as diversity in our hits. The energy contribution between ligand and every amino acid in the binding site always were key things in the ligand-receptor complex. The enrichment factor reflected the capability of a screening

application to detect active ligands (true positives) compared to random selection. Thus, its value was expected always to be greater than 1 and the higher it was, the better the enrichment performance of the virtual screening. A second enrichment metric, the Boltzmann-enhanced discrimination of receiver operating characteristic (BEDROC) was also used as a way to ensure that the results and conclusions were significant and generalized the receiver operating characteristic (ROC) that addressed the “early scoring problem” by Boltzmann weighting the hits based on how early they were retrieved. Based on the recovery rate of actives against the total 1020 compounds, 20 were known inhibitors of human A_{2A} receptor and 1000 were the decoy set which represented inactives. Where 5 point (A3, D9, R13, R14 and R15) that showed EF at 1% is 11.6 and GH is 0.28 which were considerable for the selection process, 4 point (A3, D9, R14 and R15) showed EF at 1% is 9.5 and GH is 0.246 and 3point (A3, D9 and R15) showed EF at 1% is 8.44 and GH is 0.81.

5.2.4. Docking analysis of compounds in human A_{2A} receptor

5125 compounds obtained separately by filtering the ASINEX database with structure-based ADRRR, ADRR and DRP hypotheses were initially docked to Human A_{2A} receptor in HTVS mode and scored with glide scoring function. 20% top scoring (~1025) molecules were redocked using SP docking and the top 10% of (~106) were redocked using XP docking [GScore values (-11.4 to -8.26 kcal/mol)]. The docked hits from the SP showed a sharp decrease in their GScore values from -12.09 kcal/mol to almost -9 kcal/mol and after -9 kcal/mol, the decrease in GScore values was significantly smaller. Therefore, cutoff GScore value was chosen as -9.00 kcal/mol for docking hits of XP run. Total of 33 compounds were selected for visual inspection based on number of Hbonds, docking and fitness scores, from which 9 compounds were selected and procured from ASINEX. The chemical structures of these nine hits are illustrated in **Figure 5.4**.

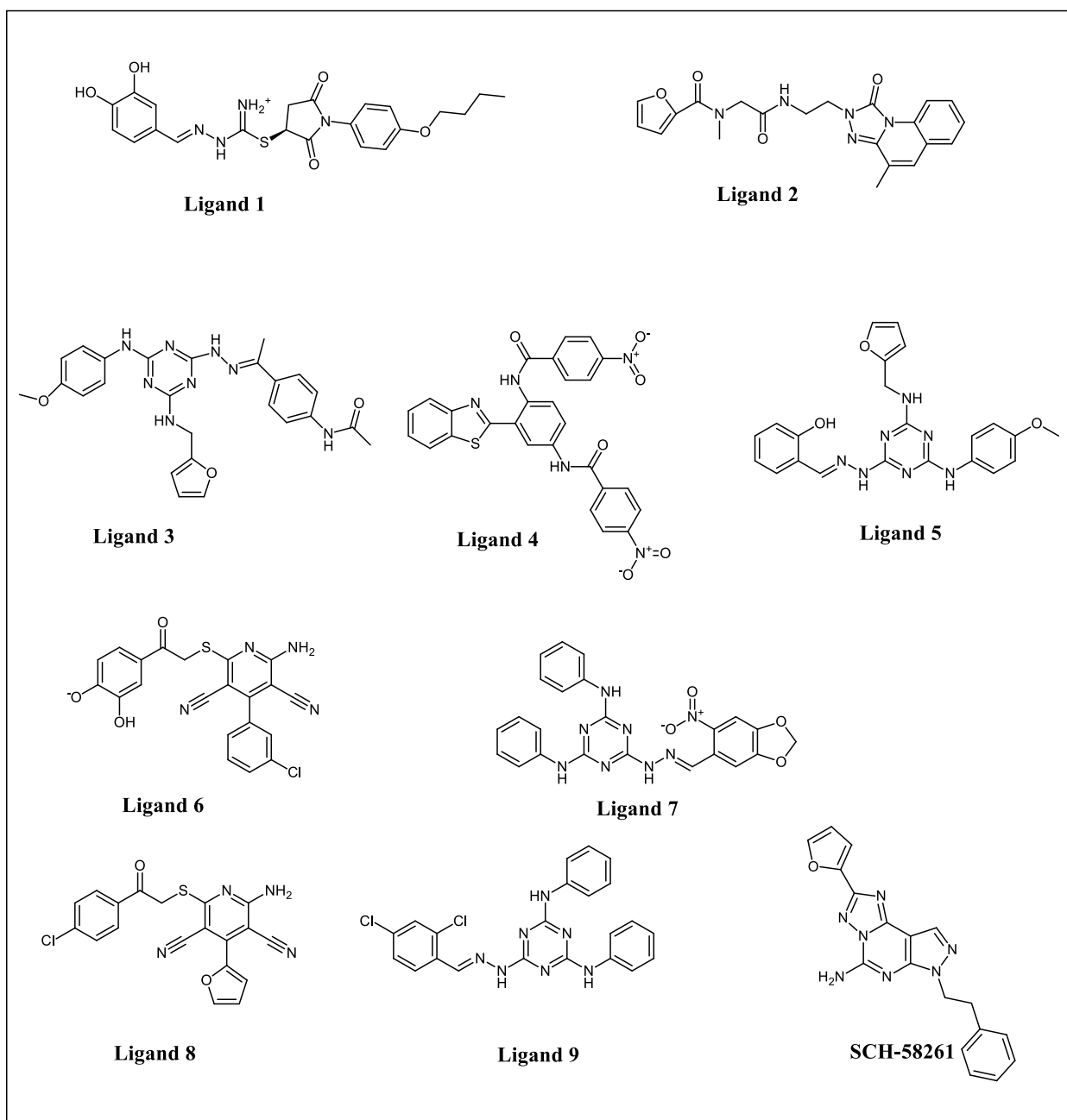


Figure 5.4: 2D chemical structures of top nine compounds and selective A_{2A} receptor antagonist (SCH-58261).

All these top 9 hits showed good docking score (-8.84 to -11.62) and interaction with important amino acids, such as, ASN253 and GLU169 and also with THR88, ASN181, and stacking interactions with HIS250, PHE168 and TYR271 amino acid residues, were well fit in the active site cavity of the protein. The docking score, H-bond and important interactions of these hits can be seen in **Table 5.2**. ADME Properties of Hits were calculated using the

QikProp module of the Schrodinger suite (**Table 5.3**). Predicted binding pose of best hit (Ligand 9) with key interactions in the binding site of human A_{2A} receptor is represented in **Figure 5.5**. Ligand interaction pictures of lead molecules from Ligand 1 to 9 along with crystal structure (3EML) can be seen in **Figure 5.6**.

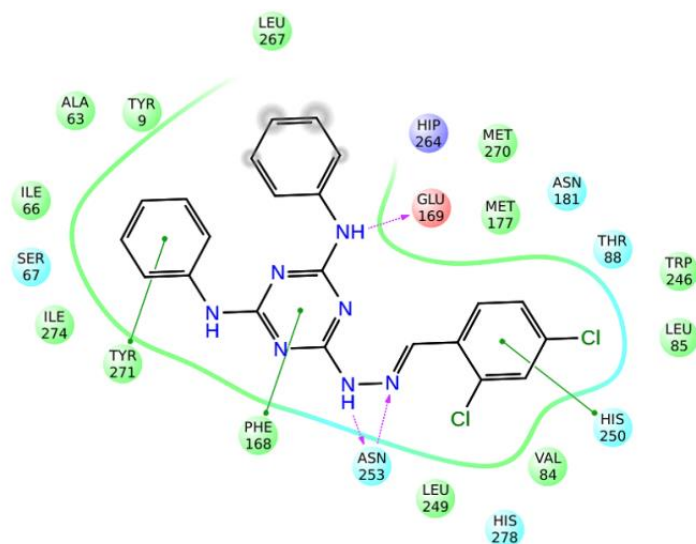
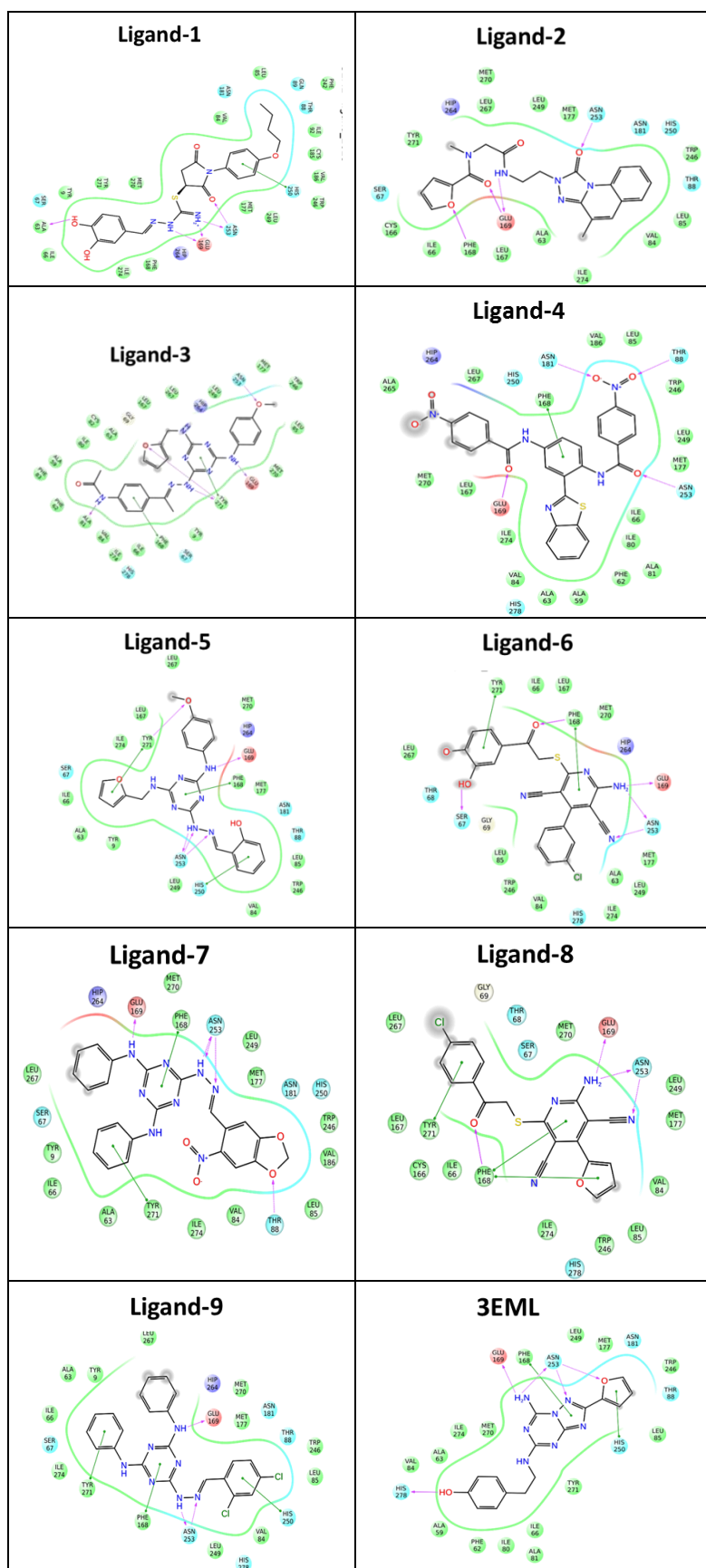


Figure 5.5: Interaction picture of most active compound (Ligand 9).

Figure 5.6: Ligand interaction pictures of lead molecules from Ligand 1 to 9 along with crystal structure (3EML).



Title	Docking Score	Glide Score	HBond	Fitness	Hbond forming AA	Stacking interaction:	Asinex-No
Ligand 1	-11.19	-11.64	5	1.79	Asn253, Glu169, Ala68	His250	BAS00105071
Ligand 2	-11.59	-11.59	4	1.58	Asn253, Glu169, Phe168	—	SYN13193209
Ligand 3	-11.14	-11.18	4	1.81	Asn253, Glu169, Tyr271, Ala81	Tyr271, Phe168	BAS00384626
Ligand 4	-10.22	-10.22	4	1.62	Asn253, Glu169, Asn181, Thr88	Phe168	BAS00470856
Ligand 5	-10.11	-10.15	4	2	Asn253, Glu169, Tyr271	Tyr271, His250	BAS00323139
Ligand 6	-8.84	-10.91	5	1.53	Asn253, Glu169, Phe168, Ser67	Phe168, Tyr271	BAS01369614
Ligand 7	-11.46	-11.46	4	2.31	Asn253, Glu169, Thr88	Tyr271, Phe168	BAS00350387
Ligand 8	-10.2	-10.2	4	1.94	Asn253, Glu169, Phe168	Phe168, Tyr271	BAS01178619
Ligand 9	-11.62	-11.62	3	2.13	Asn253, Glu169	Tyr271, Phe168, His250	BAS00137616
Crystal ligand	-9.01	-9.01	5	2.21	Asn253, Glu169, His278	Phe168, His250	PDB ID(3EML)

Table 5.2: *In silico* parameters (Docking Score, Glide Score, Fitness Scores, Hbond interacting amino acids, π - π stacking interactions of nine Asinex compounds including crystal ligand (3EML).

Table 5.3: ADME prediction for designed 9 compounds from Asinex database

Compd	MW ^(a)	QPlogPo/w ^(b)	QPlogS ^(c)	QPlogHERG ^(d)	QPPCaco ^(e)	QPlogBB ^(f)	% Human oral absorption ^(g)	Rule of five ^(h)
Ligand 1	456.52	2.52	-5.45	-6.97	37.2	-3.18	69.79	0
Ligand 2	431.45	3.54	-5.81	-8.11	623.85	-1.61	100	0
Ligand 3	470.45	3.37	-6.64	-7.27	633.73	-1.3	83.84	1
Ligand 4	458.52	4.32	-6.42	-7.4	1143.04	-1.23	100	0
Ligand 5	539.52	3.93	-8.34	-8.02	19.28	-3.06	47.06	2
Ligand 6	394.83	2.61	-6.43	-6.23	75.87	-1.94	75.85	0
Ligand 7	436.87	1.9	-6.79	-6.43	8.96	-3.31	55.12	0
Ligand 8	450.33	5.23	-7.06	-7.86	1716.35	-0.5	100	1
Ligand 9	407.43	2.37	-4.33	-5.37	346.81	-1.27	86.26	0

^a MW: molecular weight (acceptable range: 130 to 725); ^b Predicted octanol/water partition coefficient logP (acceptable range: -2.0 to 6.5); ^c Predicted aqueous solubility (-6.5 to 0.5); ^d Predicted IC50 value for blockage of HERG K⁺ channels.(below -5); ^e Predicted apparent Caco-2 cell permeability in nm/sec (<25 poor; >500 great); ^f Predicted brain/blood partition coefficient (-3.0 to 1.2); ^g Percent human oral absorption (<25% is poor and >80% is high); ^h Rule of 5 violation (mol_MW < 500, QPlogPo/w < 5, donorHB ≤5, acceptHB≤10).

5.3. Biology

5.3.1. Effect of ethanol on Cyclic AMP

From earlier reports it was found that $A_{2A}AR$ is expressed by MCF-7 breast cancer cells (Etique *et al.*, 2009). When MCF-7 cells were exposed to acute alcohol causes, there was an increase in extracellular adenosine by inhibiting adenosine uptake via nucleoside transporter (Matos *et al.*, 2013) that activated the A_2 adenosine receptor, which led to an increase in cAMP levels. Treatment of these cells with specific $A_{2A}AR$ antagonists prevented alcohol-induced increase in cAMP levels.

When MCF-7 breast cancer cells were treated for 24 h with different concentrations of ethanol, we observed 0.1% ethanol-treated cells showed increased cAMP levels for 3-4 times compared to untreated control cells (**Figure 5.7**). The levels of cyclic AMP accumulated in MCF-7 breast cancer cell lines stimulated by 0.1% ethyl alcohol over a period of 24 h were investigated. To assess that, a simple HPLC method has been developed and validated for the quantitative estimation of cAMP in ethanol treated MCF-7 cell lines.

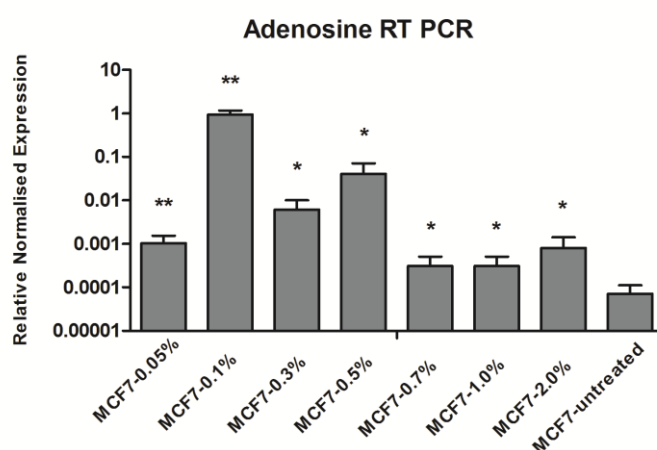


Figure 5.7: RT-PCR of adenosine in MCF-7 cells (Conc. of ethanol. Vs Normalized expression) Relative normalized expression of A_{2A} in Ethyl alcohol induced MCF-7 cell lines. The mRNA expression values were given as mean \pm SD normalised to GAPDH levels

in each sample. Y-axis values represent number of mRNA copies relative to the number of GAPDH copies in the sample. A significant increase was noticed in the expression of A_{2A} in comparison to ethyl alcohol treated cells to naive (*P<0.05) and (**P<0.01) at 95% confidence intervals.

5.3.2. Validation of Cyclic AMP Peak

Validation of peak for cyclic AMP in tissue extracts (MCF-7 cells) was carried out using the following methods: 1) by comparing the retention time of sample peak with a reference standard (Cyclic AMP) 2) co-chromatography of sample with a reference standard. For validation of cyclic AMP peak, chromatograms of tissue extracts were compared with chromatograms of standard Cyclic AMP. Chromatogram of a cyclic AMP reference standard which has a peak with a retention time of 4.1 min is shown in (**Figure 5.8**). Sample peaks present at a retention time of 4.1 min were tentatively identified as cyclic AMP alone in whole cell lysate (**Figure 5.9**).

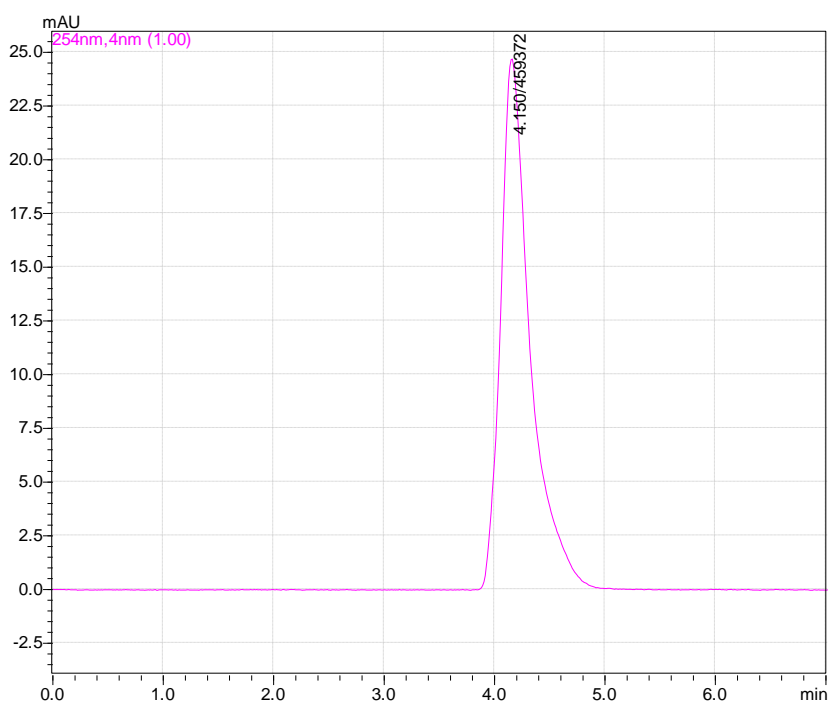


Figure 5.8: HPLC Chromatogram of standard cAMP at a concentration of 12.5ppm

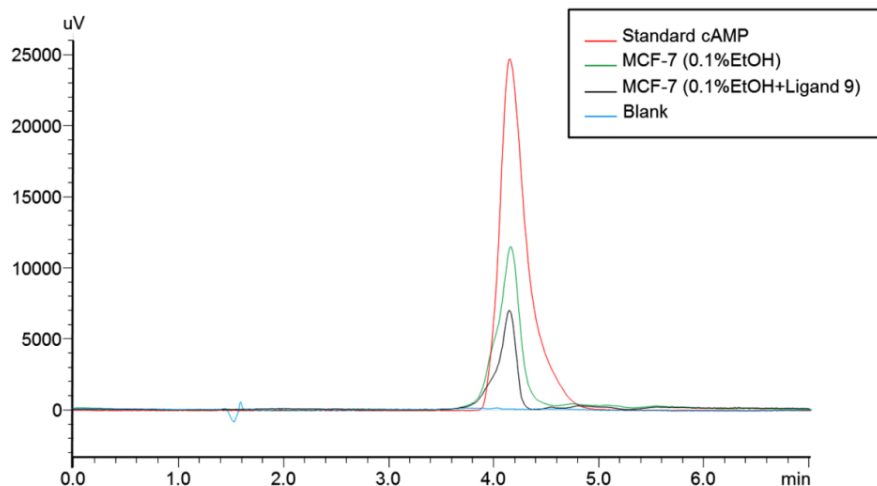


Figure 5.9: Over lay of HPLC Chromatogram of standard cAMP and Ligand 9 along with blank.

5.3.3. Linearity

The mean regression equation of standard curve for cAMP was $y = 34409x + 37972$, where y presented peak area and x was the concentration of cAMP. Calibration curve was linear over the studied concentration range (3.125–100 ppm) with a correlation coefficient more than 0.99 (**Figure 5.10**).

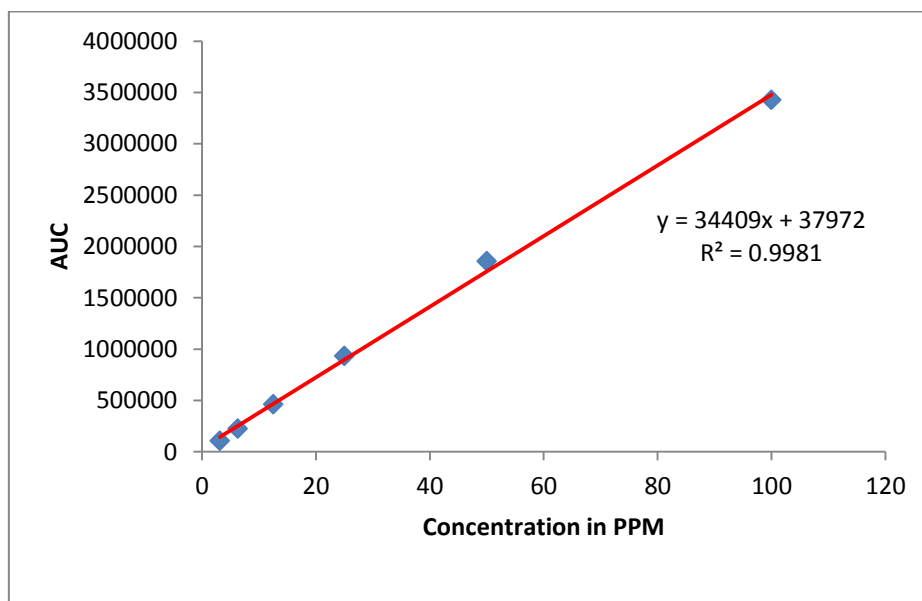


Figure 5.10: Calibration curve of standard cAMP.

In the HPLC assay, all the nine compounds and the standard A_{2A} antagonist were tested at different concentrations (25 μM, 12.5 μM, 6.25 μM, 3.125 μM and 1.5 μM) and % inhibitions were calculated by taking 0.1% alcohol (for 24h) treated cells as control to determine IC₅₀ of all compounds using Graphpad prism software. The representative dose response curves (DRC) were shown in **Figure 5.11**. Out of nine compounds, seven compounds displayed cAMP inhibitory IC₅₀ <100 μM, of which six compounds demonstrated IC₅₀ < 50 μM, five compounds showed IC₅₀ < 10 μM and one compound (Ligand 9) was found to decrease cAMP level at an IC₅₀ of 2.065 μM. Ligand 9 emerged as the most promising lead as the cAMP inhibitory IC₅₀ of Ligand 9 (2.065μM) was almost similar to the cAMP inhibitory IC₅₀ of standard selective A_{2A} receptor antagonist SCH-58261(1.399 μM),

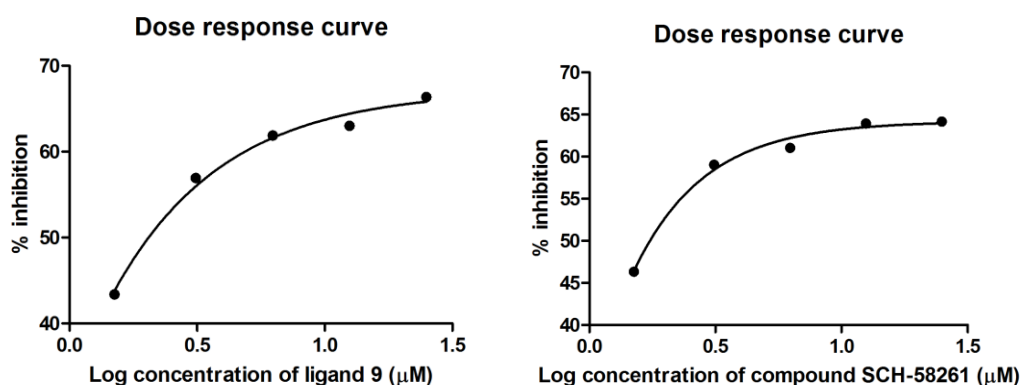


Figure 5.11: Dose-response curve of top active compound (Ligand 9) Vs SCH-58261.

Selectivity index (SI) is a comparison of the amount of therapeutic agent that causes biological effect to the amount that causes toxicity to understand specificity. Results are shown in **Table 5.4**. All compounds have shown >1 SI, which represent that compounds were selective towards disease model. Comparatively Ligand 2 and 9 have shown SI of >300 and 285.8 respectively.

Table 5.4: Biological data of selected Asinex molecules

Compd	IC ₅₀ (μM) ^a	CC ₅₀ (μM) ^b	EC ₅₀ (μM) ^c	SI (CC ₅₀ /EC ₅₀)
Ligand 1	>25	21.422±0.541	1.542±0.412	13.909
Ligand 2	6.263±0.33	63.143±4.121	0.021±0.005	>300
Ligand 3	6.485±0.09	7.129±1.547	1.342±0.063	5.313
Ligand 4	18.44±0.08	5.312±1.419	0.164±0.054	32.392
Ligand 5	>25	6.143±0.543	0.357±0.098	17.198
Ligand 6	>25	8.743±3.214	0.412±0.074	21.213
Ligand 7	7.287±0.18	7.124±4.127	1.218±0.124	5.848
Ligand 8	5.855±0.39	6.123±0.621	0.148±0.094	41.371
Ligand 9	2.065±0.07	24.011±5.214	0.084±0.004	285.833
SCH-58261	1.399±0.07	66.124±5.124	1.141±0.157	57.952

^a -cAMP inhibitory concentration in MCF-7 cell lines, ^b - Cell cytotoxicity of compounds on HEK-293 cell lines, ^c - Effective concentration of compounds on 0.1% EtOH induced MCF-7 cell lines; All data presented as Mean±SEM (n=3).

5.4. Zebrafish behavioural and toxicity studies:

5.4.1. Visual assessment of seizure-like behaviour in response to PTZ and Ligand-9:

One of the typical phenomena observed during seizure-like behaviour of zebrafish is circular movement, and it is directly proportional to seizure intensity. These circular movements which we term as rotations are defined as the number of 360° turns either in clockwise or anti-clockwise direction. After recording the behavioural movements of zebrafish over a period of 8 min, rotational movements were counted manually with naked eye. According to the above definition, we found that the number of rotations increased in PTZ treated fish compared to untreated fish. At 50 and 75 mg/kg, Test compound (Ligand-9) reduced the number of rotations in a dose-dependent manner, but at 25 mg/kg, it did not have any effect (Figure 5.12).

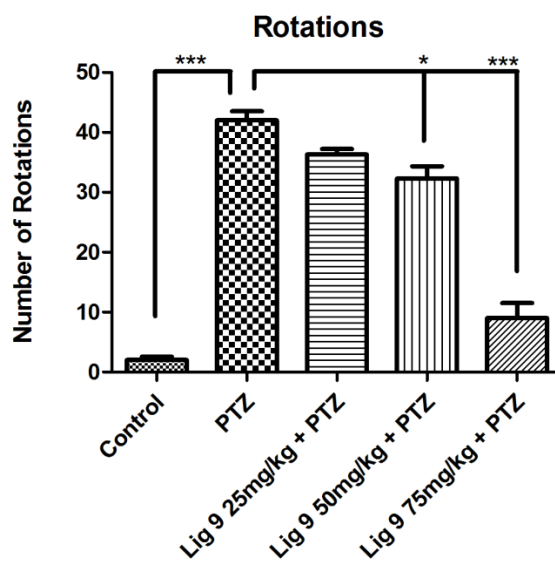


Figure 5.12: Rotational movements of orally administered Ligand 9 (25 mg/kg, 50 mg/kg, 75 mg/kg) on seizure-like activity induced by intraperitoneal injection of PTZ (220 mg/kg) (* $p < 0.05$, ** $p < 0.01$, *** $p < 0.001$).

This study represents evaluation of test compounds in PTZ induced seizure model in adult zebrafish (standard 8 min. protocol). Initially Ligand-9 was selected based on physicochemical properties and docking score for titration of dose, and based on its activity a 50 mg/kg oral dose was considered a reference dose. All test compounds were screened at 50 mg/kg oral dose and scored for seizure scores. Seizure scores were evaluated at every minute from 1 min. – 8 mins. Overall seizure score assigned to each fish was the mean seizure score over the period of 8 min observation (**Figure 5.13**).

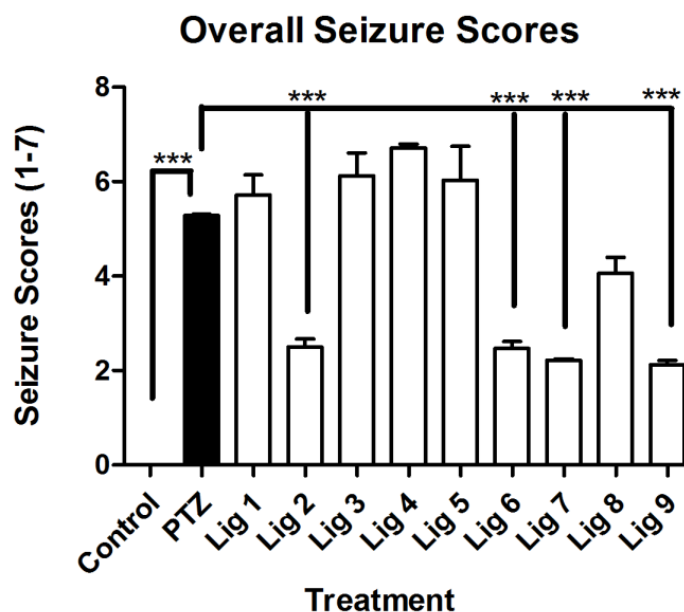


Figure 5.13: Overall Seizure Scores (Mean \pm S.E.M.) for fish treated with various compounds. Statistical analysis was carried out using One-way ANOVA followed by Tukey's Multiple Comparison Test and all treatment groups were compared with the PTZ treated group.

Test compounds numbered Ligand 2, 6, 7 and 9 showed clear anti-epileptic potential (**Figure 5.14**). Ligand 9 was convincingly most potent and effective compound to show anti-epileptic properties. Other compounds did not show any neuro-protection to the PTZ challenge (**Figure 5.15**). Result suggested that efficacious compounds were absorbed from the intestine and also penetrated the BBB. This observation warranted a need for optimising the dose of Ligand-9 at which it would show antiepileptic activity. Therefore, we carried out dose response evaluation for Ligand-9 by following the same protocol, as described in experimental setup section.

Compounds with neuroprotection(Ligands 2,6,7,9)

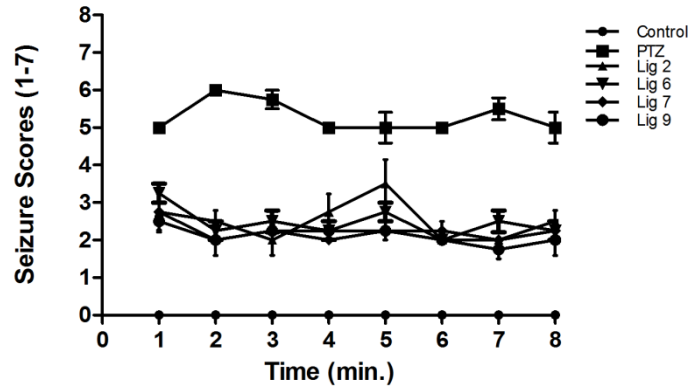


Figure 5.14: Seizure score at every minute time point, representative to neuro-protection to PTZ challenge.

Compounds with no neuroprotection (Ligands 1,3,4,5,8)

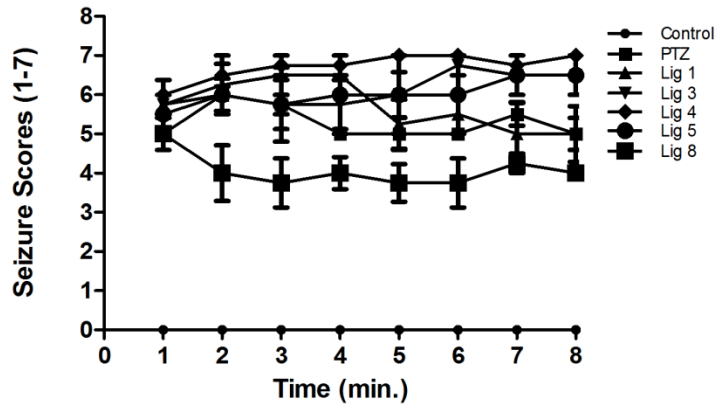


Figure 5.15: Seizure score at every minute time point, suggesting no neuro-protection to PTZ challenge.

Seizure-like activity of adult zebrafish was assessed in terms of qualitative scoring system (1–7) described in the experimental setup section. The mean seizure scores (\pm SEM) for each group (6 fish per treatment group) were plotted against the time after PTZ administration with respect to the control group (Figure 5.16).

Seizure score of ligand 9

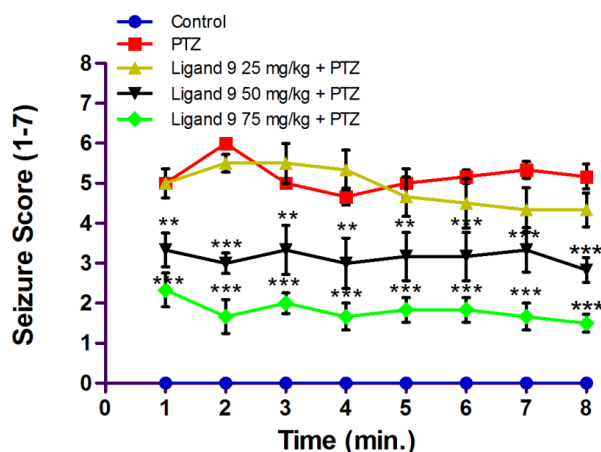


Figure 5.16: Visual assessment of seizure-like activity in adult zebrafish. Mean seizure scores (\pm SEM) for each group were assessed using a scoring system (1 through 7, see experimental setup section) after pentylenetetrazole injection with or without Ligand-9 pretreatment (* $p < 0.05$, ** $p < 0.01$, and *** $p < 0.001$). Statistical significance was analyzed as PTZ group vs. all groups.

Based on seizure score, seizure-like activity levels in PTZ-treated zebrafish were found higher than in Ligand-9-pretreated fish. Seizure scores of PTZ treated group ranging between stages 4 and 6 were statistically significant at all-time points compared to control group. Ligand-9 pre-treatment at 25 mg/kg resulted in seizure scores ranging from stages 4 to 6 which were statistically non-significant at all-time points compared to PTZ group. Pre-treatment at higher doses of 50 mg/kg and 75 mg/kg caused the fish to exhibit a seizure score ranging between stages 1 and <4 which were statistically significant compared to the PTZ group except for four time points (1,3,4 and 5 min) in the 50-mg/kg-treated group.

This study presents the evaluation of the effects of Ligand 9 pre-treatment on PTZ induced seizure-like behaviors such as excessive involuntary locomotary movements, intermittent immobility, high frequency convulsions and visible muscular spasms in an adult zebrafish. The test compounds were administered orally, and the chemoconvulsant PTZ was administered intraperitoneally. Here, we found that the drug administered in an adult

zebrafish through oral route is a simple, precise and easy method for accurate delivery of drugs. Behavioural assessment studies clearly indicate a good *in vivo* seizure model with controlled drug treatment. Furthermore, it appears to be an appropriate animal model for primary screening of drug candidates in the central nervous systems-related diseases and assessing their dose-related effectiveness.

The seizure score indicates dose dependent and statistically significant response of Ligand 9 in reversion of PTZ induced seizures starting from 25mg/kg until 75mg/kg (**Figure 5.17**).

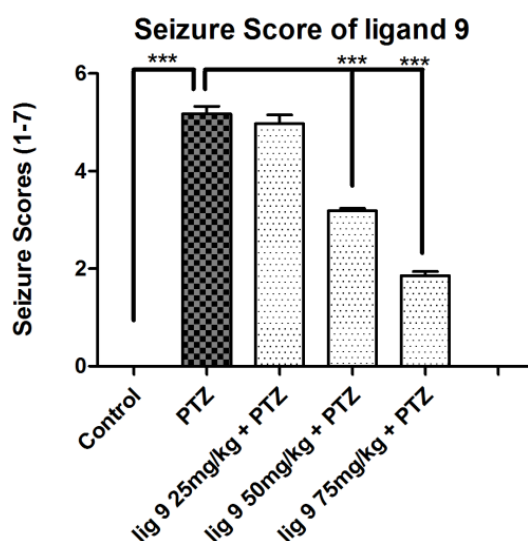


Figure 5.17: Overall Seizure Score (Mean \pm S.E.M.) for fish treated with Ligand 9 (25 mg/kg, 50 mg/kg and 75 mg/kg). Statistical analysis was carried out using One-way ANOVA followed by Tukey's Multiple Comparison Test and all treatment groups were compared with the PTZ treated group.

However, similar effect was not observed with 100 mg/kg and it was considered a saturation dose. Ligand 9 at a dose of 75mg/kg had shown better response when compared to all other groups ($P < 0.001$). Overall seizure score suggests that Ligand 9 at a dose of 75mg/kg showed maximum reversion of seizures followed by 50mg/kg. The reversion was statistically significant with P value < 0.001 . Overall, Ligand 9 pretreatment significantly suppressed 220-mg/kg pentylenetetrazole-induced increases in rotational movements and visual

assessment of seizures in a dose–response manner. After considering the above results we can conclude that Ligand 9 at the dose of 75mg/kg showed neuro-protection in PTZ induced seizure model in adult zebrafish.

5.4.2. Toxicity evaluation of potent compound (Ligand 9):

5.4.2.1. Cardiotoxicity assay: The most potent compound was further examined for zERG channel inhibition by assessing arrhythmogenic potential in a zebrafish model. Abnormalities in auriculo-ventricular beat were very minimal at 30 μ M. whereas lower concentrations of Ligand 9 did not show significant effect on heart rate & auriculo-ventricular ratio, and found to be safe (**Figures 5.18-5.19**).

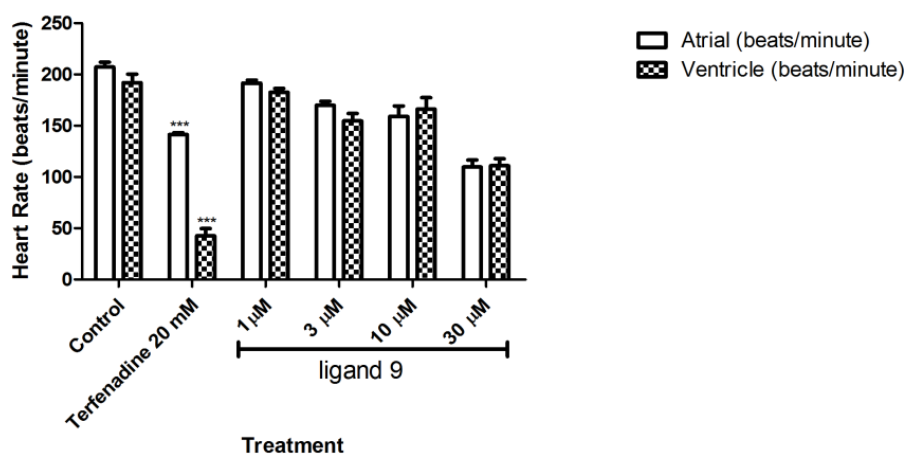


Figure 5.18: Mean (\pm S.E.M.) of the heart rates of atria and ventricles of Ligand 9 treatment groups. (* p <0.05, ** p <0.01 and *** p <0.001). Statistical significance was analyzed comparing control group vs. all groups.

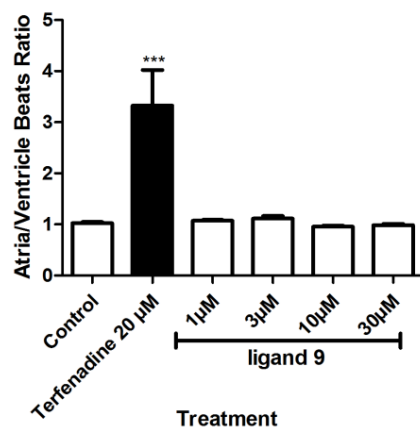


Figure 5.19: Mean (\pm S.E.M.) score of atrio ventricular ratio of Ligand 9 treatment groups. (* $p < 0.05$, ** $p < 0.01$ and *** $p < 0.001$). Statistical significance was analysed comparing control group vs all groups.

5.4.2.2. Hepatotoxicity assay: Ligand 9 at 30 μ M had significant effect on liver size and liver degeneration whereas Lower concentrations were found to be safe when compared to control (Figures 5.20-5.21).

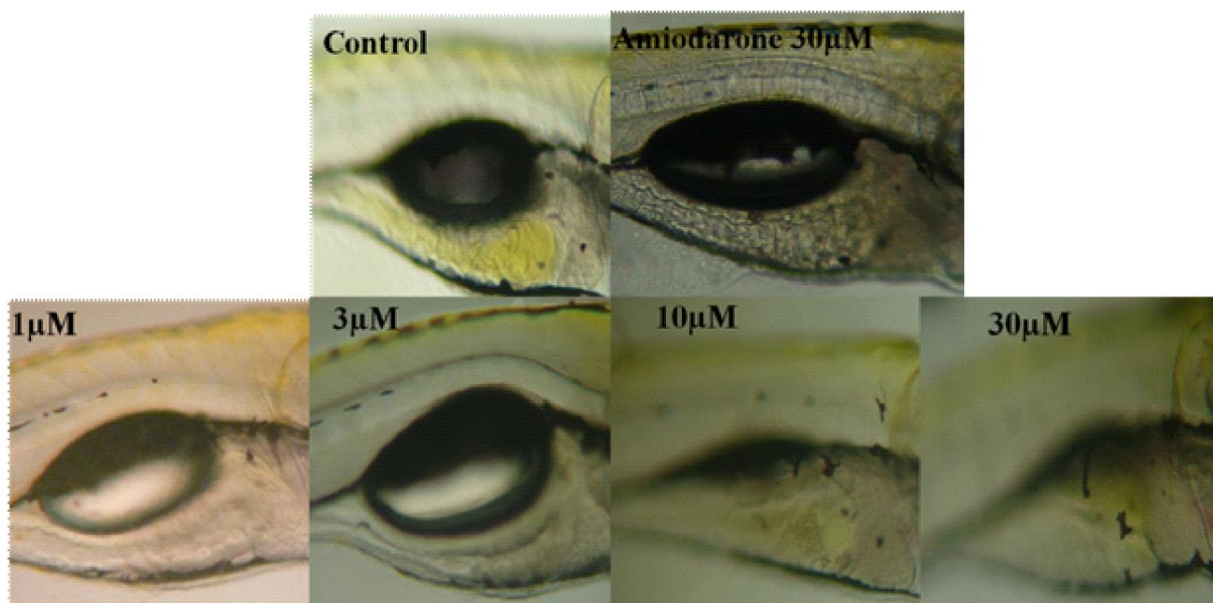


Figure 5.20: Representative images of hepatotoxicity assay.

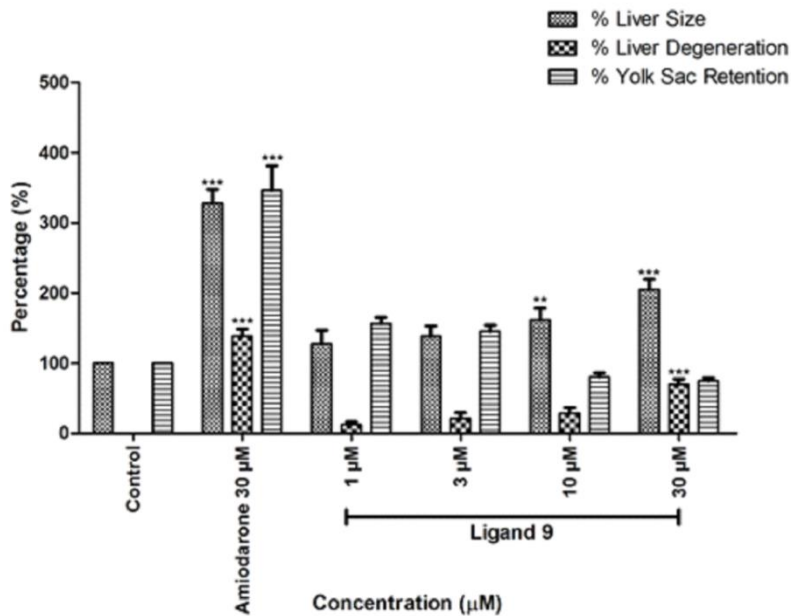


Figure 5.21: The graph represents qualitative data of % liver size, % liver degeneration & % yolk sac retention of Ligand 9 at different concentrations when compared to positive control Amiodarone.

5.4.2.3. Neurotoxicity assay: Ligand 9 did not show apoptotic activity at 1 & 3 µM whereas mild apoptotic activity was seen at 10µM, and significant apoptotic activity was seen at 30 µM (Figures 5.22-5.23).

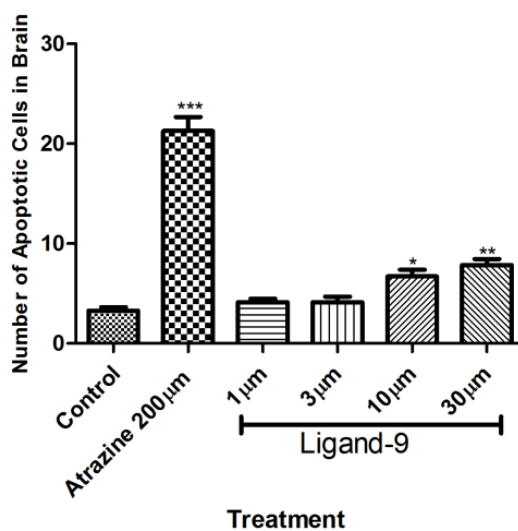


Figure 5.22: Qualitative data of Percentage Induction of apoptosis of Ligand-9 at different concentrations when compared to Atrazine.

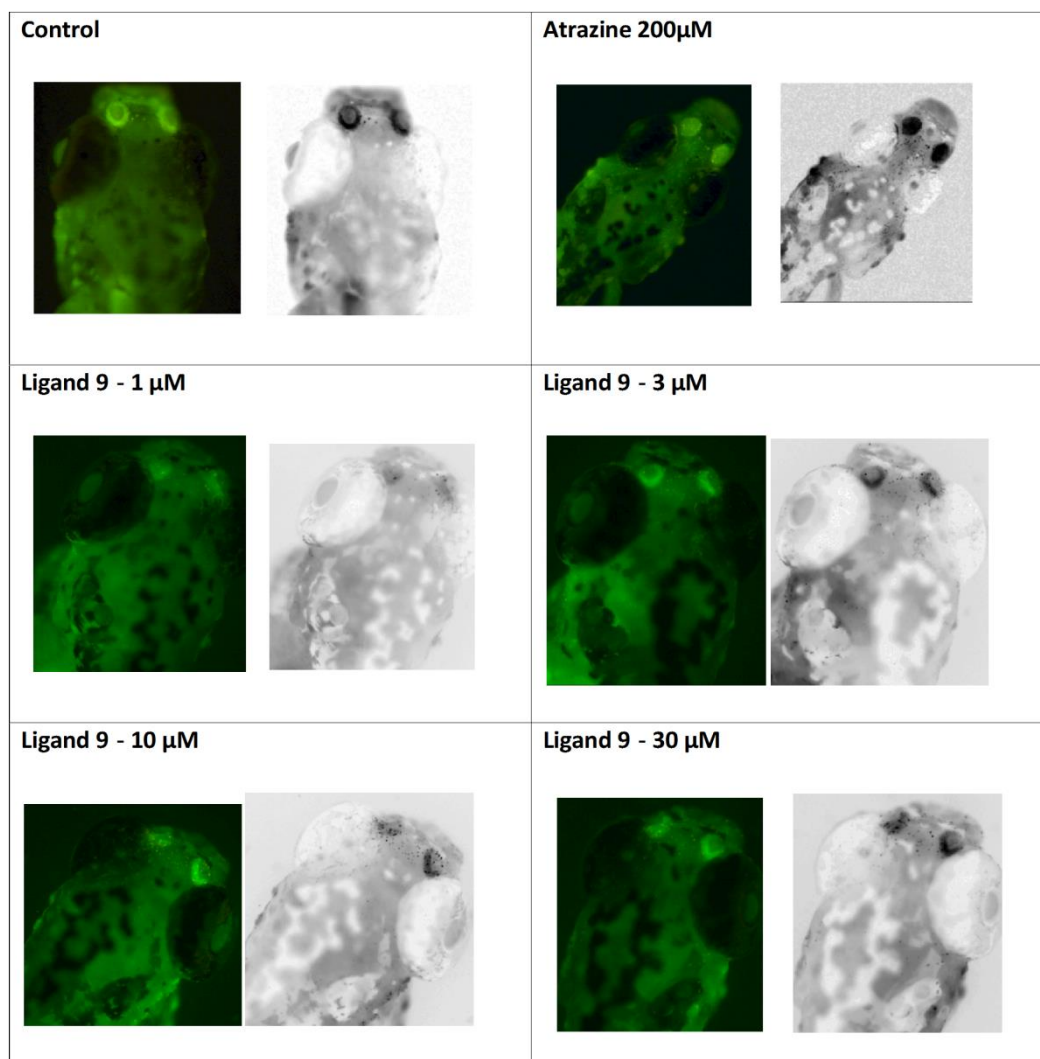


Figure 5.23: Representative images of embryos treated with compounds assayed for Apoptosis.

By considering toxicity data, Ligand 9 was found safe at lower concentrations except at 30 µM indicating an acceptable neuro, hepato, cardiovascular safety profile.

5.5. Estimation of cAMP levels by HPLC-Assay (for synthesised compounds)

In the preliminary screening, all the synthesized compounds (twenty four) were evaluated for their *in vivo* anticonvulsant activity. Compounds showed good activity in all four *in vivo*

mice/rat models (ten), and was evaluated for their *in vitro* cAMP inhibitory HPLC assay adapted as described previously and detailed extensively in the experimental section. SCH-58261 which had previously been demonstrated as a potent and selective A_{2A} receptor antagonist was used as a positive control and negative controls (without any inhibitory compounds) was used in the study. Representative dose response curves (DRC) were shown in **Figure 5.24**.

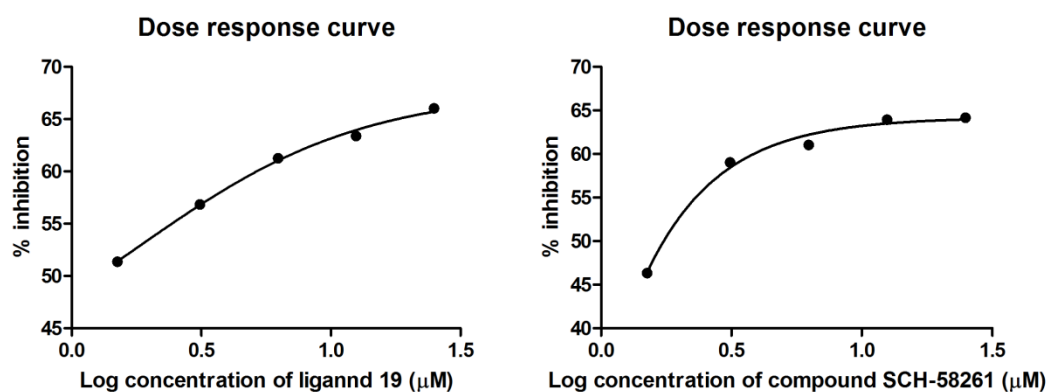


Figure 5.24: Dose-response curve of most active lead 19 and SCH-58261.

In the HPLC assay, out of ten compounds tested, eight compounds displayed cAMP inhibitory IC₅₀ <100 μM, out of which seven compounds demonstrated IC₅₀ < 20 μM, six compounds showed IC₅₀ < 10 μM and two compounds were found to decrease the cAMP level at sub-micromolar concentration (IC₅₀ < less 1 μM) which is less than the cAMP inhibitory IC₅₀ of standard selective A_{2A} receptor antagonist SCH-58261(1.399μM). Compounds 7 and 19 emerged as the most promising leads with cAMP inhibitory IC₅₀ of 0.29 and 0.96 μM respectively (**Table-5.5**).

All twenty four compounds were subjected to selectivity index analysis which is a ratio between cell cytotoxicity and growth inhibition. Among twenty four compounds, six

compounds showed SI of <1. Compounds 9,15,23,25 and 27 showed SI of >300, compounds 6 and 19 showed 285 and 190 respectively. The results are presented in **Table 5.5**.

Table 5.5: Biological data of synthesized molecules

Compd	IC ₅₀ (μM) ^a	CC ₅₀ (μM) ^b	EC ₅₀ (μM) ^c	SI (CC ₅₀ /EC ₅₀)
4	ND	8.121±1.241	0.597±0.188	13.612
5	ND	0.072±0.041	0.018±0.008	4.089
6	2.065±0.07	24.011±5.214	0.084±0.004	285.833
7	0.292±0.09	0.0212±0.001	0.033±0.024	0.491
8	1.503±0.03	0.056±0.021	2.232±0.531	0.022
9	3.977±0.10	1.765±0.213	0.003±0.001	>300
10	ND	0.084±0.016	0.720±0.231	0.114
11	2.152±0.25	0.075±0.031	0.198±0.01	0.337
12	19.89±0.08	0.148±0.054	0.165±0.01	0.848
13	>25	3.572±0.631	0.101±0.024	35.029
14	ND	0.098±0.031	0.005±0.003	17.077
15	6.203±0.21	30.578±0.614	0.057±0.012	>300
16	ND	0.123±0.063	0.535±0.021	0.225
17	ND	10.333±0.041	1.374±0.622	7.529
18	ND	0.921±0.347	0.016±0.017	54.347
19	0.966±0.02	5.092±0.631	0.03±0.018	190.005
20	ND	7.891±1.478	0.859±0.125	9.173
21	ND	0.453±0.541	0.021±0.012	21.507
22	ND	4.902±0.647	0.056±0.012	87.578
23	ND	11.201±0.031	0.014±0.005	>300
24	>25	2.327±0.654	0.156±0.031	14.814
25	ND	181.401±5.321	0.061±0.014	>300
26	ND	4.432±0.046	0.031±0.005	142.876
27	ND	40.991±5.631	0.065±0.002	>300
SCH-58261	1.399±0.07	66.124±5.124	1.141±0.157	57.952

^a-cAMP inhibitory concentration in MCF-7 cell lines, ^b-Cell cytotoxicity of compounds on HEK-293 cell lines, ^c-Effective concentration of compounds on 0.1% EtOH induced MCF-7 cell lines; all data presented as Mean ± SEM (n=3), ND-indicates compounds not determined.

5.6. Experimental section

5.6.1. Chemistry. The synthetic approach used to prepare 1,3,5-triazine-2,4,6-triamine derivatives was accomplished as presented in **Figure 5.25**. Final compounds (**4-27**) were prepared in three step reactions; first step involves S_NAr nucleophilic substitution reaction, which involves consecutive replacement of two chlorines in 2,4,6-tri chloro-1,3,5-triazine with aryl/alkyl/aliphatic amines (R_2) to afford 2,4 di-substituted 1,3,5-triazines (**2a-d**) and, subsequently, the second step involves substitution of remaining chloro group at 6th position with hydrazine hydrate in methanol to obtain a series of tri substituted 1,3,5-triazine derivatives (**3a-d**) in yields ranging 78-93%. Third step involves reaction of appropriate mono or di substituted benzaldehyde with the corresponding tri substituted 1,3,5-triazine derivatives (**3a-d**) by refluxing for 2h at 90°C in the presence of ethanol as a solvent to afford the final compounds (**4-27**) in variable good yields. Thin layer chromatography (TLC) was checked throughout the reactions to optimize for completion. Synthetic protocols used were based on the earlier reported procedures (Afonso *et al.*, 2006 and Radi *et al.*, 2010).

5.6.2. General. The homogeneity of compounds was monitored by thin layer chromatography (TLC) on silica gel 60 (pre-coated F₂₅₄ Merck plates), visualized by UV light and Iodine (I₂) treatment. Organic solutions were dried over anhydrous Na₂SO₄. Flash chromatography was performed on a Biotage Isolera with prepackaged disposable normal phase silica columns, and Chromatographies were performed using Merck 60–120 and 200–400 mesh silica gel. All ¹H and ¹³C NMR spectra were determined in DMSO-d₆ solutions with a Bruker AM-300 (300.12 MHz, 75.12 MHz) NMR spectrometer, Bruker BioSpin Corp, Germany. Chemical shifts are reported in ppm (δ) with reference to internal standard TMS. Coupling constants are referred to as *J* values in Hertz (Hz). The signals are designated as follows: s, singlet; d, doublet; dd, doublet of doublets; t, triplet; q, (quartet), m, multiplet. All reported products showed ¹H NMR and ¹³C NMR spectra in agreement with

the assigned structures. Molecular weights of synthesized compounds were checked by SHIMADZU LCMS-2020 series in ESI mode. Elemental analyses were carried out on an automatic Flash EA 1112 Series, CHN Analyzer (Thermo), and they were within $\pm 0.4\%$ of the theoretical values for C, H, and N. Melting points (M.p) were determined using a VMP-CM digital melting point apparatus and remained uncorrected. All commercially available chemicals and solvents were purchased from Sigma-Aldrich (St. Louis, USA) and used without further purification. Purity of all final compounds was determined by using HPLC (Shimadzu, Japan, (on Promosil C8 column (250 mm \times 4.6 mm, 5 μ m, 100 \AA))) and was $>95\%$.

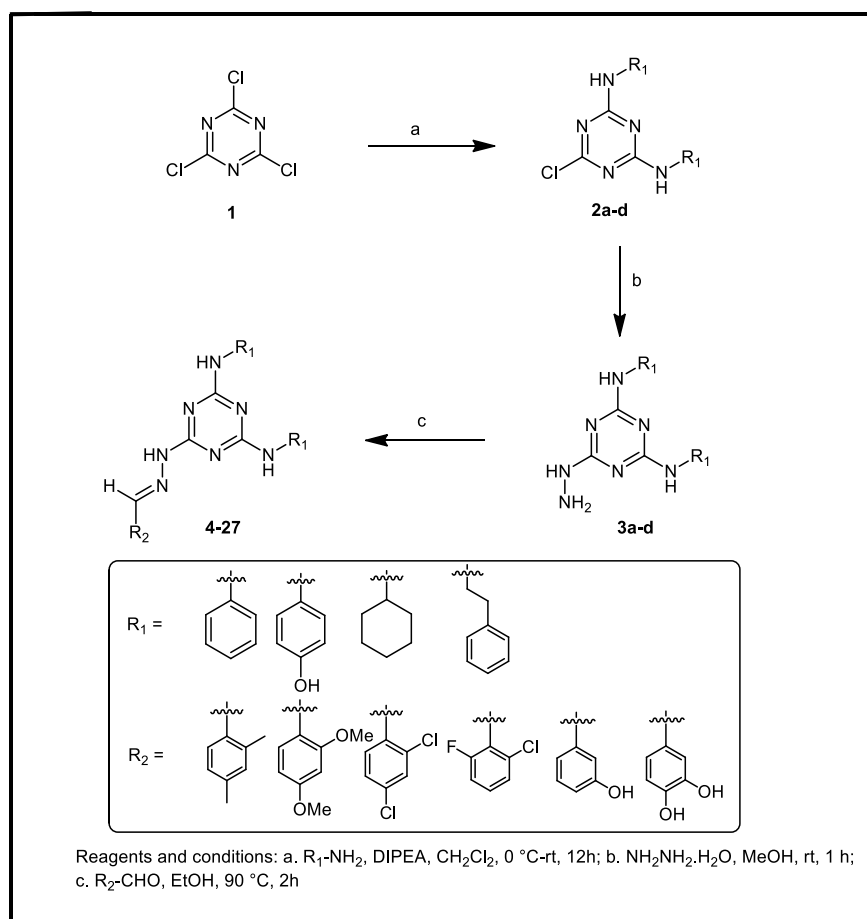


Figure 5.25: Synthetic protocol used to achieve target compounds.

5.6.3.1. General procedure for synthesis of compounds (2a-d): To a stirred solution of substituted anilines (2.1 equiv) and diisopropylethylamine (2.2 equiv) in anhydrous dichloromethane (60mL) at 0 °C under nitrogen, was added via cannula (10 min.) a solution of cyanuric chloride (1 equiv) in dichloromethane (25mL) and the reaction mixture was allowed to warm to room temperature. The reaction was monitored by TLC, after completion the mixture was partitioned between dichloromethane (50mL) and saturated aqueous sodium chloride (20mL). Aqueous phase was extracted with DCM (2*50mL), combined organic layers were dried (MgSO₄), filtered, evaporated to dryness and purified by flash chromatography by using ethyl acetate:hexane (3:7) as eluent to afford corresponding chloro derivative as a solid (80-95%).

6-Chloro-*N*²,*N*⁴-diphenyl-1,3,5-triazine-2,4-diamine (2a): To a stirred solution of aniline (1.03mL, 11.34 mmol) and diisopropylethylamine (2.067mL, 11.88 mmol) in anhydrous dichloromethane (60mL) at 0 °C under nitrogen, was added via cannula (10 min.) a solution of cyanuric chloride (1.0 g, 5.42 mmol) in dichloromethane (25mL) and the reaction mixture was allowed to warm to room temperature. The reaction was monitored by TLC, after completion the mixture was partitioned between dichloromethane (50mL) and saturated aqueous sodium chloride (20mL). Aqueous phase was extracted with DCM (2*50mL), the combined organic layers were dried (MgSO₄), filtered, evaporated to dryness and purified by flash chromatography by using ethylacetate:hexane (3:7) as eluent to afford **2a** as white solid. Yield: 89%; ¹H NMR (400 MHz, DMSO-d₆): δH. 9.23 (s, 2H), 7.83 (d, *J* = 6.0 Hz, 4H), 7.33 (d, *J* = 6.0 Hz, 4H), 7.03–6.98 (m, 2H). ESI-MS *m/z* 298.08 [M+H]⁺; Anal. Calcd for C₁₅H₁₂ClN₅: C, 60.51; H, 4.06; N, 23.52; Found: C, 60.59; H, 3.99; N, 23.64.

6-Chloro-*N*²,*N*⁴-diphenethyl-1,3,5-triazine-2,4-diamine (2b): The compound was prepared according to general procedure described above (**2a-d**) using 2-phenylethylamine (1.43mL,

11.34 mmol), diisopropylethylamine (2.067mL, 11.88 mmol), cyanuric chloride (1.0 g, 5.42 mmol) to afford **2b** as white solid. Yield: 95%; ¹H NMR (400 MHz, DMSO-d₆): δH. 9.38 (s, 2H), 7.49–7.44 (m, 4H), 7.34–7.31 (m, 6H), 3.47 (t, *J* = 8.4 Hz, 4H), 2.96 (t, *J* = 7.2 Hz, 4H). ESI-MS *m/z* 354.14 [M+H]⁺; Anal. Calcd for C₁₉H₂₀ClN₅: C, 64.49; H, 5.70; N, 19.79; Found: C, 64.32; H, 5.79; N, 19.83.

6-Chloro-*N*²,*N*⁴-dicyclohexyl-1,3,5-triazine-2,4-diamine (2c): The compound was prepared according to general procedure described above (**2a-d**) using cyclohexanamine (1.43mL, 11.34 mmol), diisopropylethylamine (2.067mL, 11.88 mmol), cyanuric chloride (1.0 g, 5.42 mmol) to afford **2c** as white solid. Yield: 85%; ¹H NMR (400 MHz, DMSO-d₆): δH. 9.72 (s, 2H), 3.54–3.51 (m, 2H), 1.98–1.51 (m, 10H), 1.29–1.01 (m, 10H). ESI-MS *m/z* 310.18 [M+H]⁺; Anal. Calcd for C₁₅H₂₄ClN₅: C, 58.15; H, 7.81; N, 22.60; Found: C, 58.22; H, 7.78; N, 22.53.

4,4-((6-Chloro-1,3,5-triazine-2,4-diyl)bis(azanediyl))diphenol (2d): The compound was prepared according to the general procedure described above (**2a-d**) using 4-aminophenol (1.237 g, 11.34 mmol), diisopropylethylamine (2.067mL, 11.88 mmol), cyanuric chloride (1.0 g, 5.42 mmol) to afford **2d** as white solid. Yield: 91%; ¹H NMR (400 MHz, DMSO-d₆): δH. 8.92 (s, 2H), 7.68 (d, *J* = 7.6 Hz, 4H), 7.14 (d, *J* = 6.8 Hz, 4H), 5.42 (s, 2H). ESI-MS *m/z* 330.07 [M+H]⁺; Anal. Calcd for C₁₅H₁₂ClN₅O₂: C, 54.64; H, 3.67; N, 21.24; Found: C, 54.72; H, 3.62; N, 21.19.

5.6.3.2. General procedure for the synthesis of compounds (3a-d): To a stirred solution of compounds **2a-d** (1 equiv) in methanol (20mL), hydrazine hydrate, 80% (3 equiv) was added and the resulting mixture was refluxed for 2 h. Two third volume of methanol was evaporated *in vacuo*, and the reaction mixture was poured into crushed ice. Resultant precipitate was collected by filtration, washed with ice cold water and dried. Then the residue was dissolved

with minimum amount of dichloromethane; by addition of petroleum ether the product precipitated as a white solid and was collected by filtration. The solid was recrystallized with 99.9% ethyl alcohol (78-93%).

6-Hydrazinyl-*N*²,*N*⁴-diphenyl-1,3,5-triazine-2,4-diamine (3a): To a stirred solution of 6-chloro-*N*²,*N*⁴-diphenyl-1,3,5-triazine-2,4-diamine (1.0 g, 3.358 mmol), in methanol (20mL), hydrazine hydrate, 80% (0.32mL, 10.074 mmol), was added and the resulting mixture was refluxed for 2 h. The two third volume of methanol was evaporated *in vacuo*, and the reaction mixture was poured into crushed ice. The resultant precipitate was collected by filtration, washed with ice cold water and dried. Then the residue was dissolved with minimum amount of dichloromethane; by addition of petroleum ether the product precipitated, and was collected by filtration. The solid was recrystallised with 99.9% ethyl alcohol to afford **3a** as white solid. Yield: 87%; ¹H NMR (400 MHz, DMSO-d₆): δH. 9.13 (s, 2H), 8.15 (s, 1H), 7.78 (d, *J* = 6.0 Hz, 4H), 7.24 (t, *J* = 7.2 Hz, 4H), 6.93 (t, *J* = 7.2 Hz, 2H), 4.23 (s, 2H). ESI-MS *m/z* 294.14 [M+H]⁺; Anal. Calcd for C₁₅H₁₅N₇: C, 61.42; H, 5.15; N, 33.43; Found: C, 61.53; H, 5.19; N, 33.19.

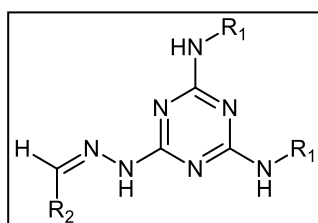
6-Hydrazinyl-*N*²,*N*⁴-diphenethyl-1,3,5-triazine-2,4-diamine (3b): The compound was prepared according to the general procedure described above (**3a-d**) using 6-chloro-*N*²,*N*⁴-diphenethyl-1,3,5-triazine-2,4-diamine (1.0 g, 2.826 mmol), in methanol (20mL), hydrazine hydrate, 80% (0.27mL, 8.478 mmol), to afford **3b** as white solid. Yield: 93%; ¹H NMR (400 MHz, DMSO-d₆): δH. 9.42 (s, 2H), 8.17 (s, 1H), 7.52–7.48 (m, 4H), 7.36–7.33 (m, 6H), 4.16 (s, 2H), 3.49 (t, *J* = 7.2 Hz, 4H), 2.99 (t, *J* = 6.8 Hz, 4H). ESI-MS *m/z* 350.2 [M+H]⁺; Anal. Calcd for C₁₉H₂₃N₇: C, 65.31; H, 6.63; N, 28.06; Found: C, 65.28; H, 6.69; N, 28.14.

***N*²,*N*⁴-Dicyclohexyl-6-hydrazinyl-1,3,5-triazine-2,4-diamine (3c):** The compound was prepared according to the general procedure described above (**3a-d**) using 6-chloro-*N*²,*N*⁴-

dicyclohexyl-1,3,5-triazine-2,4-diamine (1.0 g, 3.227 mmol), in methanol (20mL), hydrazine hydrate, 80% (0.310mL, 9.681 mmol), to afford **3c** as white solid. Yield: 81%; ¹H NMR (400 MHz, DMSO-d₆): δH. 10.72 (s, 2H), 8.19 (s, 1H), 4.28 (s, 2H), 3.74–3.72 (m, 2H), 1.96–1.48 (m, 10H), 1.31–1.02 (m, 10H). ESI-MS m/z 306.25 [M+H]⁺; Anal. Calcd for C₁₅H₂₇N₇: C, 58.99; H, 8.91; N, 32.10; Found: C, 58.96; H, 8.99; N, 32.29.

4,4-((6-Hydrazinyl-1,3,5-triazine-2,4-diyl)bis(azanediy))diphenol (3d): The compound was prepared according to the general procedure described above (**3a-d**) using 4,4-((6-chloro-1,3,5-triazine-2,4-diyl)bis(azanediy))diphenol (1.0 g, 3.032 mmol), in methanol (20mL), hydrazine hydrate, 80% (0.291mL, 9.098 mmol), to afford **3d** as white solid. Yield: 89%; ¹H NMR (400 MHz, DMSO-d₆): δH. 9.36 (s, 2H), 8.18 (s, 1H), 7.76 (d, *J* = 7.6 Hz, 4H), 7.26 (d, *J* = 8.0 Hz, 4H), 5.61 (s, 2H), 4.08 (s, 2H). ESI-MS m/z 326.13 [M+H]⁺; Anal. Calcd for C₁₅H₁₅N₇O₂: C, 55.38; H, 4.65; N, 30.14; Found: C, 55.27; H, 4.68; N, 30.08.

5.6.3.3. General procedure for synthesis of designed analogues (4-27): To a stirred solution of **3a-d** (1 equiv) in ethanol, the corresponding aldehyde (1.2 equiv) was added and the resulting mixture was refluxed for 2-3 h at 90 °C. After completion of the reaction (monitored by TLC), ethanol was removed under vacuo. Crushed ice was added to the crude reaction mixture and extracted with ethyl acetate (100mL). The organic layer was washed with brine (50 mL). The organic layer was dried over anhydrous Na₂SO₄, filtered, evaporated to dryness to get crude product which was further purified by flash chromatography by using ethylacetate:hexane (2:8) as eluent to afford desired compounds in good yield as described below. Physical data of compounds are presented in **Table 5.6**.

Table 5.6: Physical data of 1,3,5 triazine 2,4,6 triamine derivatives

Compound	R ₁	R ₂	Mol.formula	M.P.(⁰ C) ⁱ	R _f ⁱⁱ	Yield (%) ⁱⁱⁱ
4	Phenyl	2,4-dimethyl phenyl	C ₂₄ H ₂₃ N ₇	154-155	0.46	44.6
5	Phenyl	2,4-dimethoxy phenyl	C ₂₄ H ₂₃ N ₇ O ₂	168-170	0.68	62.3
6	Phenyl	2,4-dichloro phenyl	C ₂₂ H ₁₇ Cl ₂ N ₇	181-182	0.54	39.5
7	Phenyl	2-chloro 6-fluoro phenyl	C ₂₂ H ₁₇ ClFN ₇	140-142	0.48	68.2
8	Phenyl	3-hydroxy phenyl	C ₂₂ H ₁₉ N ₇ O	148-150	0.63	64.34
9	Phenyl	3,4-dihydroxy phenyl	C ₂₂ H ₁₉ N ₇ O ₂	178-179	0.55	49.92
10	Phenyl ethyl	2,4-dimethyl phenyl	C ₂₈ H ₃₁ N ₇	76-77	0.53	71.81
11	Phenyl ethyl	2,4-dimethoxy phenyl	C ₂₈ H ₃₁ N ₇ O ₂	86-87	0.58	56.32
12	Phenyl ethyl	2,4-dichloro phenyl	C ₂₆ H ₂₅ Cl ₂ N ₇	90-92	0.74	78.6
13	Phenyl ethyl	2-chloro 6-fluoro phenyl	C ₂₆ H ₂₅ ClFN ₇	78-89	0.48	81.3
14	Phenyl ethyl	3-hydroxy phenyl	C ₂₆ H ₂₇ N ₇ O	82-83	0.54	92.8
15	Phenyl ethyl	3,4-dihydroxy phenyl	C ₂₆ H ₂₇ N ₇ O ₂	108-110	0.61	88.8
16	Cyclohexyl	2,4-dimethyl phenyl	C ₂₄ H ₃₅ N ₇	152-153	0.54	42.6
17	Cyclohexyl	2,4-dimethoxy phenyl	C ₂₄ H ₃₅ N ₇ O ₂	116-117	0.63	39.8
18	Cyclohexyl	2,4-dichloro phenyl	C ₂₂ H ₂₉ Cl ₂ N ₇	139-140	0.58	66.4
19	Cyclohexyl	2-chloro 6-fluoro phenyl	C ₂₂ H ₂₉ ClFN ₇	201-203	0.52	78.2
20	Cyclohexyl	3-hydroxy phenyl	C ₂₂ H ₃₁ N ₇ O	168-169	0.58	46.3
21	Cyclohexyl	3,4-dihydroxy phenyl	C ₂₂ H ₃₁ N ₇ O ₂	136-137	0.52	42.9
22	4-hydroxy phenyl	2,4-dimethyl phenyl	C ₂₄ H ₂₃ N ₇ O ₂	157-158	0.48	48.6

23	4-hydroxy phenyl	2,4-dimethoxy phenyl	$C_{24}H_{23}N_7O_4$	188-190	0.46	62.8
24	4-hydroxy phenyl	2,4-dichloro phenyl	$C_{22}H_{17}Cl_2N_7O_2$	148-149	0.44	37.6
25	4-hydroxy phenyl	2-chloro 6-fluoro phenyl	$C_{22}H_{17}ClFN_7O_2$	149-150	0.62	56.8
26	4-hydroxy phenyl	3-hydroxy phenyl	$C_{22}H_{19}N_7O_3$	117-118	0.76	48.8
27	4-hydroxy phenyl	3,4-dihydroxy phenyl	$C_{22}H_{19}N_7O_4$	108-109	0.67	58.8

ⁱ Melting points of compounds at their decomposition. ⁱⁱ Mobile phase EtOAc: Hexane (2:8). ⁱⁱⁱ Elemental analyses for C, H, and N were within ± 0.4 % of the theoretical values.

(E)-6-(2-(2,4-Dimethylbenzylidene)hydrazinyl)-N²,N⁴-diphenyl-1,3,5-triazine-2,4

diamine (4): The compound was synthesized according to the general procedure described above (**4-27**) using 6-hydrazinyl-N²,N⁴-diphenyl-1,3,5-triazine-2,4-diamine (**3a**, 0.1 g, 0.340 mmol), 2,4-dimethylbenzaldehyde (0.057 mL, 0.409 mmol), to afford **4** as white solid. Yield: 44.6%; M.p. 153–154 °C; ¹H NMR (400 MHz, DMSO-d₆): δ H. 10.76 (s, 1H), 9.34 (s, 2H), 8.44 (s, 1H), 8.01 (d, $J = 7.2$ Hz, 1H), 7.86–7.82 (m, 4H), 7.57 (d, $J = 8.0$ Hz, 1H), 7.34–7.29 (m, 5H), 7.03–6.99 (m, 2H), 2.59 (s, 3H), 2.46 (s, 3H). ESI-MS m/z 410.2 [M+H]⁺; Anal. Calcd for $C_{24}H_{23}N_7$: C, 70.39; H, 5.66; N, 23.94; Found: C, 70.51; H, 5.61; N, 23.91. HPLC purity: 98.39% (C8 reverse phase, Acetonitrile and 10mM ammonium acetate, 60:40 at 254nm).

(E)-6-(2-(2,4-Dimethoxybenzylidene)hydrazinyl)-N²,N⁴-diphenyl-1,3,5-triazine-2,4-

diamine (5): The compound was synthesized according to the general procedure described above (**4-27**) using 6-hydrazinyl-N²,N⁴-diphenyl-1,3,5-triazine-2,4-diamine (**3a**, 0.1 g, 0.340 mmol), 2,4-dimethoxybenzaldehyde (0.067 g, 0.409 mmol), to afford **5** as buff coloured solid. Yield: 62.3%; M.p. 168–169 °C; ¹H NMR (400 MHz, DMSO-d₆): δ H. 10.83 (s, 1H), 9.31 (s, 2H), 8.44 (s, 1H), 7.84–7.80 (m, 5H), 7.29–7.25 (m, 4H), 6.99–6.95 (m, 2H), 6.66–

6.61 (m, 2H), 3.91 (s, 3H), 3.88 (s, 3H). ESI-MS m/z 442.2 [M+H]⁺; Anal. Calcd for C₂₄H₂₃N₇O₂: C, 65.29; H, 5.25; N, 22.21; Found: C, 65.36; H, 5.28; N, 22.08. HPLC purity: 95.87% (C8 reverse phase, Acetonitrile and 10mM ammonium acetate, 60:40 at 254nm).

(E)-6-(2-(2,4-Dichlorobenzylidene)hydrazinyl)-N²,N⁴-diphenyl-1,3,5-triazine-2,4-

diamine (6): The compound was synthesized according to the general procedure described above (4-27) using 6-hydrazinyl-N²,N⁴-diphenyl-1,3,5-triazine-2,4-diamine (3a, 0.1 g, 0.340 mmol), 2,4-dichlorobenzaldehyde (0.071 g, 0.409 mmol), to afford 6 as white solid. Yield: 39.5%; M.p. 181–182 °C; ¹H NMR (400 MHz, DMSO-d₆): δH. 11.29 (s, 1H), 9.42 (s, 2H), 8.54 (s, 1H), 8.02 (d, $J = 8.4$ Hz, 1H), 7.88–7.84 (m, 4H), 7.70 (s, 1H), 7.58 (d, $J = 8.0$ Hz, 1H), 7.30 (t, $J = 7.6$ Hz, 4H), 6.99 (t, $J = 6.8$ Hz, 2H). ESI-MS m/z 450.15 [M+H]⁺; Anal. Calcd for C₂₂H₁₇Cl₂N₇: C, 58.68; H, 3.81; N, 21.77; Found: C, 58.56; H, 3.78; N, 21.86. HPLC purity: 98.61% (C8 reverse phase, Acetonitrile and 10mM ammonium acetate, 60:40 at 254nm).

(E)-6-(2-(2-Chloro-6-fluorobenzylidene)hydrazinyl)-N²,N⁴-diphenyl-1,3,5-triazine-2,4-

diamine (7): The compound was synthesized according to the general procedure described above (4-27) using 6-hydrazinyl-N²,N⁴-diphenyl-1,3,5-triazine-2,4-diamine (3a, 0.1 g, 0.340 mmol), 2-chloro-6-fluorobenzaldehyde (0.064 g, 0.409 mmol), to afford 7 as white solid. Yield: 68.2%; M.p. 140–141 °C; ¹H NMR (400 MHz, DMSO-d₆): δH. 10.96 (s, 1H), 9.37 (s, 1H), 8.52 (s, 1H), 7.67 (s, 1H), 7.42–7.28 (m, 3H), 7.89–7.83 (m, 4H), 7.32–7.29 (m, 4H), 6.97–6.92 (m, 2H). ESI-MS m/z 434.15 [M+H]⁺; Anal. Calcd for C₂₂H₁₇ClFN₇: C, 60.90; H, 3.95; N, 22.60; Found: C, 60.81; H, 3.99; N, 22.69. HPLC purity: 96.21% (C8 reverse phase, Acetonitrile and 10mM ammonium acetate, 60:40 at 254nm).

(E)-3-((2-(4,6-Bis(phenylamino)-1,3,5-triazin-2-yl)hydrazono)methyl)phenol (8): The compound was synthesized according to the general procedure described above (4-27) using

6-hydrazinyl- N^2,N^4 -diphenyl-1,3,5-triazine-2,4-diamine (**3a**, 0.1 g, 0.340 mmol) , 3-hydroxybenzaldehyde (0.049 g, 0.409 mmol),) to afford **8** as white solid. Yield: 64.3%; M.p. 148–149 °C; ^1H NMR (400 MHz, DMSO- d_6): δH . 11.16 (s, 1H), 9.35 (s, 2H), 8.39 (s, 1H), 7.89–7.82 (m, 4H), 7.66–7.60 (m, 3H), 7.33–7.21 (m, 4H), 7.09–6.94 (m, 3H), 5.49 (s, 1H). ESI-MS m/z 398.15 $[\text{M}+\text{H}]^+$; Anal. Calcd for $\text{C}_{22}\text{H}_{19}\text{N}_7\text{O}$: C, 66.49; H, 4.82; N, 24.67; Found: C, 66.35; H, 4.76; N, 24.69. HPLC purity: 97.64% (C8 reverse phase, Acetonitrile and 10mM ammonium acetate, 60:40 at 254nm).

(E)-4-((2-(4,6-Bis(phenylamino)-1,3,5-triazin-2-yl)hydrazono)methyl)benzene-1,2-diol

(9): The compound was synthesized according to the general procedure described above (**4-27**) using 6-hydrazinyl- N^2,N^4 -diphenyl-1,3,5-triazine-2,4-diamine (**3a**, 0.1 g, 0.340 mmol) , 3,4-dihydroxybenzaldehyde (0.056 g, 0.409 mmol),) to afford **9** as dark brown coloured solid. Yield: 49.9%; M.p. 178–179 °C; ^1H NMR (400 MHz, DMSO- d_6): δH . 11.08 (s, 1H), 9.63 (s, 2H), 8.38 (s, 1H), 7.92–7.84 (m, 4H), 7.36–7.32 (m, 2H), 7.30–7.26 (m, 4H), 7.08–6.97 (m, 3H), 5.94 (s, 1H), 5.63 (s, 1H). ESI-MS m/z 414.15 $[\text{M}+\text{H}]^+$; Anal. Calcd for $\text{C}_{22}\text{H}_{19}\text{N}_7\text{O}_2$: C, 63.91; H, 4.63; N, 23.72; Found: C, 63.89; H, 4.68; N, 23.63. HPLC purity: 97.33% (C8 reverse phase, Acetonitrile and 10mM ammonium acetate, 60:40 at 254nm).

(E)-6-(2-(2,4-Dimethylbenzylidene)hydrazinyl)- N^2,N^4 -diphenethyl-1,3,5-triazine-2,4-

diamine (10): The compound was synthesized according to the general procedure described above (**4-27**) using 6-hydrazinyl- N^2,N^4 -diphenethyl-1,3,5-triazine-2,4-diamine (**3b**, 0.1 g, 0.286 mmol), 2,4-dimethylbenzaldehyde (0.047 mL, 0.343 mmol), to afford **10** as White crystalline solid. Yield: 71.8%; M.p. 76–77 °C; ^1H NMR (400 MHz, DMSO- d_6): δH . 10.82 (s, 1H), 9.12 (s, 2H), 8.37 (s, 1H), 7.63–7.46 (m, 5H), 7.33–7.28 (m, 6H), 7.22 (s, 1H), 7.14 (d, $J = 8.0$ Hz, 1H), 3.49 (t, $J = 7.2$ Hz, 4H), 2.92 (t, $J = 6.8$ Hz, 4H), 2.54 (s, 3H), 2.41 (s, 3H). ESI-MS m/z 466.25 $[\text{M}+\text{H}]^+$; Anal. Calcd for $\text{C}_{28}\text{H}_{31}\text{N}_7$: C, 72.23; H, 6.71; N, 21.06;

Found: C, 72.34; H, 6.67; N, 21.17. HPLC purity: 99.26% (C8 reverse phase, Acetonitrile and 10mM ammonium acetate, 60:40 at 254nm).

(E)-6-(2-(2,4-Dimethoxybenzylidene)hydrazinyl)-N²,N⁴-diphenethyl-1,3,5-triazine-2,4-diamine (11): The compound was synthesized according to the general procedure described above (4-27) using 6-hydrazinyl-N²,N⁴-diphenethyl-1,3,5-triazine-2,4-diamine (**3b**, 0.1 g, 0.286 mmol), 2,4-dimethoxybenzaldehyde (0.057 g, 0.343 mmol), to afford **11** as light brown solid. Yield: 56.3%; M.p. 86–87 °C; ¹H NMR (400 MHz, DMSO-d₆): δH. 11.21 (s, 1H), 8.92 (s, 2H), 8.43 (s, 1H), 7.71–7.52 (m, 5H), 7.38–7.31 (m, 6H), 7.22 (s, 1H), 7.13 (d, *J* = 8.4 Hz, 1H), 3.94 (s, 3H), 3.89 (s, 3H), 3.47 (t, *J* = 6.8 Hz, 4H), 2.99 (t, *J* = 7.2 Hz, 4H). ESI-MS *m/z* 498.3 [M+H]⁺; Anal. Calcd for C₂₈H₃₁N₇O₂: C, 67.59; H, 6.28; N, 19.70; Found: C, 67.51; H, 6.36; N, 19.63. HPLC purity: 95.81% (C8 reverse phase, Acetonitrile and 10mM ammonium acetate, 60:40 at 254nm).

(E)-6-(2-(2,4-Dichlorobenzylidene)hydrazinyl)-N²,N⁴-diphenethyl-1,3,5-triazine-2,4-diamine (12): The compound was synthesized according to the general procedure described above (4-27) using 6-hydrazinyl-N²,N⁴-diphenethyl-1,3,5-triazine-2,4-diamine (**3b**, 0.1 g, 0.286 mmol), 2,4-dichlorobenzaldehyde (0.060 g, 0.343 mmol), to afford **12** as white solid. Yield: 78.6%; M.p. 90–91 °C; ¹H NMR (400 MHz, DMSO-d₆): δH. 10.96 (s, 1H), 9.34 (s, 2H), 8.43 (s, 1H), 8.21–7.98 (m, 2H), 7.29–7.16 (m, 11H), 3.49 (t, *J* = 7.6 Hz, 4H), 2.94 (t, *J* = 6.4 Hz, 4H). ESI-MS *m/z* 506.15 [M+H]⁺; Anal. Calcd for C₂₆H₂₅Cl₂N₇: C, 61.66; H, 4.98; N, 19.36; Found: C, 61.75; H, 4.87; N, 19.34. HPLC purity: 96.28% (C8 reverse phase, Acetonitrile and 10mM ammonium acetate, 60:40 at 254nm).

(E)-6-(2-(2-Chloro-6-fluorobenzylidene)hydrazinyl)-N²,N⁴-diphenethyl-1,3,5-triazine-2,4-diamine (13): The compound was synthesized according to the general procedure described above (4-27) using 6-hydrazinyl-N²,N⁴-diphenethyl-1,3,5-triazine-2,4-diamine (**3b**,

0.1 g, 0.286 mmol), 2-chloro-6-fluorobenzaldehyde (0.054 g, 0.343 mmol), to afford **13** as White crystalline solid. Yield: 81.3%; M.p. 78–79 °C; ¹H NMR (400 MHz, DMSO-d₆): δH. 10.86 (s, 1H), 9.21 (s, 2H), 8.46 (s, 1H), 7.31–7.24 (m, 5H), 7.11–6.98 (m, 8H), 3.42 (t, *J* = 7.2 Hz, 4H), 2.96 (t, *J* = 8.8 Hz, 4H). ESI-MS *m/z* 490.2 [M+H]⁺; Anal. Calcd for C₂₆H₂₅ClFN₇: C, 63.73; H, 5.14; N, 20.01; Found: C, 63.76; H, 5.02; N, 20.13. HPLC purity: 98.17% (C8 reverse phase, Acetonitrile and 10mM ammonium acetate, 60:40 at 254nm).

(E)-3-((2-(4,6-Bis(phenethylamino)-1,3,5-triazin-2-yl)hydrazono)methyl)phenol (14):

The compound was synthesized according to the general procedure described above (**4-27**) using 6-hydrazinyl-N²,N⁴-diphenethyl-1,3,5-triazine-2,4-diamine (**3b**, 0.1 g, 0.286 mmol), 3-hydroxybenzaldehyde (0.042 g, 0.343 mmol), to afford **14** as white solid. Yield: 92.8%; M.p. 82–83 °C; ¹H NMR (400 MHz, DMSO-d₆): δH. 11.03 (s, 1H), 9.24 (s, 1H), 8.51 (s, 1H), 7.42–7.35 (m, 7H), 7.24–6.92 (m, 8H), 5.44 (s, 1H), 3.44 (t, *J* = 7.2 Hz, 4H), 2.93 (t, *J* = 8.0 Hz, 4H). ESI-MS *m/z* 454.25 [M+H]⁺; Anal. Calcd for C₂₆H₂₇N₇O: C, 68.85; H, 6.00; N, 21.62; Found: C, 68.78; H, 6.08; N, 21.66. HPLC purity: 96.78% (C8 reverse phase, Acetonitrile and 10mM ammonium acetate, 60:40 at 254nm).

(E)-4-((2-(4,6-Bis(phenethylamino)-1,3,5-triazin-2-yl)hydrazono)methyl)benzene-1,2-

diol (15): The compound was synthesized according to the general procedure described above (**4-27**) using 6-hydrazinyl-N²,N⁴-diphenethyl-1,3,5-triazine-2,4-diamine (**3b**, 0.1 g, 0.286 mmol), 3,4-dihydroxybenzaldehyde (0.047 g, 0.343 mmol), to afford **15** as white solid. Yield: 88.8%; M.p. 108–109 °C; ¹H NMR (400 MHz, DMSO-d₆): δH. 10.21 (s, 1H), 9.24 (s, 1H), 9.09 (s, 1H), 7.87 (s, 1H), 7.28–7.19 (m, 10H), 7.08 (s, 1H), 6.91–6.73 (m, 4H), 3.46 (t, *J* = 7.2 Hz, 4H), 2.84 (t, *J* = 6.4 Hz, 4H). ESI-MS *m/z* 470.2 [M+H]⁺; Anal. Calcd for C₂₆H₂₇N₇O₂: C, 66.51; H, 5.80; N, 20.88; Found: C, 66.44; H, 5.71; N, 20.94. HPLC purity: 97.26% (C8 reverse phase, Acetonitrile and 10mM ammonium acetate, 60:40 at 254nm).

(E)-N²,N⁴-Dicyclohexyl-6-(2-(2,4-dimethylbenzylidene)hydrazinyl)-1,3,5-triazine-2,4-diamine (16): The compound was synthesized according to the general procedure described above (4-27) using N²,N⁴-dicyclohexyl-6-hydrazinyl-1,3,5-triazine-2,4-diamine (3c, 0.1 g, 0.327 mmol), 2, 4-dimethylbenzaldehyde (0.054 mL, 0.392 mmol), to afford 16 as white coloured solid. Yield: 42.6%; M.p. 152–153 °C; ¹H NMR (400 MHz, DMSO-d₆): δH. 10.69 (s, 1H), 8.24 (s, 1H), 7.57 (d, *J* = 7.6 Hz, 1H), 7.21–7.11 (m, 2H), 6.72 (s, 2H), 3.76–3.66 (m, 2H), 1.93–1.59 (m, 10H), 1.34–1.08 (m, 10H), 2.53 (s, 3H), 2.45 (s, 3H). ESI-MS *m/z* 422.3 [M+H]⁺; Anal. Calcd for C₂₄H₃₅N₇: C, 68.38; H, 8.37; N, 23.26; Found: C, 68.42; H, 8.44; N, 23.13. HPLC purity: 95.47% (C8 reverse phase, Acetonitrile and 10mM ammonium acetate, 60:40 at 254nm).

(E)-N²,N⁴-Dicyclohexyl-6-(2-(2,4-dimethoxybenzylidene)hydrazinyl)-1,3,5-triazine-2,4-diamine (17): The compound was synthesized according to the general procedure described above (4-27) using N²,N⁴-dicyclohexyl-6-hydrazinyl-1,3,5-triazine-2,4-diamine (3c, 0.1 g, 0.327 mmol), 2, 4-dimethoxybenzaldehyde (0.065 g, 0.392 mmol), to afford 17 as white solid. Yield: 39.8%; M.p. 116–117 °C; ¹H NMR (400 MHz, DMSO-d₆): δH. 10.67 (s, 1H), 8.29 (s, 1H), 7.62 (d, *J* = 7.2 Hz, 1H), 6.93–6.81 (m, 2H), 6.73 (s, 2H), 3.94 (s, 3H), 3.89 (s, 3H), 3.58–3.46 (m, 2H), 1.92–1.55 (m, 10H), 1.28–1.02 (m, 10H). ESI-MS *m/z* 454.3 [M+H]⁺; Anal. Calcd for C₂₄H₃₅N₇O₂: C, 63.55; H, 7.78; N, 21.62; Found: C, 63.44; H, 7.72; N, 21.74. HPLC purity: 99.25% (C8 reverse phase, Acetonitrile and 10mM ammonium acetate, 60:40 at 254nm).

(E)-N²,N⁴-Dicyclohexyl-6-(2-(2,4-dichlorobenzylidene)hydrazinyl)-1,3,5-triazine-2,4-diamine (18): The compound was synthesized according to the general procedure described above (4-27) using N²,N⁴-dicyclohexyl-6-hydrazinyl-1,3,5-triazine-2,4-diamine (3c, 0.1 g, 0.327 mmol), 2, 4-dichlorobenzaldehyde (0.068 g, 0.392 mmol), to afford 18 as off white

solid. Yield: 66.4%; M.p. 139–140 °C; ¹H NMR (400 MHz, DMSO-d₆): δH. 10.84 (s, 1H), 8.52 (s, 1H), 8.25 (s, 1H), 6.78 (s, 2H), 8.02 (d, *J* = 7.2 Hz, 1H), 7.59 (d, *J* = 8.0 Hz, 1H), 3.66–3.60 (m, 2H), 1.98–1.64 (m, 10H), 1.38–1.06 (m, 10H). ESI-MS *m/z* 462.2 [M+H]⁺; Anal. Calcd for C₂₂H₂₉Cl₂N₇: C, 57.14; H, 6.32; N, 21.20; Found: C, 57.22; H, 6.39; N, 21.16. HPLC purity: 96.14% (C8 reverse phase, Acetonitrile and 10mM ammonium acetate, 60:40 at 254nm).

(*E*)-6-(2-(2-Chloro-6-fluorobenzylidene)hydrazinyl)-N²,N⁴-dicyclohexyl-1,3,5-triazine-2,4-diamine (19): The compound was synthesized according to the general procedure described above (**4-27**) using N²,N⁴-dicyclohexyl-6-hydrazinyl-1,3,5-triazine-2,4-diamine (**3c**, 0.1 g, 0.327 mmol), 2-chloro-6-fluorobenzaldehyde (0.062 g, 0.392 mmol), to afford **19** as white solid. Yield: 78.2%; M.p. 201–202 °C; ¹H NMR (400 MHz, DMSO-d₆): δH. 10.73 (s, 1H), 8.27 (s, 1H), 7.41 – 7.24 (m, 3H), 6.75 (s, 2H), 3.80–3.61 (m, 2H), 1.99–1.50 (m, 10H), 1.32–1.01 (m, 10H). ESI-MS *m/z* 446.25 [M+H]⁺; Anal. Calcd for C₂₂H₂₉ClFN₇: C, 59.25; H, 6.55; N, 21.99; Found: C, 59.28; H, 6.51; N, 22.03. HPLC purity: 95.96% (C8 reverse phase, Acetonitrile and 10mM ammonium acetate, 60:40 at 254nm).

(*E*)-3-((2-(4,6-Bis(cyclohexylamino)-1,3,5-triazin-2-yl)hydrazono)methyl)phenol (20): The compound was synthesized according to the general procedure described above (**4-27**) using N²,N⁴-dicyclohexyl-6-hydrazinyl-1,3,5-triazine-2,4-diamine (**3c**, 0.1 g, 0.327 mmol), 3-hydroxybenzaldehyde (0.047 g, 0.392 mmol), to afford **20** as white solid. Yield: 46.3%; M.p. 168–169 °C; ¹H NMR (400 MHz, DMSO-d₆): δH. 10.59 (s, 1H), 8.31 (s, 1H), 6.77 (s, 2H), 7.52–7.42 (m, 3H), 7.34 (t, *J* = 7.6 Hz, 1H), 5.43 (s, 1H), 3.55–3.46 (m, 2H), 1.93–1.58 (m, 10H), 1.34–1.07 (m, 10H). ESI-MS *m/z* 410.25 [M+H]⁺; Anal. Calcd for C₂₂H₃₁N₇O: C, 64.52; H, 7.63; N, 23.94; Found: C, 64.58; H, 7.56; N, 23.92. HPLC purity: 97.84% (C8 reverse phase, Acetonitrile and 10mM ammonium acetate, 60:40 at 254nm).

(E)-4-((2-(4,6-Bis(cyclohexylamino)-1,3,5-triazin-2-yl)hydrazono)methyl)benzene-1,2-

diol (21): The compound was synthesized according to the general procedure described above (**4-27**) using N²,N⁴-dicyclohexyl-6-hydrazinyl-1,3,5-triazine-2,4-diamine (**3c**, 0.1 g, 0.327 mmol), 3, 4-dihydroxybenzaldehyde (0.054 g, 0.392 mmol), to afford **21** as white solid. Yield: 42.9%; M.p. 136–137 °C; ¹H NMR (400 MHz, DMSO-d₆): δH. 10.73 (s, 1H), 8.29 (s, 1H), 6.81 (s, 2H), 7.54–7.48 (m, 2H), 6.94 (s, 1H), 5.68 (s, 2H), 3.62–3.47 (m, 2H), 1.89–1.54 (m, 10H), 1.36–1.08 (m, 10H). ESI-MS m/z 426.25 [M+H]⁺; Anal. Calcd for C₂₂H₃₁N₇O₂: C, 62.10; H, 7.34; N, 23.04; Found: C, 62.27; H, 7.23; N, 23.09. HPLC purity: 99.18% (C8 reverse phase, Acetonitrile and 10mM ammonium acetate, 60:40 at 254nm).

(E)-4,4-(((6-(2-(2,4-Dimethylbenzylidene)hydrazinyl)-1,3,5-triazine-2,4-

diyl)bis(azanediy))diphenol (22): The compound was synthesized according to the general procedure described above (**4-27**) using 4,4-(((6-hydrazinyl-1,3,5-triazine-2,4-diyl)bis(azanediy))diphenol (**3d**, 0.1 g, 0.307 mmol), 2, 4-dimethylbenzaldehyde (0.051 mL, 0.368 mmol), to afford **22** as Dark brown solid. Yield: 48.6%; M.p. 157–159 °C; ¹H NMR (400 MHz, DMSO-d₆): δH. 10.12 (s, 1H), 8.98 (s, 2H), 8.49 (s, 1H), 7.76–7.67 (m, 5H), 7.23 (s, 1H), 7.14 (d, *J* = 7.2 Hz, 1H), 6.92–6.86 (m, 4H), 5.48 (s, 2H), 2.54 (s, 3H), 2.47 (s, 3H). ESI-MS m/z 442.2 [M+H]⁺; Anal. Calcd for C₂₄H₂₃N₇O₂: C, 65.29; H, 5.25; N, 22.21; Found: C, 65.38; H, 5.13; N, 22.17. HPLC purity: 96.57% (C8 reverse phase, Acetonitrile and 10mM ammonium acetate, 60:40 at 254nm).

(E)-4,4-(((6-(2-(2,4-Dimethoxybenzylidene)hydrazinyl)-1,3,5-triazine-2,4

diyl)bis(azanediy))diphenol (23): The compound was synthesized according to the general procedure described above (**4-27**) using 4,4-(((6-hydrazinyl-1,3,5-triazine-2,4-diyl)bis(azanediy))diphenol (**3d**, 0.1 g, 0.307 mmol), 2, 4-dimethoxybenzaldehyde (0.061 g, 0.368 mmol), to afford **23** as light brown solid. Yield: 62.8%; M.p. 188–189 °C; ¹H NMR

(400 MHz, DMSO-d₆): δH. 10.18 (s, 1H), 9.01 (s, 2H), 8.46 (s, 1H), 7.81–7.78 (m, 5H), 7.65–7.59 (m, 4H), 6.94–6.85 (m, 2H), 5.44 (s, 2H), 3.89 (s, 3H), 3.84 (s, 3H). ESI-MS m/z 474.2 [M+H]⁺; Anal. Calcd for C₂₄H₂₃N₇O₄: C, 60.88; H, 4.90; N, 20.71; Found: C, 60.79; H, 4.97; N, 20.76. HPLC purity: 95.79% (C8 reverse phase, Acetonitrile and 10mM ammonium acetate, 60:40 at 254nm).

(E)-4,4-((6-(2-(2,4-Dichlorobenzylidene)hydrazinyl)-1,3,5-triazine-2,4-

diyl)bis(azanediy))diphenol (24): The compound was synthesized according to the general procedure described above **(4-27)** using 4,4-((6-hydrazinyl-1,3,5-triazine-2,4-diyl)bis(azanediy))diphenol (**3d**, 0.1 g, 0.307 mmol), 2, 4-dichlorobenzaldehyde (0.064 g, 0.368 mmol), to afford **24** as light brown solid. Yield: 37.6%; M.p. 148–1149 °C; ¹H NMR (400 MHz, DMSO-d₆): δH. 11.21 (s, 1H), 9.36 (s, 2H), 8.50 (s, 1H), 8.01 (d, *J* = 8.4 Hz, 1H), 7.92 (s, 1H), 7.76–7.71 (m, 4H), 7.59 (d, *J* = 6.8 Hz, 1H), 6.91–6.86 (m, 4H), 5.46 (s, 2H). ESI-MS m/z 482.05 [M+H]⁺; Anal. Calcd for C₂₂H₁₇Cl₂N₇O₂: C, 54.78; H, 3.55; N, 20.33; Found: C, 54.72; H, 3.41; N, 20.36. HPLC purity: 99.31% (C8 reverse phase, Acetonitrile and 10mM ammonium acetate, 60:40 at 254nm).

(E)-4,4-((6-(2-(2-Chloro-6-fluorobenzylidene)hydrazinyl)-1,3,5-triazine-2,4-

diyl)bis(azanediy))diphenol (25): The compound was synthesized according to the general procedure described above **(4-27)** using 4,4-((6-hydrazinyl-1,3,5-triazine-2,4-diyl)bis(azanediy))diphenol (**3d**, 0.1 g, 0.307 mmol), 2-chloro-6-fluorobenzaldehyde (0.058 g, 0.368 mmol), to afford **25** as light brown solid. Yield: 56.8%; M.p. 149–150 °C; ¹H NMR (400 MHz, DMSO-d₆): δH. 10.76 (s, 1H), 9.19 (s, 2H), 8.45 (s, 1H), 7.86–7.79 (m, 4H), 7.43–7.26 (m, 3H), 6.92–6.87 (m, 4H), 5.42 (s, 2H). ESI-MS m/z 466.05 [M+H]⁺; Anal. Calcd for C₂₂H₁₇ClFN₇O₂: C, 56.72; H, 3.68; N, 21.05; Found: C, 56.68; H, 3.76; N, 21.09.

HPLC purity: 96.53% (C8 reverse phase, Acetonitrile and 10mM ammonium acetate, 60:40 at 254nm).

(E)-4,4-((6-(2-(3-Hydroxybenzylidene)hydrazinyl)-1,3,5-triazine-2,4-

diyl)bis(azanediy))diphenol (26): The compound was synthesized according to the general procedure described above (4-27) using 4,4-((6-hydrazinyl-1,3,5-triazine-2,4-diyl)bis(azanediy))diphenol (**3d**, 0.1 g, 0.307 mmol), 3-hydroxybenzaldehyde (0.040 g, 0.368 mmol), to afford **26** as Dark brown solid. Yield: 48.8%; M.p. 117–118 °C; ¹H NMR (400 MHz, DMSO-d₆): δH. 11.08 (s, 1H), 9.28 (s, 2H), 8.49 (s, 1H), 7.83–7.72 (m, 6H), 7.39–7.12 (m, 6H), 5.42 (s, 2H), 5.24 (s, 1H). ESI-MS m/z 430.15 [M+H]⁺; Anal. Calcd for C₂₂H₁₉N₇O₃: C, 61.53; H, 4.46; N, 22.83; Found: C, 61.59; H, 4.33; N, 22.78. HPLC purity: 95.13% (C8 reverse phase, Acetonitrile and 10mM ammonium acetate, 60:40 at 254nm).

(E)-4-((2-(4,6-Bis((4-hydroxyphenyl)amino)-1,3,5-triazin-2-

yl)hydrazono)methyl)benzene-1,2-diol (27): The compound was synthesized according to the general procedure described above (4-27) using 4,4-((6-hydrazinyl-1,3,5-triazine-2,4-diyl)bis(azanediy))diphenol (**3d**, 0.1 g, 0.307 mmol), 3,4-dihydroxybenzaldehyde (0.050 g, 0.368 mmol), to afford **27** as Dark yellow crystalline solid. Yield: 58.8%; M.p. 108–109 °C; ¹H NMR (400 MHz, DMSO-d₆): δH. 10.84 (s, 1H), 9.32 (s, 2H), 8.39 (s, 1H), 7.78–7.56 (m, 6H), 7.11–6.95 (m, 5H), 5.44 (s, 1H), 5.37 (s, 2H), 5.29 (s, 1H). ESI-MS m/z 446.15 [M+H]⁺; Anal. Calcd for C₂₂H₁₉N₇O₄: C, 59.32; H, 4.30; N, 22.01; Found: C, 59.37; H, 4.25; N, 22.08. HPLC purity: 96.46% (C8 reverse phase, Acetonitrile and 10mM ammonium acetate, 60:40 at 254nm).

Spectral representation of most active compounds like compounds 19 and 6 (Mass chromatogram, ¹H NMR and ¹³C NMR spectra) were shown in **Figures 5.26-5.30**. Ligand

interaction pictures and structures of lead molecules from Ligand 4 to 27 were shown in **Figures 5.33-5.35**.

5.6.4. Structure-activity relationship: Structure–activity relationships were depicted based on *in vivo* pharmacological activity of 1,3,5-triazine-2,4,6-triamine derivatives in four different antiepileptic models.

Chief substitutions for development of SAR were made on the core moiety (1,3,5 triazine ring) of parent lead compound, where, proximal aryl ring and distal aryl rings were substituted with different electron donating, electron withdrawing, aryl, alkyl and alicyclic groups. Specifically, proximal aryl ring was substituted with various electron donating groups such as methyl and methoxy; and electron withdrawing groups such as fluorine and chlorine groups at various positions on the ring. Whereas, distal aryl rings were replaced with phenyl ethyl, cyclohexyl and 4-hydroxy phenyl groups by withstanding proximal aryl ring substitutions to attain respective combinations.

Replacement of two chlorine atoms at 2, 4 positions of the parent compound (**6**) by electron releasing substituents like methyl, methoxy groups (**4, 5**) resulted in decreased activity in all four *in vivo* models with no neurotoxicity. Introduction of electron withdrawing substituents such as chlorine and fluorine at positions 2- and 6- respectively (**7**) in proximal aryl ring results in increased activity. Proximal aryl ring with substitution of hydroxyl group as mono substitution at position 3 (**8**) resulted in slight increase in activity whereas, di substitution at positions 3 and 4 (**9**) displayed increase in activity in contrast to parent compound **6** as well as compound **8**.

Replacement of distal phenyl rings (R1) of parent compound (**6**) with phenyl ethyl group (**12**), and 4-hydroxy phenyl ring (**24**) showed increase in activity whereas, with cyclohexyl ring (**18**) showed decrease in activity.

Distal phenyl rings replacements in compound **7** (proximal phenyl ring with substituted 2,6 chloro and fluoro groups) with phenyl ethyl group (**13**) showed slight increase in activity and with cyclohexyl ring (**19**) showed increase in activity in all four *in vivo* models (Table-6). Conversely, substitution of 4-hydroxy phenyl ring (**25**) showed decrease in activity even in comparison with parent compound (**6**).

Distal phenyl rings replacements in compound **8** (proximal phenyl ring with hydroxyl function at position 3) with phenyl ethyl group (**14**) and cyclohexyl ring (**20**) showed decrease in activity whereas, complete loss of activity was found with 4-hydroxy phenyl ring (**26**).

Distal phenyl rings replacements in compound **9** (proximal phenyl ring with substituted 3,4 di hydroxyl moieties) with phenyl ethyl group (**15**), cyclohexyl ring (**21**) and 4-hydroxy phenyl ring (**27**) showed decrease in activity.

Distal phenyl rings replacements in compound **4** (proximal phenyl ring with substituted 3,4 di methyl groups) with phenyl ethyl group (**10**) showed slight increase in activity, whereas cyclohexyl ring (**16**) and 4-hydroxy phenyl ring (**22**) showed decrease in activity.

Distal phenyl rings replacements in compound **5** (proximal phenyl ring with substituted 3, 4 di methoxy groups) with phenyl ethyl group (**11**) and 4-hydroxy phenyl ring (**23**) showed slight increase in activity, whereas cyclohexyl ring (**17**) showed decrease in activity.

In vivo pharmacological activity was mainly influenced by variations in substituents on the aryl ring at the proximal end. Electron donating substitutions at proximal phenyl ring such as methyl (**4**, **10**, **16** and **22**), methoxy (**5**, **11**, **17** and **23**) hydroxyl groups (**8**, **9**, **14**, **15**, **20**, **21**, **26** and **27**) in combination of various replacements at the distal phenyl rings led to decreasing activity. Electron withdrawing substitutions at proximal phenyl ring (**6**, **7**, **12**, **13**, **18**, **19**, **24**,

and **25**) in combination of various replacements at the distal phenyl rings led to better activity. In particular, it appears that compound **7** with 2-chloro, 6-fluoro substitutions on the proximal phenyl ring and cyclohexyl ring at the distal phenyl ring showed significant activity at 30 mg/kg in all four *in vivo* animal models (MES,sc PTZ,sc STY and scPIC), and emerged as promising candidates without neurotoxicity.

Figure 5.26: MASS spectra of compound 19

<Spectrum>

Line#:1 R.Time:0.600(Scan#:37)
MassPeaks:168
RawMode:Averaged 0.400-0.767(25-47) BasePeak:446.250(3534666)
BG Mode:Averaged 0.000-0.367(1-23) Segment 1 - Event 1

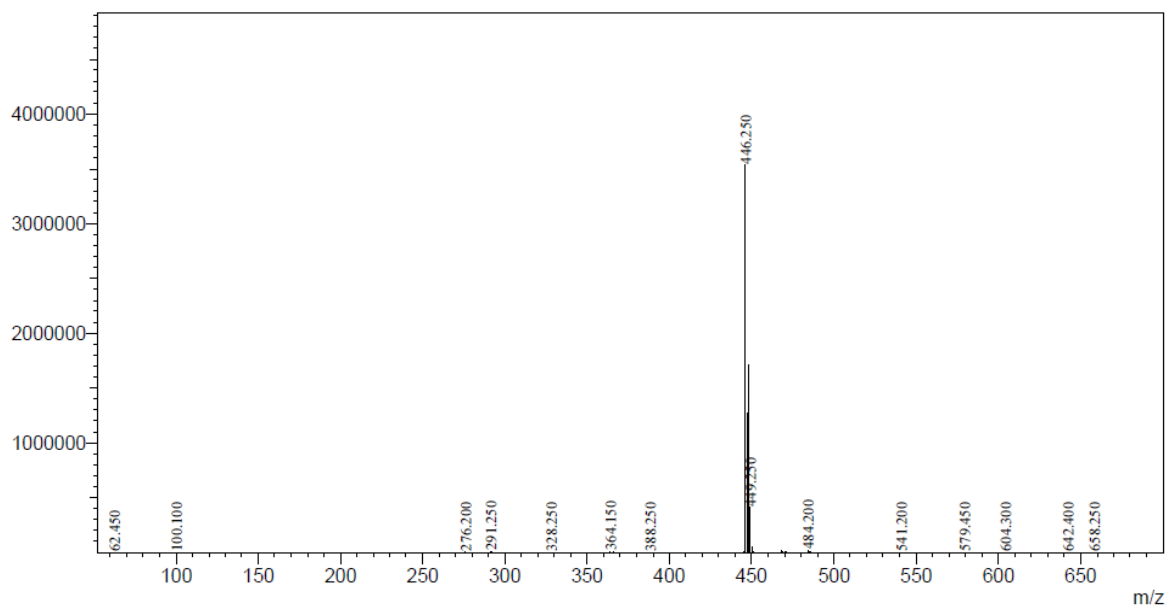


Figure 5.27: Spectral representation ^1H NMR spectra of most active compound **19**

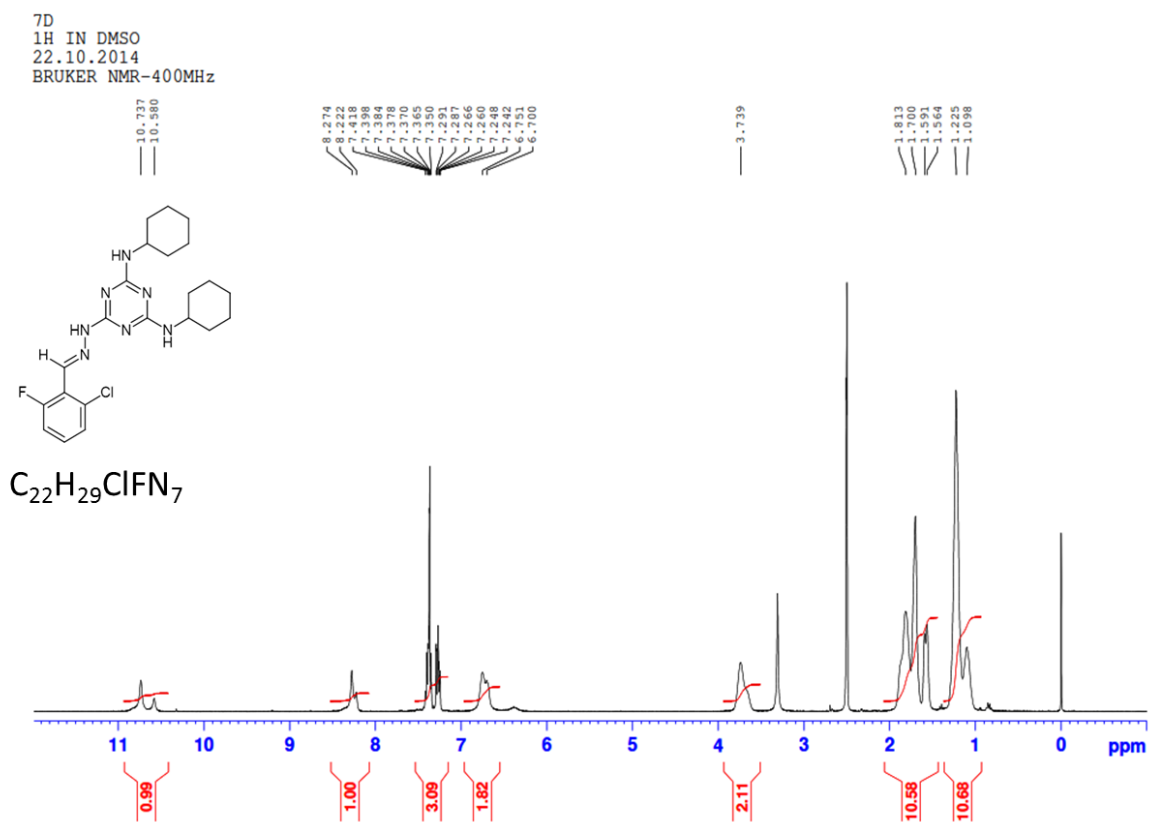


Figure 5.28: Spectral representation ¹³C NMR spectra of most active compound 19

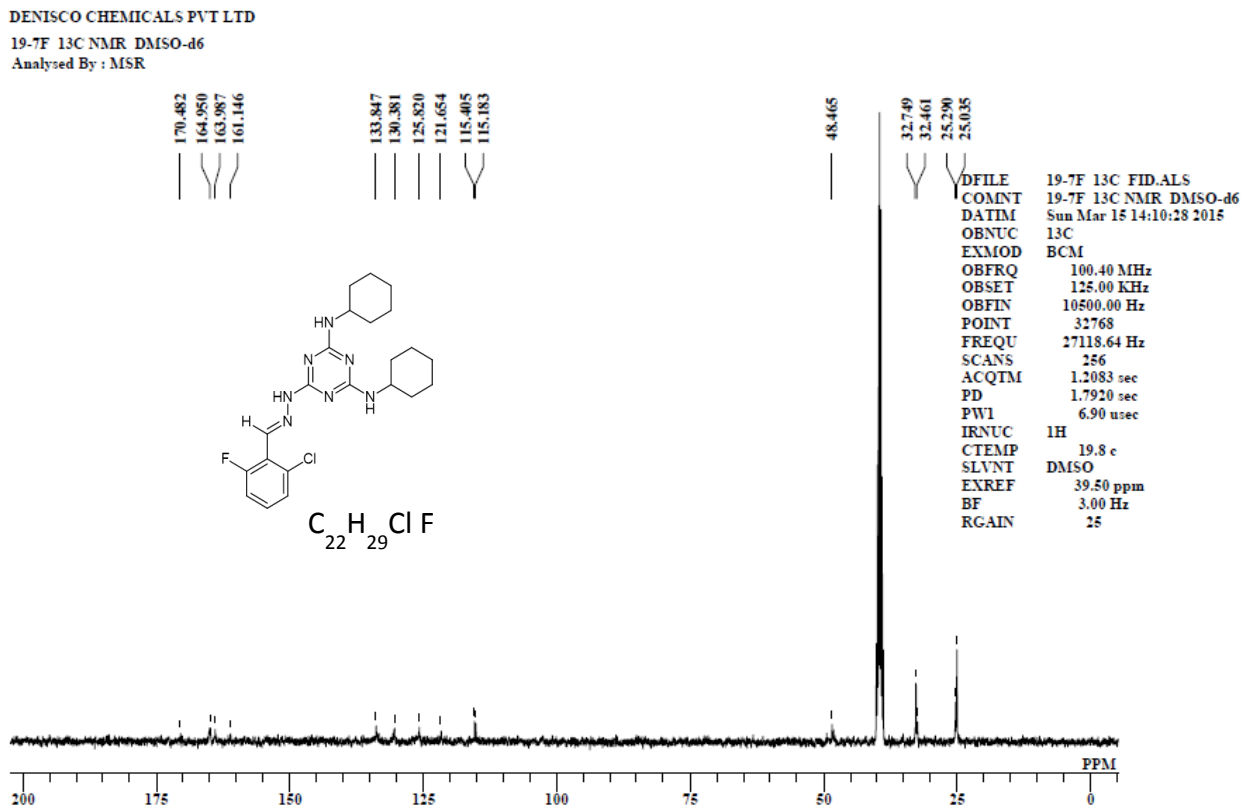


Figure 5.29: MASS spectra of compound 6

<Spectrum>

Line#:1 R.Time:0.833(Scan#:51)
MassPeaks:306
RawMode:Averaged 0.633-1.267(39-77) BasePeak:450.15(2240470)
BG Mode:Averaged 0.000-0.600(1-37) Segment 1 - Event 1

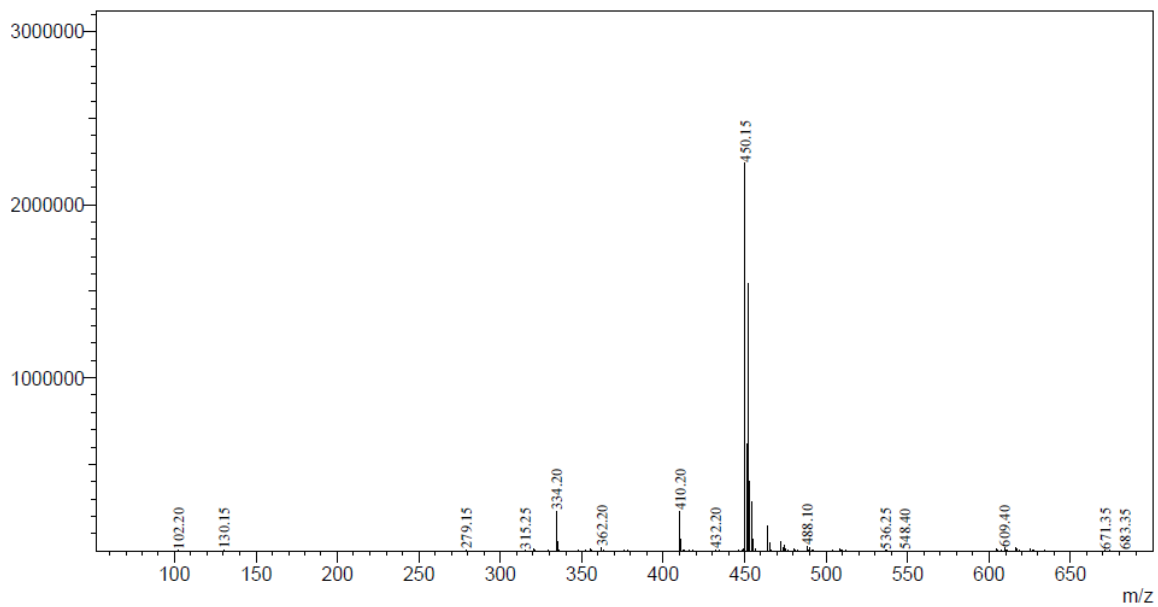
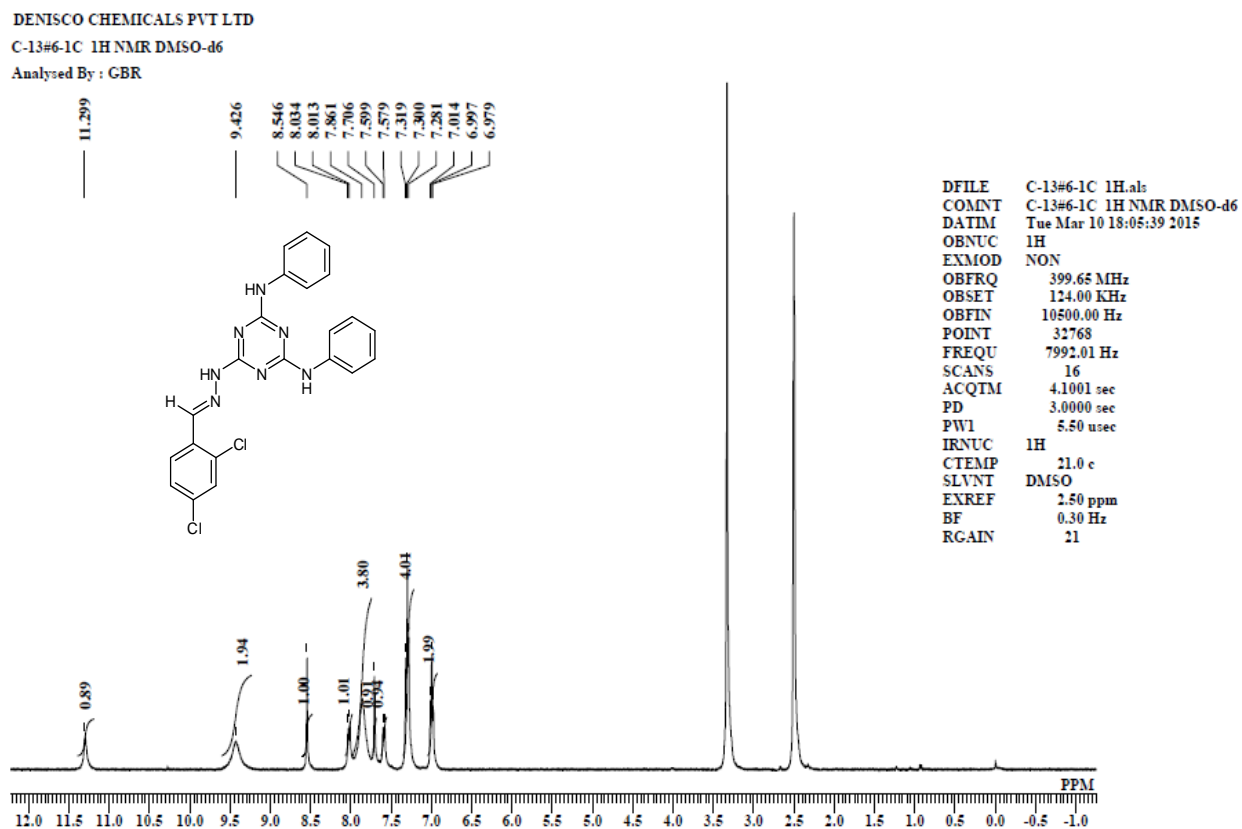


Figure 5.30: Spectral representation ^1H NMR spectra of most active compound 6



5.6.5. Purity analyses

All the final compounds were checked for purity with a common method for detection which was developed using a Shimadzu HPLC system. Chromatographic separation procedure was achieved on basis of method development protocol described in detail in materials and methods section. HPLC chromatograms of representative compounds **6 and 19** are displayed in **Figures 5.31 and 5.32** respectively where, the drug peak in aqueous method was resolved at retention time 4.16 and 17.96 minutes respectively. All the areas of visible peaks were added manually and the whole area was estimated to assess the purity of single drug peak. Compounds **6 and 19** have been shown 98.60% and 95.96% purity respectively. All the remaining compounds were estimated using the same aqueous method and were, on an average, found above 95% purity.

<Chromatogram>

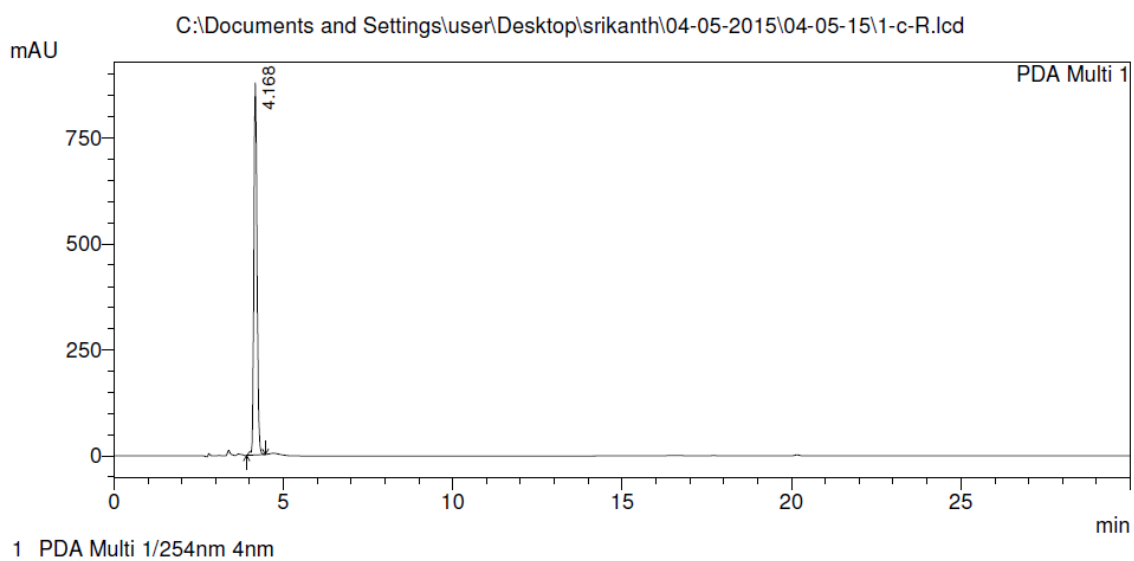


Figure 5.31: HPLC chromatogram of most active compound **6** with 98.60% purity.

<Chromatogram>

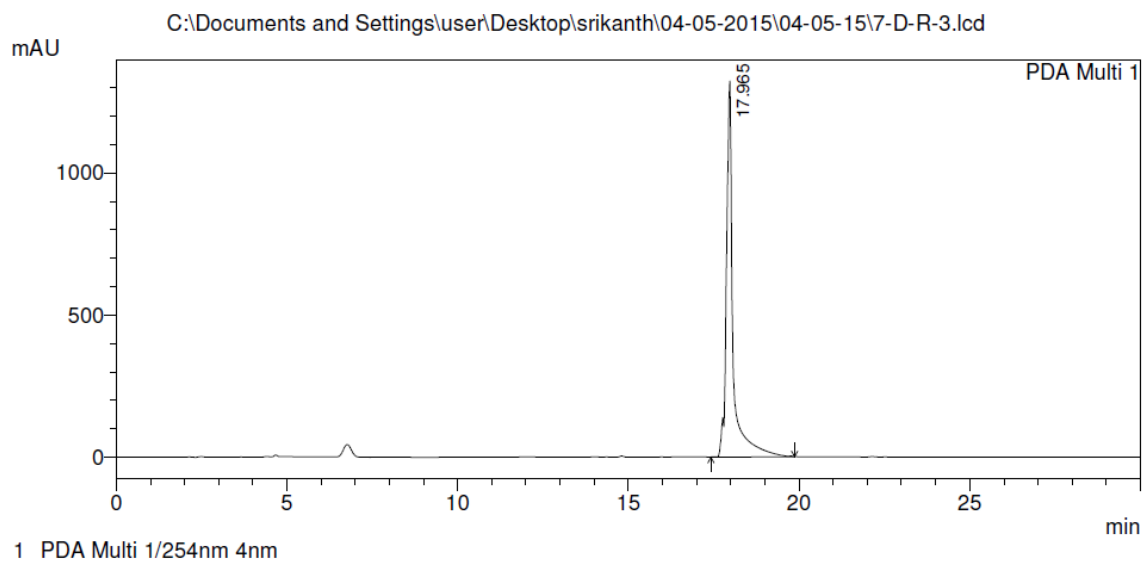


Figure 5.32: HPLC chromatogram of most active compound **19** with 95.96% purity.

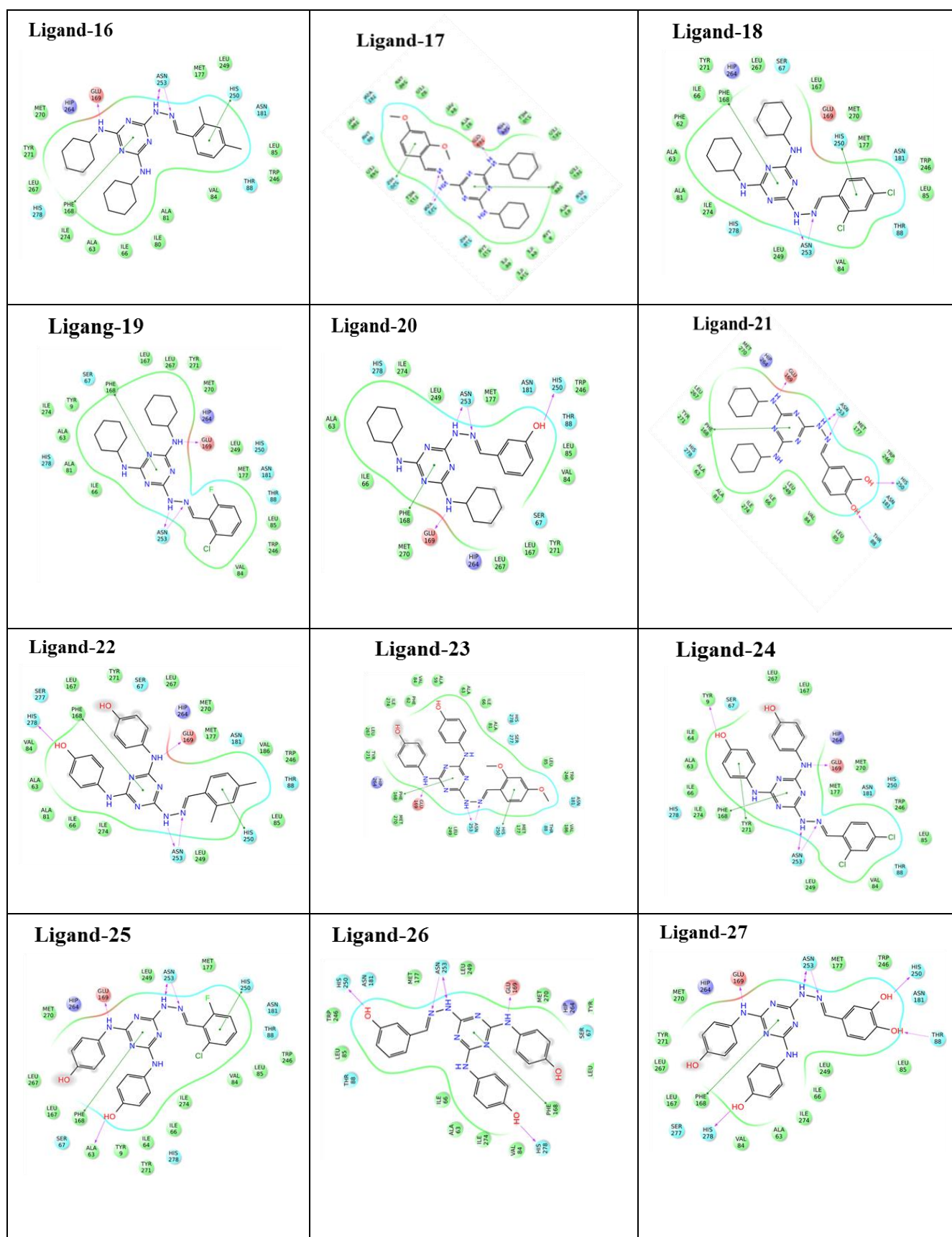


Figure 5.34: Ligand interaction pictures of lead molecules from Ligand 16 to 27.

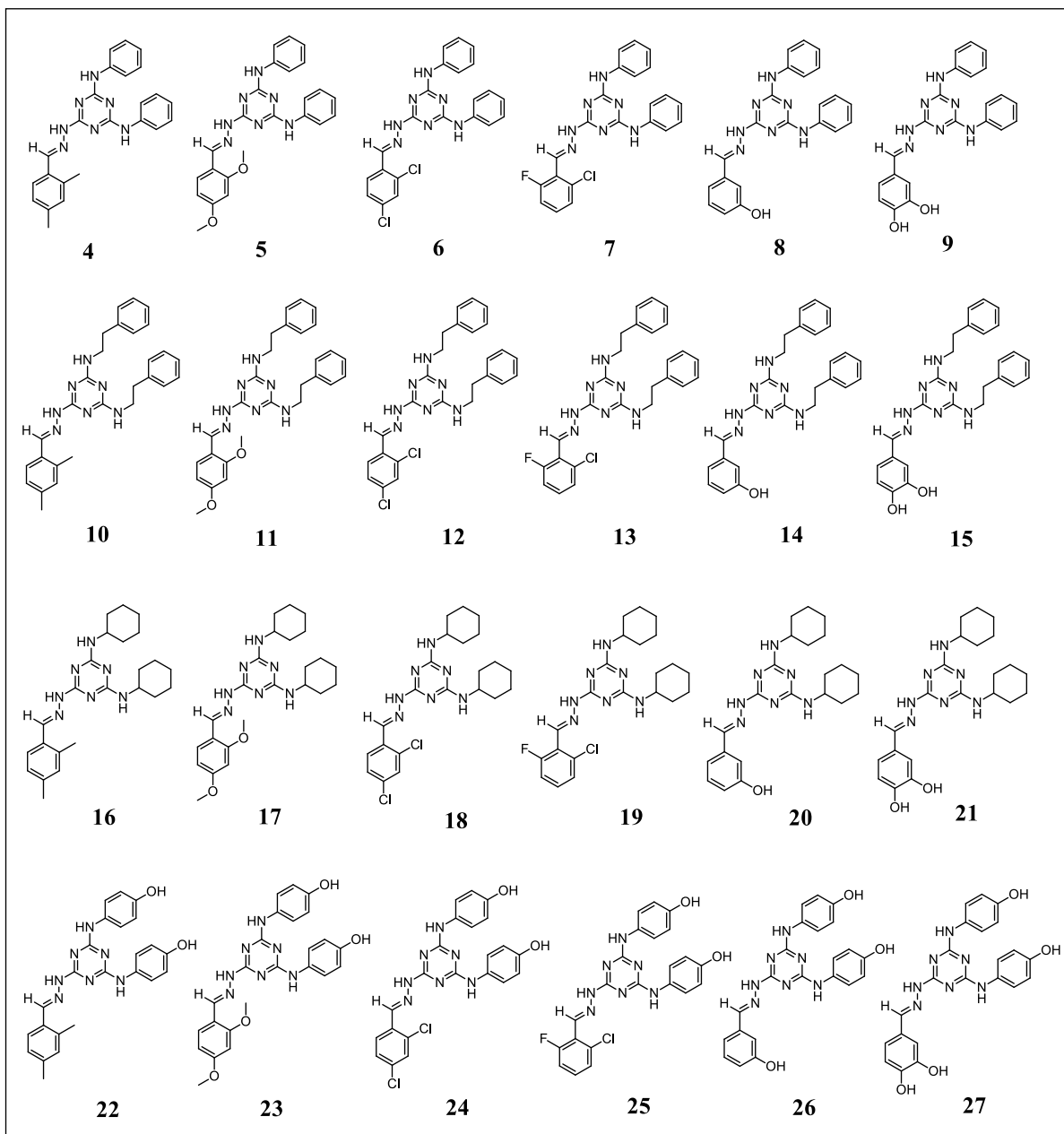


Figure 5.35: Structures of 24 synthetic lead molecules.

5.7. Pharmacological activity:

Rotarod test was used to determine acute neurological toxicity. Anticonvulsant and neurotoxicity test results for the titled compounds in the mice/rat i.p. MES, scPTZ, scSTY, scPIC and NT screens are reported in the **Table 5.7**, along with the literature data for standard antiepileptic drugs. The titled 1,3,5-triazine-2,4,6-triamine derivatives (**4-27**) were administered at 300, 100 and 30 mg/kg doses in ip/sc routes. Seven out of twenty four compounds screened against neurotoxicity test failed in protecting the animals during the observation period at doses 300 and 100 mg/kg (Initial 2 hrs. followed by 15 days). The seven compounds which showed neurotoxicity were not considered for further screening studies(sc STY and sc PIC models) but all 24 compounds were screened in MES and sc PTZ models. In the preliminary MES screen, the compounds of 1,3,5-triazine-2,4,6-triamine derivatives except **5**, **16** and **17** showed protection, indicative of their ability to prevent seizure spread. Compounds that were active at 30 mg/kg include **7, 9, 11, 12, 14, 19** and **24** at both 0.5 h & 4h time periods; compounds that were active at 100 mg/kg include **6, 8, 13, 15, 18, 20, 23** and **25** at both 0.5h & 4h time periods, whereas 10 and 27 showed protection at higher dose (300 mg/kg). Compounds **6-9, 11-15, 18-20, 23-25** were active at both 0.5 h & 4h time periods; hence these compounds exhibited prolonged duration of action. Other compounds that showed rapid onsets (0.5 h) with shorter duration of action are **4** and **22** and the compounds **21** and **26** showed activity only at 4h time point (late onset of action).

In the subcutaneous pentylenetetrazole (scPTZ) screen, a test used to identify compounds that elevated seizures threshold, twenty compounds showed protection at different doses (30, 100, 300 mg/kg) except **4, 22, 23** and **26**. At 30 mg/kg six compounds (**4-5, 9, 11, 13, and 19**) showed protection at both 0.5 h & 4h time periods; compounds that were active at 100 mg/kg include **8, 10, 12, 14-15, 18, 20-21, 24, 25** and **27** at both 0.5h & 4h time periods; whereas **5**,

16 and **17** showed protection at higher dose (300 mg/kg), hence these compounds exhibited prolonged duration of action.

In the acute neurological deficit test, all compounds except **11**, **20-22**, **25** and **27** at 0.5h and compounds **18**, **20-22**, **25** and **27** at 4h showed no neurotoxicity at 100 mg/kg. Only compounds **16** and **17** showed neurotoxicity at the maximum dose administered (300mg/kg) but no neurotoxicity could be seen at 100 mg/kg.

Overall synthetic 1, 3, 5 triazine derivatives which did not show neurotoxicity (seventeen out of twenty four) were carried onto the second phase of study, which involved antiepileptic evaluation in subcutaneous strychnine (scSTY) and subcutaneous picrotoxin (scPIC)-induced seizure threshold tests. All compounds except **5**, **16-17** and **26** showed protection against scSTY model. Compounds **8**, **10**, **12-13**, **19** and **24** showed protection at 30mg/kg (0.5 and 4h) and other compounds showed activity at 100mg/kg. Except compounds **4**, **7** and **14**, all active compounds exhibited a longer duration (4h) of action. The results suggest that 1, 3, 5-triazine-2, 4, 6-triamine derivatives have the possibility of interacting in the glycine pathway.

All compounds except **16** and **17** showed protection against scPIC model. Compounds **8-9**, **13** and **19** showed protection at 30mg/kg (0.5 and 4h), and the compounds showed activity at 100mg/kg included **6-7**, **10**, **12**, **14-15**, **23** and **24**. Except compounds **4-5** and **26** all other compounds showed protection in both 0.5h and 4h intervals. This implied that 1, 3, 5-triazine-2, 4, 6-triamine derivatives could act through GABA (γ -aminobutyric acid) mediation.

In general, it appeared that all 17 compounds except **5**, **16**, **17** and **26** were found to be effective in at least two *in vivo* models, of which compounds **16** and **17** showed activity only in the scPTZ model, and were found to be neurotoxic at its anticonvulsant dose. However,

compounds **4** and **23** were effective in three animal models. Eleven compounds (**6-10, 12-15, 19** and **24**) showed activity in all the screens (MES, scPTZ, scSTY, and scPIC).

Table 5.7: Anticonvulsant activity and minimal motor impairment of 1,3,5 triazine 2,4,6 triamine derivatives

Compound	Intraperitoneal injection in mice ^a									
	MES screen		scPTZ screen		scSTY screen (Rat)		scPIC screen (Rat)		Neurotoxicity screen	
	0.5 hr.	4 hr.	0.5 hr.	4 hr.	0.5 hr.	4 hr.	0.5 hr.	4 hr.	0.5 hr.	4 hr.
4	100	—	—	—	100	—	100	—	—	—
5	—	—	300	300	—	—	100	—	—	—
6	100	100	30	30	100	100	100	100	—	—
7	30	30	30	30	100	—	100	100	—	—
8	100	100	100	100	30	30	30	30	—	—
9	30	30	30	30	100	100	30	30	—	—
10	300	300	100	100	30	30	100	100	—	—
11	30	30	30	30	X	X	X	X	100	100
12	30	30	100	100	30	30	100	100	—	—
13	100	100	30	30	30	30	30	30	—	—
14	30	30	100	100	100	—	100	100	—	—
15	100	100	100	100	100	100	100	100	—	—
16	—	—	300	300	—	—	—	—	300	300
17	—	—	300	300	—	—	—	-	300	300
18	100	100	100	100	X	X	X	X	100	100
19	30	30	30	30	30	30	30	30	—	—
20	100	100	100	100	X	X	X	X	100	100
21	—	300	100	100	X	X	X	X	100	100
22	100	—	—	—	X	X	X	X	100	100
23	100	100	—	—	100	100	100	100	—	—
24	30	30	100	100	30	30	100	100	—	—
25	100	100	100	100	X	X	X	X	100	100
26	—	300	—	—	—	—	100	—	—	—
27	300	300	100	100	X	X	X	X	100	100
Sod. Valproate	—	300	100	—	100	—	—	—	—	—
Phenytoin	30	30	—	—	—	—	X	X	100	100

^aDose of 30, 100 and 300mg/kg were administered. Figures in the table indicate minimum dose whereby bioactivity was demonstrated in half or more of the mice. The dash (—) indicates absence of activity at maximum dose administered (300mg/kg); cross (X) indicates the compounds not tested in animals.

5.8. Summary and conclusion

This study represents the results of our research work targeted at identifying a potent and selective $A_{2A}R$ antagonist. The design approach was based on structure-based e-pharmacophore modelling by employing 2.6 Å crystal structure of Human A_{2A} receptor bound to ZMA241385 was retrieved from protein data bank (PDB code: 3EML).

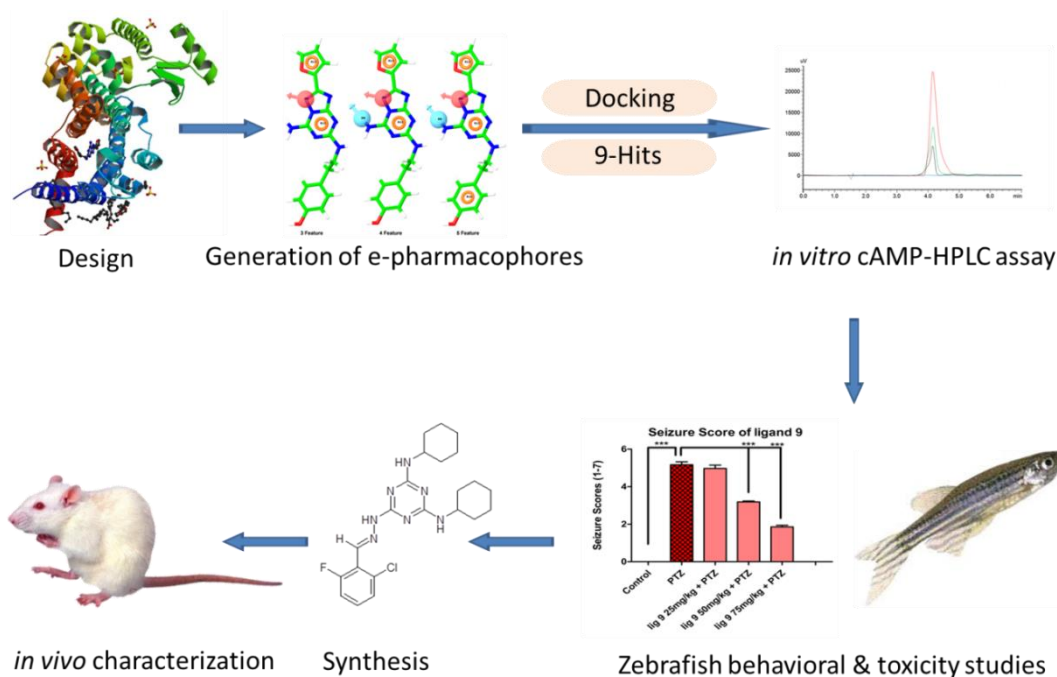


Figure 5.36: Overall workflow of anti-epileptic evaluation of A_{2A} antagonists

Nine compounds were identified, and subjected to quantitative estimation of cAMP in MCF-7 breast cancer cellines by HPLC assay method. The levels of cyclic AMP accumulated in MCF-7 breast cancer cell lines stimulated by 0.1% ethyl alcohol over a period of 24 h were investigated. For that, a simple HPLC method was developed and validated for quantitative estimation of cAMP. Validation of the peak was carried out by comparing retention time of the sample peak with a Cyclic AMP reference standard. In the HPLC assay, out of 9 compounds tested, Ligand 9 was found to have the cAMP inhibitory IC_{50} of 2.065 μ M which was almost similar/close to the cAMP inhibitory IC_{50} of standard selective A_{2A} receptor antagonist SCH-58261(1.399 μ M), hence ligand 9 emerged as the most promising lead. Ligand 9 pre-treatment significantly suppressed 220-mg/kg pentylenetetrazole-induced increases in rotational movements and visual assessment of seizures in a dose dependent manner. Ligand 9 at the dose of 75mg/kg showed neuro-protection in PTZ induced seizure model in an adult zebrafish and was found to be safe at lower concentrations except at 30 μ M

indicating an acceptable neuro, hepato, and cardiovascular safety profile. Further, Docking based SAR optimization resulted various 1, 3, 5-triazine-2, 4, 6-triamine derivatives through a facile reaction condition and has marked anticonvulsant activity against various animal models of seizures by their multiple mechanism of action in four animal models of seizures. Eleven compounds (**6-10**, **12-15**, **19** and **24**) had shown activity in all the screens (MES, scPTZ, scSTY, and scPIC), exhibiting a broad spectrum of anticonvulsant activity with no neurotoxicity. Overall compound **19** was found to be active at a dose of 30 mg/kg in all four animal models considered to be a most promising, potential lead for treatment of epilepsy. **Figure 5-36** represents overall workflow of anti-epileptic evaluation of A_{2A} antagonists starting from design to pharmacological evaluation.

**Results and discussion:
Identification of novel $A_{2B}R$ antagonists
by using Pharmacophore-Based 3D
QSAR and its anti-nociceptive and anti-
inflammatory effects**

6.1. Identification of novel $A_{2B}R$ antagonists by using pharmacophore-based 3D QSAR and its anti-nociceptive and anti-inflammatory effects

Pain is an ill-defined, complex unpleasant phenomenon, usually evoked by an internal or external noxious stimulus (nociception). Until 2006, the role of this receptor ($A_{2B}R$) has been unexplored due to the lack of selective $A_{2B}R$ agonists as well as an A_{2B} knockout mouse. Recently, Abo-Salem *et al.*, 2004 demonstrated that novel selective adenosine $A_{2B}R$ antagonists produced a similar anti-nociception to caffeine in the hot-plate test in mice. Furthermore, $A_{2B}R$ antagonists were potent in attenuating pulmonary inflammation as well as in reducing inflammatory pain and inflammatory hyperalgesia. In the present study, pharmacophore model was generated considering a dataset of 265 compounds. A five point pharmacophore model AADRR was developed. A valid 3D QSAR model was generated based on the developed pharmacophore model. This model was further validated by external validation and was further utilized to identify diverse scaffolds against A_{2B} from BITS in-house database based on the fitness and predicted activity of the hits. The present study was carried out to evaluate the anti-nociceptive and anti-inflammatory activities of $A_{2B}R$ antagonists (30 mg/kg) using acetic acid induced writhing, formalin induced paw licking, hot plate and tail immersion methods. These test compounds were further evaluated for its anti-inflammatory activity by carrageenan-induced mice paw edema. Further, we measured levels of tumour necrosis factor (TNF- α), interleukin-1 β (IL-1 β), interleukin-6 (IL-6) and nuclear factor (NF κ B) in the edema paw tissue using real-time quantitative RT-PCR analysis.

6.2. Ligand based drug design

6.2.1. Determination of pharmacophore and validation

The dataset containing a total of 265 compounds was considered in the present study which was divided into active, moderately active and inactive subsets to obtain the common pharmacophore. Compounds with pIC_{50} higher than or equal to 8.399 were considered to be active and those with less than 7.072 were considered to be inactive, remaining compounds were considered to be moderately active. Based on the threshold values set, 66 compounds were found to fall under active subset while 67 and 132 compounds were found inactive and moderately active respectively. Pharmacophore sites for all compounds were generated and a common pharmacophore was attempted to generate, which was set to match at least 61 out of 66 active compounds.

19 pharmacophore hypotheses were found to be generated for which scoring hypothesis was applied. Of these 19, five best hypotheses were selected based on the generated scores. The best five selected hypotheses are given in **Table 6.1**. Of these five, AADRR.6 was selected as better hypothesis for further QSAR studies based on survival score of 3.737, survival-inactive score of 2.248 and post hoc value of about 3.737.

Table 6.1: Top five pharmacophore hypotheses generated and given with their scoring parameters

Hypothesis	Survival	Survival-inactive	Posthoc	Energy	Activity	Inactive
AADRR.6	3.737	2.248	3.737	3.328	8.444	1.489
ADRRR.9	3.729	2.282	3.729	3.328	8.444	1.447
ADRRR.35	3.722	2.302	3.722	3.328	8.444	1.42
AADRR.42	3.722	2.36	3.722	3.328	8.444	1.362
AADRR.37	3.722	2.285	3.722	3.328	8.444	1.437

A: Acceptor atom, D: Donor atom, R: Aromatic ring features.

AADRR.6 was found to contain two hydrogen bond acceptors, one hydrogen bond donor and two ring aromatics. The selected pharmacophore with its intersite distances is shown in **Figure 6.1**. Compound **C61** with pIC_{50} **8.44** was found to overlap on to the selected

hypothesis with a maximum fitness value of 3.0. This compound was found to be one of the most active compounds against A_{2B} from the selected dataset. Further, the selected hypothesis was employed in the generation of 3D QSAR model which was further validated for its predictability. The pharmacophore-based method for QSAR generation was adopted over atom-based, so as to map and incorporate the pharmacophoric features from the developed common pharmacophore in the QSAR model. Also, another reason can be explained in terms of huge number of dataset compounds which include diversity in their structures and with many rotatable bonds, thereby making pharmacophore-based model the preferred one. The generated 3D QSAR model was subjected to PLS analysis. All data set (training and test) molecules used for pharmacophore generation and 3D QSAR study are given in **Tables 6.2 and 6.3** with their structural information, observed, predicted biological activity and fitness.

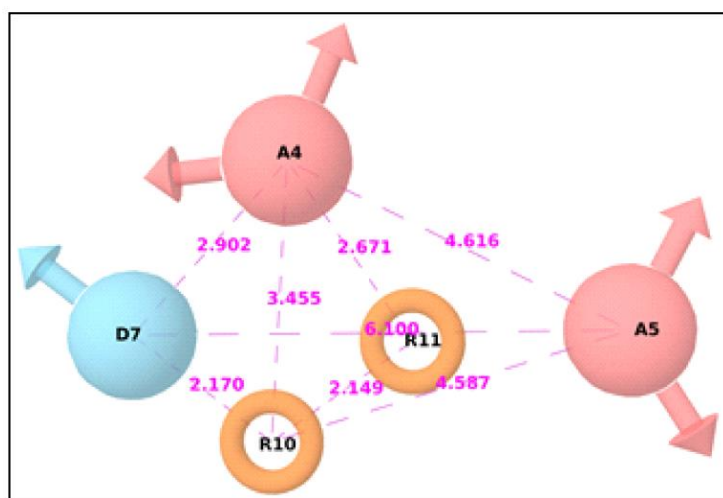
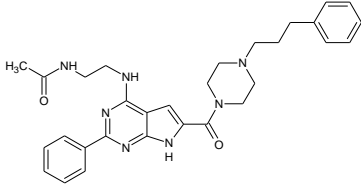
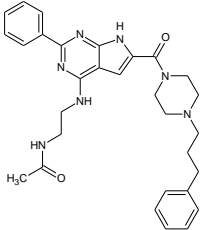
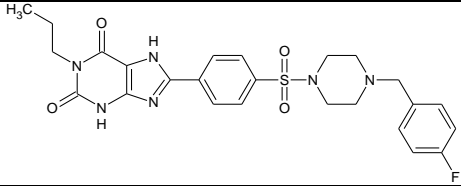
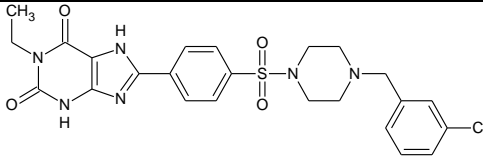
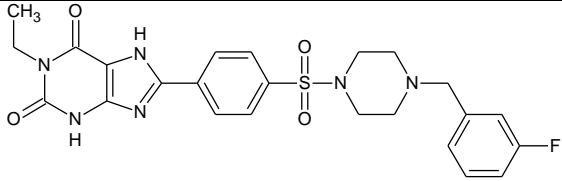
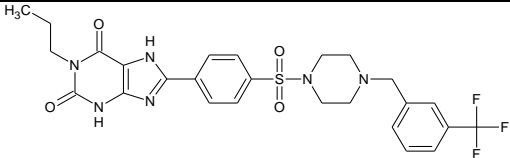
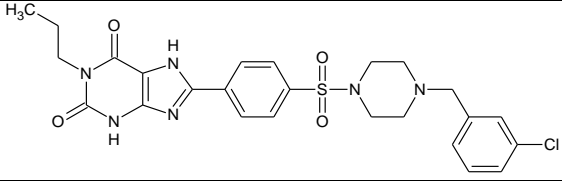
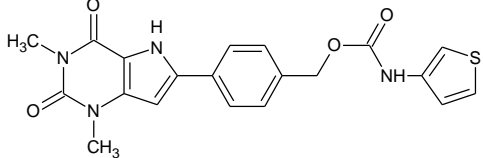
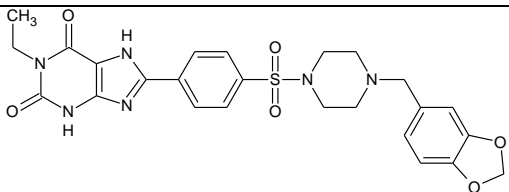
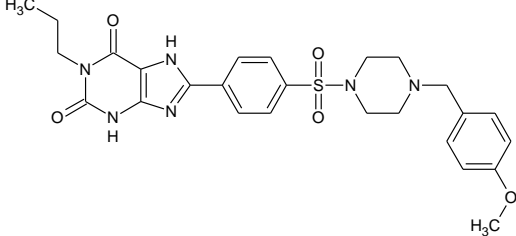
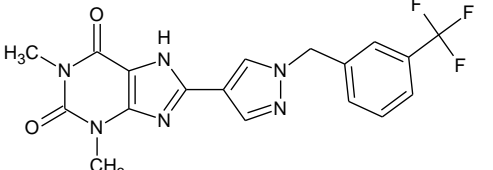
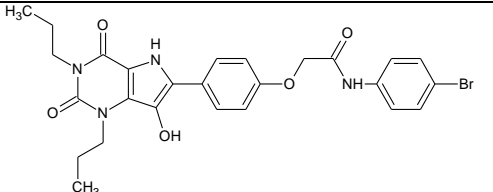
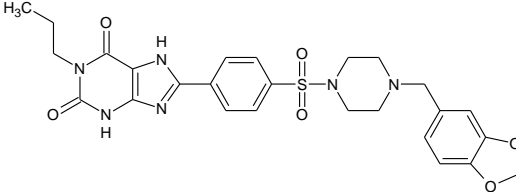
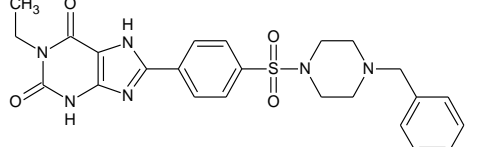
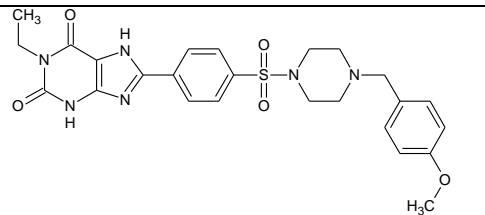
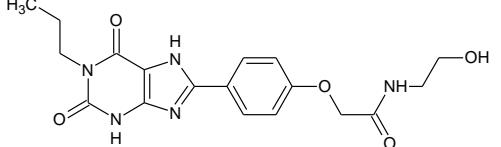
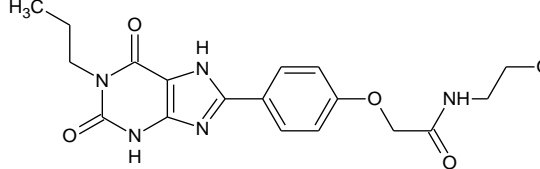
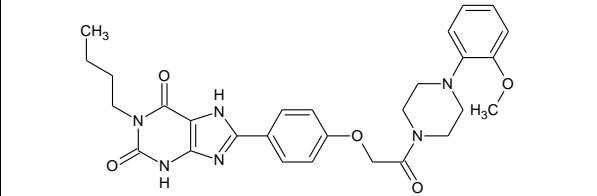
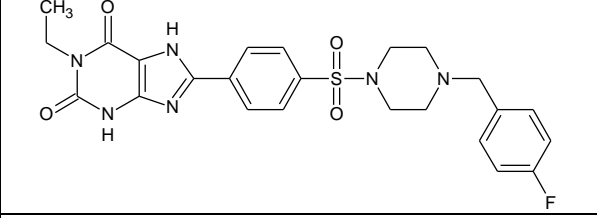
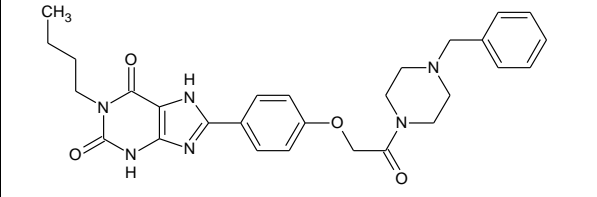
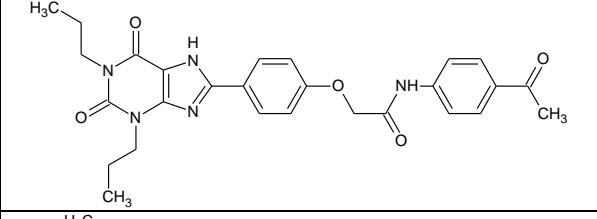
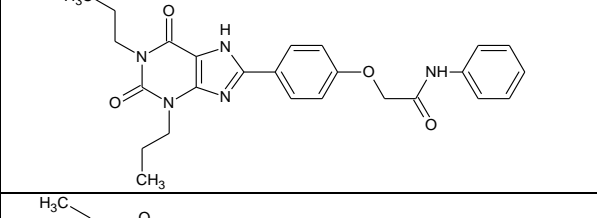
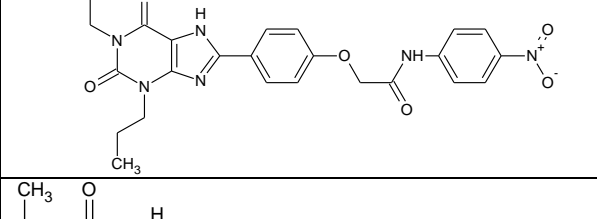
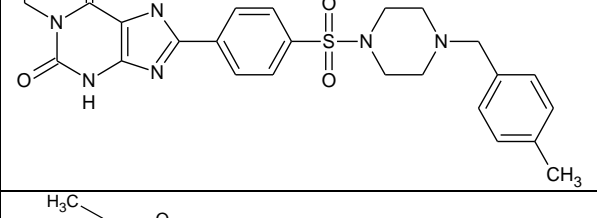
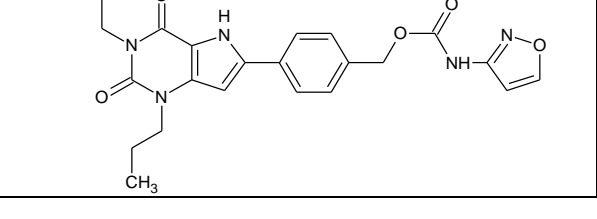


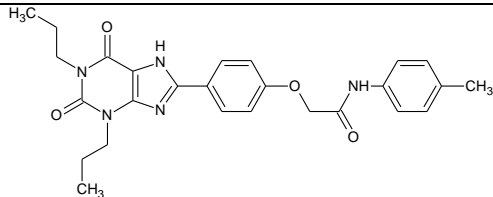
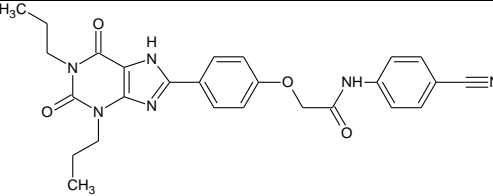
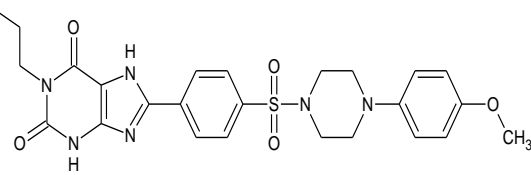
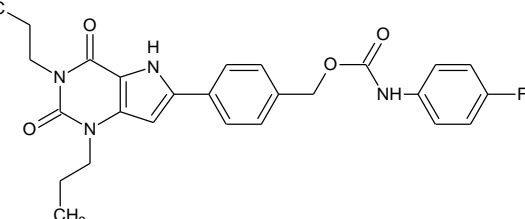
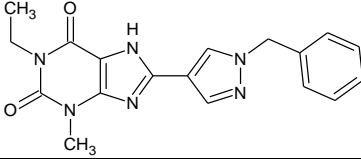
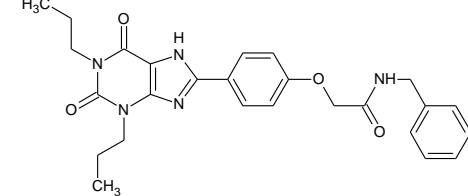
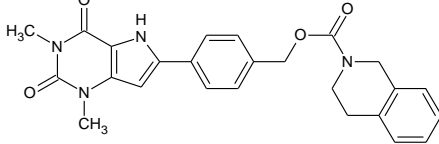
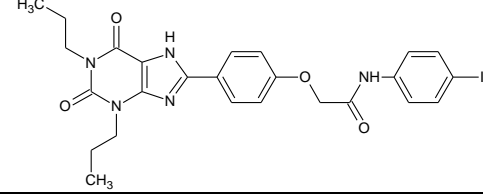
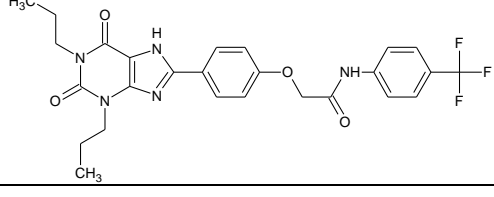
Figure 6.1: Pharmacophore hypothesis AADRR.6 with distances between pharmacophoric sites shown in pink dashed lines. All measurements are in Å units

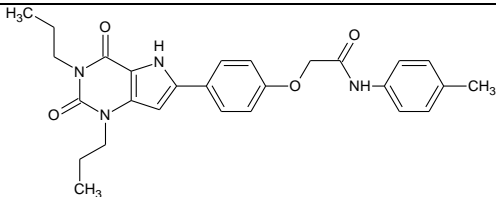
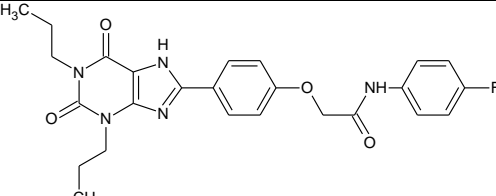
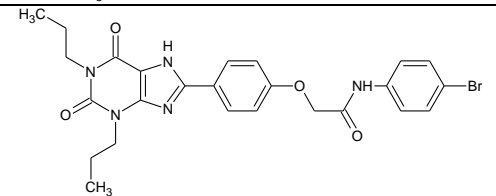
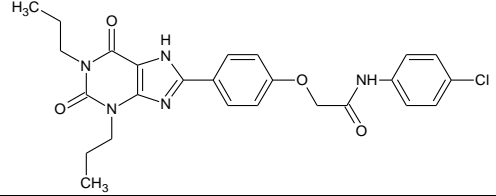
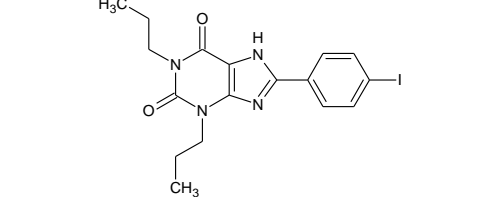
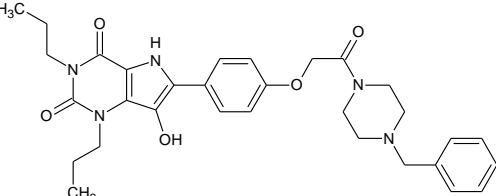
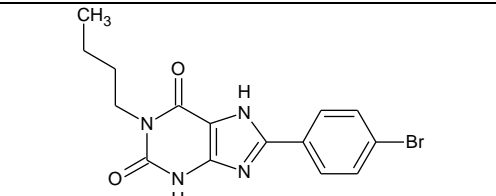
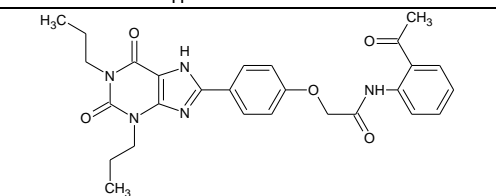
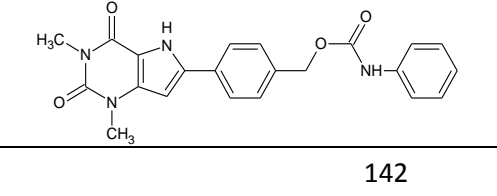
Table 6.2: Training set compounds of dataset used in QSAR model development. The observed and predicted activity along with fitness over pharmacophore model is given in table.

Compound	Ligand Name	Observed activity	Predicted activity 5	Fitness
C6		9.398	9.68	1.34
C9		9.301	9.57	1.31
C11		9.225	8.85	2.9
C12		9.215	8.93	2.97
C13		9.158	8.89	2.97
C14		9.111	8.99	2.91
C15		9.107	8.98	2.99
C16		9.097	8.82	2.62
Compound	Ligand Name	Observed	Predicted	Fitness

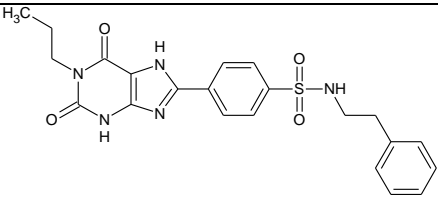
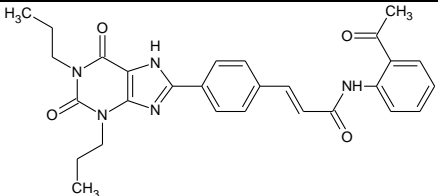
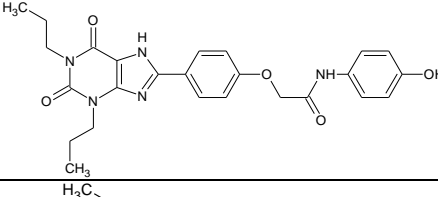
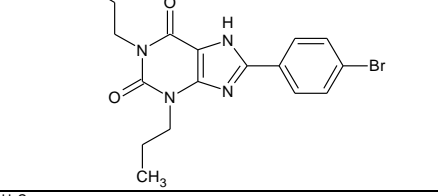
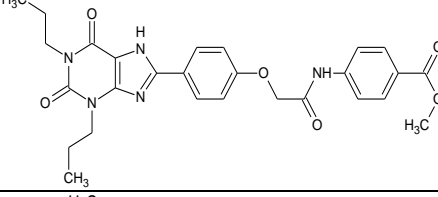
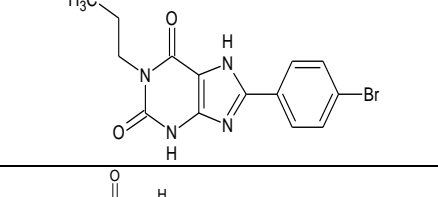
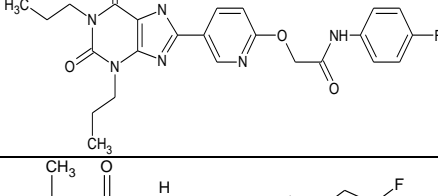
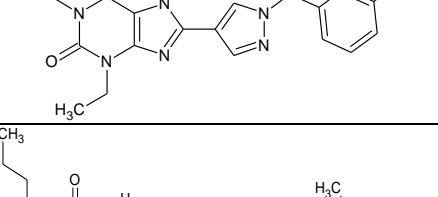
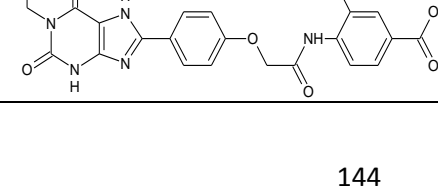
		activity	activity 5	
C18		9.058	8.88	2.93
C19		9.025	8.94	2.97
C21		9	8.72	2.59
C22		9	8.76	2.7
C23		8.975	8.93	2.94
C24		8.939	8.87	2.99
C25		8.924	8.88	2.95
C26		8.921	8.81	2.67
C27		8.921	8.81	2.67

Compound	Ligand Name	Observed activity	Predicted activity 5	Fitness
C28		8.921	8.77	2.71
C29		8.896	8.88	2.97
C30		8.886	8.88	2.7
C31		8.857	8.68	2.59
C32		8.83	8.61	2.62
C33		8.818	8.79	2.63
C34		8.801	8.87	2.97
C35		8.77	8.74	2.6

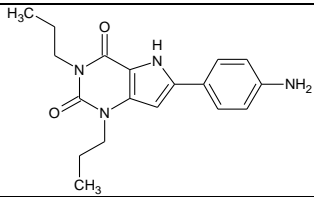
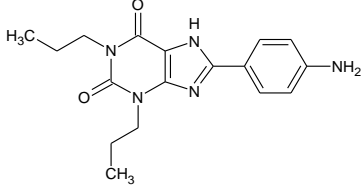
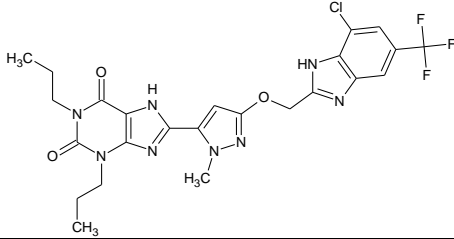
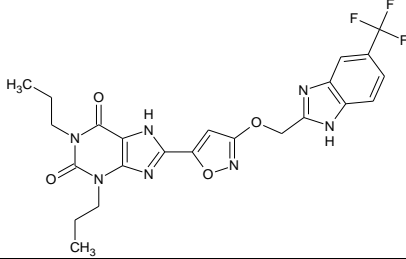
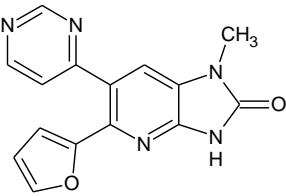
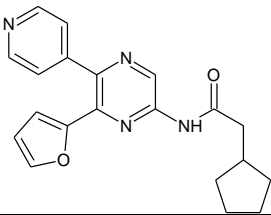
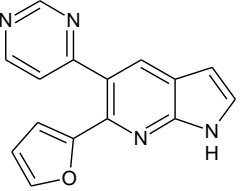
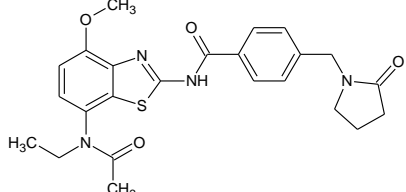
Compound	Ligand Name	Observed activity	Predicted activity 5	Fitness
C36		8.726	8.84	2.63
C37		8.706	8.75	2.62
C38		8.701	8.59	2.71
C39		8.699	8.64	2.6
C40		8.699	8.65	2.66
C41		8.69	8.59	2.63
C42		8.678	8.76	2.64
C43		8.672	8.67	2.62
C44		8.67	8.8	2.63

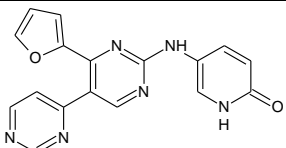
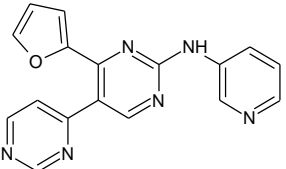
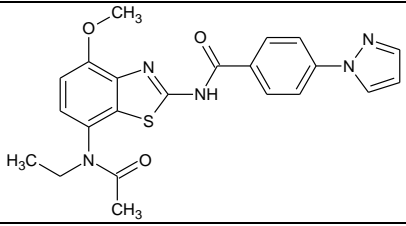
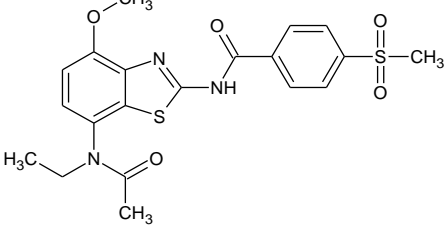
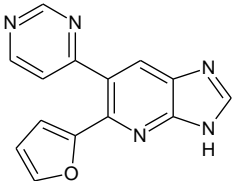
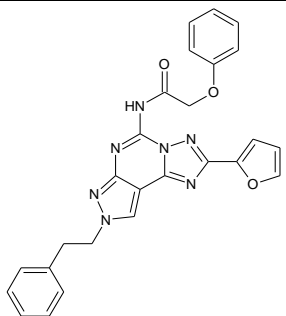
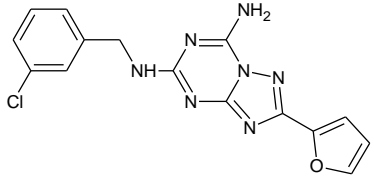
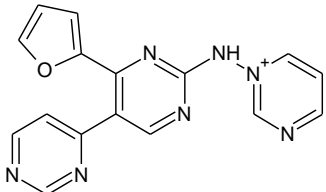
Compound	Ligand Name	Observed activity	Predicted activity 5	Fitness
C45		8.658	8.71	2.71
C46		8.654	8.58	2.62
C47		8.629	8.71	2.62
C48		8.607	8.83	2.63
C49		8.602	8.48	2.57
C50		8.585	8.56	2.66
C51		8.569	8.37	2.61
C52		8.562	8.71	2.65
C53		8.553	8.73	2.63

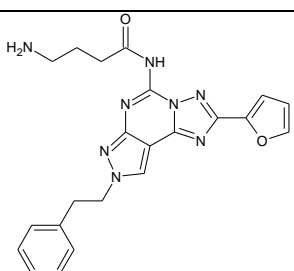
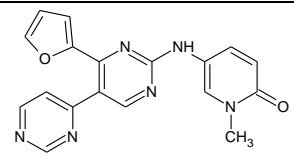
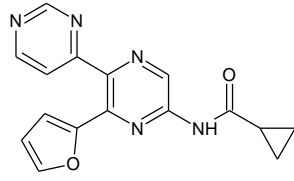
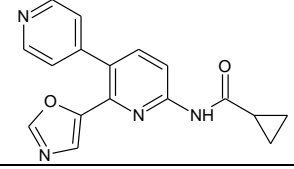
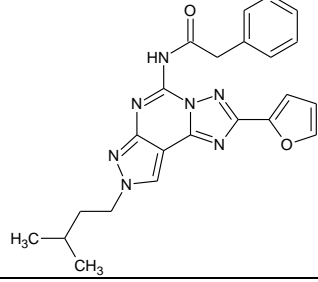
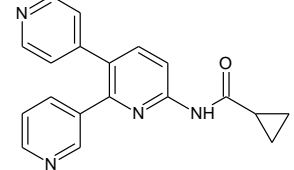
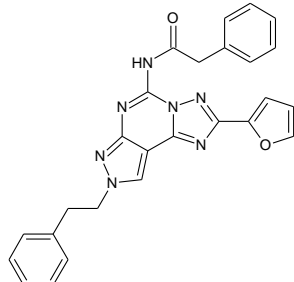
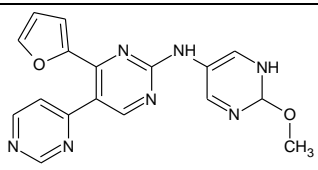
Compound	Ligand Name	Observed activity	Predicted activity 5	Fitness
C54		8.538	8.71	2.75
C55		8.519	8.52	2.71
C56		8.495	8.7	2.61
C57		8.476	8.6	2.55
C58		8.47	8.7	2.62
C59		8.469	8.4	1.24
C60		8.456	8.37	2.52
C61		8.444	8.93	3

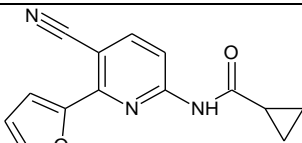
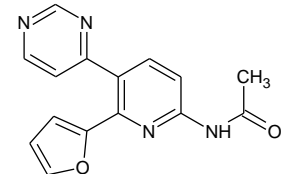
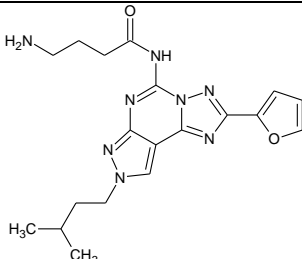
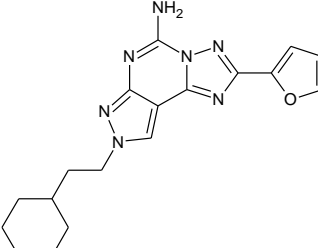
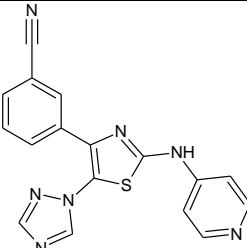
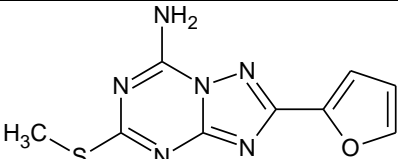
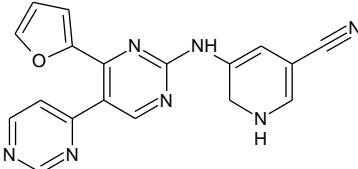
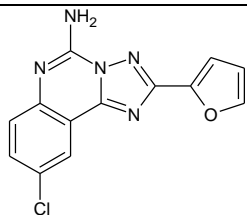
Compound	Ligand Name	Observed activity	Predicted activity 5	Fitness
C62		8.441	8.48	2.75
C63		8.438	8.45	2.49
C64		8.431	8.4	2.68
C65		8.42	8.4	2.57
C66		8.406	8.63	2.67
C70		8.357	8.27	2.55
C73		8.319	8.31	2.62
C77		8.301	8.59	2.62
C78		8.276	8.43	2.61

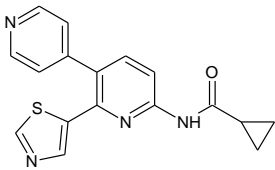
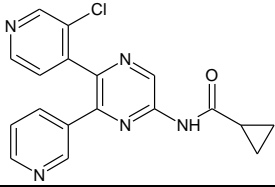
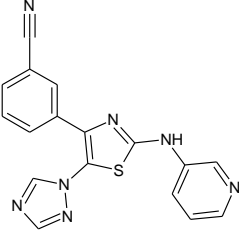
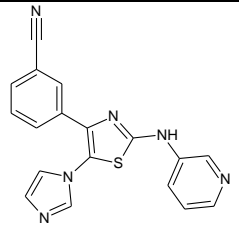
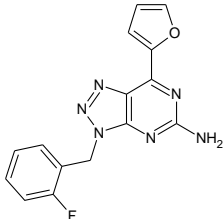
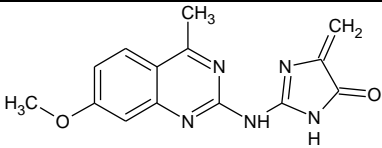
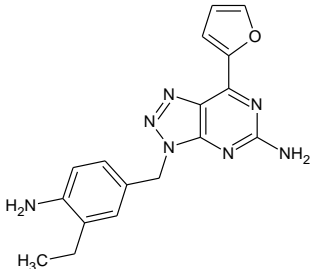
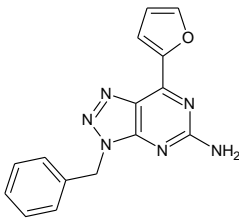
Compound	Ligand Name	Observed activity	Predicted activity 5	Fitness
C84		8.26	8.13	2.51
C85		8.26	8.19	2.73
C90		8.222	8.27	2.59
C93		8.187	8.03	2.55
C96		8.155	8.44	2.75
C100		8.124	8.5	2.8
C102		8.111	8.28	2.62
C103		8.108	8.44	2.62
C104		8.092	8.16	2.64

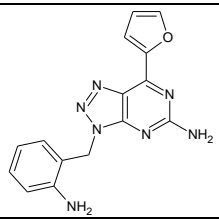
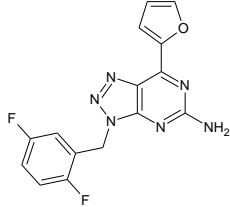
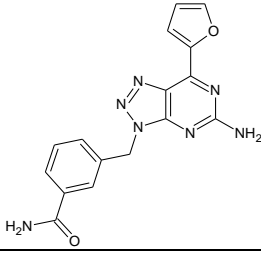
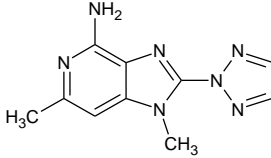
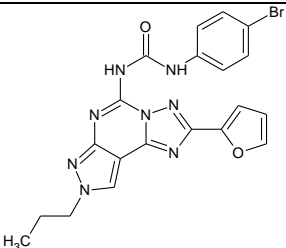
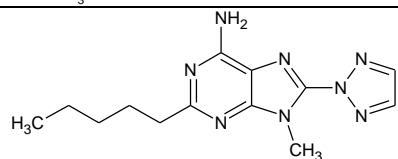
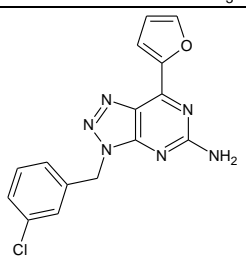
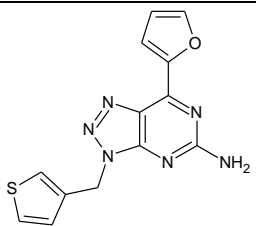
Compound	Ligand Name	Observed activity	Predicted activity 5	Fitness
C106		8.051	8.07	2.53
C108		8.046	8.19	2.56
C109		8.027	8.07	2.46
C114		8	8.25	2.55
C117		7.959	7.73	1.57
C121		7.921	7.82	1.64
C125		7.886	7.8	1.55
C128		7.854	7.74	1.31

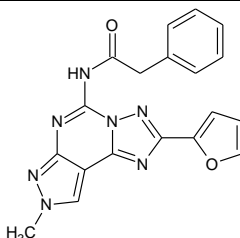
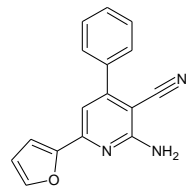
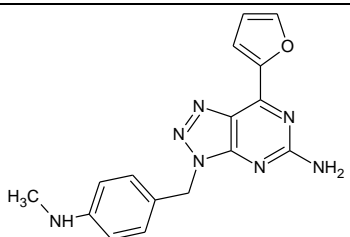
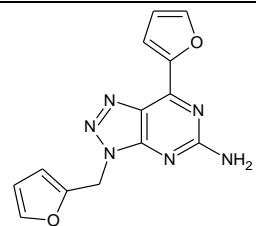
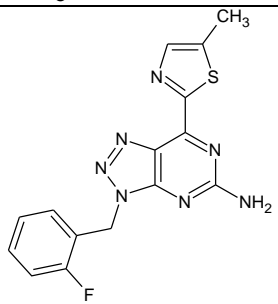
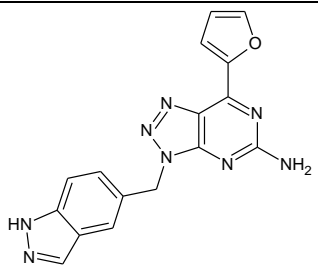
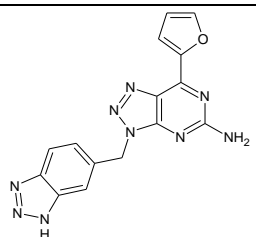
Compound	Ligand Name	Observed activity	Predicted activity 5	Fitness
C130		7.796	7.67	1.61
C133		7.77	7.67	1.63
C136		7.745	7.66	1.29
C139		7.721	7.74	1.3
C142		7.678	7.8	1.55
C145		7.658	7.56	1.47
C149		7.627	7.72	1.15
C151		7.62	7.47	1.56

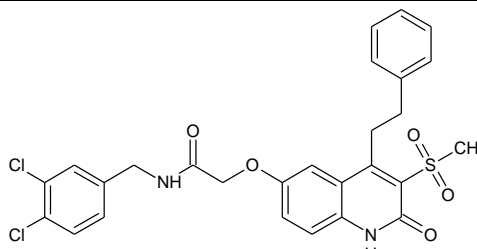
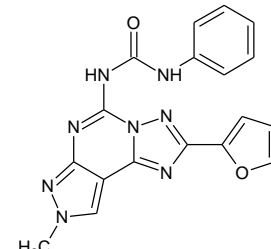
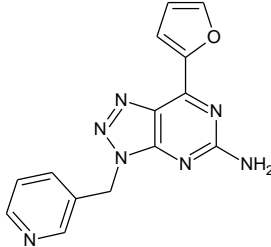
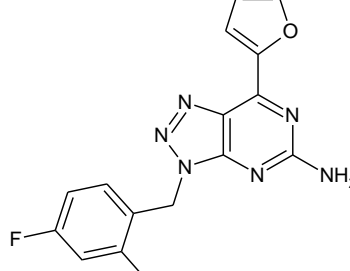
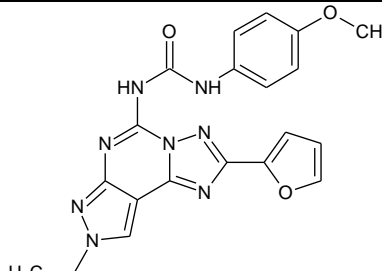
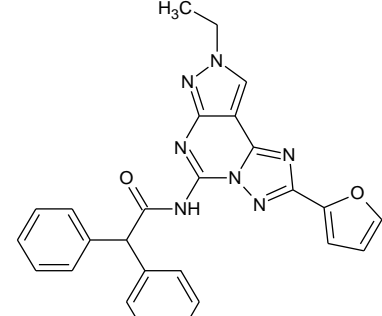
Compound	Ligand Name	Observed activity	Predicted activity 5	Fitness
C155		7.559	7.57	1.49
C158		7.553	7.37	1.06
C159		7.538	7.51	1.64
C162		7.523	7.31	1.46
C164		7.509	7.31	1.49
C169		7.481	7.51	1.18
C173		7.456	7.54	1.47
C176		7.409	7.26	0.99

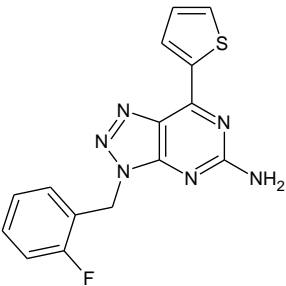
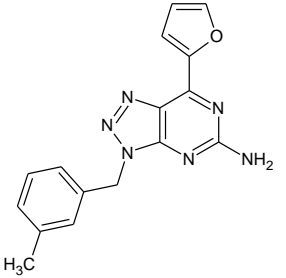
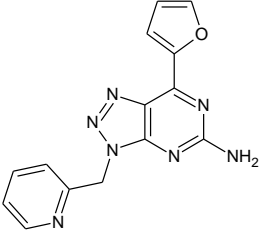
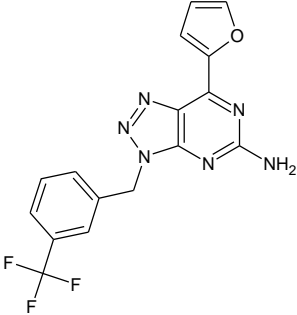
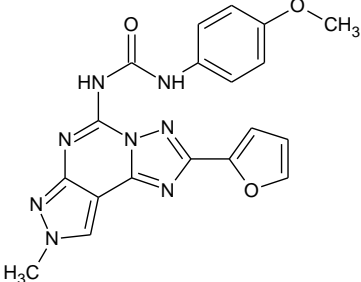
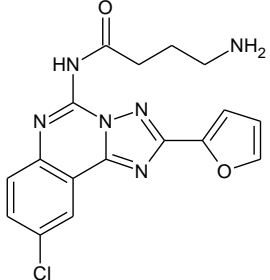
Compound	Ligand Name	Observed activity	Predicted activity 5	Fitness
C178		7.387	7.12	1.35
C182		7.328	7.31	1.33
C185		7.277	7.14	1.51
C187		7.253	7.18	1.36
C190		7.208	7.12	1.47
C192		7.187	6.93	1.43
C193		7.161	7.38	1.04
C195		7.149	6.81	1.4

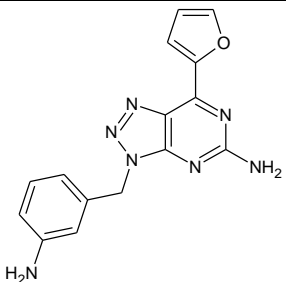
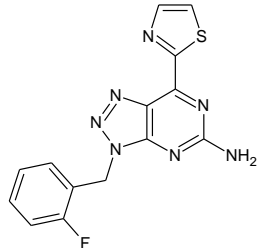
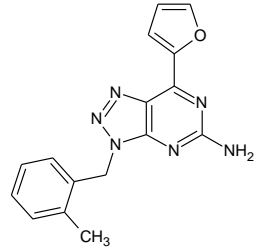
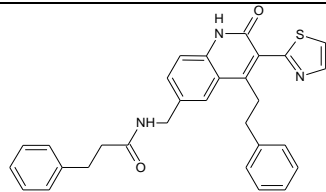
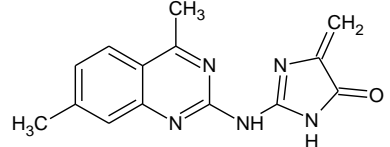
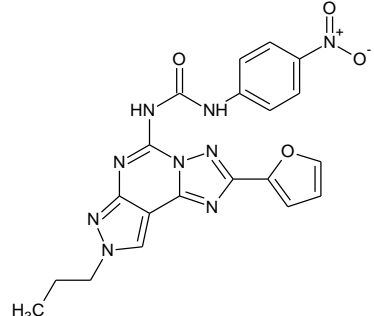
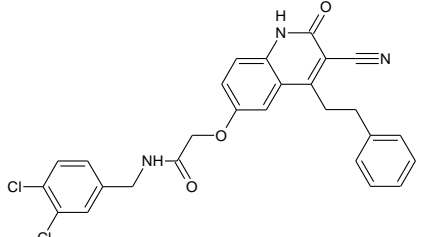
Compound	Ligand Name	Observed activity	Predicted activity 5	Fitness
C198		7.108	7.32	1.24
C199		7.071	6.99	1.35
C200		7.066	7.17	1.47
C201		7.036	6.82	0.97
C202		6.963	6.67	1.6
C203		6.951	6.61	1.43
C204		6.928	6.72	1.53
C205		6.914	6.71	1.55

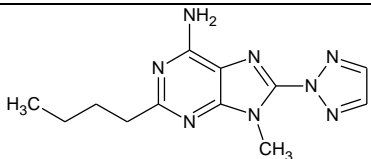
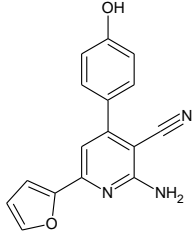
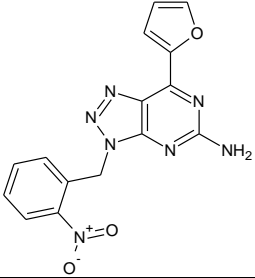
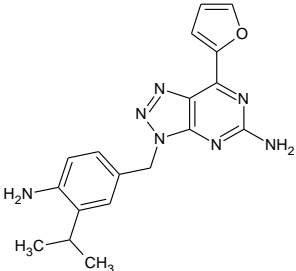
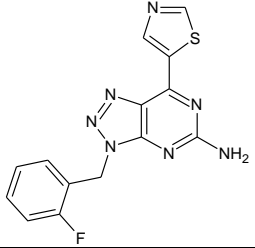
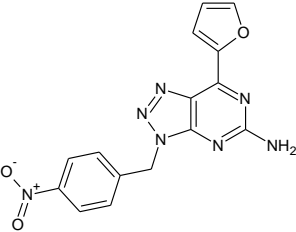
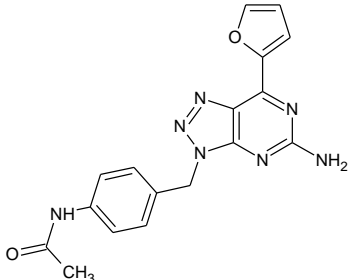
Compound	Ligand Name	Observed activity	Predicted activity 5	Fitness
C206		6.91	6.84	1.55
C207		6.893	6.74	1.54
C208		6.879	6.7	1.55
C209		6.854	6.52	1.29
C210		6.824	6.67	1.49
C211		6.815	6.65	1.3
C212		6.796	6.53	1.56
C213		6.785	6.64	1.57

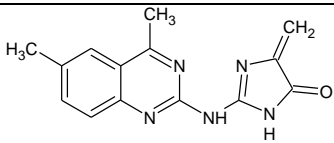
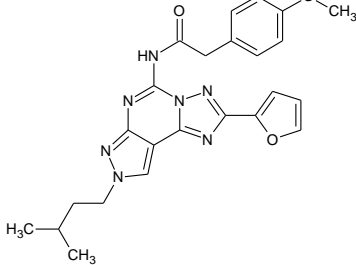
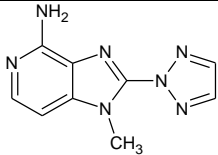
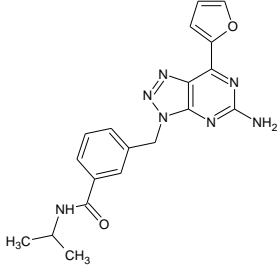
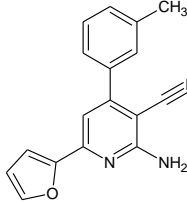
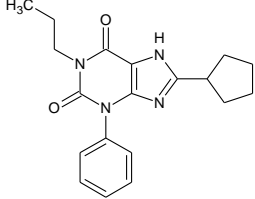
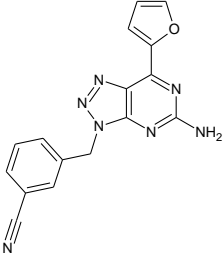
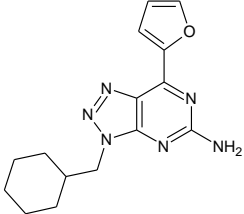
Compound	Ligand Name	Observed activity	Predicted activity 5	Fitness
C214		6.783	6.98	1.51
C215		6.77	6.62	1.29
C216		6.742	6.7	1.54
C217		6.717	6.69	1.57
C218		6.701	6.7	1.55
C219		6.686	6.74	1.53
C220		6.686	6.6	1.54

Compound	Ligand Name	Observed activity	Predicted activity 5	Fitness
C221		6.676	6.58	1.53
C222		6.654	6.72	1.51
C223		6.648	6.61	1.56
C224		6.646	6.67	1.6
C225		6.611	6.69	1.49
C226		6.606	6.79	1.47

Compound	Ligand Name	Observed activity	Predicted activity 5	Fitness
C227		6.606	6.75	1.5
C228		6.595	6.5	1.56
C229		6.588	6.7	1.56
C230		6.587	6.51	1.54
C231		6.583	6.6	1.49
C232		6.569	6.6	1.35

Compound	Ligand Name	Observed activity	Predicted activity 5	Fitness
C233		6.569	6.53	1.56
C234		6.567	6.61	1.53
C235		6.55	6.72	1.55
C236		6.536	6.44	1.37
C237		6.535	6.5	1.43
C238		6.516	6.6	1.48
C239		6.471	6.34	1.35

Compound	Ligand Name	Observed activity	Predicted activity 5	Fitness
C240		6.453	6.56	1.3
C241		6.432	6.63	1.29
C242		6.417	6.63	1.55
C243		6.401	6.67	1.53
C244		6.374	6.4	1.52
C245		6.357	6.63	1.53
C246		6.354	6.62	1.53

Compound	Ligand Name	Observed activity	Predicted activity 5	Fitness
C247		6.351	6.56	1.46
C248		6.337	6.72	1.48
C249		6.286	6.44	1.27
C250		6.227	6.4	1.53
C251		6.208	6.48	1.29
C252		6.204	6.84	2.41
C253		6.201	6.4	1.55
C254		6.198	6.35	1.56

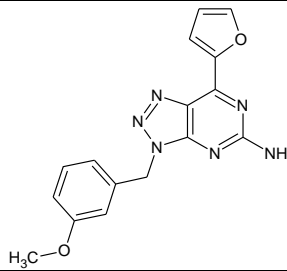
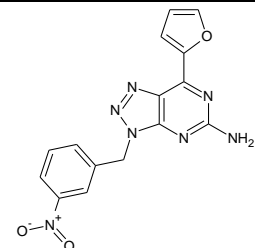
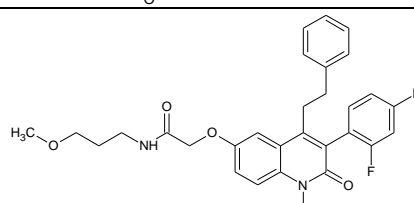
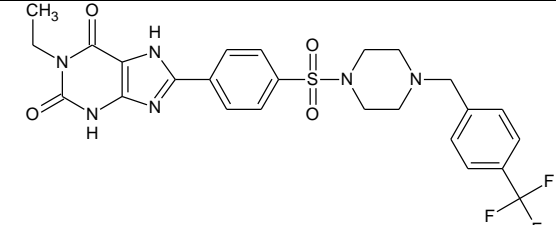
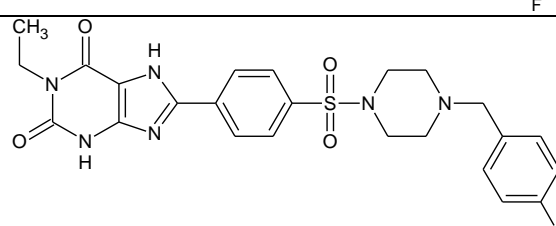
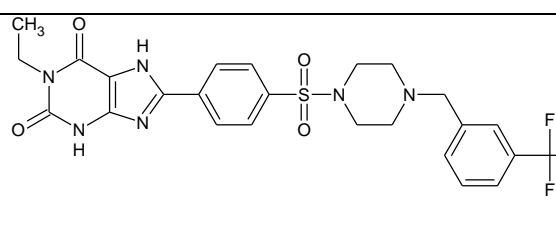
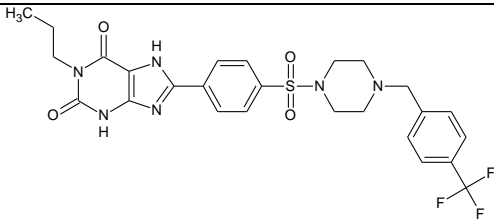
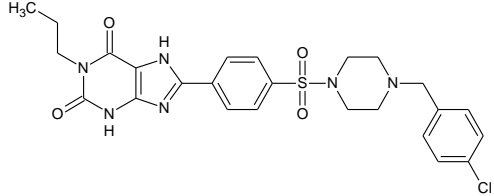
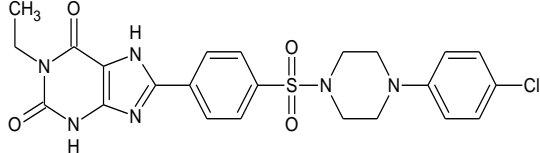
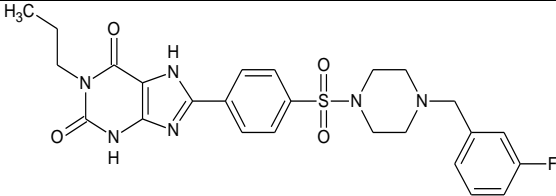
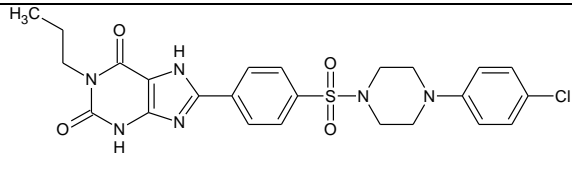
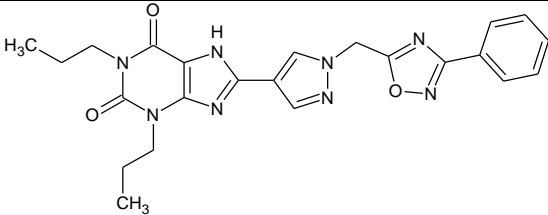
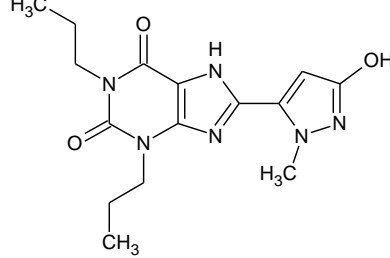
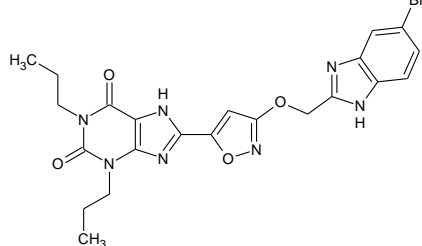
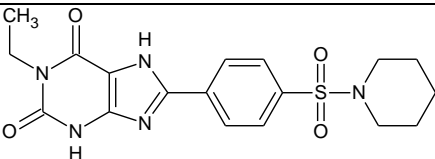
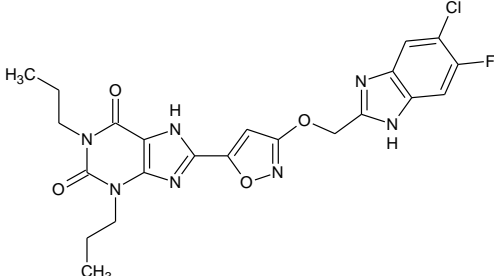
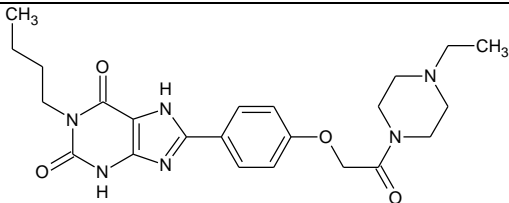
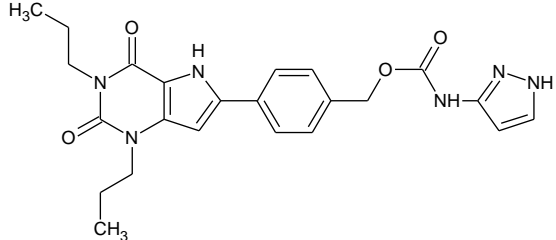
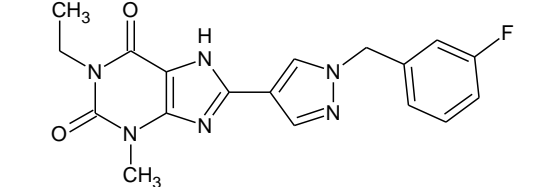
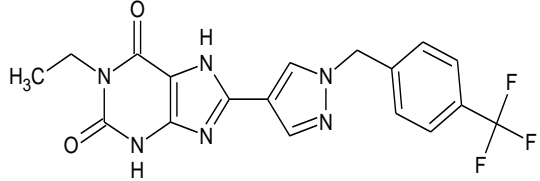
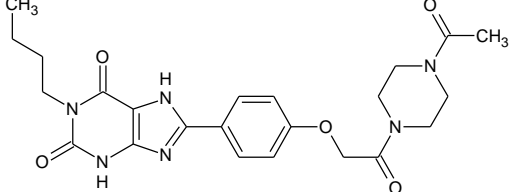
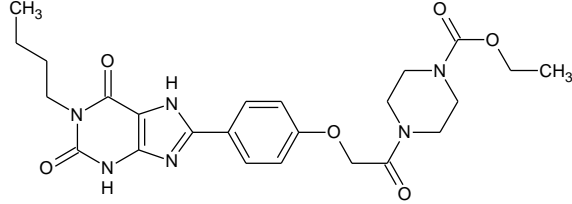
Compound	Ligand Name	Observed activity	Predicted activity 5	Fitness
C255		6.192	6.42	1.55
C256		6.19	6.58	1.53
C257		6.169	6.09	1.13

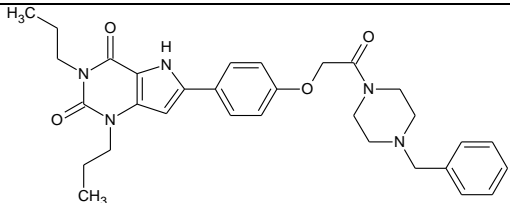
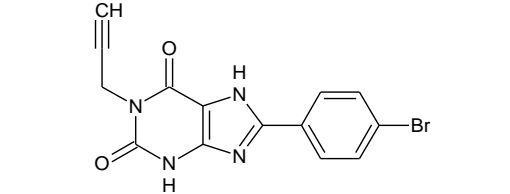
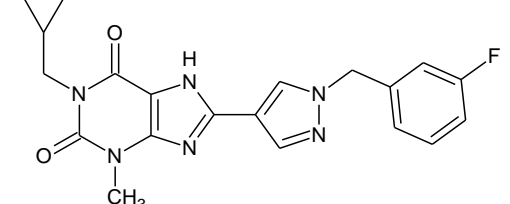
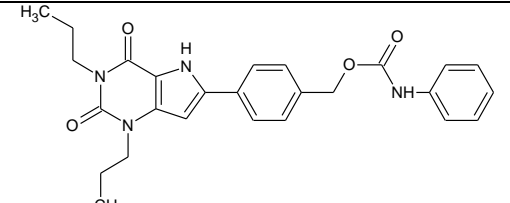
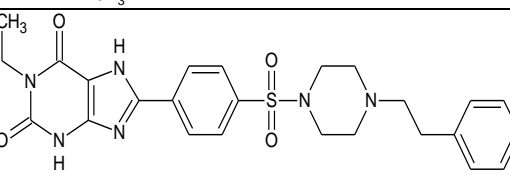
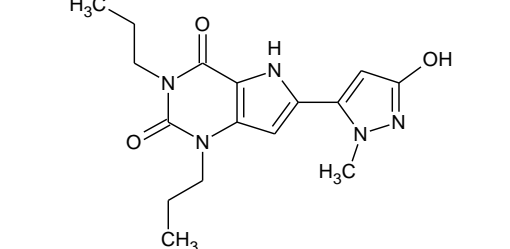
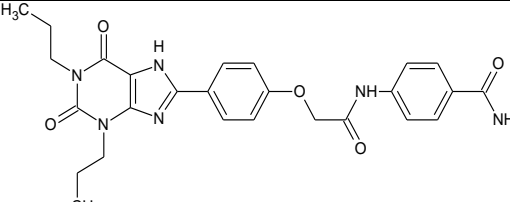
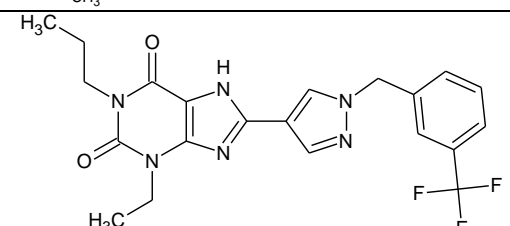
Table 6.3: Test set compounds of dataset used in QSAR model development. The observed and predicted activity along with the fitness over pharmacophore model is given in table.

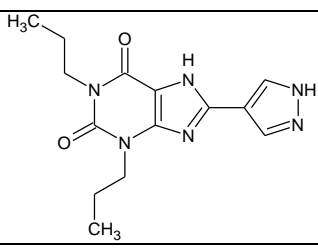
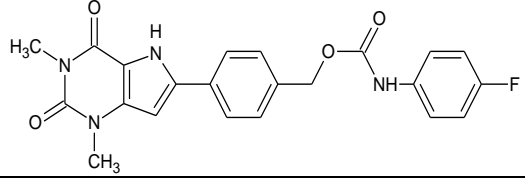
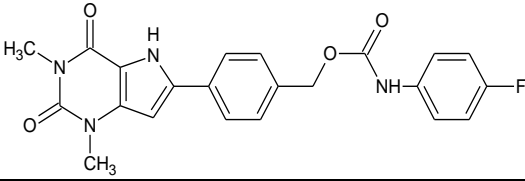
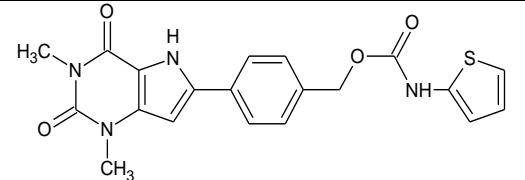
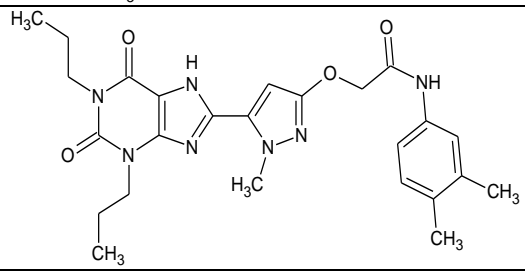
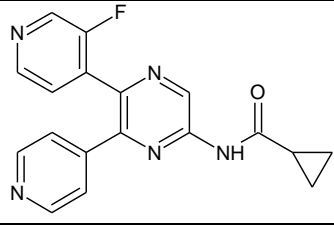
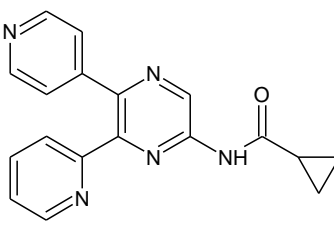
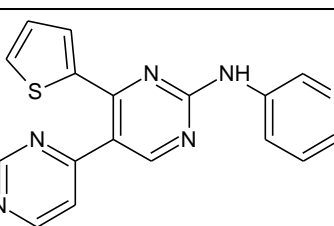
Compound	Ligand Name	Observed Activity	Predicted Activity 5	Fitness
C1		9.804	8.87	2.9
C2		9.668	8.88	2.97
C3		9.551	8.93	2.9

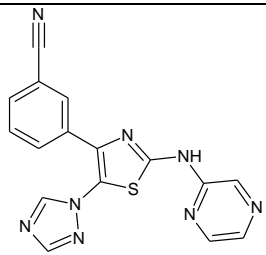
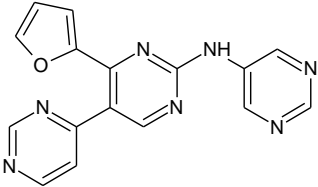
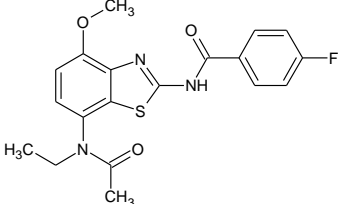
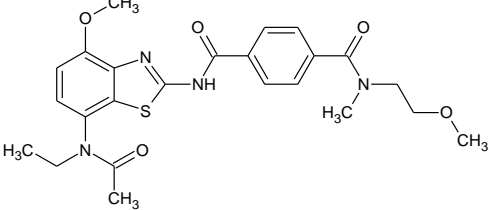
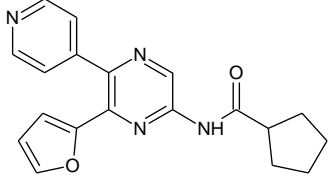
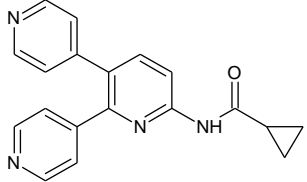
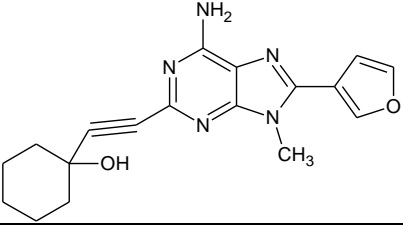
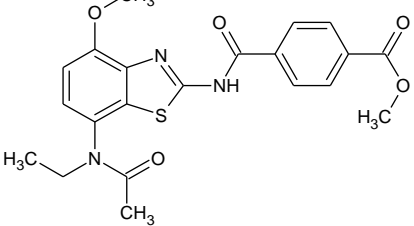
Compound	Ligand Name	Observed activity	Predicted activity 5	Fitness
C4		9.519	8.93	2.91
C5		9.406	8.94	2.99
C7		9.391	8.54	2.71
C8		9.351	8.95	2.98
C10		9.257	8.61	2.72
C20		9	8.21	2.71
C67		8.398	7.79	2.52
C68		8.387	8.37	2.52

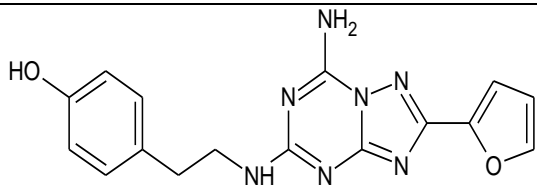
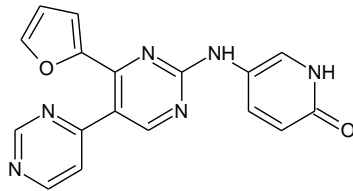
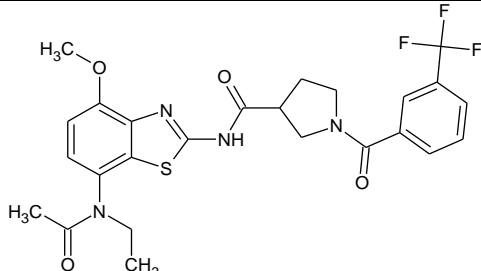
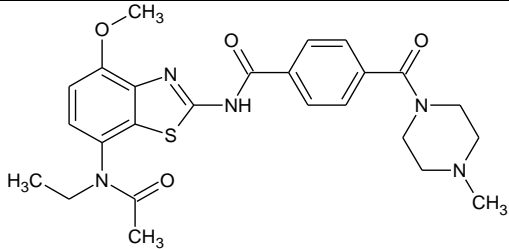
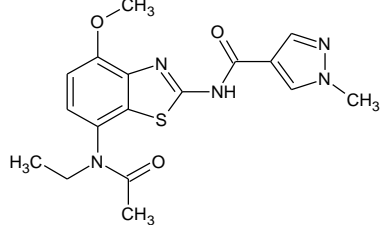
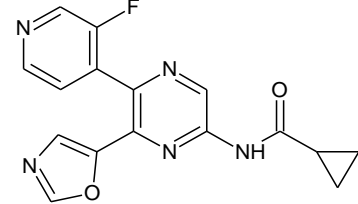
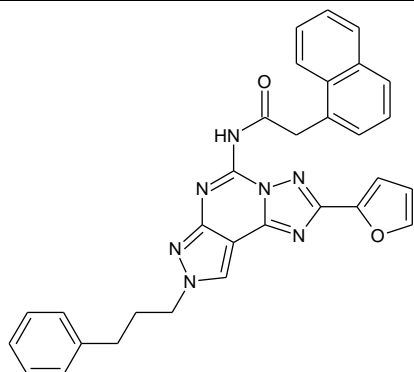
Compound	Ligand Name	Observed activity	Predicted activity 5	Fitness
C69		8.377	8.41	2.7
C71		8.349	8.39	2.71
C72		8.328	8	2.52
C74		8.31	8.03	2.56
C75		8.308	8.54	2.6
C76		8.301	8.24	2.5
C79		8.266	8.59	2.59
C80		8.266	8.6	2.61

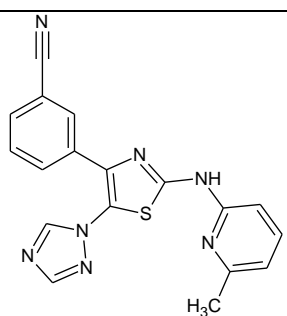
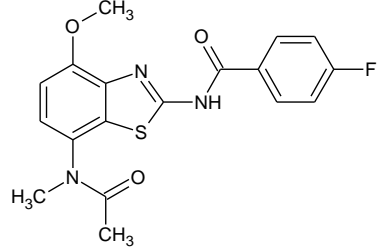
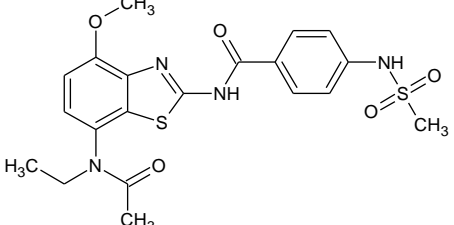
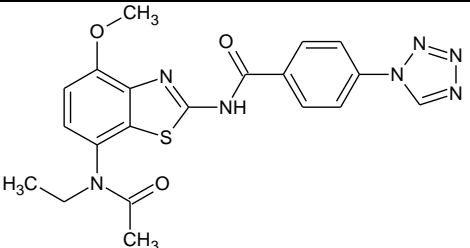
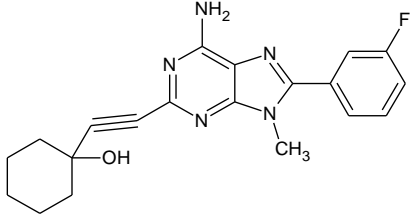
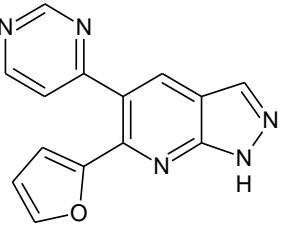
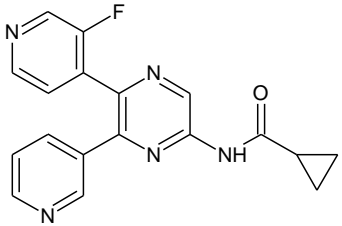
Compound	Ligand Name	Observed activity	Predicted activity 5	Fitness
C81		8.265	8.49	2.75
C82		8.26	8.36	2.5
C83		8.26	8.76	2.72
C86		8.229	8.41	2.6
C87		8.222	8.22	2.65
C88		8.222	8.32	2.69
C89		8.222	8.78	2.78
C91		8.215	8.64	2.76

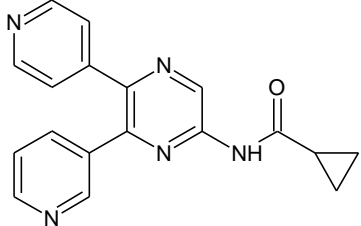
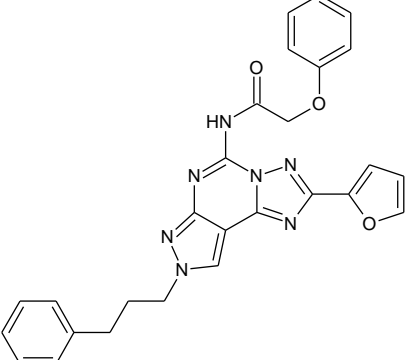
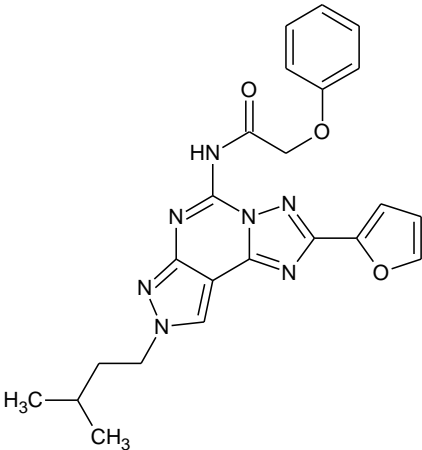
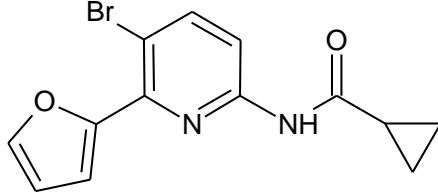
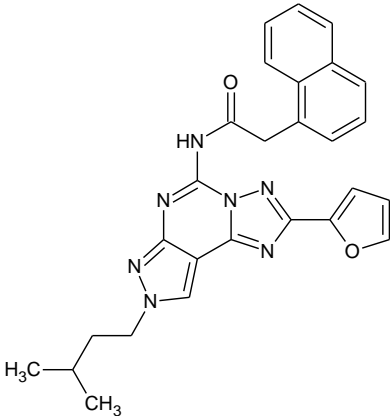
Compound	Ligand Name	Observed activity	Predicted activity 5	Fitness
C92		8.208	8.53	2.58
C94		8.167	8.33	2.6
C95		8.155	8.69	2.66
C97		8.149	8.44	2.59
C98		8.126	8.79	2.84
C99		8.125	7.54	2.51
C101		8.111	8.55	2.63
C105		8.081	8.24	2.62

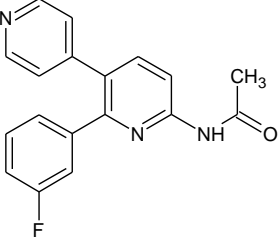
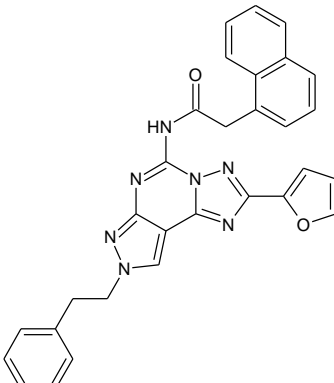
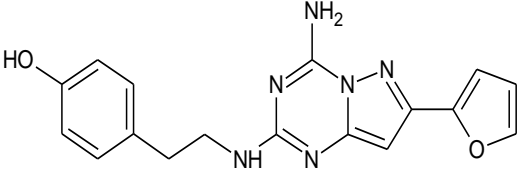
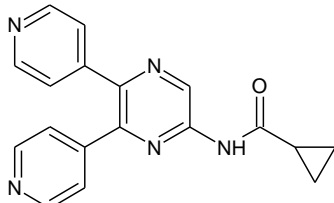
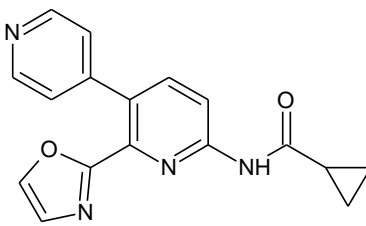
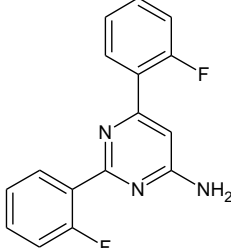
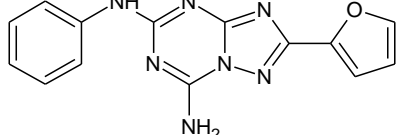
Compound	Ligand Name	Observed activity	Predicted activity 5	Fitness
C107		8.046	7.58	2.51
C110		8.022	8.74	2.62
C111		8.005	8.6	2.56
C112		8	8.65	2.61
C113		8	8.15	2.62
C115		7.959	6.95	1.35
C116		7.959	7.59	1.57
C118		7.921	7.69	1.4

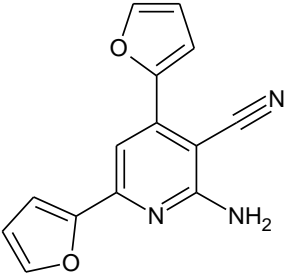
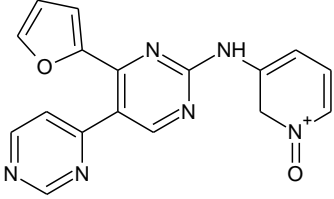
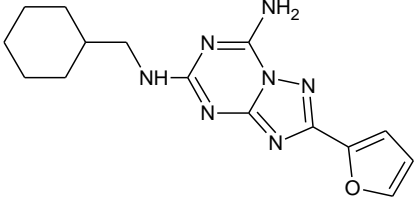
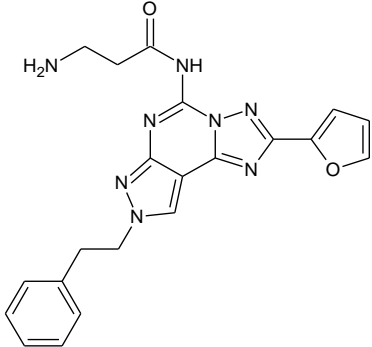
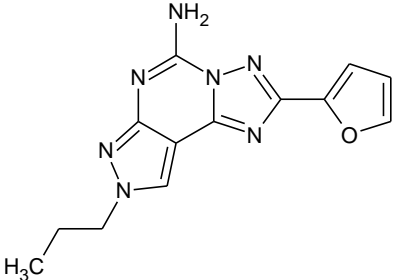
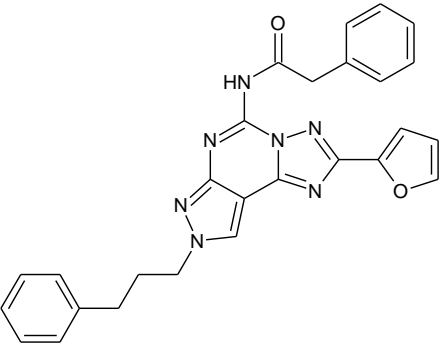
Compound	Ligand Name	Observed activity	Predicted activity 5	Fitness
C119		7.921	7.51	1.48
C120		7.921	7.44	1.62
C122		7.886	7.55	1.31
C123		7.886	7.7	1.43
C124		7.886	7.81	1.66
C126		7.854	7.07	1.38
C127		7.854	6.29	1.52
C129		7.824	7.6	1.3

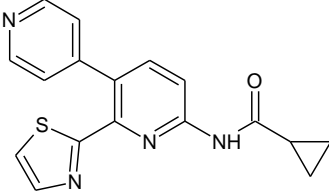
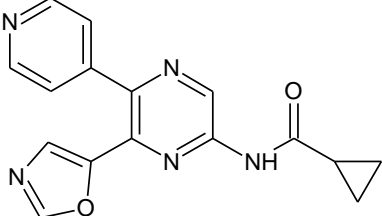
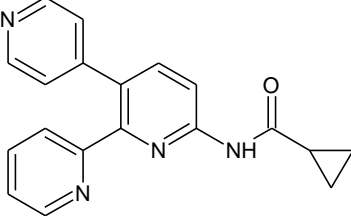
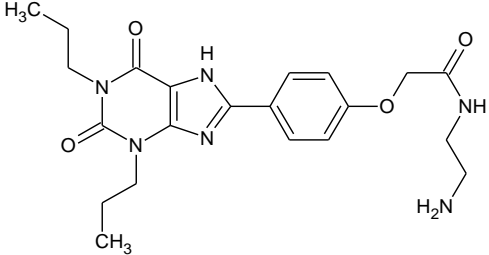
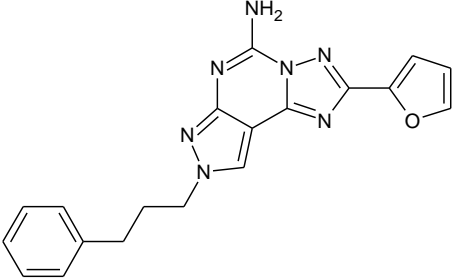
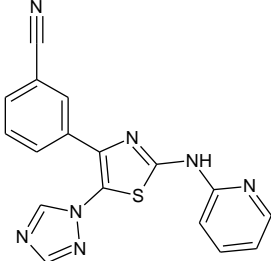
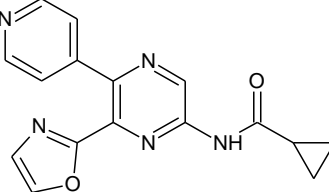
Compound	Ligand Name	Observed activity	Predicted activity 5	Fitness
C131		7.783	7.74	1.52
C132		7.77	7.41	1.05
C134		7.745	7.14	1.3
C135		7.745	7.94	1.47
C137		7.721	7.55	1.42
C138		7.721	7.62	1.65
C140		7.699	7.2	1.45

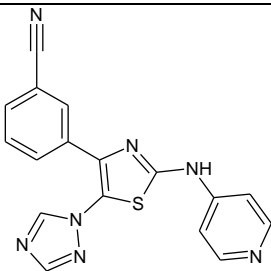
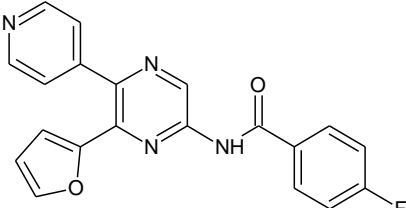
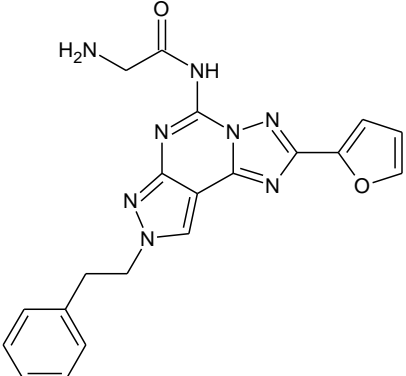
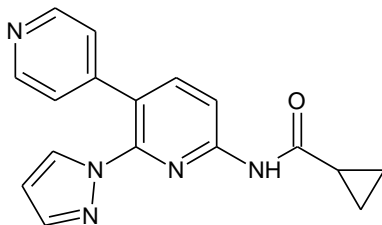
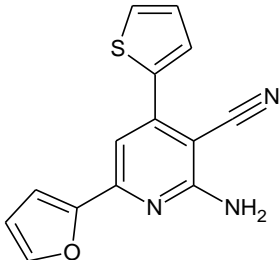
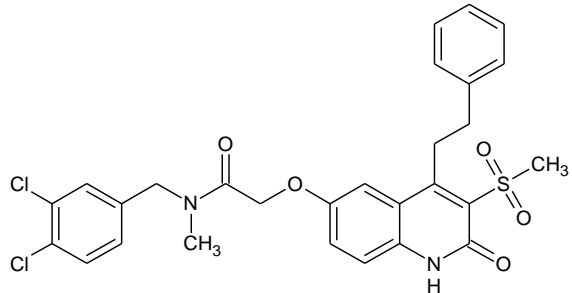
Compound	Ligand Name	Observed activity	Predicted activity 5	Fitness
C141		7.699	7.6	1.47
C143		7.658	7.48	1.31
C144		7.658	7.39	1.43
C146		7.638	7.58	1.29
C147		7.638	6.35	1.51
C148		7.638	7.71	1.55
C150		7.62	6.96	1.35

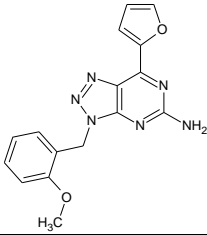
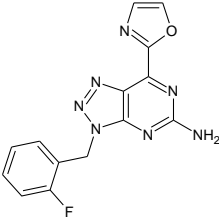
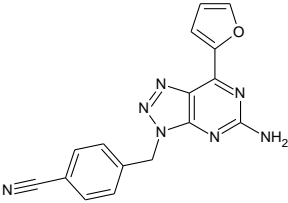
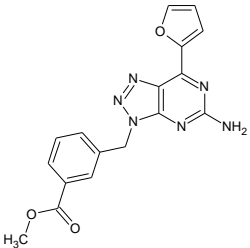
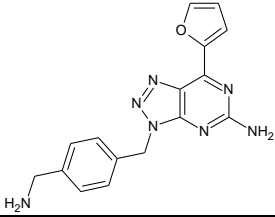
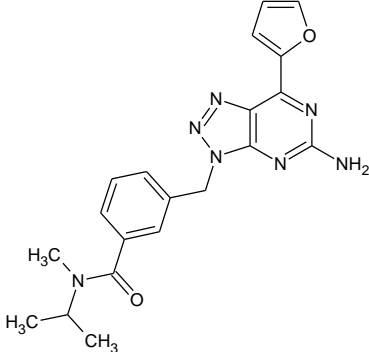
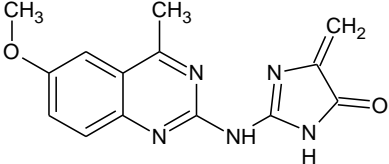
Compound	Ligand Name	Observed activity	Predicted activity 5	Fitness
C152		7.602	6.9	1.36
C153		7.602	7.32	1.46
C154		7.602	7.42	1.48
C156		7.553	7.33	1.2
C157		7.553	7.36	1.47

Compound	Ligand Name	Observed activity	Predicted activity 5	Fitness
C160		7.523	7.09	1.37
C161		7.523	7.4	1.45
C163		7.509	7.46	1.51
C165		7.495	6.9	1.36
C166		7.495	7.19	1.38
C167		7.495	6.91	1.4
C168		7.481	7.48	1.16

Compound	Ligand Name	Observed activity	Predicted activity 5	Fitness
C170		7.469	6.65	1.38
C171		7.469	7.58	1.64
C172		7.456	7.29	1.45
C174		7.425	7.45	1.49
C175		7.419	7.03	1.39
C177		7.398	7.22	1.47

Compound	Ligand Name	Observed activity	Predicted activity 5	Fitness
C179		7.377	6.93	1.3
C180		7.367	7.64	1.66
C181		7.328	7.23	1.22
C183		7.319	8.28	2.61
C184		7.316	7.06	1.35
C186		7.276	7.32	1.46
C188		7.252	7.59	1.67

Compound	Ligand Name	Observed activity	Predicted activity 5	Fitness
C189		7.208	7.28	1.48
C191		7.201	7.64	1.69
C194		7.155	7.46	1.5
C196		7.143	7.14	1.21
C197		7.125	6.64	1.3
C258		6.149	6.97	1.54

Compound	Ligand Name	Observed activity	Predicted activity 5	Fitness
C259		6.13	6.97	1.26
C260		6.078	6.75	1.6
C261		6.053	6.63	1.55
C262		6.042	6.67	1.54
C263		6.038	6.61	1.55
C264		6.028	6.42	1.53
C265		6.025	6.6	1.48

6.2.2. 3D QSAR model development and PLS analysis

For a QSAR model to be valid, one of the crucial components includes reliable predictability of the model. This predictive power of the model was validated in the present study using both internal and external validation. Internal validation of the model was carried out using PLS analysis. For this purpose, total dataset was divided into training and test sets which include 162 and 103 compounds respectively. A total of 5 PLS factors were applied in the present study in developing QSAR model. Leave one out (LOO) method of cross validation was employed for the training and test set molecules. The LOO cross validated R^2 and Q^2 should be greater than 0.6 and 0.55 respectively to obtain valid predictability of the model. The LOO cross validated R^2 value for the training set was found to be 0.9661 and Q^2 for test set was found to be 0.5839 indicating predictive ability of the developed model.

Various numerical parameters involved in the validation of QSAR model other than R^2 and Q^2 are Pearson correlation coefficient (R), standard deviation (SD), root mean square error (RMSE) and variance ratio (F). 'F' indicates statistical significance of the model which was found to be 888.6 and the lesser value of P, 1.2e-112, indicates a greater degree of confidence. The goodness of predictive ability of the model and its robustness were depicted by lesser values of SD and RMSE which were observed to be 0.1811 and 0.4912 respectively.

Figure 6.2 shows regression plot between the observed and the predicted pIC50s of compounds. From the above internal validation and scatter plot, it was observed that the observed values were in accordance with corresponding predicted values.

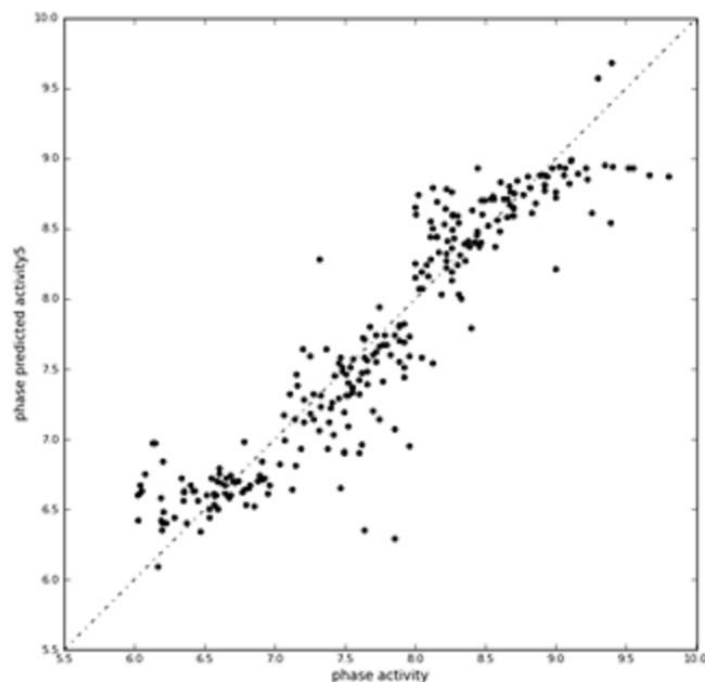


Figure 6.2: Scatter plot plotted between observed versus predicted activity

6.2.3. External validation of 3D QSAR model

The LOO cross validated R^2 and Q^2 values obtained from internal validation are important in assessing predictive ability of the QSAR model. But it is not only these parameters which explain the predictability of the model. It also depends on the correlation coefficient R and the predicted r^2 obtained from external validation. Hence, in the present study we performed external validation for the developed model using observed and predicted activities for both training set and test set compounds. Validation of the model resulted in excellent squared correlation coefficient of 0.926 indicating robustness of the model. The cross validated correlation coefficient (r^2_{cv}) was also found to be greater with a value of 0.858 confirming predictive ability of the model. The predictive correlation coefficient (r^2_{pred}) was also found to be good enough with 0.594. The slope of the regression line (k) passing through origin was found to be 0.999 which was obtained by plotting experimental activity versus predicted activity of dataset. Two other important parameters indicating predictive ability of the model, modified r^2 (r^2_{mod}) r^2_o , were found to be 0.7908 and 0.999 respectively confirming robustness

of the model. Observed from these internal and external validations, it can be summarized that the developed model has a reliable predictive ability based on the structural features of known A_{2B} inhibitors, and can be further considered in the discovery of such novel leads as A_{2B} antagonists. Results of external statistical validation of developed 3D QSAR model for hypothesis AADRR.6 was shown in **Table 6.4**.

Table 6.4: Results of external statistical validation of developed 3D QSAR model for hypothesis AADRR.6

External validation [¥]	Parameter calculated	Limitations
r_{cv}^2	0.858	$r_{cv}^2 > 0.5$
R	0.926	Must be close to 1
r_{pred}^2	0.594	$r_{pred}^2 > 0.6$
k value	0.999	$0.85 \leq k \leq 1.15$
r_0^2	0.999	$r_0^2 > 0.5$
r_m^2	0.791	$r_m^2 > 0.5$

[¥] r_{cv}^2 : Cross validated coefficient, R: correlation coefficient between actual and predicted activities, r_{pred}^2 : predictive correlation coefficient, k: slope value of regression line, r_0^2 : observed correlation coefficient, r_m^2 : modified squared correlation coefficient.

6.2.4. Contour map analyses

Various structural insights can be obtained by analyzing the visual effects generated by 3D QSAR model over molecular features of the compounds which can be useful in lead optimization studies in the field of drug discovery. Analysis of contour maps for the generated pharmacophore hypothesis by 3D QSAR model outlined the crucial functional groups and their positions in order to exhibit better A_{2B} inhibitory activity by the compounds. Contour cubes analyses of most active and the least active compounds considered are given in **Figures 6.3, 6.4 and 6.5**.

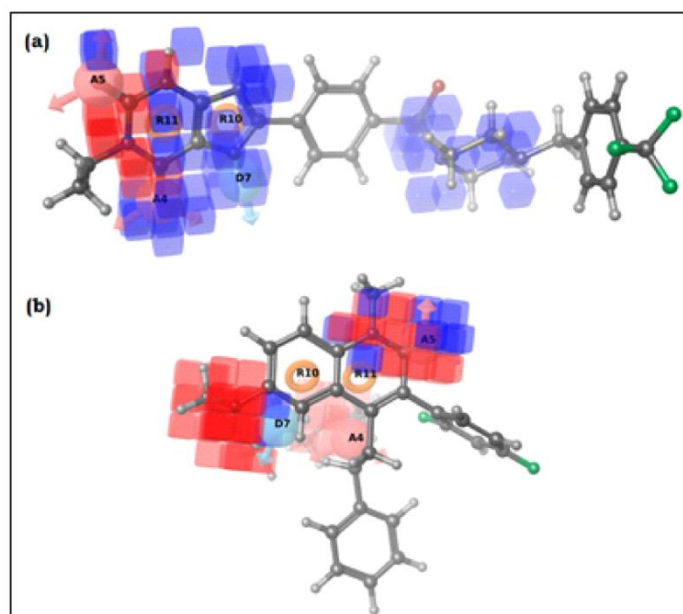


Figure 6.3: 3D QSAR contour map representation for hydrogen bond acceptor property for most active compound **C1** and least active compound **C257**.

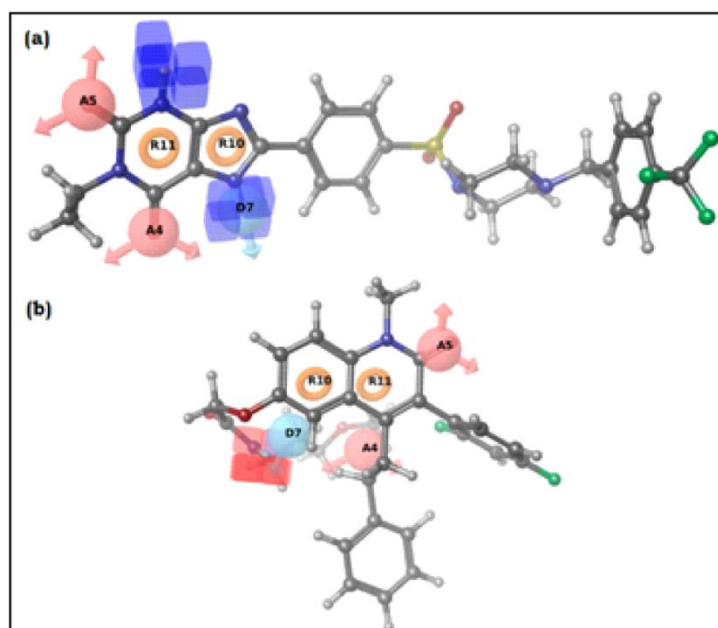


Figure 6.4: 3D QSAR contour map representation for hydrogen bond donor property for most active compound **C1** and least active compound **C257**.

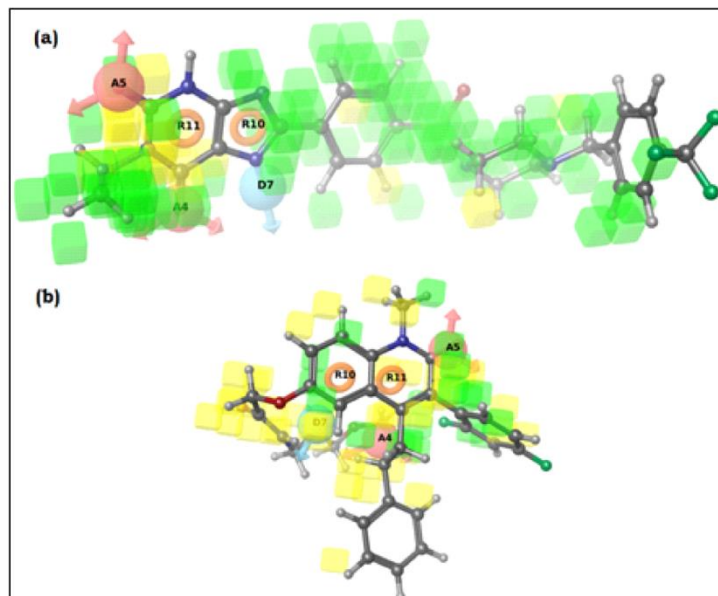


Figure 6.5: 3D QSAR contour map representation for hydrophobic property for most active compound **C1** and least active compound **C257**.

Figure 6.3 represents contour map analysis for hydrogen bond acceptor activity, while **figure 6.4** represents for hydrogen bond donor activity and the **figure 6.5** represents the contour map analysis for hydrophobic nature of molecules. In the present study, compound **C1** with pIC_{50} 9.804 was considered most active compound with a fitness of 2.9 with respect to the generated pharmacophore model AADRR.6. Compound **C257** with pIC_{50} 6.169 and fitness 1.13 was considered least active compound for the contour map analysis. In **figure 6.3**, blue cubes indicate favorable regions in the compound while red cubes indicate unfavorable regions for hydrogen bond acceptor activity. Similarly, in **figure 6.4**, blue and red cubes indicate favorable and unfavorable regions of compounds for hydrogen bond donor activity. In **figure 6.5**, green cubes indicate favorable regions and yellow cubes indicate unfavorable regions for hydrophobic groups. **Figure 6.3** indicates comparison of hydrogen bond acceptor property in most active compound **C1** (**figure 6.3(a)**) and least active compound **C257** (**figure 6.3(b)**). The favored blue cubes were observed predominantly at 1-ethyl-3,7-dihydro-1H-purine-2,6-dione moiety of compound **C1** where two ketonic oxygen atoms readily accept

hydrogen bonding. Also the favourable hydrogen bond acceptor nature was observed at sulphonyl group attached to the piperazine ring. In case of least active compound, **C257**, disfavored red cubes were observed at dihydroquinoline group, suggesting the substitution of dihydropurine-2, 6-dione group in order to increase A_{2B} inhibitory activity.

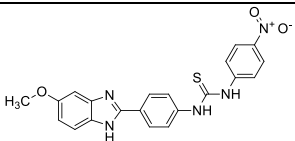
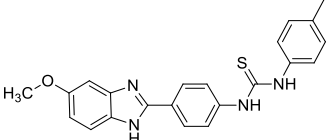
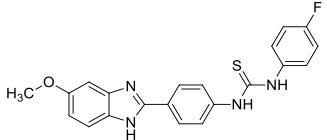
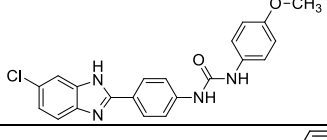
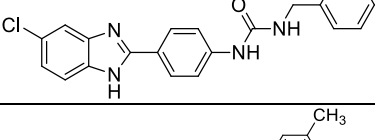
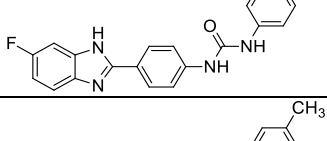
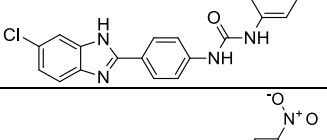
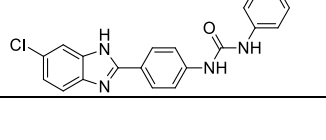
Hydrogen bond donor map analysis for the most active and least active compounds showed favorable blue cubes at the nitrogen atoms with hydrogen atom in the purine ring of compound **C1** (**figure 6.4(a)**) indicating their importance in the A_{2B} inhibitory activity in contrast to compound **C257**. The blue favored cubes were not found in compound **C257** and the unfavorable red cubes were found on the substituted groups of dihydroquinoline moiety (**figure 6.4(b)**). The final contour map analysis of most active and least active compounds for their hydrophobic groups is shown in **figure 6.5**. Favorable green cubes were observed almost throughout the structure of the most active compound **C1** owing to the presence of bulky groups like ethyl on purine ring, hydrophobic natured purine, phenyl, piperazine and the terminal substituted phenyl ring. Favorable green cubes were also observed in compound **C257** owing to the presence of hydrophobic moieties in the compound. Also, unfavorable cubes were observed towards other substituted regions indicating the substitution of these regions with phenyl, and piperazine moieties increasing the A_{2B} inhibitory activity.

In a nutshell, based on these observations, it was observed that presence of ketonic oxygens and amine groups is crucial for a compound to be an A_{2B} inhibitor. Also such compound with bulky hydrophobic moieties is well suitable as A_{2B} inhibitor as observed from compound **C1**. Some hydrophobic substitutions on phenyl groups of compound **C1** can further increase hydrophobicity of the molecule which may increase its A_{2B} inhibitory activity.

Therefore, predicted 3D QSAR model was well validated for its predictability and further analyzed for identification of structural features necessary for a compound to act as A_{2B} inhibitor which plays a crucial role in the field of drug discovery.

The pharmacophore model developed was further employed in the screening of in-house BITS database to identified compounds with similar chemical features. The model was set to screen matching at least 3 out of 5 compounds. The retrieved hits were screened based on their predicted activity and fitness which allowed us to select 15 compounds for further in-vitro evaluation. The selected hits along with their chemical structures, predicted activity and fitness are given in **Table 6.5**.

Table 6.5: Selected hits based on their predicted activity and fitness to model AADRR.6

Compound	Structure	Predicted Activity 5 (pIC ₅₀)	Fitness
RS-1		8.145	1.902
RS-2		8.151	1.888
RS-3		8.115	1.887
RS-4		7.148	1.105
RS-5		7.144	1.109
RS-6		7.128	1.109
RS-7		7.124	1.109
RS-8		7.114	1.102

RS-9		7.311	1.446
RS-10		6.973	1.370
RS-11		7.459	1.437
RS-12		7.464	1.452
RS-13		7.05	0.805
RS-14		7.351	1.441
RS-15		7.643	1.407

6.2.5. ADME analysis

The in-silico pharmacokinetic parameters for selected hits were evaluated so as to understand the drug likeliness of compounds. QikProp module was utilized for the same in the present study whose results are given in **Table 6.6** (Schrodinger L, 2012; QikProp v3.5). All the selected 15 hits were found with good partition coefficient (QPlogPo/w) which was crucial in studying the absorption and distribution pattern of the hits. The QPPCaco, predicted apparent Caco-2 cell permeability in nm/sec, for the 15 hits were found to be in the range of 60 – 2344. This parameter was crucial in identifying estimation of cell permeability in biological membranes and their metabolism. The QPlogBB for the compounds were found in the range of -0.098 to -2.19, which were in-between acceptable range. The percentage oral absorption for compounds was found in the range of 66.75 - 100. All the compounds were found within

the permissible ranges of pharmacokinetic parameters which were further carried forward for in-vitro studies.

Table 6.6: Predicted ADME properties for selected 15 compounds

Hits	QPlogPo/w [§]	QPlogHERG [¥]	QPPCaco [€]	QPlogBB ^Ω	% Human Oral Absorption ^Σ
RS1	4	-7.23	280.99	-1.37	94.19
RS2	4.97	-7.22	2344.87	-0.23	100
RS3	4.89	-7.19	2346.87	-0.098	100
RS4	4.15	-6.01	831.48	-0.53	100
RS5	4.02	-6.11	832.45	-0.45	100
RS6	4.07	-5.97	831.81	-0.52	100
RS7	4.34	-6.02	832.01	-0.48	100
RS8	3.37	-6.02	99.86	-1.63	82.44
RS9	1.94	-6.09	75.92	-1.99	71.94
RS10	3.17	-6.4	162.29	-1.4	85.08
RS11	2.02	-6.2	86.82	-1.99	73.48
RS12	2.95	-6.18	725.01	-0.78	95.42
RS13	2.59	-6.46	124	-1.62	79.6
RS14	1.36	-6.12	60.01	-2.19	66.75
RS15	4.66	-7.99	694.53	-1.28	100

[§] Predicted octanol/water partition co-efficient log p (acceptable range from -2.0 to 6.5).

[¥] Predicted IC₅₀ value for blockage of HERG K⁺ channels (concern below -5.0).

[€] Predicted Caco-2 cell permeability in nm/s (acceptable range: <25 is poor and >500 is great).

^Ω Predicted brain/blood partition coefficient (acceptable range from -3.0 to 1.2)

^Σ Percentage of human oral absorption (<25% is poor and >80% is high).

6.3. Gene expression analysis of A_{2A} and A_{2B} in PC3 and DU145 cell lines

Gene expression levels of A_{2A} and A_{2B} AR subtypes, in two prostate cancer cell lines, PC-3 and DU145 (**Figure 6.6**), were compared using real-time quantitative RT-PCR analysis. Wei *et al.*, 2013, reported that A_{2B}AR expression in different prostate cancer cell lines was more compared to other A₁, A_{2A} and A₃ receptors. We further tested in our lab conditions, hence in PC3 cell lines A_{2B} was found to show more than 10⁴ fold increases in the expression than A_{2A}. PC3 cells were selected as *in vitro* system to screen inhibitors designed for A_{2B} *in silico* by 3D QSAR model.

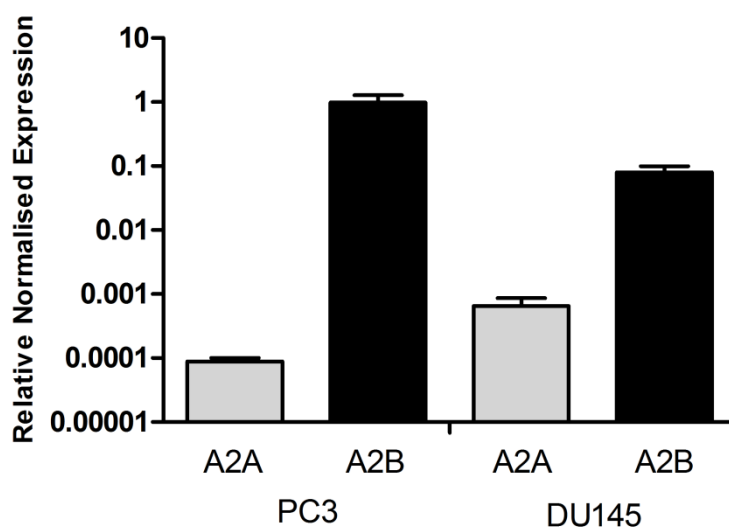


Figure 6.6: Determination of gene expression analysis of A_{2A} and A_{2B} adenosine receptors (ARs) in two prostate cancer cell lines

6.4. *In vitro* cAMP assay

The levels of cyclic AMP accumulated in PC-3 prostate cancer cell lines over a period of 24 h were investigated. To assess that, a simple HPLC method has been developed and validated for quantitative estimation of cAMP in PC-3 cell lines. Validation of the peak for cyclic AMP in PC-3 cells was carried out by comparing the retention time of sample peak with standard Cyclic AMP (RT 4.1 min). Sample peaks present at a retention time of 4.1 min were

tentatively identified as cyclic AMP alone in whole cell lysate. The representative dose response curves (DRC) were shown in **Figure 6.7**.

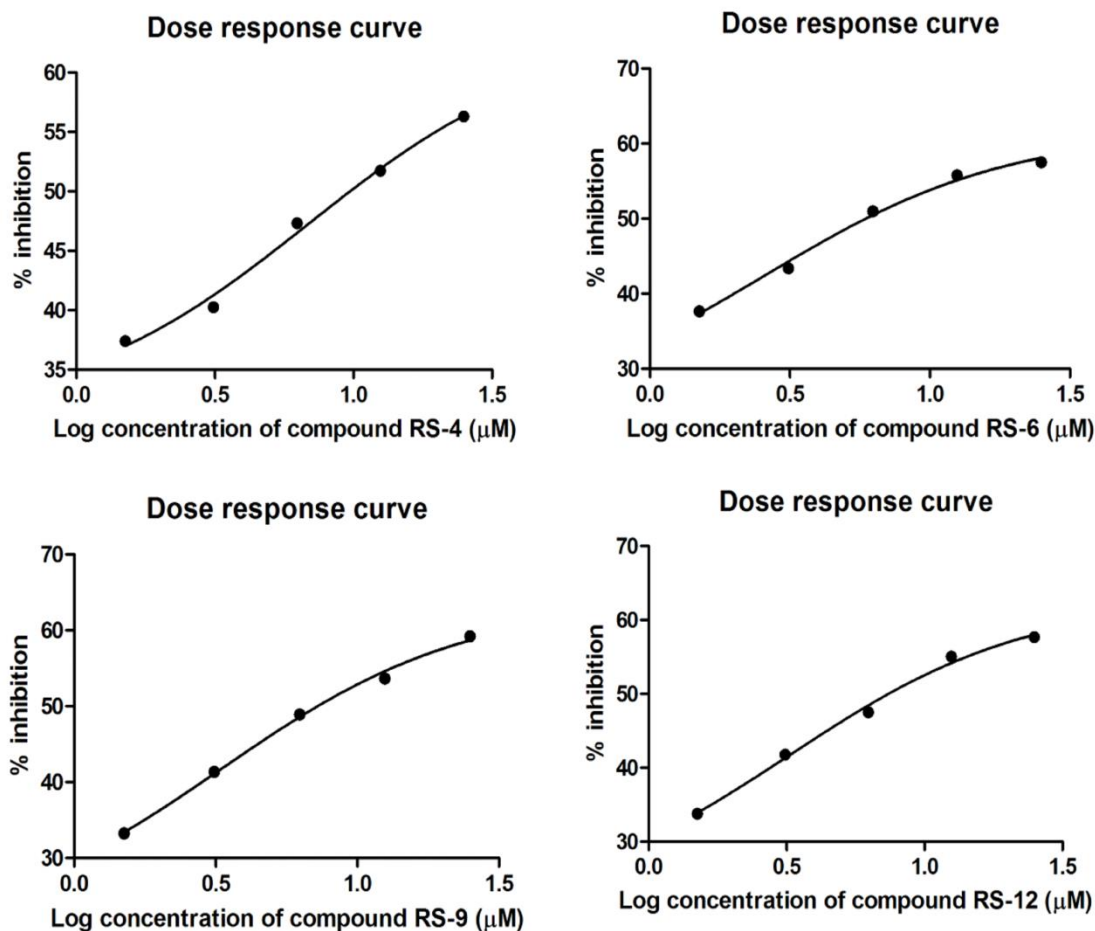


Figure 6.7: Dose-response curves of top active compounds (RS-4, 6, 9, and 12).

Out of 15 compounds, 10 compounds were found to show $\text{IC}_{50} > 100 \mu\text{M}$ and 5 compounds have shown $\text{IC}_{50} < 20 \mu\text{M}$. Compounds RS-4, 6, 9, 12 and 15 found to show IC_{50} of 10.08, 7.015, 8.36, 8.58 and 19.99 μM respectively. Out of these, compounds RS-6 and RS-9 showed least IC_{50} of 7.015 μM and 8.36 μM respectively, to reduce cAMP level in PC3 cell lines. Hence, **RS-6** and **RS-9** emerged as most promising leads from the in-vitro cAMP inhibitory assay.

6.5. Selectivity index analysis

Selectivity index (SI) is a comparison of amount of therapeutic agent that causes biological effect to the amount that causes toxicity to understand specificity. The results are shown in **Table 6.7**. Out of fifteen compounds nine compounds have shown >1 SI which represents that compounds were selective towards disease model. Comparatively RS-4, 6 and 9 have shown SI of 132.18, 216.17 and 607.88 respectively.

Table 6.7: Biological data of the selected compounds from in house database

Test compound	IC ₅₀ (μM) ^a	CC ₅₀ (μM) ^b	EC ₅₀ (μM) ^c	SI (CC ₅₀ /EC ₅₀)
RS-1	>100μM	8.11±0.74	317.31±4.88	0.02
RS-2	>100μM	0.75±0.08	114.08±3.72	0.01
RS-3	>100μM	0.14±0.04	17.42±1.47	0.01
RS-4	10.08±0.28	3.57±0.18	0.03±0.01	132.18
RS-5	>100μM	30.57±2.67	654.87±5.93	0.05
RS-6	7.01±0.30	11.24±1.31	0.05±0.01	216.17
RS-7	>100μM	7.88±0.86	4.77±0.31	1.65
RS-8	>100μM	4.90±0.27	11.32±0.77	0.43
RS-9	8.36±0.37	10.33±1.25	0.02±0.01	607.88
RS-10	>100μM	2.32±0.19	0.20±0.02	11.38
RS-11	>100μM	181.42±3.88	1240±8.98	0.15
RS-12	8.58±0.35	4.43±0.14	0.09±0.01	47.62
RS-13	>100μM	40.99±2.59	6.40±0.25	6.40
RS-14	>100μM	3.57±0.17	2.36±0.96	1.51
RS-15	19.99±0.50	0.75±0.08	0.38±0.04	1.96

^a-cAMP inhibitory concentration in PC-3 cell lines, ^b - Cell cytotoxicity of compounds on HEK-293 cell lines, ^c - Effective concentration of compounds on PC-3 cell lines; All data presented as Mean ± SEM (n=3).

6.6. Pharmacological evaluation

6.6.1. Neurotoxicity screening

In the present study, neurotoxicity was assessed using two animal models, *viz* rotarod and actophotometer based screening. Compounds were administered at three dose levels (300, 100 and 30 mg/kg). Minimal motor impairment was measured by rotarod test and neurotoxicity was indicated by the inability of the animal to maintain balance on the rotating rod for at least 2 min. In these acute neurotoxicity assays, all four test compounds exhibited motor deficit at the highest tested dose (300 mg/kg) up to 2 h post administration (**Table 6.8**). But at a dose of 100 mg/kg two compounds (RS-9 and RS-12) were found non-toxic in rotarod test and RS-12 was found non-toxic in actophotometer assay. However, none of the compound was found toxic at lower dose (30 mg/kg). Thus, we decided to proceed with a lower dose (30 mg/kg) for further *in vivo* experiments. The results of neurotoxicity assays clearly indicate that all four compounds show neurotoxicity at high doses (300 and 100 mg/kg). Thus, we further carried out our *in vivo* experiments with a lower dose (30 mg/kg).

Table 6.8: Neurotoxic Activity of test Compounds.

Test Group	Neurotoxicity ^a			
	Rotarod		Actophotometer	
	1h	2h	1h	2h
RS-4	100	100	100	100
RS-6	100	100	100	100
RS-9	100	300	100	100
RS-12	100	300	100	300

^a Neurotoxicity screening of test compounds. Dose of 30, 100 and 300mg/kg were administered. Figures in the table indicate the minimum dose whereby bioactivity was demonstrated in half or more of the mice.

6.6.2. *In vivo* anti-nociceptive evaluation

Acetic acid induced writhing and formalin induced paw licking are the best pain models that mainly involve peripheral mechanisms whereas hot plate test and tail flick tests are the models of pain that involve central mechanisms (Muhammad *et al.*, 2014). In order to identify the possible central and peripheral effects of the test substances, anti-nociceptive evaluation was done by subjecting the test compounds preliminary for acetic acid induced writhing test and formalin induced flinching test and then thermal induced pain models like hot plate test and tail immersion tests.

6.6.2.1. Acetic acid induced writhing model in mice

In acetic acid induced writhing test, all test compounds (RS-4, 6, 9 and 12) produced significant ($p < 0.05-0.001$) reduction in the number of writhing in mice. The test compound RS-9 at 30 mg/kg i.p, the percent reduction of writhing was 90.20%, as compared to the control group, whereas the standard drug indomethacin (10 mg/kg p.o.) showed a reduction of 89.22%, indicating no significant difference between test compound RS-9 and standard. Effect of RS-9 at 30 mg/kg i.p. was better than the standard drug, indomethacin. Results of acetic acid induced writhing method in mice were tabulated in **Table 6.9**.

Table 6.9: Effect of test compounds (RS-4, 6, 9 and RS-12) on Acetic acid induced writhing model in mice

Groups	Drugs	Dose (mg/kg) i.p	Mean \pm SEM	% decrease in wriths
I	Control	—	68.000 \pm 2.309	0.00
II	Indomethacin	10	7.333 \pm 1.201***	89.22
III	RS-4	30	59.333 \pm 0.881**	12.75
IV	RS-6	30	53.667 \pm 3.282*	21.08
V	RS-9	30	6.667 \pm 0.881***	90.20
VI	RS-12	30	15.000 \pm 1.527***	77.94

All the values are expressed as mean \pm SEM (n=3), *P < 0.05; ** P < 0.01; *** P < 0.001 significant compared with control. Data were analysed by using One-way ANOVA followed by Dunnett's Multiple Comparison Test.

The inflammatory pain produced by acetic acid is due to the liberation of endogenous substances that excite pain nerve ending. The acetic acid induced writhing is a more convenient model for screening of test compounds which shows their antinociceptive effect by inhibiting the synthesis of prostaglandin (Ochi *et al.*, 2000). All test compounds (RS-4, 6, 9 and 12) showed significant reduction in acetic acid induced writhing as compared to vehicle control ($p < 0.05-0.001$). Based on the above results, decrease in the number of writhings indicated that all the four test compounds might exert their anti-nociceptive activity by inhibiting the synthesis of prostaglandin or action of prostaglandin.

6.6.2.2. Formalin induced paw licking model in mice

In Formalin induced paw licking test, administration of test compound RS-9 at 30 mg/kg i.p. produced significant ($p < 0.001$) reduction in paw licking time (53.33 sec) as compared to the control group (108.0 sec) in the early phase. However, the standard drug, indomethacin (10 mg/kg p.o.) exhibited a reduction of paw licking time of 49.0 sec. But in late phase, the test compounds RS-9 and RS-12 decreased the duration of paw licking to 28.33 sec and 50.33 sec

respectively from 85.0 sec of control group. On the other hand, the standard drug indomethacin (10 mg/kg p.o.) exhibited a reduction of paw licking time of 25.33 sec in the late phase. But RS-6 at 30 mg/kg i.p. produced no significant reduction in paw licking time as compared to the control group both in the early and late phases. The results of formalin induced paw licking model in mice were tabulated in **Table 6.10**. The formalin induced paw licking model comprises a distinct biphasic nociceptive responses including early phase (0-5 min) and late phase (20-30 min). This test gives a clear idea about possible mechanism involved in its anti-nociceptive effect of test compound. Drugs that inhibit first phase of the formalin test have the ability to alleviate neurogenic pain while the drugs that inhibit second phase of the test have the ability to inhibit inflammatory pain. In our study, test compounds RS-4, 9 and 12 decreased reaction time (paw licking time) in both early phase and late phase at 30 mg/kg i.p. suggesting that these compounds have the ability to alleviate neurogenic pain in the early phase and to inhibit inflammatory pain in the late phase.

Table 6.10: Effect of test compounds (RS-4, 6, 9 and RS-12) on Formalin induced paw licking model in mice:

Groups	Dose (mg/kg) i.p	Licking time (sec)			
		Early phase (sec)	% decrease in licking	Late phase (sec)	% decrease in licking
Control	—	108.00 ± 2.08	0.00	85.00 ± 1.15	0.00
Indomethacin	10	49.00 ± 2.08***	54.20	25.33 ± 1.76***	76.32
RS-4	30	88.33 ± 1.76**	17.45	74.33 ± 1.20*	30.53
RS-6	30	97.67 ± 3.84	8.72	79.33 ± 2.03	25.86
RS-9	30	53.33 ± 2.90***	50.16	28.33 ± 1.45***	73.52
RS-12	30	87.33 ± 4.37**	18.38	50.33 ± 2.72***	52.96

All the values are expressed as mean \pm SEM (n=3), *P < 0.05; ** P < 0.01; *** P < 0.001 significant compared with control. Data were analysed by using One-way ANOVA followed by Dunnett's Multiple Comparison Test.

6.6.2.3. Eddy's hot-plate test in mice

In Eddy's hot-plate test, the reaction time in test compound (RS-4, 6, 9 and 12) treated groups increased significantly ($p < 0.05-0.001$) in comparison to the control group except RS-6 at 120 min. Maximum effect was observed in RS-9 at the dose viz. 30 mg/kg i.p. at 90 min which showed a reaction time of 14.97 sec, whereas the standard drug indomethacin (10 mg/kg i.p.) showed a reaction time of 14.19 sec. All test compounds were also showed dose dependent activity. Results of Hot plate method in mice were seen in **Table 6.11**. Hot plate test is mainly used for detection of various types of analgesics drugs from spinal origin. Paw licking and jumping are the two types of behavioural responses seen in hotplate test (neurogenic model). In hot plate test, all four test compounds have shown significant central analgesic activity ($p < 0.05-0.001$) as compared to the vehicle treated control group.

Table 6.11: Effect of test compounds (RS-4, 6, 9 and RS-12) on Eddy's hot-plate test in mice

Groups	Dose (mg/kg) i.p	Reaction time (sec)				
		0 min	30 min	60 min	90 min	120 min
		Mean \pm SEM	Mean \pm SEM	Mean \pm SEM	Mean \pm SEM	Mean \pm SEM
Control	—	5.29 \pm 0.17	6.22 \pm 0.06	7.52 \pm 0.10	8.16 \pm 0.13	7.94 \pm 0.13
Indomethacin	10	5.62 \pm 0.06	10.14 \pm 0.08***	13.48 \pm 0.34***	14.19 \pm 0.14***	13.02 \pm 0.21***
RS-4	30	5.28 \pm 0.23	7.58 \pm 0.11*	7.86 \pm 0.57	9.70 \pm 0.38*	10.04 \pm 0.21***
RS-6	30	5.37 \pm 0.22	6.55 \pm 0.53	7.34 \pm 0.21	7.89 \pm 0.19	9.50 \pm 0.34*
RS-9	30	5.87 \pm 0.18	7.93 \pm 0.27**	13.97 \pm 0.89***	14.97 \pm 0.66***	14.27 \pm 0.46***
RS-12	30	5.53 \pm 0.51	8.06 \pm 0.62**	12.73 \pm 0.53***	13.62 \pm 0.36***	9.90 \pm 0.56**

All the values are expressed as mean \pm SEM (n=3), *P < 0.05; ** P < 0.01; *** P < 0.001 significant compared with control. Data were analysed by using Two-way ANOVA followed by Bonferroni post-tests.

6.6.2.4. Tail immersion test in mice

In Tail immersion test, reaction time in test compound (RS-9 and RS-12) treated groups increased significantly ($p < 0.05-0.01$) in comparison to the control group. Maximum effect was observed in RS-9 at the dose 30 mg/kg i.p. at 60 min which showed a reaction time of 2.61 sec, and the standard drug indomethacin (10 mg/kg i.p.) showed a reaction time of 3.56 sec, whereas, reaction time in the vehicle treated control group was 2.12 at 60 min, clearly indicating the activity of compound RS-9. However, in this test, the compounds (RS-4 and RS-6) at 30 mg/kg dose did not increase the response latency compared to vehicle control group. The results of tail immersion test in mice were tabulated in **Table 6.12**. In tail flick test, only two compounds (RS-9 and RS-12) have shown significant central analgesic activity ($p < 0.05-0.01$) as compared to the vehicle treated control group, and test compounds RS-4 and RS-6 did not show any significant activity.

Table 6.12: Effect of test compounds (RS-4, 6, 9 and RS-12) on Tail immersion test in mice:

Groups	Dose (mg/kg) i.p	Reaction time (sec)				
		0 min	30 min	60 min	90 min	120 min
		Mean \pm SEM	Mean \pm SEM	Mean \pm SEM	Mean \pm SEM	Mean \pm SEM
Control	—	2.05 \pm 0.04	2.04 \pm 0.05	2.12 \pm 0.04	2.01 \pm 0.13	2.10 \pm 0.09
Indomethacin	10	2.07 \pm 0.09	2.41 \pm 0.04*	3.56 \pm 0.10***	4.16 \pm 0.08***	2.58 \pm 0.05**
RS-4	30	2.05 \pm 0.10	2.11 \pm 0.09	2.01 \pm 0.12	2.07 \pm 0.12	2.04 \pm 0.17
RS-6	30	2.08 \pm 0.12	2.12 \pm 0.11	2.15 \pm 0.16	2.20 \pm 0.08	2.13 \pm 0.08
RS-9	30	2.33 \pm 0.11	2.43 \pm 0.05*	2.61 \pm 0.11**	2.45 \pm 0.04**	2.47 \pm 0.09*
RS-12	30	2.09 \pm 0.08	2.13 \pm 0.10	2.52 \pm 0.08*	2.42 \pm 0.09*	2.19 \pm 0.07

All values are expressed as mean \pm SEM (n=3), *P < 0.05; ** P < 0.01; *** P < 0.001 significant compared with control. Data were analysed using Two-way ANOVA followed by Bonferroni post-tests.

Based on the results obtained from hot plate and tail flick tests, we can conclude that RS-9 and RS-12 were found to be effective in both the thermal induced pain models. Initially test compounds (RS-4, 9 and 12) were selected based on the results obtained from *in vivo* anti-nociceptive activity evaluation in both chemical and thermal induced pain models, and were subjected to carrageenan-induced paw edema in mice (a standard experimental procedure of acute inflammation) (Rosa *et al.*, 1972), for evaluation of its anti-inflammatory activity. Carrageenan-induced paw edema is believed to involve biphasic responses (Vinegar *et al.*, 1969). The first phase of inflammation is due to the release of serotonin and histamine, and the second phase is due to the release of bradykinins, prostaglandins, protease and lysosomes (Crunkhorn *et al.*, 1971). All three test compounds were screened at 30 mg/kg intra peritoneal dose and after 30 minutes carrageenan was administered at a dose of 50 μ L through sub plantar region of hind limb. Pre and post changes in paw volume were measured.

6.7. Effects of test compounds RS-4, RS-9 and RS-12 on carrageenan-induced mice paw edema

It was observed that test compound **RS-9** and **RS-12** (30 mg/kg) and Indomethacin (10 mg/kg) significantly inhibited development of carrageenan-induced paw edema after three, four and five hours of treatment ($p < 0.001$). The effects of test compounds RS-4, RS-9 and RS-12 on carrageenan-induced mice paw edema are shown in **Figure 6.8.1**.

Figure 6.8.1: Carrageenan-induced mice paw edema

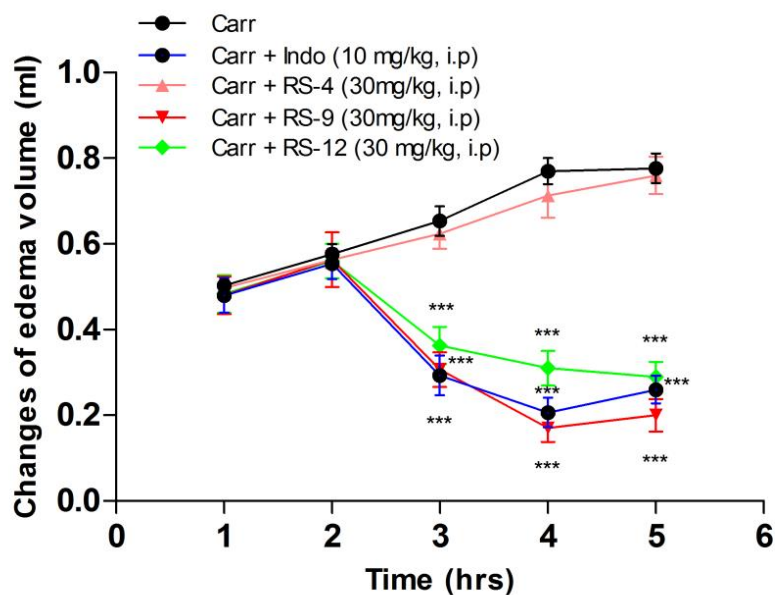


Figure 6.8.1: Effects of test compounds (RS-4, RS-9 and RS-12) and Indomethacin on carrageenan-induced mice paw edema. Each value was represented as mean \pm S.E.M. *** $p < 0.001$ when compared to the carrageenan group (two-way ANOVA followed by Bonferroni posttests).

From the above results, test compound RS-9 and RS-12 were found to be most potent at third and fourth hour after administration of carrageenan in test compound pre-treated mice, which showed clear anti-inflammatory activity in carrageenan-induced paw edema in mice. This explains inhibition of second phase of inflammation. But test compound RS-4 did not show any anti-inflammatory activity to the carrageenan challenge. In order to optimise the dose of RS-9 at which it showed anti-inflammatory activity, we carried out the dose response evaluation by following the same protocol as described in materials and methods section. It was observed that test compound **RS-9** (10 mg/kg) significantly inhibited development of carrageenan-induced paw edema after three, four and five hours of treatment ($p < 0.05-0.01$). Test compounds **RS-9** (30 mg/kg) significantly inhibited development of carrageenan-induced paw edema after three, four and five hours of treatment ($p < 0.001$). The dose response evaluation of test compound RS-9 on carrageenan-induced mice paw edema is

shown in **Figures 6.8.2**. Overall, pre-treatment of RS-9 significantly inhibited carrageenan-induced paw edema in a dose-dependent manner.

Figure 6.8.2: Dose response evaluation of RS-9 on carrageenan induced mice paw edema

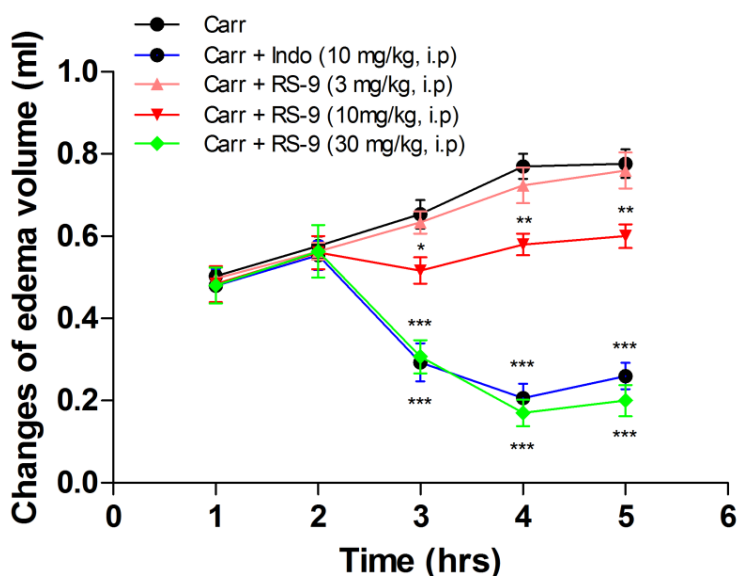


Figure 6.8.2: Effects of test compound RS-9 (3, 10 and 30 mg/kg) and Indomethacin on carrageenan-induced mice paw edema. Each value was represented as mean \pm S.E.M. * $p < 0.05$, ** $p < 0.01$, *** $p < 0.001$ when compared to the carrageenan group (two-way ANOVA followed by Bonferroni posttests).

6.8. Effects of test compounds RS-4, RS-9 and RS-12 on TNF- α , IL-1 β , IL-6 and NF κ B levels

When compared to normal group, the levels of TNF- α , IL-1 β , IL-6 and NF κ B were increased significantly in the carrageenan treatment group. The increased TNF- α levels were decreased by treatment with RS-9 and RS-12 (30 mg/kg) and Indomethacin (10 mg/kg) ($p < 0.01$ –0.001). The increased IL-6 levels were decreased by treatment with RS-9 and RS-12 (30 mg/kg) and Indomethacin at 10 mg/kg ($p < 0.01$). However, there are no significant changes on the NF κ B levels by treatment with test compounds (RS-4 and 12), except RS-9 ($p < 0.05$). The effects of test compounds RS-4, RS-9 and RS-12 on TNF- α , IL-1 β , IL-6 and NF κ B levels are shown in **Figure 6.9**. In the present study, we found that the levels of TNF- α , IL-6

and NF κ B diminished significantly in the edema paw tissues of mice by treatment with test compounds (RS-4, RS-9 and RS-12). However, there are no significant changes on the IL-1 β levels by treatment with all three test compounds occur. Among the three tested compounds RS-9 was found to diminish the levels of all three inflammatory mediators like TNF- α , IL-6 and NF κ B but not IL-1 β level suggesting its underlying mechanism of anti-inflammatory action. Further studies will be carried out to understand the reason why RS-9 inhibits the levels of TNF- α , IL-6 and NF κ B but not IL-1 β . To conclude, RS-9 at a dose of 30mg/kg produced a marked anti-inflammatory activity by inhibiting mediators of acute inflammation in carrageenan-induced mice paw edema.

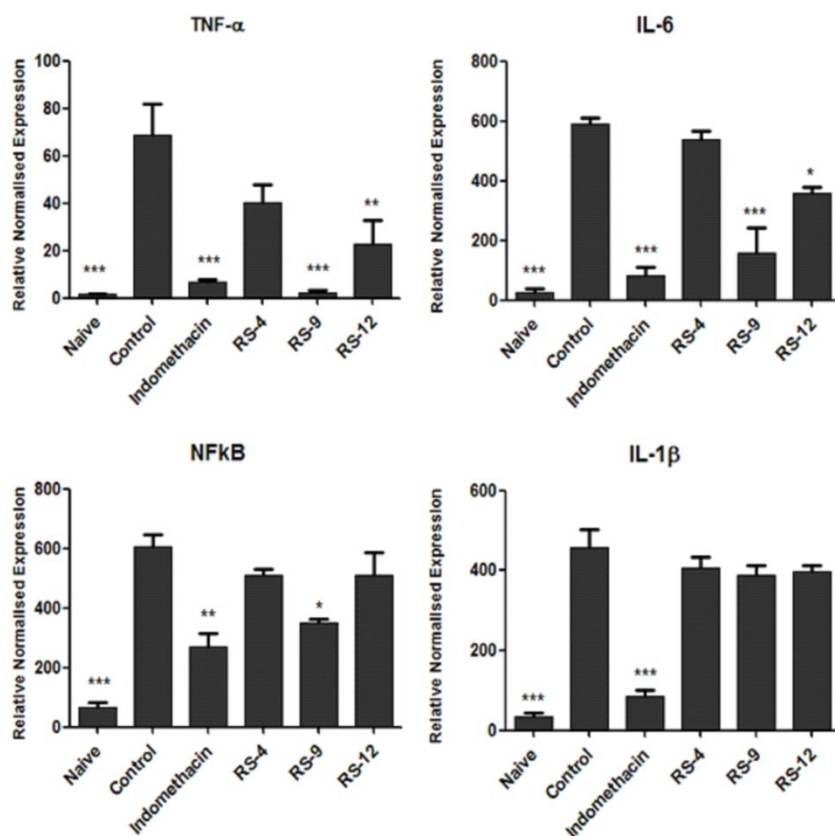


Figure 6.9: Normalised gene expression levels of pro inflammatory cytokines in carrageenan-induced edema paws with test compounds RS-4, RS-9 and RS-12 and indomethacin ($n=3$). The mRNA expression values are given as mean \pm SD normalised to GAPDH levels in each sample. Y-axis values represent number of mRNA copies relative to number of GAPDH copies in the sample. * $p < 0.05$; ** $p < 0.01$; *** $p < 0.001$ as compared to the carrageenan group (Two-way ANOVA followed by Tukey's Multiple Comparison Test).

6.9. Summary and conclusion

In the present study, we attempted to identify the structural requirements for a compound to act as A_{2B} inhibitor based on reported inhibitors employing pharmacophore model development and 3D QSAR analysis. Here, a dataset containing 265 compounds with an activity range of 0.157-944 nM was considered in the development of pharmacophore model which resulted in a five point model, AADRR.6. Pharmacophore-based 3D QSAR analysis was carried out which resulted in statistically significant parameters, $R^2 = 0.9661$ and $Q^2 = 0.5839$. Further, visual analysis of 3D QSAR generated contour cubes for the most active and the least active compounds of the dataset and provided structural requirements for a compound to be an A_{2B} inhibitor. The pharmacophore based screening of in-house compound database resulted in the identification of 15 hits based on their predicted activity and fitness. In conclusion, the test compounds selected from the results of cAMP-HPLC assay produced an anti-nociceptive effect when assessed in thermal models of nociception including hot plate test and tail immersion test, and also in chemical models of nociception including acetic acid induced writhing test and formalin induced paw licking tests. Test compound RS-9 was found to possess promising anti-nociceptive and anti-inflammatory properties, and the exact mechanism of action - whether it is central or peripheral - was not known. Further studies will be carried out to ascertain the mechanism of action involved in its anti-nociceptive and anti-inflammatory properties. Finally, we can conclude that RS-9 emerged as a novel $A_{2B}R$ antagonist and it may be further developed into a therapeutic agent for treatment or prevention of acute pain and inflammatory diseases. However, this is the first investigation against the role of $A_{2B}R$ antagonists in both anti-nociceptive and anti-inflammatory action.

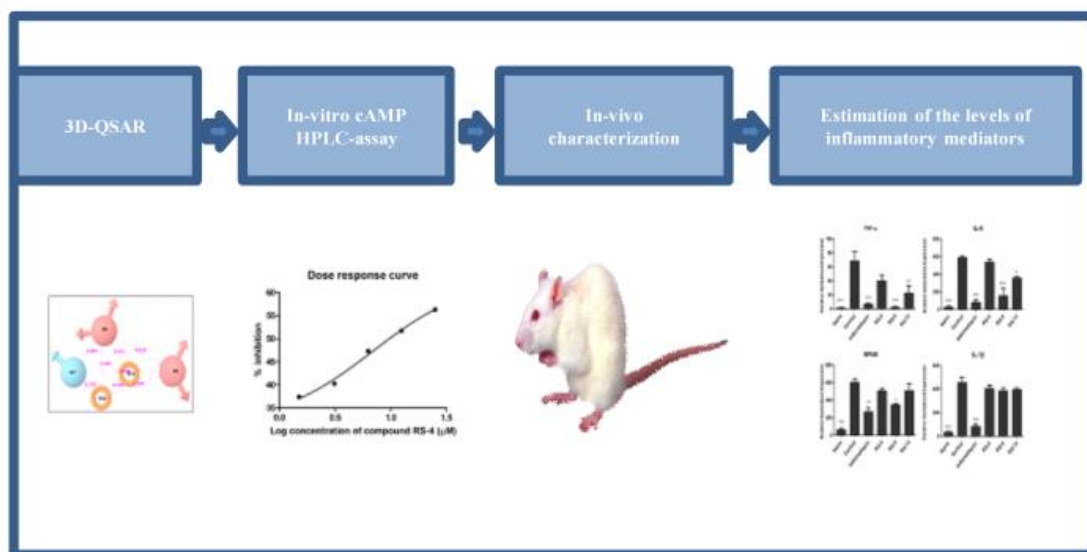


Figure 6.10: Overall workflow of anti-nociceptive and anti-inflammatory effect of A_{2B} antagonists

Recapitulation and future perspectives

Part-1

Recapitulation

- In the present work, we have attempted to design novel diverse A_{2A}R antagonists, which has crucial role in epilepsy.
- By utilising the knowledge of computer assisted drug design strategy, such as, structure based drug design, a pharmacophore model was generated to screen promising molecules from a large dataset of a commercial library (ASINEX) as A_{2A}R inhibitors. Hit molecules attained were subjected for docking based virtual screening methods to predict the binding interactions between the protein crystal structure active site and the molecule, to screen out the best hits.
- Total of 33 compounds were selected for visual inspection based on the number of H-bonds, docking and fitness scores, from which 9 compounds were selected and procured from ASINEX.
- The levels of cyclic AMP accumulated in MCF-7 breast cancer cell lines stimulated by 0.1% ethyl alcohol over a period of 24 h were investigated. To assess that a simple HPLC method has been developed and validated for the quantitative estimation of cAMP in ethanol treated MCF-7 cell lines.
- In the HPLC assay, out of 9 compounds tested, **Ligand 9** was found to decrease the cAMP level at an IC₅₀ of 2.065 µM, and it was found to be almost similar to the cAMP inhibitory IC₅₀ of standard selective A_{2A} receptor antagonist SCH-58261(1.399 µM). Hence, ligand 9 emerged as the most promising lead.
- All the compounds have shown >1 SI which represents that compounds were selective towards disease model. Comparatively Ligand 2 and 9 have shown SI of >300 and 285 respectively.

- These nine compounds were subjected to evaluate their anti-epileptic potential in adult zebrafish model and the potent compound was subjected to toxicity studies in larval zebrafish model. Test compounds, Ligand 2, 6, 7 and 9 showed clear anti-epileptic potential at 50 mg/kg.
- Ligand 9 at the dose of 75mg/kg showed neuro-protection in PTZ induced seizure model in an adult zebrafish and was found to be safe at lower concentrations except at 30 μ M indicating an acceptable neuro, hepato, and cardiovascular safety profile.
- A total of 24 analogues from parent compound **Ligand 9** with different modifications were designed with computational methodologies and synthesized as part of lead optimization.
- Synthesized and purified 24 analogues were subjected to the *in vitro* cyclic AMP assay, growth inhibition (HEK) and cell cytotoxicity assessments (MCF-7), to check the selectivity index towards cancerous cells rather than normal cells.
- All the 24 synthesized compounds were tested for preliminary *in vivo* Anti-epileptic behavioral assays (MES and sc PTZ) at 300, 100 and 30 mg/kg doses in ip/sc routes. 7 out of 24 compounds screened against neurotoxicity tests (Rotarod and Actophotometer) failed in protecting the animals during the observation period (Initial 2 hrs. followed by 15 days). Thus the 7 compounds which showed neurotoxicity were not considered for further screening studies (sc STY and sc PIC models) but all 24 compounds were screened in MES and sc PTZ models.
- Overall, eleven compounds (**6-10, 12-15, 19** and **24**) showed activity in all the screens (MES, scPTZ, scSTY, and scPIC), exhibiting a broad spectrum of anticonvulsant activity with no neurotoxicity. Compound **19** was found to be active at a dose of 30 mg/kg in all four animal models considered to be a most promising, potential lead for the treatment of epilepsy.

Future perspectives

- Our designed molecules may provide novel platform for development of the next generation of 1, 3, 5-triazine analogs as A_{2A}R antagonists in the treatment of epilepsy.
- Further studies like radio ligand binding assay and Cyclic AMP accumulation assay (by using the Sigma Direct cyclic AMP Enzyme Immunoassay kit) could be performed to confirm its A_{2A}R inhibitory action.
- Structural modification of lead **compound 19** could be useful for further molecular development with improved bioactivity.

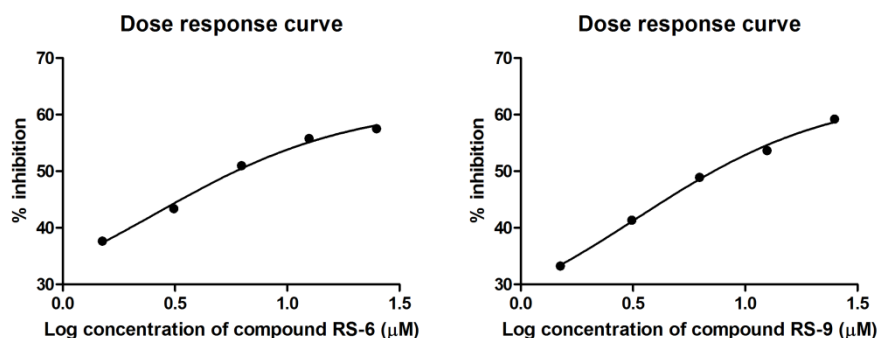
- Further studies like pharmacokinetics, pharmacodynamics and toxicity evaluation are still required to develop their higher analogs and elucidate its putative mechanism of action as anticonvulsant.
- Advancement of candidate compounds presented in this thesis along a drug development path would require a significant investment in medicinal chemistry, preclinical and clinical studies.

Part-2

Recapitulation

- With the intention of developing novel inhibitors of A_{2B}R to attenuate acute inflammation in neurological disorders and its anti-nociceptive effects, we explored the pharmacophore model development and 3D QSAR analysis.
- The dataset containing a total of 265 compounds with an activity range of 0.157-944 nM was considered in the present study to obtain the common pharmacophore.
- 19 pharmacophore hypotheses were found to be generated for which scoring hypothesis was applied. Of these 19, five best hypotheses were selected based on the generated scores.
- Further, the selected hypothesis a five point model, AADRR was employed in generation of 3D QSAR model which was further validated for its predictability. The generated 3D QSAR model was subjected to PLS analysis.
- Further, the visual analysis of 3D QSAR generated contour cubes for the most active and the least active compounds of the dataset providing structural requirements for a compound to be an A_{2B} inhibitor.
- The pharmacophore based screening of in-house compound database resulted in the identification of 15 hits based on their predicted activity and fitness.
- Gene expression levels of A_{2A} and A_{2B} AR subtypes, in two prostate cancer cell lines, PC-3 and DU145, were compared using real-time quantitative RT-PCR analysis, and PC3 cells were selected as *in vitro* system to screen inhibitors designed for A_{2B} *in silico* by 3D QSAR model.
- The levels of cyclic AMP accumulated in PC-3 prostate cancer cell lines over a period of 24 h were investigated. These 15 analogues were subjected to the *in vitro* cyclic AMP assay, growth inhibition (HEK) and cell cytotoxicity assessments (PC-3), to check the selectivity index towards cancerous cells rather than normal cells.

- Out of these 15 compounds RS-6 and RS-9 showed least IC₅₀ of 7.015 μM and 8.36 μM respectively, to reduce cAMP level in PC3 cell lines. Hence, RS-6 and RS-9 were emerged as most promising leads from the in-vitro cAMP inhibitory assay.



- All the compounds have shown >1 SI which represent that compounds were selective towards disease model. Comparatively RS-4, 6 and 9 have shown SI of 132.185, 216.173 and 607.882 respectively.
- Out of 15 compounds, 5 compounds showed cyclic AMP inhibitory IC₅₀ of less than 100. However, RS 15 has shown less SI than the remaining four compounds. Hence these four compounds were selected for further evaluation of their anti-nociceptive as well as anti-inflammatory potential.
- In order to identify the possible central and peripheral effects of the test substances, anti-nociceptive evaluation was done by subjecting the test compounds preliminary for acetic acid induced writhing test and formalin induced flinching test and then thermal induced pain models like hot plate test and tail immersion tests.
- Based on the results obtained from acetic acid induced writhing test and formalin induced paw licking test, it was found that RS-4, 9 and 12 were found effective in both the models, whereas, RS-9 and RS-12 were found to be effective in both the thermal induced pain models (hot plate and tail flick tests).
- Initially test compounds (RS-4, 9 and 12) were selected based on the results obtained from *in vivo* anti-nociceptive activity evaluation in both chemical and thermal induced pain models, and were subjected to carrageenan induces paw edema in mice.
- It was observed that the test compound RS-9 and RS-12 (30 mg/kg) and Indomethacin (10 mg/kg) significantly inhibited development of carrageenan-induced paw edema after three, four and five hours of treatment ($p < 0.001$).
- In the gene expression analysis of test compounds on inflammatory mediators by RT-PCR studies, it was found that the levels of TNF- α , IL-6 and NF κ B were diminished

significantly in the edema paw tissues of mice by treatment with test compounds (RS-4, RS-9 and RS-12). However, there are no significant changes occurred on the IL-1 β levels by treatment with all the three test compounds.

- To conclude, RS-9 at the dose of 30 mg/kg produced a marked anti-inflammatory activity by inhibiting mediators of acute inflammation in carrageenan-induced mice paw edema. Hence, RS-9 emerged as a novel A_{2B}R antagonist and it may be further developed into a therapeutic agent for treatment or prevention of acute pain and inflammatory diseases.

Future perspectives

- This is the first investigation against the role of A_{2B}R antagonists in both anti-nociceptive and anti-inflammatory action which provides a novel platform for young researchers.
- Further studies like radio ligand binding assay and Cyclic AMP accumulation assay (by using the Sigma Direct cyclic AMP Enzyme Immunoassay kit) could be performed to confirm its A_{2B} inhibitory action.
- Structural modification of lead compound RS-9 could be useful for further molecular development with improved bioactivity.
- Studies are still required to confirm chronic pharmacodynamic and pharmacokinetic profile of the active molecules including safety profile.
- Test compound RS-9 was found to possess promising anti-nociceptive and anti-inflammatory properties, of which the exact mechanism of action was not known, whether it is central or peripheral. Further studies will be carried out to ascertain the mechanism of action involved in its anti-nociceptive and anti-inflammatory properties.
- Further studies will be carried out to understand the reason why RS-9 inhibits the levels of TNF- α , IL-6 and NF κ B but not IL-1 β .

References

- Abo-Salem OM, Hayallah AM, Bilkei-Gorzo A, Filipek B, Zimmer A, Muller CE. Antinociceptive effects of novel A2B adenosine receptor antagonists. *Journal of Pharmacology and Experimental Therapeutics*. 2004 Jan 1;308(1):358-66.
- Afonso CA, Lourenco NM, Rosatella AD. Synthesis of 2,4,6-Tri-substituted-1,3,5-Triazines. *Molecules*. 2006 Jan 31;11(1):81-102.
- Akkari R, Burbiel JC, Hockemeyer J, Muller CE. Recent progress in the development of adenosine receptor ligands as anti-inflammatory drugs. *Current topics in medicinal chemistry*. 2006 Jul 1;6(13):1375-99.
- Alderton W, Berghmans S, Butler P, Chassaing H, Fleming A, Golder Z, Richards F, Gardner I. Accumulation and metabolism of drugs and CYP probe substrates in zebrafish larvae. *Xenobiotica*. 2010 Aug 1;40(8):547-57.
- Antonioli L, Fornai M, Colucci R, Ghisu N, Tuccori M, Del Tacca M, Blandizzi C. Regulation of enteric functions by adenosine: pathophysiological and pharmacological implications. *Pharmacology & therapeutics*. 2008 Dec 31;120(3):233-53.
- Arslan G, Fredholm BB. Stimulatory and inhibitory effects of adenosine A2A receptors on nerve growth factor-induced phosphorylation of extracellular regulated kinases 1/2 in PC12 cells. *Neuroscience letters*. 2000 Oct 13;292(3):183-86.
- Auchampach JA, Caughey GH, Linden J. A2B and not A3 adenosine receptors mediate degranulation of canine BR mastocytoma cells. *Drug Dev. Res*. 1996;37:147.
- Azdad K, Gall D, Woods AS, Ledent C, Ferre S, Schiffmann SN. Dopamine D2 and adenosine A2A receptors regulate NMDA-mediated excitation in accumbens neurons through A2A–D2 receptor heteromerization. *Neuropsychopharmacology*. 2009 Mar 1;34(4):972-86.
- Banote RK, Koutarapu S, Chennubhotla KS, Chatti K, Kulkarni P. Oral gabapentin suppresses pentylenetetrazole-induced seizure-like behavior and cephalic field potential in adult zebrafish. *Epilepsy & Behavior*. 2013 Apr 30;27(1):212-19.
- Baraldi PG, Baraldi S, Saponaro G, Preti D, Romagnoli R, Piccagli L, Cavalli A, Recanatini M, Moorman AR, Zaid AN, Varani K. Novel 1, 3-dipropyl-8-(3-benzimidazol-2-yl-

- methoxy-1-methylpyrazol-5-yl) xanthines as potent and selective A2B adenosine receptor antagonists. *Journal of medicinal chemistry*. 2012 Jan 11;55(2):797-811.
- Baraldi PG, Tabrizi MA, Gessi S, Borea PA. Adenosine receptor antagonists: translating medicinal chemistry and pharmacology into clinical utility. *Chemical reviews*. 2008 Jan 9;108(1):238-63.
- Baraldi PG, Tabrizi MA, Preti D, Bovero A, Romagnoli R, Fruttarolo F, Zaid NA, Moorman AR, Varani K, Gessi S, Merighi S. Design, synthesis, and biological evaluation of new 8-heterocyclic xanthine derivatives as highly potent and selective human A2B adenosine receptor antagonists. *Journal of medicinal chemistry*. 2004 Mar 11;47(6):1434-47.
- Beghi E. Efficacy and tolerability of the new antiepileptic drugs: comparison of two recent guidelines. *The Lancet Neurology*. 2004 Oct 31;3(10):618-21.
- Begley CE, Annegers JF, Lairson DR, Reynolds TF, Hauser WA. Cost of epilepsy in the United States: a model based on incidence and prognosis. *Epilepsia*. 1994 Nov 1;35(6):1230-43.
- Belikoff BG, Hatfield S, Georgiev P, Ohta A, Lukashev D, Buras JA, Remick DG, Sitkovsky M. A2B adenosine receptor blockade enhances macrophage-mediated bacterial phagocytosis and improves polymicrobial sepsis survival in mice. *The Journal of Immunology*. 2011 Feb 15;186(4):2444-53.
- Berghmans S, Hunt J, Roach A, Goldsmith P. Zebrafish offer the potential for a primary screen to identify a wide variety of potential anticonvulsants. *Epilepsy research*. 2007 Jun 30;75(1):18-28.
- Berkovic SF. Treatment with anti-epileptic drugs. *Australian family physician*. 2005 Dec;34(12):1017.
- Berman RF, Fredholm BB, Aden U, O'Connor WT. Evidence for increased dorsal hippocampal adenosine release and metabolism during pharmacologically induced seizures in rats. *Brain research*. 2000 Jul 28;872(1):44-53.
- Bilkei-Gorzo A, Abo-Salem OM, Hayallah AM, Michel K, Muller CE, Zimmer A. Adenosine receptor subtype-selective antagonists in inflammation and hyperalgesia. *Naunyn-Schmiedeberg's archives of pharmacology*. 2008 Mar 1;377(1):65-76.

- Boison D, Singer P, Shen HY, Feldon J, Yee BK. Adenosine hypothesis of schizophrenia—opportunities for pharmacotherapy. *Neuropharmacology*. 2012 Mar 31;62(3):1527-43.
- Boissier JR, Simon P. [Action of caffeine on the spontaneous motility of the mouse]. *Archives internationales de pharmacodynamie et de therapie*. 1965 Nov;158(1):212-21.
- Borrmann T, Hinz S, Bertarelli DC, Li W, Florin NC, Scheiff AB, Müller CE. 1-Alkyl-8-(piperazine-1-sulfonyl) phenylxanthines: development and characterization of adenosine A2B receptor antagonists and a new radioligand with subnanomolar affinity and subtype specificity. *Journal of medicinal chemistry*. 2009 May 27;52(13):3994-4006.
- Burnstock G, Cocks T, Crowe R, Kasakov L. PURINERGIC INNERVATION OF THE GUINEA-PIG URINARY BLADDER. *British journal of pharmacology*. 1978 May 1;63(1):125-38.
- Cacciari B, Pastorin G, Bolcato C, Spalluto G, Bacilieri M, Moro S. A2B adenosine receptor antagonists: recent developments. *Mini reviews in medicinal chemistry*. 2005 Dec 1;5(12):1053-60.
- Castelhano A, McKibben B, Steinig A, inventors; Osi Pharmaceuticals, Inc., assignee. Pyrrolopyrimidine A2B selective antagonist compounds, their synthesis and use. United States patent US 7,645,754. 2010 Jan 12.
- Catena E, Gunella G, Monici PP, Oliani C. Evaluation of the risk/benefit ratio of bamiphylline in the treatment of chronic obstructive lung disease. *Italian J Chest Dis*. 1988;42:419-26.
- Cekic C, Sag D, Li Y, Theodorescu D, Strieter RM, Linden J. Adenosine A2B receptor blockade slows growth of bladder and breast tumors. *The Journal of Immunology*. 2012 Jan 1;188(1):198-205.
- Chakraborty C, Hsu CH, Wen ZH, Lin CS, Agoramoorthy G. Zebrafish: a complete animal model for in vivo drug discovery and development. *Current drug metabolism*. 2009 Feb 1;10(2):116-24.
- Chaudhari GH, Chennubhotla KS, Chatti K, Kulkarni P. Optimization of the adult zebrafish ECG method for assessment of drug-induced QTc prolongation. *Journal of pharmacological and toxicological methods*. 2013 Apr 30;67(2):115-20.

- Cheung AW, Brinkman J, Firooznia F, Flohr A, Grimsby J, Gubler ML, Guertin K, Hamid R, Marcopulos N, Norcross RD, Qi L. 4-Substituted-7-N-alkyl-N-acetyl 2-aminobenzothiazole amides: drug-like and non-xanthine based A2B adenosine receptor antagonists. *Bioorganic & medicinal chemistry letters*. 2010 Jul 15;20(14):4140-46.
- Chomczynski. P. A reagent for the single-step simultaneous isolation of RNA, DNA and proteins from cell and tissue samples. *BioTechniques*. 1993; 15(3):532-4, 536-7.
- Coulter DA. Epilepsy-associated plasticity in γ -aminobutyric acid receptor expression, function, and inhibitory synaptic properties. *International review of neurobiology*. 2001 Dec 31;45:237-52.
- Crescioli S, Spinazzi A, Plebani M, Pozzani M, Mapp CE, Boschetto P, Fabbri LM. Theophylline inhibits early and late asthmatic reactions induced by allergens in asthmatic subjects. *Annals of allergy*. 1991 Mar;66(3):245-51.
- Crunkhorn P, Meacock SC. Mediators of the inflammation induced in the rat paw by carrageenin. *British Journal of Pharmacology*. 1971 Jul 1;42(3):392-402.
- Csoka B, Nemeth ZH, Rosenberger P, Eltzhig HK, Spolarics Z, Pacher P, Selmezy Z, Kosco B, Himer L, Vizi ES, Blackburn MR. A2B adenosine receptors protect against sepsis-induced mortality by dampening excessive inflammation. *The Journal of Immunology*. 2010 Jul 1;185(1):542-50.
- De Zwart M, Vollinga RC, Beukers MW, Slegers DF, von Frijtag Drabbe Künzel JK, de Groote M, Ijzerman AP. Potent antagonists for the human adenosine A2B receptor. Derivatives of the triazolotriazine adenosine receptor antagonist ZM241385 with high affinity. *Drug development research*. 1999 Nov 1;48(3):95-103.
- Dhalla AK, Shryock JC, Shreeniwas R, Belardinelli L. Pharmacology and therapeutic applications of A1 adenosine receptor ligands. *Current topics in medicinal chemistry*. 2003 Feb 1;3(4):369-85.
- Dixon SL, Smondyrev AM, Rao SN. PHASE: a novel approach to pharmacophore modeling and 3D database searching. *Chemical biology & drug design*. 2006 May 1;67(5):370-2.
- Dohrman DP, Diamond I, Gordon AS. The role of the neuromodulator adenosine in alcohol's actions. *Alcohol Research and Health*. 1997 Jan 1;21(2):136.

- Doweyko AM. 3D-QSAR illusions. *Journal of computer-aided molecular design*. 2004 Jul 1;18(7-9):587-96.
- Dragunow M, Goddard GV, Lavery R. Is adenosine an endogenous anticonvulsant? *Epilepsia*. 1985 Oct 1;26(5):480-7.
- Dunwiddie TV, Masino SA. The role and regulation of adenosine in the central nervous system. *Annual review of neuroscience*. 2001 Mar;24(1):31-55.
- Dunwiddie TV. Adenosine and suppression of seizures. *Advances in neurology*. 1999;79:1001.
- During MJ, Spencer DD. Adenosine: a potential mediator of seizure arrest and postictal refractoriness. *Annals of neurology*. 1992 Nov 1;32(5):618-24.
- Eastwood P, Esteve C, Gonzalez J, Fonquerna S, Aiguade J, Carranco I, Domenech T, Aparici M, Miralpeix M, Albertí J, Córdoba M. Discovery of LAS101057: a potent, selective, and orally efficacious A2B adenosine receptor antagonist. *ACS medicinal chemistry letters*. 2010 Dec 20;2(3):213-18.
- Eastwood P, Gonzalez J, Paredes S, Nueda A, Domenech T, Alberti J, Vidal B. Discovery of N-(5, 6-diarylpyridin-2-yl) amide derivatives as potent and selective A2B adenosine receptor antagonists. *Bioorganic & medicinal chemistry letters*. 2010 Mar 1;20(5):1697-700.
- Eddy NB, Leimbach D. Synthetic analgesics. II. Dithienylbutenyl- and dithienylbutylamines. *Journal of Pharmacology and Experimental Therapeutics*. 1953 Mar 1;107(3):385-93.
- Eisenach JC, Rauck RL, Curry R. Intrathecal, but not intravenous adenosine reduces allodynia in patients with neuropathic pain. *Pain*. 2003 Sep 30;105(1):65-70.
- El Yacoubi M, Ledent C, Parmentier M, Costentin J, Vaugeois JM. Evidence for the involvement of the adenosine A2A receptor in the lowered susceptibility to pentylenetetrazol-induced seizures produced in mice by long-term treatment with caffeine. *Neuropharmacology*. 2008 Jul 31;55(1):35-40.
- Eliceiri BP, Gonzalez AM, Baird A. Zebrafish model of the blood-brain barrier: morphological and permeability studies. *The Blood-Brain and Other Neural Barriers: Reviews and Protocols*. 2011:371-78.

- Ellenbogen KA, O'Neill G, Prystowsky EN, Camm JA, Meng L, Lieu HD, Jerling M, Shreeniwas R, Belardinelli L, Wolff AA, TEMPEST Study Group. Trial to evaluate the management of paroxysmal supraventricular tachycardia during an electrophysiology study with tecadenoson. *Circulation*. 2005 Jun 21;111(24):3202-208.
- Elnatan A, Mitchelson F. A simple and rapid HPLC assay for quantitating cyclic AMP accumulation in intact cell preparations. *Journal of pharmacological and toxicological methods*. 1994 Feb 1;31(1):47-51.
- Elzein E, Kalla RV, Li X, Perry T, Gimbel A, Zeng D, Lustig D, Leung K, Zablocki J. Discovery of a novel A2B adenosine receptor antagonist as a clinical candidate for chronic inflammatory airway diseases. *Journal of medicinal chemistry*. 2008 Mar 6;51(7):2267-78.
- Esteve C, Nueda A, Diaz JL, Beleta J, Cardenas A, Lozoya E, Cadavid MI, Loza MI, Ryder H, Vidal B. New pyrrolopyrimidin-6-yl benzenesulfonamides: Potent A2B adenosine receptor antagonists. *Bioorganic & medicinal chemistry letters*. 2006 Jul 15;16(14):3642-45.
- Etherington LA, Frenguelli BG. Endogenous adenosine modulates epileptiform activity in rat hippocampus in a receptor subtype-dependent manner. *European Journal of Neuroscience*. 2004 May 1;19(9):2539-50.
- Etique N, Grillier-Vuissoz I, Lecomte J, Flament S. Crosstalk between adenosine receptor (A2A isoform) and ER α mediates ethanol action in MCF-7 breast cancer cells. *Oncology reports*. 2009 Apr 1;21(4):977-81.
- Ezeamuzie CI, Khan I. The role of adenosine A2 receptors in the regulation of TNF- α production and PGE-2 release in mouse peritoneal macrophages. *International immunopharmacology*. 2007 Apr 30;7(4):483-90.
- Fedele DE, Li T, Lan JQ, Fredholm BB, Boison D. Adenosine A1 receptors are crucial in keeping an epileptic focus localized. *Experimental neurology*. 2006 Jul 31;200(1):184-90.
- Feoktistov I, Biaggioni I. Adenosine A2B receptors. *Pharmacological reviews*. 1997 Dec 1;49(4):381-402.

- Feoktistov I, Murray JJ, Biaggioni I. Positive modulation of intracellular Ca^{2+} levels by adenosine A2B receptors, prostacyclin, and prostaglandin E1 via a cholera toxin-sensitive mechanism in human erythroleukemia cells. *Molecular pharmacology*. 1994 Jun 1;45(6):1160-67.
- Fernandez F, Caamano O, Nieto MI, Lopez C, Garcia-Mera X, Stefanachi A, Nicolotti O, Loza MI, Brea J, Esteve C, Segarra V. 1, 3-Dialkyl-8-N-substituted benzyloxycarbonylamino-9-deazaxanthines as potent adenosine receptor ligands: Design, synthesis, structure–affinity and structure–selectivity relationships. *Bioorganic & medicinal chemistry*. 2009 May 15;17(10):3618-29.
- Fiebich BL, Biber K, Gyufko K, Berger M, Bauer J, Van Calker D. Adenosine A2B receptors mediate an increase in interleukin (IL)-6 mRNA and IL-6 protein synthesis in human astrogloma cells. *Journal of neurochemistry*. 1996 Apr 1;66(4):1426-31.
- Fleming A, Alderton WK. Zebrafish in pharmaceutical industry research: finding the best fit. *Drug Discovery Today: Disease Models*. 2013 May 31;10(1):e43-50.
- Fozard JR, Ellis KM, Dantas MF, Tigani B, Mazzoni L. Effects of CGS 21680, a selective adenosine A2A receptor agonist, on allergic airways inflammation in the rat. *European journal of pharmacology*. 2002 Mar 8;438(3):183-88.
- Fozard JR, McCarthy C. Adenosine receptor ligands as potential therapeutics in asthma. *Current opinion in investigational drugs (London, England: 2000)*. 2002 Jan;3(1):69-77.
- Fredholm BB, Abbracchio MP, Burnstock G, Dubyak GR, Harden TK, Jacobson KA, Schwabe U, Williams M. Towards a revised nomenclature for P1 and P2 receptors. *Trends in pharmacological sciences*. 1997 Mar;18(3):79.
- Fredholm BB, Arslan G, Halldner L, Kull B, Schulte G, Wasserman W. Structure and function of adenosine receptors and their genes. *Naunyn-Schmiedeberg's archives of pharmacology*. 2000 Nov 1;362(4-5):364-74.
- Fredholm BB, Chern Y, Franco R, Sitkovsky M. Aspects of the general biology of adenosine A2A signaling. *Progress in neurobiology*. 2007 Dec 31;83(5):263-76.

- Fredholm BB, Cunha RA, Svenningsson P. Pharmacology of adenosine A2A receptors and therapeutic applications. *Current topics in medicinal chemistry*. 2003 Feb 1;3(4):413-26.
- Fredholm BB, IJzerman AP, Jacobson KA, Klotz KN, Linden J. International Union of Pharmacology. XXV. Nomenclature and classification of adenosine receptors. *Pharmacological reviews*. 2001 Dec 1;53(4):527-52.
- French JA, Kanner AM, Bautista J, Abou-Khalil B, Browne T, Harden CL, Theodore WH, Bazil C, Stern J, Schachter SC, Bergen D. Efficacy and tolerability of the new antiepileptic drugs I: Treatment of new onset epilepsy Report of the Therapeutics and Technology Assessment Subcommittee and Quality Standards Subcommittee of the American Academy of Neurology and the American Epilepsy Society. *Neurology*. 2004 Apr 27;62(8):1252-60.
- French JA, Kanner AM, Bautista J, Abou-Khalil B, Browne T, Harden CL, Theodore WH, Bazil C, Stern J, Schachter SC, Bergen D. Efficacy and tolerability of the new antiepileptic drugs II: Treatment of refractory epilepsy Report of the Therapeutics and Technology Assessment Subcommittee and Quality Standards Subcommittee of the American Academy of Neurology and the American Epilepsy Society. *Neurology*. 2004 Apr 27;62(8):1261-73.
- Gessi S, Varani K, Merighi S, Cattabriga E, Pancaldi C, Szabadkai Y, Rizzuto R, Klotz KN, Leung E, Mac Lennan S, Baraldi PG. Expression, pharmacological profile, and functional coupling of A2B receptors in a recombinant system and in peripheral blood cells using a novel selective antagonist radioligand, [3H] MRE 2029-F20. *Molecular pharmacology*. 2005 Jun 1;67(6):2137-47.
- Gillespie RJ, Bamford SJ, Botting R, Comer M, Denny S, Gaur S, Griffin M, Jordan AM, Knight AR, Lerpiniere J, Leonardi S. Antagonists of the human A2A adenosine receptor. 4. Design, synthesis, and preclinical evaluation of 7-aryltriazolo [4, 5-d] pyrimidines. *Journal of medicinal chemistry*. 2008 Dec 10;52(1):33-47.
- Goldsmith P, Fleming A, inventors; Fleming Angeleen L, assignee. Screening methods employing zebrafish and the blood brain barrier. United States patent application US 10/566,888. 2005 Feb 17.

- Grahner B, Winiwarter S, Lanzner W, Mueller CE. Synthesis and structure-activity relationships of deazaxanthines: analogs of potent A1-and A2-adenosine receptor antagonists. *Journal of medicinal chemistry*. 1994 May;37(10):1526-34.
- Hagberg H, Andersson P, Lacarewicz J, Jacobson I, Butcher S, Sandberg M. Extracellular adenosine, inosine, hypoxanthine, and xanthine in relation to tissue nucleotides and purines in rat striatum during transient ischemia. *Journal of neurochemistry*. 1987 Jul 1;49(1):227-31.
- Harada H, Asano O, Hoshino Y, Yoshikawa S, Matsukura M, Kabasawa Y, Niijima J, Kotake Y, Watanabe N, Kawata T, Inoue T. 2-Alkynyl-8-aryl-9-methyladenines as novel adenosine receptor antagonists: Their synthesis and structure-activity relationships toward hepatic glucose production induced via agonism of the A2B receptor. *Journal of medicinal chemistry*. 2001 Jan 18;44(2):170-9.
- Hasko G, Pacher P, Deitch EA, Vizi ES. Shaping of monocyte and macrophage function by adenosine receptors. *Pharmacology & therapeutics*. 2007 Feb 28;113(2):264-75.
- Hauser RA, Schwarzschild MA. Adenosine A2A Receptor Antagonists for Parkinson's Disease. *Drugs & aging*. 2005 Jun 1;22(6):471-82.
- Hayallah AM, Sandoval-Ramírez J, Reith U, Schobert U, Preiss B, Schumacher B, Daly JW, Müller CE. 1, 8-Disubstituted xanthine derivatives: synthesis of potent A2B-selective adenosine receptor antagonists. *Journal of medicinal chemistry*. 2002 Mar 28;45(7):1500-10.
- Hill A, Mesens N, Steemans M, Xu JJ, Aleo MD. Comparisons between in vitro whole cell imaging and in vivo zebrafish-based approaches for identifying potential human hepatotoxicants earlier in pharmaceutical development. *Drug metabolism reviews*. 2012 Feb 1;44(1):127-40.
- Hirose S, Okada M, Kaneko S, Mitsudome A. Are some idiopathic epilepsies disorders of ion channels? A working hypothesis. *Epilepsy research*. 2000 Oct 2;41(3):191-204.
- Huber A, Padrun V, Deglon N, Aebischer P, Mohler H, Boison D. Grafts of adenosine-releasing cells suppress seizures in kindling epilepsy. *Proceedings of the National Academy of Sciences*. 2001 Jun 19;98(13):7611-6.

- Hunnskaar S, Hole K. The formalin test in mice: dissociation between inflammatory and non-inflammatory pain. *Pain*. 1987 Jul 31;30(1):103-14.
- Hutchinson SA, Scammells PJ. A1 adenosine receptor agonists: medicinal chemistry and therapeutic potential. *Current pharmaceutical design*. 2004 Jul 1;10(17):2021-39.
- Jacobson KA, Gao ZG. Adenosine receptors as therapeutic targets. *Nature Reviews Drug Discovery*. 2006 Mar 1;5(3):247-64.
- Jacobson KA. Adenosine A3 receptors: novel ligands and paradoxical effects. *Trends in pharmacological sciences*. 1998 May 1;19(5):184-91.
- Jordan JE, Zhao ZQ, Sato H, Taft S, Vinten-Johansen J. Adenosine A2 receptor activation attenuates reperfusion injury by inhibiting neutrophil accumulation, superoxide generation and coronary endothelial adherence. *Journal of Pharmacology and Experimental Therapeutics*. 1997 Jan 1;280(1):301-9.
- Jung KY, Kim SK, Gao ZG, Gross AS, Melman N, Jacobson KA, Kim YC. Structure–activity relationships of thiazole and thiadiazole derivatives as potent and selective human adenosine A3 receptor antagonists. *Bioorganic & medicinal chemistry*. 2004 Feb 1;12(3):613-23.
- Kalla RV, Elzein E, Perry T, Li X, Gimbel A, Yang M, Zeng D, Zablocki J. Selective, high affinity A2B adenosine receptor antagonists: N-1 monosubstituted 8-(pyrazol-4-yl) xanthines. *Bioorganic & medicinal chemistry letters*. 2008 Feb 15;18(4):1397-401.
- Kalla RV, Zablocki J, Tabrizi MA, Baraldi PG. Recent developments in A2B adenosine receptor ligands. *Adenosine Receptors in Health and Disease 2009* (pp. 99-122). Springer Berlin Heidelberg.
- Kalla RV, Zablocki J. Progress in the discovery of selective, high affinity A2B adenosine receptor antagonists as clinical candidates. *Purinergic signalling*. 2009 Mar 1;5(1):21-29.
- Kari G, Rodeck U, Dicker AP. Zebrafish: an emerging model system for human disease and drug discovery. *Clinical Pharmacology & Therapeutics*. 2007 Jul 1;82(1):70-80.
- Kim SA, Marshall MA, Melman N, Kim HS, Müller CE, Linden J, Jacobson KA. Structure–activity relationships at human and rat A2B adenosine receptors of xanthine derivatives

- substituted at the 1-, 3-, 7-, and 8-positions. *Journal of medicinal chemistry*. 2002 May 23;45(11):2131-38.
- Kim YC, Ji XD, Melman N, Linden J, Jacobson KA. Anilide derivatives of an 8-phenylxanthine carboxylic congener are highly potent and selective antagonists at human A2B adenosine receptors. *Journal of medicinal chemistry*. 2000 Mar 23;43(6):1165-72.
- Klinger M, Kudlacek O, Seidel MG, Freissmuth M, Sexl V. MAP kinase stimulation by cAMP does not require RAP1 but SRC family kinases. *Journal of Biological Chemistry*. 2002 Sep 6;277(36):32490-7.
- Koeppen M, Eckle T, Eltzschig HK. Interplay of hypoxia and A2B adenosine receptors in tissue protection. *Advances in pharmacology*. 2011 Jul 13;61:145.
- Koga K, Kurokawa M, Ochi M, Nakamura J, Kuwana Y. Adenosine A2A receptor antagonists KF17837 and KW-6002 potentiate rotation induced by dopaminergic drugs in hemi-Parkinsonian rats. *European journal of pharmacology*. 2000 Nov 24;408(3):249-55.
- Kolachala V, Asamoah V, Wang L, Obertone TS, Ziegler TR, Merlin D, Sitaraman SV. TNF- α upregulates adenosine 2B (A2B) receptor expression and signaling in intestinal epithelial cells: a basis for A2bR overexpression in colitis. *Cellular and molecular life sciences*. 2005 Nov 1;62(22):2647-57.
- Kolachala VL, Bajaj R, Chalasani M, Sitaraman SV. Purinergic receptors in gastrointestinal inflammation. *American Journal of Physiology-Gastrointestinal and Liver Physiology*. 2008 Feb 1;294(2):G401-10.
- Koster R, Anderson M, De Beer EJ. Acetic acid-induced analgesic screening. *FEDERATION PROCEEDINGS*. 1959; 18: 412.
- Krall RL, Penry JK, White BG, Kupferberg HJ, Swinyard EA. Antiepileptic drug development: II. Anticonvulsant drug screening. *Epilepsia*. 1978 Aug 1;19(4):409-28.
- Ledent C, Vaugeois JM, Schiffmann SN, Pedrazzini T, El Yacoubi M, Vanderhaeghen JJ, Costentin J, Heath JK, Vassart G, Parmentier M. Aggressiveness, hypoalgesia and high blood pressure in mice lacking the adenosine A2A receptor. *Nature*. 1997 Aug 14;388(6643):674-8.

- Li X, Kang H, Liu X, Liu Z, Shu K, Chen X, Zhu S. Effect of adenosine A2A receptor antagonist ZM241385 on amygdala-kindled seizures and progression of amygdala kindling. *Journal of Huazhong University of Science and Technology [Medical Sciences]*. 2012 Apr;32:257-64.
- Linden J. Cloned adenosine A3 receptors: pharmacological properties, species differences and receptor functions. *Trends in pharmacological sciences*. 1994 Aug 31;15(8):298-306.
- Liu J, Cheng ML, Shi JZ, Yang Q, Wu J, Li CX, Waalkes MP. Differential effects between Maotai and ethanol on hepatic gene expression in mice: possible role of metallothionein and heme oxygenase-1 induction by Maotai. *Experimental Biology and Medicine*. 2006 Oct 1;231(9):1535-41.
- Liu J, Qu W, Saavedra JE, Waalkes MP. The nitric oxide donor, O₂-vinyl 1-(pyrrolidin-1-yl) diazen-1-ium-1, 2-diolate (V-PYRRO/NO), protects against cadmium-induced hepatotoxicity in mice. *Journal of Pharmacology and Experimental Therapeutics*. 2004 Jul 1;310(1):18-24.
- Livingston M, Heaney LG, Ennis M. Adenosine, inflammation and asthma—a review. *Inflammation research*. 2004 Apr 1;53(5):171-78.
- Londos C, Cooper DM, Wolff J. Subclasses of external adenosine receptors. *Proceedings of the National Academy of Sciences*. 1980 May 1;77(5):2551-54.
- Mantri M, de Graaf O, van Veldhoven J, Göblyös A, von Frijtag Drabbe Künzel JK, Mulder-Krieger T, Link R, de Vries H, Beukers MW, Brussee J, IJzerman AP. 2-Amino-6-furan-2-yl-4-substituted nicotinonitriles as A2A adenosine receptor antagonists. *Journal of medicinal chemistry*. 2008 Jul 19;51(15):4449-55.
- Matos M, Augusto E, Agostinho P, Cunha RA, Chen JF. Antagonistic interaction between adenosine A2A receptors and Na⁺/K⁺-ATPase- α 2 controlling glutamate uptake in astrocytes. *The Journal of Neuroscience*. 2013 Nov 20;33(47):18492-502.
- Matsumoto T, Tostes RC, Webb RC. Alterations in vasoconstrictor responses to the endothelium-derived contracting factor uridine adenosine tetraphosphate are region specific in DOCA-salt hypertensive rats. *Pharmacological Research*. 2012 Jan 31;65(1):81-90.

- Matulenko MA, Paight ES, Frey RR, Gomtsyan A, DiDomenico S, Jiang M, Lee CH, Stewart AO, Yu H, Kohlhaas KL, Alexander KM. 4-Amino-5-aryl-6-arylethynylpyrimidines: Structure–activity relationships of non-nucleoside adenosine kinase inhibitors. *Bioorganic & medicinal chemistry*. 2007 Feb 15;15(4):1586-605.
- McGuinness BF, Ho KK, Stauffer TM, Rokosz LL, Mannava N, Kultgen SG, Saionz K, Klon A, Chen W, Desai H, Rogers WL. Discovery of novel quinolinone adenosine A2B antagonists. *Bioorganic & medicinal chemistry letters*. 2010 Dec 15;20(24):7414-20.
- McIntire WE, MacCleery G, Garrison JC. The G protein β subunit is a determinant in the coupling of Gs to the β 1-adrenergic and A2A adenosine receptors. *Journal of Biological Chemistry*. 2001 May 11;276(19):15801-9.
- McNamara JO. Emerging insights into the genesis of epilepsy. *Nature*. 1999 Jun 24;399:A15-22.
- Meldrum BS, Akbar MT, Chapman AG. Glutamate receptors and transporters in genetic and acquired models of epilepsy. *Epilepsy research*. 1999 Sep 30;36(2):189-204.
- Mitra. I, P. P. Roy, S. Kar, P. K. Ojha and K. Roy, *J. Chemometrics*, 2010, 24, 22-33.
- Mittelstadt SW, Hemenway CL, Craig MP, Hove JR. Evaluation of zebrafish embryos as a model for assessing inhibition of hERG. *Journal of pharmacological and toxicological methods*. 2008 Apr 30;57(2):100-5.
- Mogul DJ, Adams ME, Fox AP. Differential activation of adenosine receptors decreases N-type but potentiates P-type Ca^{2+} current in hippocampal CA3 neurons. *Neuron*. 1993 Feb 28;10(2):327-34.
- Monopoli A, Casati C, Lozza G, Forlani A, Ongini E. Cardiovascular pharmacology of the A2A adenosine receptor antagonist, SCH 58261, in the rat. *Journal of Pharmacology and Experimental Therapeutics*. 1998 Apr 1;285(1):9-15.
- Muhammad N. In-Vivo Models for Management of Pain. *Pharmacology & Pharmacy*. 2014 Jan 1;5(1):92.
- Muller CE, Jacobson KA. Recent developments in adenosine receptor ligands and their potential as novel drugs. *Biochimica et Biophysica Acta (BBA)-Biomembranes*. 2011 May 31;1808(5):1290-308.

- Muller CE, Stein B. Adenosine receptor antagonists: structures and potential therapeutic applications. *Current Pharmaceutical Design*. 1996 Oct 1;2(5):501-30.
- Muller CE. Adenosine receptor ligands-recent developments part I. Agonists. *Current medicinal chemistry*. 2000 Dec 1;7(12):1269-88.
- Mustafa SJ, Nadeem A, Fan M, Zhong H, Belardinelli L, Zeng D. Effect of a specific and selective A2B adenosine receptor antagonist on adenosine agonist AMP and allergen-induced airway responsiveness and cellular influx in a mouse model of asthma. *Journal of Pharmacology and Experimental Therapeutics*. 2007 Mar 1;320(3):1246-51.
- Neves SR, Ram PT, Iyengar R. G protein pathways. *Science*. 2002 May 31;296(5573):1636-9.
- Nishizaki T, Nagai K, Nomura T, Tada H, Kanno T, Tozaki H, Li XX, Kondoh T, Kodama N, Takahashi E, Sakai N. A new neuromodulatory pathway with a glial contribution mediated via A2A adenosine receptors. *Glia*. 2002 Aug 1;39(2):133-47.
- Ochi T, Motoyama Y, Goto T. The analgesic effect profile of FR122047, a selective cyclooxygenase-1 inhibitor, in chemical nociceptive models. *European journal of pharmacology*. 2000 Mar 10;391(1):49-54.
- Odashima M, Bamias G, Rivera-Nieves J, Linden J, Nast CC, Moskaluk CA, Marini M, Sugawara K, Kozaiwa K, Otaka M, Watanabe S. Activation of A2A adenosine receptor attenuates intestinal inflammation in animal models of inflammatory bowel disease. *Gastroenterology*. 2005 Jul 31;129(1):26-33.
- Pagonopoulou O, Efthimiadou A, Asimakopoulos B, Nikolettos NK. Modulatory role of adenosine and its receptors in epilepsy: possible therapeutic approaches. *Neuroscience research*. 2006 Sep 30;56(1):14-20.
- Palmer TM, Stiles GL. Identification of an A2A adenosine receptor domain specifically responsible for mediating short-term desensitization. *Biochemistry*. 1997 Jan 28;36(4):832-8.
- Pan X, Tan N, Zeng G, Huang H, Yan H. 3D QSAR studies on ketoamides of human cathepsin K inhibitors based on two different alignment methods. *European journal of medicinal chemistry*. 2010 Feb 28;45(2):667-81.

- Papassotiropoulos A, Hock C, Nitsch RM. Genetics of interleukin 6: implications for Alzheimer's disease. *Neurobiology of aging*. 2001 Dec 31;22(6):863-71.
- Peakman MC, Hill SJ. Adenosine A2B-receptor-mediated cyclic AMP accumulation in primary rat astrocytes. *British journal of pharmacology*. 1994 Jan 1;111(1):191-8.
- Pierce KD, Furlong TJ, Selbie LA, Shine J. Molecular cloning and expression of an adenosine A2b receptor from human brain. *Biochemical and biophysical research communications*. 1992 Aug 31;187(1):86-93.
- Pitkanen A, Sutula TP. Is epilepsy a progressive disorder? Prospects for new therapeutic approaches in temporal-lobe epilepsy. *The Lancet Neurology*. 2002 Jul 31;1(3):173-81.
- Poulsen SA, Quinn RJ. Adenosine receptors: new opportunities for future drugs. *Bioorganic & medicinal chemistry*. 1998 Jun 30; 6(6):619-41.
- Radi M, Botta M, Falchi F, Maga G, Baldanti F, Paolucci S, inventors; Universita Degli Studi Di Siena, Consiglio Nazionale Delle Ricerche, assignee. Compounds with ddx3 inhibitory activity and uses thereof. United States patent application US 13/499,547. 2010 Oct 4.
- Ralevic V, Burnstock G. Effects of purines and pyrimidines on the rat mesenteric arterial bed. *Circulation research*. 1991 Dec 1; 69(6):1583-90.
- Rao VS, Rao A, Karanth KS. Anticonvulsant and neurotoxicity profile of *Nardostachys jatamansi* in rats. *Journal of ethnopharmacology*. 2005 Dec 1; 102(3):351-56.
- Rebola N, Porciúncula LO, Lopes LV, Oliveira CR, Soares-da-Silva P, Cunha RA. Long-term Effect of Convulsive Behavior on the Density of Adenosine A1 and A2A Receptors in the Rat Cerebral Cortex. *Epilepsia*. 2005 Jul 1;46(s5):159-65.
- Riekenberg S, Farhat K, Debarry J, Heine H, Jung G, Wiesmüller KH, Ulmer AJ. Regulators of G-protein signalling are modulated by bacterial lipopeptides and lipopolysaccharide. *FEBS journal*. 2009 Feb 1;276(3):649-59.
- Rigoulot MA, Leroy C, Koning E, Ferrandon A, Nehlig A. Prolonged Low-dose Caffeine Exposure Protects Against Hippocampal Damage but Not Against the Occurrence of Epilepsy in the Lithium-pilocarpine Model in the Rat. *Epilepsia*. 2003 Apr 1;44(4):529-35.

- Rivkees SA, Reppert SM. RFL9 encodes an A2B-adenosine receptor. *Molecular Endocrinology*. 1992 Oct;6(10):1598-604.
- Rodrigues RJ, Alfaro TM, Rebola N, Oliveira CR, Cunha RA. Co-localization and functional interaction between adenosine A2A and metabotropic group 5 receptors in glutamatergic nerve terminals of the rat striatum. *Journal of neurochemistry*. 2005 Feb 1;92(3):433-41.
- Rosa M. Biological properties of carrageenan. *Journal of Pharmacy and Pharmacology*. 1972 Feb 1;24(2):89-102.
- Roseti C, Martinello K, Fucile S, Piccari V, Mascia A, Di Gennaro G, Quarato PP, Manfredi M, Esposito V, Cantore G, Arcella A. Adenosine receptor antagonists alter the stability of human epileptic GABA_A receptors. *Proceedings of the National Academy of Sciences*. 2008 Sep 30;105(39):15118-23.
- Roseti C, Palma E, Martinello K, Fucile S, Morace R, Esposito V, Cantore G, Arcella A, Giangaspero F, Aronica E, Mascia A. Blockage of A2A and A3 adenosine receptors decreases the desensitization of human GABA_A receptors microtransplanted to *Xenopus* oocytes. *Proceedings of the National Academy of Sciences*. 2009 Sep 15;106(37):15927-31.
- Rosi S, McGann K, Hauss-Wegrzyniak B, Wenk GL. The influence of brain inflammation upon neuronal adenosine A2B receptors. *Journal of neurochemistry*. 2003 Jul 1;86(1):220-27.
- Rybaczyk L, Wunderlich JE, Needleman B, Melvin S, Grants I, Huang K, Christofi FL. Differential dysregulation of ADORA3, ADORA2A, ADORA2B, and P2RY14 expression profiles from 34 purine-genes in mucosal biopsies and peripheral blood mononuclear cells in inflammatory bowel diseases. *Gastroenterology* 2007 Apr 1 (Vol. 132, No. 4, pp. A246-A246).
- Ryzhov S, Novitskiy SV, Carbone DP, Biaggioni I, Zaynagetdinov R, Goldstein AE, Dikov MM, Feoktistov I. Host A 2B adenosine receptors promote carcinoma growth. *Neoplasia*. 2008 Sep 30;10(9):987-95.

- Sanchez-Mateo CC, Bonkanka CX, Hernandez-Perez M, Rabanal RM. Evaluation of the analgesic and topical anti-inflammatory effects of *Hypericum reflexum* L. fil. *Journal of ethnopharmacology*. 2006 Aug 11;107(1):1-6.
- Sawynok J, Reid A, Liu XJ. Involvement of mast cells, sensory afferents and sympathetic mechanisms in paw oedema induced by adenosine A1 and A2B/3 receptor agonists. *European journal of pharmacology*. 2000 Apr 21;395(1):47-50.
- Schaddelee MP, Groenendaal D, DeJongh J, Cleypool CG, IJzerman AP, De Boer AG, Danhof M. Population pharmacokinetic modeling of blood-brain barrier transport of synthetic adenosine A1 receptor agonists. *Journal of Pharmacology and Experimental Therapeutics*. 2004 Dec 1;311(3):1138-46.
- Schrodinger, LLC, Phase, version 3.4, New York, NY, 2011.
- Schrodinger, LLC: LigPrep, version 2.5; New York, NY, 2012.
- Schrodinger. L, ConfGen, version 2.3, New York, NY, 2012.
- Schrodinger. L, MacroModel, version 9.10, New York, NY, 2012.
- Schrodinger. L, QikProp, version 3.5, New York, NY, 2012.
- Schulte G, Fredholm BB. Human adenosine A1, A2A, A2B, and A3 receptors expressed in Chinese hamster ovary cells all mediate the phosphorylation of extracellular-regulated kinase 1/2. *Molecular pharmacology*. 2000 Sep 1;58(3):477-82.
- Schuermann G, Ebert RU, Chen J, Wang B, Kühne R. External validation and prediction employing the predictive squared correlation coefficient — Test set activity mean vs training set activity mean. *Journal of chemical information and modeling*. 2008 Oct 28;48(11):2140-45.
- Sebastiao AM. Adenosine and epilepsy—thinking beyond A1 receptors. *Purinergic signalling*. 2010 Mar 1;6(1):1-2.
- Sharma MC, Sharma S. 3D-quantitative structure-activity relationship analysis of some 2-substituted halogen benzimidazoles analogues with antimycobacterial activity. *Int. J. Chem. Tech. Res*. 2010;2(1):606-14.

- Shryock JC, Belardinelli L. Adenosine and adenosine receptors in the cardiovascular system: biochemistry, physiology, and pharmacology. *The American journal of cardiology*. 1997 Jun 19;79(12):2-10.
- Shukla MK, Mishra PC. Structure-activity relationship for some xanthines as adenosine A1 receptor antagonists, bronchodilators and phosphodiesterase inhibitors: an electric field mapping approach. *Journal of Molecular Structure: THEOCHEM*. 1995 Sep 20;340(1):159-67.
- Spicuzza L, Di Maria G, Polosa R. Adenosine in the airways: implications and applications. *European journal of pharmacology*. 2006 Mar 8;533(1):77-88.
- Stefanachi A, Brea JM, Cadavid MI, Centeno NB, Esteve C, Loza MI, Martinez A, Nieto R, Ravina E, Sanz F, Segarra V. 1-, 3- and 8-substituted-9-deazaxanthines as potent and selective antagonists at the human A2B adenosine receptor. *Bioorganic & medicinal chemistry*. 2008 Mar 15;16(6):2852-69.
- Stefanachi A, Nicolotti O, Leonetti F, Cellamare S, Campagna F, Loza MI, Brea JM, Mazza F, Gavuzzo E, Carotti A. 1, 3-Dialkyl-8-(hetero) aryl-9-OH-9-deazaxanthines as potent A2B adenosine receptor antagonists: design, synthesis, structure–affinity and structure–selectivity relationships. *Bioorganic & medicinal chemistry*. 2008 Nov 15;16(22):9780-89.
- Stevens B, Porta S, Haak LL, Gallo V, Fields RD. Adenosine: a neuron-glia transmitter promoting myelination in the CNS in response to action potentials. *Neuron*. 2002 Dec 5;36(5):855-68.
- Stewart M, Steinig AG, Ma C, Song JP, McKibben B, Castelhana AL, MacLennan SJ. [3 H] OSIP339391, a selective, novel, and high affinity antagonist radioligand for adenosine A2B receptors. *Biochemical pharmacology*. 2004 Jul 15;68(2):305-12.
- Strickberger SA, Man KC, Daoud EG, Goyal R, Brinkman K, Knight BP, Weiss R, Bahu M, Morady F. Adenosine-induced atrial arrhythmia: a prospective analysis. *Annals of internal medicine*. 1997 Sep 15;127(6):417-22.
- Sullivan GW, Fang G, Linden J, Scheld WM. A2A adenosine receptor activation improves survival in mouse models of endotoxemia and sepsis. *Journal of Infectious Diseases*. 2004 May 15;189(10):1897-1904.

- Sun CX, Zhong H, Mohsenin A, Morschl E, Chunn JL, Molina JG, Belardinelli L, Zeng D, Blackburn MR. Role of A2B adenosine receptor signaling in adenosine-dependent pulmonary inflammation and injury. *The Journal of clinical investigation*. 2006 Aug 1;116(8):2173-82.
- Sweeney MI. Neuroprotective effects of adenosine in cerebral ischemia: window of opportunity. *Neuroscience & Biobehavioral Reviews*. 1997 Dec 31;21(2):207-17.
- Swinyard EA, Brown WC, Goodman LS. Comparative assays of antiepileptic drugs in mice and rats. *Journal of Pharmacology and Experimental Therapeutics*. 1952 Nov 1;106(3):319-30.
- Tautenhahn M, Leichsenring A, Servetini I, Pesic M, Sperlagh B, Norenberg W, Illes P. Purinergic modulation of the excitatory synaptic input onto rat striatal neurons. *Neuropharmacology*. 2012 Mar 31;62(4):1756-66.
- Tian GF, Azmi H, Takano T, Xu Q, Peng W, Lin J, Oberheim N, Lou N, Wang X, Zielke HR, Kang J. An astrocytic basis of epilepsy. *Nature medicine*. 2005 Sep 1;11(9):973-81.
- Tome AR, Silva H, Cunha RA. Role of the purinergic neuromodulation system in epilepsy. *Open Neurosci. J*. 2010;4:64-83.
- Tsujita Y, Muraski J, Shiraishi I, Kato T, Kajstura J, Anversa P, Sussman MA. Nuclear targeting of Akt antagonizes aspects of cardiomyocyte hypertrophy. *Proceedings of the National Academy of Sciences*. 2006 Aug 8;103(32):11946-51.
- Tucker AL, LiGuo JI, Holeton D, Taylor AJ, Linden J. Dominance of Gs in doubly Gs/Gi-coupled chimaeric A1/A2A adenosine receptors in HEK-293 cells. *Biochemical Journal*. 2000 Nov 15;352(1):203-10.
- Van der Hoeven D, Wan TC, Gizewski ET, Kreckler LM, Maas JE, Van Orman J, Ravid K, Auchampach JA. A role for the low-affinity A2B adenosine receptor in regulating superoxide generation by murine neutrophils. *Journal of Pharmacology and Experimental Therapeutics*. 2011 Sep 1;338(3):1004-12.
- Van Meerloo J, Kaspers GJ, Cloos J. Cell sensitivity assays: the MTT assay. *Cancer cell culture: methods and protocols*. 2011:237-45.

- Varani K, Caramori G, Vincenzi F, Adcock I, Casolari P, Leung E, MacLennan S, Gessi S, Morello S, Barnes PJ, Ito K. Alteration of adenosine receptors in patients with chronic obstructive pulmonary disease. *American journal of respiratory and critical care medicine*. 2006 Feb 15;173(4):398-406.
- Varani K, Caramori G, Vincenzi F, Tosi A, Barczyk A, Contoli M, Casolari P, Triggiani M, Hansel T, Leung E, MacLennan S. Oxidative/nitrosative stress selectively altered A2B adenosine receptors in chronic obstructive pulmonary disease. *The FASEB Journal*. 2010 Apr 1;24(4):1192-204.
- Vidal B, Nueda A, Esteve C, Domenech T, Benito S, Reinoso RF, Pont M, Calbet M, López R, Cadavid MI, Loza MI. Discovery and characterization of 4'-(2-furyl)-N-pyridin-3-yl-4, 5'-bipyrimidin-2'-amine (LAS38096), a potent, selective, and efficacious A2B adenosine receptor antagonist. *Journal of medicinal chemistry*. 2007 May 31;50(11):2732-36.
- Vinegar R, Schreiber W, Hugo R. Biphasic development of carrageenin edema in rats. *Journal of pharmacology and experimental therapeutics*. 1969 Mar 1;166(1):96-103.
- Volpini R, Costanzi S, Vittori S, Cristalli G, Klotz KN. Medicinal chemistry and pharmacology of A2B adenosine receptors. *Current topics in medicinal chemistry*. 2003 Feb 1;3(4):427-43.
- Walmsley SR, Farahi N, Peyssonnaud C, Johnson RS, Cramer T, Sobolewski A, Condliffe AM, Cowburn AS, Johnson N, Chilvers ER. Hypoxia-induced neutrophil survival is mediated by HIF-1 α -dependent NF- κ B activity. *The Journal of experimental medicine*. 2005 Jan 3;201(1):105-15.
- Wei Q, Costanzi S, Balasubramanian R, Gao ZG, Jacobson KA. A2B adenosine receptor blockade inhibits growth of prostate cancer cells. *Purinergic signalling*. 2013 Jun 1;9(2):271-80.
- Wei W, Du C, Lv J, Zhao G, Li Z, Wu Z, Haskó G, Xie X. Blocking A2B adenosine receptor alleviates pathogenesis of experimental autoimmune encephalomyelitis via inhibition of IL-6 production and Th17 differentiation. *The Journal of Immunology*. 2013 Jan 1;190(1):138-46.

- Westerfield M. The zebrafish book: a guide for the laboratory use of zebrafish (*Danio rerio*). University of Oregon press; 2000.
- Xu K, Bastia E, Schwarzschild M. Therapeutic potential of adenosine A2A receptor antagonists in Parkinson's disease. *Pharmacology & therapeutics*. 2005 Mar 31;105(3):267-310.
- Yang D, Zhang Y, Nguyen HG, Koupenova M, Chauhan AK, Makitalo M, Jones MR, Hilaire CS, Seldin DC, Toselli P, Lamperti E. The A2B adenosine receptor protects against inflammation and excessive vascular adhesion. *The Journal of clinical investigation*. 2006 Jul 3;116(7):1913-23.
- Yogeeswari P, Ragavendran JV, Sriram D, Nageswari Y, Kavya R, Sreevatsan N, Vanitha K, Stables J. Discovery of 4-aminobutyric acid derivatives possessing anticonvulsant and antinociceptive activities: a hybrid pharmacophore approach. *Journal of medicinal chemistry*. 2007 May 17;50(10):2459-67.
- Yuzlenko O, Kiec-Kononowicz K. Potent adenosine A1 and A2A receptors antagonists: recent developments. *Current medicinal chemistry*. 2006 Dec 1;13(30):3609-25.
- Zablocki J, Elzein E, Kalla R. A2B adenosine receptor antagonists and their potential indications. *Expert Opinion on Therapeutic Patents*. 2006 Oct 1;16(10):1347-57.
- Zablocki J, Kalla R, Perry T, Palle V, Varkhedkar V, Xiao D, Piscopio A, Maa T, Gimbel A, Hao J, Chu N. The discovery of a selective, high affinity A2B adenosine receptor antagonist for the potential treatment of asthma. *Bioorganic & medicinal chemistry letters*. 2005 Feb 1;15(3):609-12.
- Zang L, Morikane D, Shimada Y, Tanaka T, Nishimura N. A novel protocol for the oral administration of test chemicals to adult zebrafish. *Zebrafish*. 2011 Dec 1;8(4):203-10.
- Zhang Y, Dai Y, Wen J, Zhang W, Grenz A, Sun H, Tao L, Lu G, Alexander DC, Milburn MV, Carter-Dawson L. Detrimental effects of adenosine signaling in sickle cell disease. *Nature medicine*. 2011 Jan 1;17(1):79-86.
- Zhong H, Belardinelli L, Maa T, Feoktistov I, Biaggioni I, Zeng D. A2B adenosine receptors increase cytokine release by bronchial smooth muscle cells. *American journal of respiratory cell and molecular biology*. 2004 Jan;30(1):118-125.

Zhong H, Wu Y, Belardinelli L, Zeng D. A2B adenosine receptors induce IL-19 from bronchial epithelial cells, resulting in TNF- α increase. American journal of respiratory cell and molecular biology. 2006 Nov;35(5):587-92.

Zhou Y, Schneider DJ, Blackburn MR. Adenosine signaling and the regulation of chronic lung disease. Pharmacology & therapeutics. 2009 Jul 31;123(1):105-16.

APPENDIX

LIST OF PUBLICATIONS

FROM THESIS WORK

1. **R. Srikanth**, A. Reshma, K. Pushkar, D. Sriram, P. Yogeewari. "Structure based Drug Design, Synthesis and Screening of Adenosine A_{2A}R Antagonists as Novel Anti-epileptic drugs." *EPILEPSIA*, 2014, 55, 5.
2. **Racharla Srikanth**, Reshma Alokam, Gangadhar Matharasala, Sushruth Jay, Pushkar Kulkarni, Raghavender Medishetti, Swapna Yellanki, Dharmarajan Sriram, Perumal Yogeewari. Design, Synthesis, and Pharmacological Evaluation of Novel 1,3,5-triazine-2,4,6-triamine derivatives as Potent and Selective A_{2A} Adenosine Receptor Antagonists in the treatment of Epilepsy (*Indian Patent application in process*).
3. **Racharla Srikanth**, Suryadevara Priyanka, Gangadhar Matharasala, Reshma Alokam, Dharmarajan Sriram, Perumal Yogeewari. Identification of novel A_{2B}R antagonists by using Pharmacophore-Based 3D-QSAR and its Anti-nociceptive and Anti-inflammatory effects. *European Journal of Pharmaceutical Sciences (Under communication)*.

OTHER PUBLICATIONS

1. Reshma Alokam, **Srikanth Racharla**, Madhu Babu Battu, Gangadhar Matharasala, Dharmarajan Sriram, Perumal Yogeewari. "Design of Dual inhibitors of ROCK-I and NOX-2 for the treatment of neuroinflammatory disorders." *Cell and Molecular Neurobiology (Under communication)*.
2. Ram K Mishra, **Srikanth Racharla**, Reshma Alokam, Sarthak M Singhal, Aquib Gaus, Geethasai Sreevatsav, Gangadhar Matharasala, Dharmarajan Sriram, Perumal Yogeewari. "2,6-Diaminopyrimidines as Rho-Kinase Inhibitors Useful for the Treatment of Neurological Disorders Including Diabetic Neuropathy." *European journal of medicinal chemistry (Under communication)*.
3. Ram Kumar Mishra, **Srikanth Racharla**, Deepak Kumar Sharma, Gangadhar Matharsala, Reshma Alokam, Piyush Bafna, Dharmarajan Sriram and Perumal Yogeewari. Design of Novel Protein Kinase C- β Inhibitors for the Treatment of Neurological Complications of Diabetes. *Journal of Neuroscience Research (Under communication)*.

PAPERS PRESENTED AT NATIONAL/INTERNATIONAL CONFERENCES

1. **R. Srikanth**, A. Reshma, K. Pushkar, D. Sriram, P. Yogeewari. "Structure based drug design, synthesis and screening of adenosine A_{2A}R antagonists as novel antiepileptic drugs." **11th European Congress on Epileptology**, Stockholm, Sweden, 29th June-3rd July, **2014**.
2. **Srikanth Racharla**, Dharmarajan Sriram, Perumal Yogeewari. "Anti-nociceptive and Anti-inflammatory effects of novel adenosine A_{2B}R antagonists. **Current Trends in Pharmaceutical Science (CTPS 2012)**, BITS-Pilani, Hyderabad campus, Hyderabad, Nov **2012**.
3. **R. Srikanth**, Kiran Gangarapu. "Novel structural hybrids of substituted triazine derivatives as antitumor agents" **International Conference on Recent Advances in Drug Discovery**, 22nd-24th Oct, **2010**, University College of Pharmaceutical sciences, Kakatiya University, Warangal.

BIOGRAPHY OF SRIKANTH RACHARLA

Mr. Srikanth Racharla completed his Bachelor of Pharmacy from St.Peters Institute of Pharmaceutical Sciences; Kakatiya University, Warangal in the year 2006, and M.S (Pharmacy) Medicinal chemistry from National Institute of Pharmaceutical Education and Research (NIPER), Kolkata. He has about 2 years of academic experience in teaching at S.R College of Pharmacy, Ananthasagar, Warangal from 2009-2011. He has been appointed as DST INSPIRE Fellow at Birla Institute of Technology and Science, Pilani, Hyderabad campus from 2011-2016 under the supervision of Prof. P. Yogeewari. He has published five scientific publications in well-renowned international journals. He has presented papers at various national and international conferences. He was recently awarded Indian Council of Medical Research (ICMR)-International travel grant, New Delhi and 11th ECE-Travel Bursary Award, to present his part of research work as oral presentation on title—Structure based drug design, Synthesis and Screening of adenosine A_{2A} antagonists as novel antiepileptic drugs at the 11th European Congress on Epileptology, Stockholm, Sweden, 29th June-3rd July, 2014.

BIOGRAPHY OF PROF. P. YOGEESWARI

Prof. P. Yogeeswari is presently working in the capacity of Professor, Department of Pharmacy and Associate Dean (Sponsored Research and Consultancy Division), Birla Institute of Technology and Science, Pilani, Hyderabad Campus. She received her Ph.D. degree in 2001 from Banaras Hindu University, Varanas, UP. She has been involved in research for the last 15 years and in teaching for 14 years. APTI honoured her with YOUNG PHARMACY TEACHER AWARD for the year 2007. In 2010, ICMR honored her by awarding “Shakuntala Amir Chand Award” for excellent biomedical research. She has been awarded “Excellence in Pain Research and Management in Developing Countries” in IASP 2014 under the basic science research category in Argentina. She has collaborations with various national and international organizations that include National Institute of Health, Bethesda, USA; National Institute of Mental Health and Neurosciences, Bangalore; Karolinska Institute, Stockholm, Sweden; National Institute of Immunology, New Delhi, India; Pasteur Institute, University of Lille, France; Bogomoletz Institute of Physiology National Academy of Science, Ukraine and Faculty of Medicine of Porto, Porto, Portugal. She has more than 290 research publications to her credit and five Indian Patents. She is an expert reviewer of many international journals like Journal of Medicinal Chemistry (ACS), Journal of Chemical Information & Modeling (ACS, USA), Bioorganic Medicinal Chemistry (Elsevier), Recent Patents on CNS Drug Discovery (Bentham), etc. She has also co-authored a textbook on Organic Medicinal Chemistry with Dr. D Sriram titled “Medicinal Chemistry” published by Pearson Education. She is a lifetime member of Association of Pharmacy Teachers of India and Indian Pharmacological Society. She has successfully completed many sponsored projects and is currently handling projects sponsored by DST, DBT INDO-BRAZIL, ICMR-INSERM, and CSIR. She has guided sixteen Ph.D students and currently five students are pursuing their Ph.D. work.